

VNIVERSITAT DE VALÈNCIA

Departament d'Òptica, Facultat de Física



Contributions
to the Quantum Optics of
Multi-mode Optical Parametric Oscillators

PhD dissertation by

Carlos Navarrete-Benlloch

Under the supervision of

Eugenio Roldán Serrano

and

Germán J. de Valcárcel Gonzalvo

Valencia, Spain; December, 2011

AGRADECIMIENTOS [ACKNOWLEDGEMENTS]

Escribir los agradecimientos de esta tesis genera en mí una doble sensación de felicidad. El primer motivo es obvio: ello significa que el final de este largo (pero bonito) camino que ha supuesto redactar tan pensado documento está llegando a su fin, lo cual no es poco, ya que meses atrás me parecía que el camino era infinito (tras escribir cada apartado, siempre tenía la sensación de que había algo más que decir, algo más sobre lo que incidir, algo más que matizar... la paradoja de Zenón parecía más real que nunca). Sin embargo, la mayor parte de la alegría que supone escribir estos agradecimientos viene de otro sitio: pensar en a quién agradecer y cómo, me hace recordar el camino exacto que me ha llevado a este punto, recordar a las personas y los momentos que han supuesto (en mayor o menor medida) puntos de inflexión en mi vida, que me han ayudado a elegir qué dirección tomar en cada bifurcación; y claro, teniendo en cuenta lo contento que me ha hecho la física y lo que le rodea desde que entré en la universidad, recordar tales cosas no puede suponer más que una tremenda alegría.

En este sentido, sin duda son mis padres los primeros a los que debo mi agradecimiento (tanto cronológicamente, fueron los primeros que estuvieron ahí para mí, como cuantitativamente). Corren tiempos en los que siento que la economía es el motor fundamental de la mayor parte de la gente, tiempos en los que estamos constantemente bombardeados con la idea de que el camino a la felicidad es acumular dinero (y poder, a ser posible); pero también siento que he conseguido desligarme de tal “movimiento”, que he conseguido encontrar dos cosas en la vida, la ciencia y la música, de las cuales puedo plantearme vivir, a la vez que sentirme feliz y realizado haciéndolas. Pues bien, puedo decir con total certeza que tal logro es fruto de los valores que mis padres me han inculcado desde pequeño. Ellos siempre me han proporcionado todos los medios que estuvieran a su alcance y todo el apoyo posible para hacer aquello que quisiera, eso sí, siempre que consiguiera convencerles de dos cosas: que lo haría esforzándome al máximo de verdad, y, sobre todo, que lo haría únicamente mientras me hiciera realmente feliz; las palabras dinero, futuro, o triunfo, no estaban en su discurso.

Quizás quien más ha “sufrido” mi faceta de científico es Susana, mi novia, compañera de andanzas en la vida, y mayor inspiración durante los últimos 8 años. No puedo más que agradecerle la paciencia infinita que tiene conmigo; del futuro sólo espero que las cosas buenas que conllevan compartir la vida con un científico-músico superen como hasta ahora la inestabilidad y las incomodidades (vida en el extranjero, noches y fines de semana de trabajo, etc...) intrínsecas a dicho “título”. Bien sabes que “te vull” aunque a veces no te lo diga lo suficiente.

En lo que a la parte científica se refiere, no cabe ninguna duda de que a quien más tengo que agradecer es a mis directores Eugenio y Germán; desde el principio (y hablamos de antes de terminar la carrera de Física) me hicieron sentir como un colaborador más con el potencial de aportar buenas ideas a la investigación que estuviésemos desarrollando, a la vez que pusieron a mi disposición todos los medios posibles para transferirme toda la física que almacenan (que no es poca). Pero más allá de lo puramente científico, me siento orgulloso de que me hayan dejado entrar en sus vidas hasta el punto de haberse convertido en dos de las personas que más aprecio y en las que más me apoyo a día de hoy. Desde luego, Eugenio y Germán, no aspiro más que a convertirme el día de mañana en alguien tan digno y merecedor de cariño, respeto y admiración como vosotros.

Hay gente que piensa que por ser hijo único no tengo hermanos, pero de una de las cosas que más orgulloso me siento es de haber demostrado que dicha gente se equivoca: Apa, Pabl, Fons, Alberto y Rika son prueba de ello. Apa y Pabl han estado ahí casi desde que puedo recordar; juntos hemos pasado por casi todo lo que se puede pasar, y hemos sobrevivido! Mi vida sin Fons, ciertamente habría sido completamente distinta; a él no le debo únicamente su amistad totalmente desinteresada, sino también el haberme abierto musicalmente, y con ello haber contribuido radicalmente a que mi vida sea como es ahora. Alberto es el que más tardó en llegar a mi vida, pero se ha convertido en quien mejor entiende esta faceta tan importante de mi vida que es la ciencia; no conozco persona más sincera y falta de maldad o egoísmo (vale, quizá Fons!), por lo cual tiene mi más sincera admiración. Rika fue mi pilar básico durante los primeros años de carrera, los cuales dudo que hubieran sido tan productivos y realizadores sin su presencia; sólo puedo darle las gracias por esos años que vivimos juntos, y decirle cuánto echo de menos la sensación de tenerle a mi (y estar a su) lado.

Me siento muy afortunado de contar con una familia que siempre me hace sentir especial, a la vez que me pone los pies en la tierra (lo cual no es sencillo trabajando en cosas tan abstractas como la Física Teórica, o tan intensas como la Música). Siento que una parte de cada uno de vosotros está en mi interior, tanto de los que me han criado: mi Abuelo Manolo, mi Yaya Lola, mi Tía Loles, y mis Tíos Pepa y Chani; como de los que me he criado: mi Teta Jose y mis Primos Rafa, Patricia, Dani y Carola. No me gustaría olvidarme tampoco de los nuevos miembros de la familia que han ido apareciendo con el tiempo: mis sobrinitos Pablo y Alicia, y mis “cuñaos” Paco, Sergi, Vicky, y Silvia; ni tampoco de mis “tíos y primos postizos”, en especial de mi tía Jose y mi tío Pedro, que tan buenas palabras guardan siempre para mí.

También me gustaría agradecer a mi “familia por extensión”, la familia de Su, a la cual tengo muy presente cada día y considero una parte muy relevante de mi vida. Muchas gracias a “Los Mayores” (Paloma, Carlos y Amparo) y a “Los Jóvenes” (Emi, Moni, y Mir), por abrirme las puertas de sus vidas sin trabas (bueno, aunque a Mir le costó un poco más que los demás... jejeje).

Me es imposible trazar la trayectoria que me ha llevado a este momento sin recordar a todos los profesores que me han influenciado e inspirado a lo largo de mi vida. Dentro de éstos, quizás los más importantes, porque sin ellos dudo que me hubiese dado cuenta de que la Física y las Matemáticas son mi vocación, son mis profesores del instituto (del “cole”, como nosotros lo llamamos). Encarna Giner fue sin duda la que más me abrió los ojos y a la que con más cariño recuerdo; cuando menos lo esperaba, ella me mostró lo bonitas que pueden llegar a ser las matemáticas, y me dejó maravillado tras hacerme entender que sólo requieren de comprenderlas (y no de memorizarlas) para utilizarlas e interiorizarlas. Mi mayor suerte fue su formación en Física Teórica (a la que yo finalmente me he dedicado), ya que le permitió introducirme en el mundo de la Relatividad General y la Geometría Diferencial hacia el final de nuestro tiempo juntos. Chenchó Pascual, mi gran profesor de Física, fue el primer profesor que nos planteó preguntas interesantes, con ánimo real de que fuéramos nosotros, los estudiantes, los que encontraríamos las respuestas; cuando creía que las Matemáticas eran mi vocación, él me hizo ver que la Física es precisamente la aplicación de éstas al mundo real, la forma en que preguntamos a la naturaleza para obtener respuestas a las preguntas más fundamentales, y con ello me hizo encontrar mi vocación real, la Física Teórica. Siendo científico, quizás algo más sorprendente es el hecho de que cuando pienso en los profesores que más me motivaron en dicha época, mi profesor de Lengua Castellana, Ángel Umbert, sea de los primeros que me viene a la cabeza; gracias a él también, aunque no sepa verbalizar muy bien porqué exactamente (al margen de que fuera, sin duda, uno de los mejores profesores que he tenido nunca).

Durante mi último año de instituto tuve la suerte de participar en la Olimpiada de Física, lo cual me permitió recibir “clases avanzadas” de Física de mano de varios profesores de la Universitat de València y la Universidad Politécnica de Valencia. La experiencia fue inolvidable, y no puedo más que agradecer a dichos profesores su entrega desinteresada que tanto me motivó a coger el camino de la Física finalmente con el fin de seguir aprendiendo y convertirme en un docente como ellos algún día. Guardo especial cariño a Fernando Tena, que se encargó de “cuidar” a los olímpicos valencianos durante la fase española, y que fue quien más me inspiró durante todas las fases, así como a Amparo Pons, José Luis Cruz, Miguel Andrés y Paco Pomer.

La carrera de Física cumplió sobradamente con mis expectativas en lo que a disfrutar aprendiendo se refiere; años atrás nunca hubiese pensado que una “actividad intelectual” podría llenarme y motivarme tanto. No obstante, esto no hubiese sido posible sin el esfuerzo de algunos profesores a los que ahora me gustaría agradecer explícitamente: José María Ibáñez (Cálculo y Evolución Estelar), José María Martí (Álgebra y Dinámica de Fluidos), Ramón Cases (Lab. Física General y Física Nuclear y de Partículas), José Luis Cruz (Física General y Ondas Electromagnéticas), Domingo Martínez (Física General y Lab. Electromagnetismo), Eugenio Roldán (Física General, Óptica Cuántica y Óptica No lineal), Albert Ferrando (Física General), Pas García (Óptica Geométrica y Procesos Estocásticos en Fotónica), Carlos Ferreira (Óptica Geométrica), Julio Pellicer (Termodinámica), Chantal Ferrer (Mecánica y Ondas), Jon Marcaide (Astronomía y Astrofísica), Juan Zúñiga (Métodos Numéricos), Juan Carlos Soriano (Óptica y Procesos Estocásticos en Fotónica), José María Isidro (Física Cuántica), Vicente Muñoz (Electromagnetismo), Juanfran Sánchez (Electromagnetismo), Kiko Botella (Lab. Física Cuántica y Mecánica Cuántica Avanzada), Pepe Navarro Salas (Geometría Diferencial, Variedades y Topología, y Teoría Cuántica de Campos en Espacios Curvos), Benito Gimeno (Electrodinámica), Nuria Rius (Mecánica Teórica y Teoría Cuántica de Campos a Temperatura Finita), Manuel Vicente Vacas (Mecánica Cuántica), Miguel Andrés (Ondas Electromagnéticas), Vladimir García (Física Estadística), Germán de Valcárcel (Óptica Cuántica y Óptica No Lineal), Fernando Silva (Óptica Cuántica), Ramón Lapiedra (Relatividad General y Cosmología), Toni Pich (Teoría Cuántica de Campos y Cromodinámica Cuántica), Javier García (Procesos Estocásticos en Fotónica), Pepe Bernabeu (Teoría Electrodébil), Vicent Giménez (Teoría Cuántica de Campos en el Retículo), así como a Armando Pérez y Arcadi Santamaria, a Pedro Fernández y Javier Urcheguía (ambos de la Universidad Politécnica de Valencia), y a Juan León (del Instituto de Física Fundamental del CSIC en Madrid), que, aunque no me dieron clase, contribuyeron a mis ganas de iniciar la carrera investigadora. Por razones obvias de espacio, me es imposible explicar los motivos concretos por los cuales cada uno de estos profesores puso su

granito de arena (o saco de arena en muchos casos) para convertirme en el investigador que soy hoy en día, pero estoy seguro de que la mayoría de ellos conocen perfectamente sus contribuciones particulares.

Por otro lado, uno siempre empieza la universidad con un poco de nerviosismo, sobre todo porque nunca sabe con qué tipo de gente se va a encontrar en clase (especialmente alguien como yo, que estudió todos los cursos anteriores en el mismo centro, con lo cual no hizo el cambio del “colegio” al “instituto”). Por suerte, gran parte de la culpa de que sienta que la carrera de Física me llenó tanto la tienen precisamente los compañeros con los que comencé a estudiarla: Rika, Ave, Bego, Diana, Javi (Alicante), Javi (Aragorn), Susana, Carlos, Raúl y Víctor, son a los que más cariño tengo, sobre todo porque son con los que más contacto sigo teniendo (aunque no me olvido de Juan, María Luisa y Ali!). Algo más tarde (hacia tercero), llegaron otros compañeros a los que también aprecio mucho: Alberto, David y Sergio; y algo más tarde aún, ya en la época del doctorado, conocí a Zahara e Isa, que me han ayudado de varias formas en la recta final del doctorado. Me alegro de que supiéramos ver que el camino correcto era el de compartir y ayudarnos los unos a los otros tanto como pudiéramos (algo que parece trivial, pero que no muchas clases hacen); no es casualidad que no sean pocos los profesores que afirman que hemos sido “el curso más gratificante que han dado”, gracias y enhorabuena compañeros!

2006 fue un año muy especial: es el año en el que terminé la carrera, a la vez que aprendía los fundamentos de la Biología Molecular y la Ingeniería Genética a través de mi participación en el proyecto iGEM. Aprender esas ramas de la Biología es algo que llevaba años queriendo hacer, pero que nunca pensé que podría realizar de verdad, y me gustaría agradecer en especial a Arnau, Emilio, Alberto, Cate, Chevi, Gus, Carlos, Cris, Diana, Minerva, Albert, Pedro, Javi y Jesús, por haber generado el ambiente científico y humano perfecto para desarrollar tal labor. Nunca olvidaré el año que pasamos juntos y las experiencias que vivimos (tanto nuestros primeros congresos científicos —en MIT ni más ni menos, eso sí fue “colarse” en el mundo de la investigación por la puerta grande—, como las carreras de sillas en el laboratorio); mi tiempo con vosotros es con lo que comparo cualquier otro momento de mi carrera investigadora cuando quiero saber si de verdad estoy siendo feliz en lo que hago, no se puede ir con más ilusión a un laboratorio de con la que iba en aquella época.

Quiero agradecer también a los miembros del grupo de Óptica Cuántica y No Lineal en el que trabajo, tanto a los presentes como a los pasados, por haberme hecho sentir en un ambiente inmejorable durante mi doctorado; me alegra poder llamar “amigos” a la mayoría de ellos. Muchas gracias en especial a Fernando Silva, que siempre me ayuda con todas sus fuerzas en cada mínima cosa que necesito; quiero que sepa que considero que, junto a Alberto y Fons (ver arriba), es la persona con menos maldad que conozco. Muchas gracias también por su inmejorable actitud a los compañeros con los que he colaborado en el grupo: Ferran Garcia (con quien comparto algunas ideas de esta tesis), Robert Höppner (pese a que no consiguiéramos hacer llegar a buen puerto nuestras ideas), Alejandro Romanelli (sin el cual no creo que hubiese hecho la parte numérica de la tesis nunca) y Joaquín Ruiz-Rivas (con quien acabo de comenzar, pero con quien ya he compartido unas cuantas alegrías!); me he encontrado muy a gusto trabajando con vosotros. No me olvido de Amparo Docavo, la persona que hace que las tareas administrativas que tan mal se me dan parezcan sencillas; gracias por tener siempre una sonrisa en la cara cuando hablamos. Isabel Pérez fue la estudiante de doctorado que allanó el camino hacia la Óptica Cuántica (la de verdad, no esa con el campo clásico, jiji) en el grupo, de forma que yo ya pude tomar el relevo con “el chip cambiado”; le agradezco que me haya tratado desde que estaba en la carrera como un amigo, y, en lo que a esta tesis se refiere, que se haya tomado la “molestia” de evaluarla (nadie mejor para hacerlo, por otro lado). Agradezco también a Víctor Sánchez por tantas conversaciones interesantes que hemos tenido sobre ciencia y lo que la rodea, y a Kestutis Staliunas por ayudarme siempre que lo he necesitado. Hago extensivos estos agradecimientos al resto de gente con la que he tenido el placer de coincidir de los grupos de Gandía (Víctor Espinosa, Javier Redondo, Rubén Picó, Paco Camarena, Joan Martínez,...) y Terrasa (Crina Cojocar, Ramón Herrero, Josep Font, Lina Maigyte,...). Por último, me gustaría dar las gracias y transmitir todo mi cariño a Ramón Corbalán y Ramón Vilaseca (Los Ramones!), cuya personalidad me inspira y tomo como modelo, por haber dejado a mi alrededor a tantos “hijos científicos de calidad” que también son algunas de las mejores personas que conozco.

Everyone who knows me knows that I’ve never been much of a traveller, especially when it is for touristic reasons; however, at a very early stage of my PhD I came to realize that travelling for scientific reasons (such as congresses or visits to research groups) is actually quite rewarding at many levels. I would have never grown to be the scientist that I am without the experiences that I’ve lived and the people that I’ve met during these “scientific travels”. In this sense, I would like to first thank Ignacio Cirac, Peter Drummond, Jeff Shapiro, and Nicolas Cerf for allowing me to become a “temporary member” of their research groups, and for treating me like a fellow researcher, giving me all the tools needed to become productive under their watch. As a PhD student it is easier to hear the not-so-nice stories about

the behaviour of top researchers than the nice ones, and meeting them has been one of the most inspiring experiences on this regard, as now I know that one can be at the very top of science without compromising his kindness and integrity.

On the other hand, if I have been any productive at all during my visits to foreign research centres, it is because I've been lucky enough to collaborate with some of the nicest people that I have ever met, and who of course I consider now my friends. I owe so much to Inés de Vega and Diego Porras, my very first collaborators (together with Ignacio) outside the shelter of my research group and my usual research area; thanks for treating me so well and have confidence in me. Fate decided that I should meet Raúl García-Patrón at the best possible time, and, by his hand, Nicolas Cerf. Both Raúl and Nicolas came as a blessing during my visit to MIT, inviting me to collaborate on a very interesting topic, and giving me all the chances to offer my opinions and ideas concerning it, even though they knew that I never worked on pure quantum information before. Finally on this list of collaborators are my dearest friends Giuseppe Patera and Chiara Molinelli; I am so glad that we are finally collaborating on something altogether, I am sure that many happy memories will be born from this collaboration!

Living in a new city and working in a new environment and topic can be a little bit overwhelming; however, if I didn't get any anxious in my three-months visits to Munich, Melbourne, and Boston it is in part because of the amazing people that I met there. I would like to thank many people for making me feel welcome and "part of something" during these visits. At the MPQ, my officemates (Heike Schwager, Philipp Hauke, and Christine Muschik), "the Spanish crowd" (apart from Diego and Inés, Mari Carmen Bañuls, Maria Eckholt, Miguel Aguado, Lucas Lamata, and Oriol Romero), Veronika Lechner (always a ray of sunshine in the cold Munich!), Gèza Giedke (pure kindness), Albert Schliesser (oh my god! an experimentalist on this list!), as well as David NÓvoa, Christina Krauss, Mikel Sanz, Sébastien Perseguers, Eric Kessler, Fernando Patawski, Matteo Rizzi, and Maarten van den Nest. In Melbourne I had the best housemate possible, Simon Gorman, an amazing musician (animateur!), father of the two sweetest/craziest little blondies in the world (Scarlett and Sapphire) and with the coolest sister (Rachel!); I also had the chance to meet some of the best musicians that I know, such as Chris Hale or Gian Slater (thanks to Esther for hooking me up with Chris!). The working environment at the ACQAO in Swinburne University was excellent thanks to Tim Vaughan, Margaret Reid, Qionyi He, Peter Hannaford, Xia-Ji Liu, Hui Hu, and the kind Tatiana Tchernova, who helped me with the administrative issues. I had the chance to start writing this dissertation while living halfway between Harvard and MIT, what was actually an incredibly inspiring experience, highly amplified by spending lots and lots of time with my dear friend David Adjashvili in the many restaurants that the area has to offer, and specially at "our office", the Atomic Bean Cafe, with the best waitress ever, Sam! I also thank Chelsea Martínez, my "orientation friend" María Ramírez, my officemate Niv Chandrasekaran, and the Quantum Girls (Veronika Stelmakh, Valentina Schettini, and Maria Tengner), for being such a wonderful people.

Una parte muy importante de mi vida durante los últimos 12 años ha sido la música. Al primero que debo mi agradecimiento en este sentido es a Pabl, mi "pareja musical", con quien he compartido todos y cada uno de los proyectos en los que he participado. Guardo además mucho cariño hacia la gente con la que Pabl y yo formamos nuestra primera banda, Desyrius, especialmente a Vero, Fran y José Ángel, así como a la gente de nuestra segunda banda, Fuego Fatuo (Hada, Empar y Vicent son lo que recuerdo más vívidamente), la cual nos permitió dar el salto hacia el proyecto totalmente instrumental y abierto a cualquier estilo musical en el que llevamos trabajando ya 7 años, Versus Five. Mis agradecimientos a los miembros originales de Vs5 (Borja, Diego y Dani), por poner tanta ilusión en un proyecto a priori tan "friki", y hacer con ello que empezara a funcionar. También a la gente que ha ido dejando su huella en este proyecto tan gratificante a nivel personal (Moli, Marcos, Luis y Raúl) y a los compañeros del resto de bandas de Valencia con las que hemos interactuado (Vahladian, "los Groovers", y Non Essential en especial). Y, sobre todo, muchas gracias a la gente que ha participado en la banda en los últimos tiempos: los Versus (Riki, Osvaldo, Xavi, Javi, Víctor y —por poco no llegas a esta lista de agradecimientos— David!), los "crew" (Apa, Alberto, Rika, Ferrándiz y Fons), los ingenieros (Jorge y Alberto), los diseñadores (Juanma e Isma) y las colaboraciones (Voro y David).

El final de mi doctorado ha sido (y en parte sigue siendo) un momento de relativa ansiedad, sobre todo por la incertidumbre acerca de lo que vendrá luego, y la perspectiva de un cambio obligatorio respecto a una situación en la que me siento muy cómodo y feliz. No obstante, hay un par de "tareas periódicas" que me han ayudado a llevar mejor esta situación: el frontón y las "cenas de los miércoles". Quiero agradecer a la gente con la que juego o he jugado a frontón estos últimos dos años (aproximadamente), especialmente a Alberto, Rafa, Antonio (mi compañero!), Joaquín, Juan, Pablo, Manu y los Joses; mucha de la ansiedad que siento se va en cada raquetazo y en cada conversación que mantenemos. Igualmente, agradezco a la gente de las cenas de los miércoles, en especial a Cyn, Paty, Carlos, Gonzalo, Belén, Sergio, Amparo y Ana; no sabéis cuánto me hacen olvidar la ansiedad de la que hablaba las risas que nos pegamos.

Finalmente, muchas gracias a Alfredo Luis (un sol!), Giuseppe Patera, Isabel Pérez, Alberto Aparici, y mis directores por haberse tomado el tiempo de corregir mi tesis, así como a Antonio Garrido, que ha puesto tanto esfuerzo en la edición (impresión y encuadernación) de esta tesis.

En definitiva, muchas gracias a todos los que habéis contribuido en mayor o menor medida a que llegue hasta el punto en el que me encuentro ahora; sé que me arriesgado mucho al confeccionar una lista tan específica, ya que, teniendo en cuenta el poco tiempo que he tenido para hacerla, la probabilidad de que haya olvidado a alguien es alta. Aún así, me gustaría que se entendiera este esfuerzo como una muestra real de mi gratitud, y si alguien siente que “le he olvidado”, tan sólo decirle que probablemente tenga razón y que no se lo tome a mal: lo he intentado!

Un abrazo a todos!

Carlos.

CONTENTS

<i>Agradecimientos</i> [<i>Acknowledgements</i>]	iii
1. <i>Introduction</i>	1
1.1 Squeezed states of light: Generation and applications	1
1.2 Overview of the thesis	1
1.2.1 The quantum optics behind squeezing, entanglement, and OPOs.	1
1.2.2 Original results: New phenomena in multi-mode OPOs.	4
2. <i>The quantum harmonic oscillator</i>	7
2.1 Classical analysis of the harmonic oscillator	7
2.2 Hilbert space of the harmonic oscillator and number states	8
2.3 Coherent states	10
2.3.1 Connection to classical mechanics	10
2.3.2 Properties of the coherent states	11
2.3.3 Phase space sketch of coherent states	13
2.4 Squeezed states	14
2.4.1 Definition and relevance	14
2.4.2 Minimum uncertainty squeezed states	15
2.5 Entangled states	16
2.5.1 The EPR argument and quantum non-locality	16
2.5.2 Entanglement and the two-mode squeezing operator	17
2.5.3 Enhancing entanglement by addition and subtraction of excitations	19
2.6 The harmonic oscillator in phase space	21
2.6.1 Phase space distributions	21
2.6.2 The positive P distribution	23
2.6.3 Fokker–Planck and stochastic Langevin equations	24
3. <i>Quantization of the electromagnetic field in an optical cavity</i>	27
3.1 Light as an electromagnetic wave	27
3.2 Quantization in free space: Plane waves and polarization	28
3.2.1 Quantization in terms of plane waves	28
3.2.2 Vector character of the fields and polarization	30
3.3 Paraxial optics and transverse modes	32
3.3.1 Optical beams and the paraxial approximation	32
3.3.2 Transverse modes	33
3.4 Quantization in an optical cavity	37
3.4.1 Geometrical optics: Propagation through optical elements and stable optical cavities	37
3.4.2 Considerations at a non-reflecting interface	39
3.4.3 Modes of an optical resonator	40
3.4.4 Quantization of the electromagnetic field inside a cavity	43
4. <i>Quantum theory of open cavities</i>	45
4.1 The open cavity model	45
4.2 Heisenberg picture approach: The quantum Langevin equation	46
4.3 Schrödinger picture approach: The master equation	47
4.4 Relation of the model parameters to physical parameters	49
4.5 Quantum-optical phenomena with optical lattices	50
4.5.1 The basic idea	51

4.5.2	Superradiant phenomenology	53
5.	<i>Detection of the output field</i>	59
5.1	The output field	59
5.2	Ideal detection: An intuitive picture of photo- and homodyne detection	60
5.3	Real photodetection: The photocurrent and its power spectrum	62
5.4	Real homodyne detection: Squeezing and the noise spectrum	65
6.	<i>Quantum description and basic properties of OPOs</i>	69
6.1	Dielectric media and nonlinear optics	69
6.1.1	Linear dielectrics and the refractive index	70
6.1.2	Second order nonlinear dielectrics and frequency conversion	71
6.2	Quantum model for a general OPO	74
6.3	Squeezing properties of the DOPO	78
6.3.1	The DOPO within the positive P representation	78
6.3.2	Classical analysis of the DOPO	80
6.3.3	Quantum analysis of the DOPO: linearization and noise spectrum	83
6.3.4	Effect of signal detuning	86
6.4	Entanglement properties of the OPO	88
6.4.1	The OPO within the positive P representation	88
6.4.2	Classical analysis of the OPO	89
6.4.3	The OPO below threshold: Signal–idler entanglement	90
6.4.4	The OPO above threshold: Twin beams	91
7.	<i>Basic phenomena in multi–mode OPOs</i>	95
7.1	Pump clamping as a resource for noncritically squeezed light	95
7.1.1	Introducing the phenomenon through the simplest model	95
7.1.2	Generalization to many down–conversion channels: The OPO output as a multi–mode non–classical field	98
7.2	Noncritically squeezed light via spontaneous symmetry breaking	98
7.2.1	The basic idea	98
7.2.2	The two–transverse–mode DOPO and spontaneous rotational symmetry breaking	99
8.	<i>Deep study of spontaneous symmetry breaking through the 2tmDOPO</i>	105
8.1	On canonical pairs and noise transfer	105
8.2	Homodyne detection with a fixed local oscillator	106
8.3	Beyond the considered approximations	109
8.3.1	Beyond the adiabatic elimination of the pump	109
8.3.2	Numerical simulation of the nonlinear equations	110
9.	<i>The 2tmDOPO with injected signal</i>	113
9.1	Model of the 2tmDOPO with injected signal	113
9.2	Classical steady states and their stability	114
9.2.1	The one–mode solution	114
9.2.2	The two–mode solution	116
9.2.3	Summary	118
9.3	Quantum properties of the non-injected mode	118
10.	<i>Type II OPO: Polarization symmetry breaking and frequency degeneracy</i>	121
10.1	Spontaneous polarization symmetry breaking	121
10.2	From nondegenerate to degenerate operation	122
11.	<i>DOPOs tuned to arbitrary transverse families</i>	127
11.1	The model	127
11.2	Classical emission	128
11.3	Quantum properties	130
11.4	Tuning squeezing through the pump shape	131

12. <i>Conclusions and outlook</i>	135
12.1 Summary of the original research on OPOs	135
12.2 Outlook	139
12.2.1 Temporal symmetry breaking	139
12.2.2 Self-phase-locked two-transverse-mode type II OPO	140
12.2.3 Effect of anisotropy	140
 Appendix	 143
A. <i>Quantum description of physical systems</i>	145
A.1 Classical mechanics	145
A.1.1 The Lagrangian formalism	145
A.1.2 The Hamiltonian formalism	146
A.1.3 Observables and their mathematical structure	146
A.2 The mathematical language of quantum mechanics: Hilbert spaces	148
A.2.1 Finite-dimensional Hilbert spaces	148
A.2.2 Linear operators in finite-dimensional Hilbert spaces	149
A.2.3 Generalization to infinite dimensions	151
A.2.4 Composite Hilbert spaces	153
A.3 The laws of quantum mechanics	153
A.3.1 A brief historical introduction	153
A.3.2 The axioms of quantum mechanics	154
 B. <i>Linear stochastic equations with additive noise</i>	 159
 C. <i>Linearization of the 2tmDOPO Langevin equations</i>	 161
 D. <i>Correlation functions of $\cos \theta(\tau)$ and $\sin \theta(\tau)$</i>	 163
 E. <i>Details about the numerical simulation of the 2tmDOPO equations</i>	 165
 Bibliography	 166

1. INTRODUCTION

I have divided this introductory chapter into two blocks. From the research point of view, this thesis is devoted to the study of multi-mode quantum phenomena in optical parametric oscillators (OPOs), which, as will become clear as one goes deeper into the dissertation, means the generation of squeezed states of light; in the first part of this introduction I review what these class of states are, and comment on the state of the art of their generation and applications. On the other hand, from a thematic perspective this thesis is quite unusual: Two-thirds of the dissertation are devoted to a self-contained text about the fundamentals of quantum optics as applied to the field of squeezing and entanglement, and specially to the modeling of OPOs, while only one-third of it is devoted to the original research that I have developed during my PhD student years; a detailed discussion about the organization of the thesis is then tackled in the second part of this introduction.

1.1 *Squeezed states of light: Generation and applications*

One of the most amazing predictions offered by the quantum theory of light is what has been called vacuum fluctuations: Even in the absence of photons (vacuum), the value of the fluctuations of some observables are different from zero. These fluctuations cannot be removed by improving the experimental instrumental, and hence, they are a source of non-technical noise (quantum noise), which seems to establish a limit for the precision of experiments involving light.

During the late 1970s and mid-1980s, ways for overcoming this fundamental limit were predicted and experimentally demonstrated [1]. In the case of the quadratures of light (equivalent to the position and momentum of a harmonic oscillator), the trick was to eliminate (squeeze) quantum noise from one quadrature at the expense of increasing the noise of its canonically conjugated one in order to preserve their Heisenberg uncertainty relation. States with this property are called squeezed states, and they can be generated by means of nonlinear optical processes. Even though the initial experiments were performed with materials having third order nonlinearities [2], nowadays the most widely used nonlinear materials are $\chi^{(2)}$ -crystals, whose induced polarization has a quadratic response to the applied light field [3]. Inside such crystals it takes place the process of parametric-down conversion, in which photons of frequency $2\omega_0$ are transformed into correlated pairs of photons at lower frequencies ω_1 and ω_2 such that $2\omega_0 = \omega_1 + \omega_2$; when working at frequency degeneracy $\omega_1 = \omega_2 = \omega_0$, the down-converted field can be shown to be in a squeezed state [1].

In order to increase the nonlinear interaction, it is customary to introduce the nonlinear material inside an optical cavity; when $\chi^{(2)}$ -crystals are used, such a device is called an optical parametric oscillator (OPO). To date, the best squeezing ever achieved is a 93% of noise reduction with respect to vacuum [4] (see also [5, 6]), and frequency degenerate optical parametric oscillators (DOPOs) are the systems holding this record.

Apart from fundamental reasons, improving the quality of squeezed light is an important task because of its applications. Among these, the most promising ones appear in the fields of quantum information with continuous variables [7, 8] (as mixing squeezed beams with beam splitters offers the possibility to generate multipartite entangled beams [9, 10]) and high-precision measurements (such as beam displacement and pointing measurements [11, 12] or gravitational wave detection [13, 14]).

In this thesis we offer new phenomena with which we hope to help increasing the capabilities of future optical parametric oscillators as sources of squeezed light.

1.2 *Overview of the thesis*

1.2.1 *The quantum optics behind squeezing, entanglement, and OPOs.*

As I have already commented, most of this dissertation is not dedicated to actual research, but to a self-contained introduction to the physics of squeezing, entanglement, and OPOs¹. Let me first expose the reasons why I made this decision.

¹ There are several books which talk about many of the questions that I introduce in this part of the dissertation, see for example [15, 16, 17, 18, 19, 20, 21, 22, 3, 23, 24, 25].

First of all, after four years interiorizing the mathematical language and physical phenomena of the quantum optics field, I've come to develop a certain personal point of view of it (note that "personal" does not necessarily mean "novel", at least not for every aspect of the field). I felt like this dissertation was my chance to proof myself up to what point I have truly made mine this field I will be supposed to be an expert in (after completion of my PhD); I believe that evaluation boards could actually evaluate the PhD candidate's expertise more truthfully with this kind of dissertation, rather than with one built just by gathering in a coherent, expanded way the articles published over his/her post-graduate years.

On the other hand, even though there is a lot of research devoted to OPOs and squeezing in general, it doesn't exist (to my knowledge) any book in which all the things needed to understand this topic are explained in a fully self-contained way, specially in the multi-mode regime in which the research of this thesis focuses. As a PhD student, I have tried to make myself a self-contained composition of the field, spending quite a long time going through all the books and articles devoted to it that I've become aware of. I wanted my thesis to reflect this huge part of my work, which I felt that could be helpful for researchers that would like to enter the exciting field of quantum optics.

Let me now make a summary of what the reader will find in this first two-thirds of the thesis (numbering of this list's items follows the actual numbering of the dissertation chapters, see the table of contents):

- A. The true starting point of the thesis is Appendix A. The goal of this chapter is the formulation of the axioms of quantum mechanics as I feel that are more suited to the formalism to be used in quantum optics.

In order to properly introduce these, I first review the very basics of classical mechanics making special emphasis on the Hamiltonian formalism and the mathematical structure that observable quantities have on it. I then summarize the theory of Hilbert spaces, putting special care in the properties of the infinite-dimensional ones, as these are the most relevant ones in quantum optics.

After a brief historical quote about how the quantum theory was built during the first third of the XX century, I introduce the axioms of quantum mechanics trying to motivate them as much as possible from three points of view: Mathematical consistency, capacity to incorporate experimental observations, and convergence to classical physics in the limits in which we know that it works.

I decided to relegate this part to an appendix, rather to the first chapter, because I felt that even though some readers might find my formulation and motivation of the axioms a little bit different than what they are used to, in essence all what I explain here is supposed to be of common undergraduate knowledge, and I preferred to start the thesis in some place new for any person coming from outside the field of quantum optics.

2. In the second chapter I introduce the quantum description of the one-dimensional harmonic oscillator (which I show later to be of fundamental interest for the quantum theory of light), and study different properties of it. In particular, I start by showing that its associated Hilbert space is infinite-dimensional, and that its energy is quantized. Furthermore, I explain that the energy of the oscillator is not zero in its quantum mechanical ground state (the vacuum state) owed to uncertainties on its quadratures, which are just dimensionless versions of its position and momentum.

I then introduce some special quantum mechanical states of the oscillator. First, coherent states as the states which allow us to make the correspondence between the quantum and classical descriptions, that is, the states whose associated experimental statistics lead to the observations expected for a classical harmonic oscillator; I discuss in depth how when the oscillator is in this state, its amplitude and phase are affected by the vacuum fluctuations.

I introduce then the main topic of the thesis: The squeezed states. To motivate their definition, I first explain how the phase and amplitude fluctuations can destroy the potential application of oscillators as sensors when the signals that we want to measure are tiny, and define squeezed states as states which have the uncertainty of its phase or amplitude below the level that these have in a coherent or vacuum state. I also show how to generate them via unitary evolution, that is, by making the oscillator evolve with a particular Hamiltonian.

Entangled states of two oscillators are introduced immediately after. In order to motivate them, I first show how their conception lead Einstein, Podolsky, and Rosen to believe that they had proved the inconsistency of quantum mechanics; their arguments felt so reasonable, that this apparent paradox was actually a puzzle for several decades. I then define rigorously the concept of entangled states, explaining that they can be understood as states in which the oscillators share correlations which go beyond what is classically allowed, what is accomplished by making use of the superposition principle, the main difference between the classical and quantum descriptions. I also show that these states can be generated via unitary evolution, and build a specially important class of such states: The two-mode squeezed vacuum states.

In this same section I will be able to introduce the first original result of the thesis [26, 27]: I show how by adding or subtracting excitations locally on the oscillators, the entanglement of these class of states can be enhanced; I

developed this part of the work at the Massachusetts Institute of Technology in collaboration with Raúl García-Patrón, Nicolas Cerf, Jeff H. Shapiro, and Seth Lloyd during a three-months visit to that institution in 2010. In the last part of this chapter I explain how one can make a quantum mechanical formulation of the harmonic oscillator relying solely on distributions in phase space. This appears to suggest that quantum mechanics enters the dynamics of classical systems just as additional noise blurring their trajectories in phase space; however, I quickly show that, even though this picture can be quite true for some quantum mechanical states, it is not the case in general, as this quantum mechanical phase space distributions do not correspond to probability density functions in the usual sense.

I pay particular attention to one of such distributions, the positive P distribution, as during the thesis I make extensive use of it. In the last section of the chapter I show how thanks to it one can reduce the dynamics of the oscillator to a finite set of first order differential equations with noise (stochastic Langevin equations), which in general are easier to deal with than the quantum mechanical evolution equations for the state of the oscillator (von Neumann equation) or its observables (Heisenberg equations).

3. The third chapter is devoted to the quantum theory of light. In the first section I review Maxwell's theory of electromagnetism, showing that in the absence of sources light satisfies a simple wave equation, and finally defining the concept of spatial modes of light as the independent solutions of this equation consistent with the physical boundary conditions of the particular system to be studied. Then I prove that the electromagnetic field in free space can be described as a mechanical system consisting of a collection of independent harmonic oscillators—one for each spatial mode of the system (which in this case are plane-waves)—, and then proceed to develop a quantum theory of light by treating quantum mechanically these oscillators. The concept of photons is then linked to the excitations of these electromagnetic oscillators.

The reminder of the chapter is devoted to the quantization of optical beams inside an optical cavity. In order to do this, I first find the spatial modes satisfying the boundary conditions imposed by the cavity mirrors (the so-called transverse modes), showing that, in general, modes with different transverse profiles resonate inside the cavity at different frequencies. In other words, the cavity acts as a filter, allowing only the presence of optical beams having particular transverse shapes and frequencies. In the last section I prove that, similarly to free space, optical beams confined inside the cavity can be described as a collection of independent harmonic oscillators, and quantize the theory accordingly.

4. Real cavities have not perfectly reflecting mirrors, not because they don't exist, but rather because we need to be able to inject light inside the resonator, as well as study or use in applications the light that comes out from it. In this fourth chapter I apply the theory of open quantum systems to the case of having one partially transmitting mirror.

The first step is to model the open cavity system, what I do by assuming that the intracavity mode interacts with a continuous set of external modes having frequencies around the cavity resonance. Then, I study how the external modes affect the evolution of the intracavity mode both in the Heisenberg and the Schrödinger pictures. In the Heisenberg picture it is proved that the formal integration of the external modes leads to a linear damping term in the equations for the intracavity mode, plus an additional driving term consisting in a combination of external operators, the so-called input operator; this equation is known as the quantum Langevin equation (for its similarity with stochastic Langevin equations, as the input operator can be seen as kind of a quantum noise), and is the optical version of the fluctuation-dissipation theorem.

In the Schrödinger picture, on the other hand, the procedure consists in finding the evolution equation for the reduced density operator of the intracavity mode. It is shown that the usual von Neumann equation acquires an additional term which cannot be written in a Hamiltonian manner, showing that the loss of intracavity photons through the partially transmitting mirror is not a reversible process. The resulting equation is known as the master equation of the intracavity mode. This is actually the approach which we have chosen to use for most of our research, as in our case it has several advantages over the Heisenberg approach, as shown all along the research part of this thesis.

The context of open quantum systems will give me the chance to introduce the work that I develop in collaboration with Inés de Vega, Diego Porras, and J. Ignacio Cirac [28], which started during a three-months visit to the Max-Planck Institute for Quantum Optics in 2008. I will show that it is possible to simulate quantum-optical phenomena (such as superradiance) with cold atoms trapped in optical lattices; what is interesting is that being highly tunable systems, it is possible to operate them in regimes where some interesting, but yet to be observed superradiant phenomena have been predicted to appear.

5. The next chapter is devoted to the measurement techniques that are used to analyze the light coming out from the cavity. To this aim, I first relate the output field with the intracavity field and the input field driving

the cavity, a relation that can be seen as the boundary conditions in the mirror. Together with the quantum Langevin equation, this is known in quantum optics as the input–output theory.

Then I use an idealized version of a photodetector to show how the techniques of photodetection and balanced homodyne detection are somehow equivalent, respectively, to a measurement of the photon number and the quadratures of the detected field.

After this intuitive and simplified version of these detection schemes, I pass to explain how real photodetectors work. The goal of the section is to analyze which quantity is exactly the one measured via homodyne detection in real experiments, arriving to the conclusion that it is the so-called noise spectrum (kind of a correlation spectrum of the quadratures).

I then redefine the concept of squeezing in an experimentally useful manner, which, although not in spirit, differs a little from the simplified version introduced in Chapter 2 for the harmonic oscillator. Even though I introduce this new definition of squeezing by reasoning from what is experimentally accessible, it is obvious from a theoretical point of view that the simple “uncertainty below vacuum or coherent state” definition cannot be it for the output field, as it does not consist on a simple harmonic oscillator mode, but on a continuous set of modes having different frequencies around the cavity resonance.

6. Chapter 6 is the last one of this self-contained introduction to OPOs, and its goal is to develop the quantum model of OPOs, and to show that they are sources of squeezed and entangled light.

OPOs being an optical cavity with a nonlinear crystal inside, the chapter starts by giving an overview of the linear and nonlinear properties of dielectric media within Maxwell’s theory of electromagnetism. It is shown in particular, how second-order nonlinearities of dielectrics give rise to the phenomenon of parametric down-conversion: When pumped with an optical beam of frequency $2\omega_0$, the polarization of the nonlinear material is able to generate a pair of beams at frequencies ω_1 and ω_2 such that $2\omega_0 = \omega_1 + \omega_2$. It is then shown that, at the quantum level, the process can be understood as the annihilation of one pump photon, and the simultaneous creation of the pair of down-converted photons (called signal and idler photons).

The case of an OPO in which the signal and idler photons are indistinguishable, that is, they have the same frequency, polarization, and transverse structure, is then analyzed. Such a system is known as the (single-mode) degenerate optical parametric oscillator (DOPO). It is shown that the classical theory predicts that the pump power must exceed some threshold level in order for the down-converted field to be generated; quantum theory, on the other hand, predicts that the down-converted field will have large levels of squeezing when operating the DOPO close to this threshold.

Similarly, it is shown that when signal and idler are distinguishable either on frequency or polarization (or both), these form an entangled pair when working close to threshold. On the other hand, for any pump power above threshold it is shown that the signal and idler beams have perfectly correlated intensities (photon numbers): They are what is called twin beams.

This chapter is also quite important because most of the mathematical techniques used to analyze the dynamics of any OPO configuration in the thesis are introduced here.

Even though my main intention has been to stress the physical meaning of the different topics that I have introduced, I have also tried to at least sketch all the mathematical derivations needed to go from one result to the next one. Hence, even though some points are quite concise and dense, I hope the reader will find this introductory part interesting as well as understandable.

1.2.2 Original results: New phenomena in multi-mode OPOs.

In the last third of the thesis I review most of the research that I have developed in my host group, the Nonlinear and Quantum Optics group at the Universitat de València. If I had to summarize the main contribution of these research in a couple of sentences, I would say something along the following lines: “Although one can try to favour only one down-conversion channel, OPOs are intrinsically multi-mode, and their properties can be understood in terms of three phenomena: Bifurcation squeezing, spontaneous symmetry breaking, and pump clamping. Favouring the multi-mode regime is indeed interesting because one can obtain several modes showing well marked non-classical features (such as squeezing and entanglement) at any pump level above threshold”.

Apart from my supervisors Eugenio Roldán and Germán J. de Valcárcel, some of the research has been developed in collaboration with Ferran V. García-Ferrer (another PhD student in the group), and Alejandro Romanelli (a visiting professor from the Universidad de la República, in Uruguay). An extensive, analytical summary of this part of the thesis can be found in Chapter 12; here, I just want to explain the organization of this original part of the dissertation without entering too much into the specifics of each chapter (as in the previous section, numbering follows that of the actual chapters):

7. In the first completely original chapter I introduce the concept of multi-mode OPOs as those which have many down-conversion channels for a given pumped mode. As I argue right at the beginning of the chapter, I believe that, one way or another, this is actually the way in which OPOs operate.
Then, I explain how both the classical and quantum properties of such systems (that is, of general OPOs) can be understood in terms of two fundamental phenomena: Pump clamping [29] and spontaneous symmetry breaking [30, 31, 32, 33]. This general conclusion is what I consider the most important contribution of my thesis.
The most interesting feature of these phenomena is that, contrary to the usual OPO model with a single down-conversion channel, where large levels of squeezing or entanglement are found only when working close to threshold, they allow multi-mode OPOs to generate highly squeezed or entangled light at any pump level (above threshold); we talk then about a noncritical phenomenon, as the system parameters don't need to be finely (critically) tuned in order to find the desired property.
- 8,9. Most of the research I have developed during my thesis has been devoted to study in depth the phenomenon of noncritical squeezing induced by spontaneous symmetry breaking [32, 33, 29, 34, 35, 36, 37]. In this chapters, and using the most simple DOPO configuration allowing for the phenomenon (which have called two-transverse-mode DOPO, or 2tmDOPO in short), I consider several features which are specially important in order to understand up to what point the phenomenon is experimentally observable, and offers a real advantage in front of the critical generation of squeezed light [33, 36].
10. In the previous chapters the phenomenon of spontaneous symmetry breaking is introduced in the spatial degrees of freedom of the light field (in particular, the guiding example is the spontaneous breaking of the system's invariance under rotations around the propagation axis). In the first part of this chapter the phenomenon is extended to the polarization degrees of freedom of light [35], by using an OPO in which the down-converted photons are distinguishable in polarization, but have the same frequency.
It is then explained how obtaining frequency degeneracy has been only achieved in experiments by introducing birefringent elements inside the cavity [38], which actually break the symmetry of the system, hence destroying the phenomenon of spontaneous symmetry breaking. Nevertheless, we argue that some residual noncritical squeezing should survive, and discuss that it has been indeed observed in a previous experiment [38].
The final part of the chapter is devoted to prove that frequency degeneracy can be also obtained by a different strategy consisting on the injection of an optical beam at the degenerate frequency inside the cavity [37].
11. In the last chapter I consider the system in which we originally predicted the phenomenon of pump clamping: A DOPO in which several transverse modes coexist at the down-converted frequency [29]. I show that using clever cavity designs, it is possible to get large levels of squeezing in many transverse modes at the same time, what could be interesting for quantum information protocols requiring multipartite entanglement (quantum correlations shared between more than two parties).

I would like to remind the reader that an extended summary of these part can be found on the concluding chapter. Let me now make a summary of the publications derived from my PhD research:

1. C. Navarrete-Benlloch, E. Roldán, and G. J. de Valcárcel
Non-critically squeezed light via spontaneous rotational symmetry breaking.
Physical Review Letters **100**, 203601 (2008).
2. C. Navarrete-Benlloch, G. J. de Valcárcel, and E. Roldán.
Generating highly squeezed Hybrid Laguerre-Gauss modes in large Fresnel number degenerate optical parametric oscillators.
Physical Review A **79**, 043820 (2009).
3. F. V. Garcia-Ferrer, C. Navarrete-Benlloch, G. J. de Valcárcel, and E. Roldán.
Squeezing via spontaneous rotational symmetry breaking in a four-wave mixing cavity.
IEEE Journal of Quantum Electronics **45**, 1404 (2009).
4. C. Navarrete-Benlloch, A. Romanelli, E. Roldán, and G. J. de Valcárcel.
Noncritical quadrature squeezing in two-transverse-mode optical parametric oscillators.
Physical Review A **81**, 043829 (2010).
5. F. V. Garcia-Ferrer, C. Navarrete-Benlloch, G. J. de Valcárcel, and E. Roldán.
Noncritical quadrature squeezing through spontaneous polarization symmetry breaking.
Optics Letters **35**, 2194 (2010).

6. C. Navarrete-Benlloch, I. de Vega, D. Porras, and J. I. Cirac.
Simulating quantum-optical phenomena with cold atoms in optical lattices.
New Journal of Physics **13**, 023024 (2011).
7. C. Navarrete-Benlloch, E. Roldán, and G. J. de Valcárcel.
Squeezing properties of a two-transverse-mode degenerate optical parametric oscillator with an injected signal.
Physical Review A **83**, 043812 (2011).

In addition to these published articles, the following ones are in preparation, close to being submitted:

8. C. Navarrete-Benlloch, R. García-Patrón, J. H. Shapiro, and N. Cerf.
Enhancing entanglement by photon addition and subtraction.
In preparation.
9. R. García-Patrón, C. Navarrete-Benlloch, S. Lloyd, J. H. Shapiro, and N. Cerf.
A new approach towards proving the minimum entropy conjecture for bosonic channels.
In preparation.
10. C. Navarrete-Benlloch, E. Roldán, and G. J. de Valcárcel.
Actively-phase-locked type II optical parametric oscillators: From non-degenerate to degenerate operation.
In preparation.
11. C. Navarrete-Benlloch and G. J. de Valcárcel.
Effect of anisotropy on the noncritical squeezing properties of two-transverse-mode optical parametric oscillators.
In preparation.

2. THE QUANTUM HARMONIC OSCILLATOR

The harmonic oscillator is one of the basic models in physics; it describes the dynamics of systems close to their equilibrium state, and hence has a wide range of applications. It is also of special interest for the purposes of this thesis, as we will see in the next chapter that the electromagnetic field can be modeled as a collection of one-dimensional harmonic oscillators.

This section is then devoted to the study of this simple system. We first explain how the one-dimensional harmonic oscillator is described in a classical context by a trajectory in phase space. The first step in the quantum description will be finding the Hilbert space by which it is described. We then show how coherent states reconcile the quantum and classical descriptions, and allow us to understand the amplitude-phase properties of the quantum oscillator. Squeezed and entangled states are then introduced; understanding the properties of these states is of major relevance for this thesis. In the context of entangled states we will have the chance to introduce the work developed by the author of the thesis during a three-months visit to the Massachusetts Institute of Technology in 2010, and where it is shown how entanglement can be enhanced by adding or subtracting excitations locally to the oscillators. We finally explain how to build rigorous phase space representations of quantum states, with special emphasis in the properties of the positive P representation, as we will make extensive use of it in this thesis.

We would like to stress that a summary of classical mechanics, Hilbert spaces, and the axioms of quantum mechanics (as well as definitions of the usual objects like the Hamiltonian, uncertainties, etc...) is exposed in Appendix A.

2.1 Classical analysis of the harmonic oscillator

Consider the basic mechanical model of a *one-dimensional harmonic oscillator*: A particle of mass m is at some equilibrium position which we take as $x = 0$; we displace it from this position by some amount a , and then a restoring force $F = -kx$ starts acting trying to bring the particle back to $x = 0$. Newton's equation of motion for the particle is therefore $m\ddot{x} = -kx$, which together with the initial conditions $x(0) = a$ and $\dot{x}(0) = v$ gives the solution $x(t) = a \cos \omega t + (v/\omega) \sin \omega t$, being $\omega = \sqrt{k/m}$ the so-called *angular frequency*. Therefore the particle will be bouncing back and forth between positions $-\sqrt{a^2 + v^2/\omega^2}$ and $\sqrt{a^2 + v^2/\omega^2}$ with periodicity $2\pi/\omega$ (hence the name 'harmonic oscillator').

Let us study now the problem from a Hamiltonian point of view. For this one-dimensional problem with no constraints, we can take the position of the particle and its momentum as the generalized coordinate and momentum, that is, $q = x$ and $p = m\dot{x}$. The restoring force derives from a potential $V(x) = kx^2/2$, and hence the Hamiltonian takes the form

$$H = \frac{p^2}{2m} + \frac{m\omega^2}{2}q^2. \quad (2.1)$$

The canonical equations read

$$\dot{q} = \frac{p}{m} \quad \text{and} \quad \dot{p} = -m\omega^2q, \quad (2.2)$$

which together with the initial conditions $q(0) = a$ and $p(0) = mv$ give the trajectory

$$\left(q, \frac{p}{m\omega}\right) = \left(a \cos \omega t + \frac{v}{\omega} \sin \omega t, \frac{v}{\omega} \cos \omega t - a \sin \omega t\right), \quad (2.3)$$

where we normalize the momentum to $m\omega$ for simplicity. Starting at the phase space point $(a, v/\omega)$ the system evolves drawing a circumference of radius $R = \sqrt{a^2 + v^2/\omega^2}$ as shown in Figure 2.1, returning to its initial point at times $t_k = 2\pi k/\omega$, with $k \in \mathbb{N}$. This circular trajectory could have been derived without even solving the equations of motion, as the conservation of the Hamiltonian $H(t) = H(0)$ leads directly to $q^2 + p^2/m^2\omega^2 = R^2$, which is exactly the circumference of Figure 2.1. This is a simple example of the power of the Hamiltonian formalism.

There is another useful description of the harmonic oscillator, the so called *amplitude-phase* or *complex* representation. The amplitude and phase refer to the polar coordinates in phase space, say $\mu = \sqrt{q^2 + p^2/m^2\omega^2}$ and $\varphi = \arctan(p/m\omega q)$, as shown in Figure 2.1. In terms of these variables, the trajectory reads simply $(\mu, \varphi) = (R, \varphi_0 - \omega t)$, with $\varphi_0 = \arctan(v/\omega a)$, so that the evolution is completely described by a linear time variation of the oscillator's

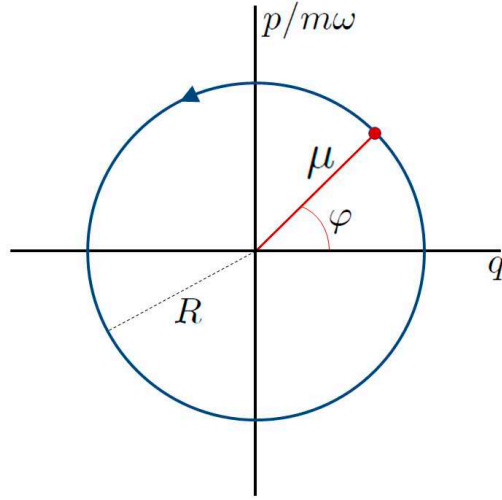


Fig. 2.1: Phase space trajectory of the classical harmonic oscillator.

phase. From these variables we can define the complex variable $\nu = \mu \exp(i\varphi) = q + (i/m\omega)p$, in terms of which the trajectory reads $\nu(t) = R \exp[i(\varphi_0 - \omega t)]$, and the Hamiltonian can be written as

$$H = \frac{m\omega^2}{2} \nu^* \nu. \quad (2.4)$$

The pair $\{\nu, \nu^*\}$ is known as the *normal variables* of the oscillator.

2.2 Hilbert space of the harmonic oscillator and number states

The easiest way to understand the structure of the Hilbert space associated to the one-dimensional harmonic oscillator is by finding the eigensystem of its associated Hamiltonian operator. According to the axioms of quantum mechanics which we review in Appendix A, the operator corresponding to its classical Hamiltonian (2.1) is

$$\hat{H} = \frac{\hat{p}^2}{2m} + \frac{m\omega^2}{2} \hat{q}^2, \quad (2.5)$$

where \hat{q} and \hat{p} are the self-adjoint operators associated to the position and momentum of the oscillator. At a first sight, this Hamiltonian may seem difficult to diagonalize because it is a combination of two non-commuting observables, as according to Axiom III we have $[\hat{q}, \hat{p}] = i\hbar$, see (A.28). However, we can write it in an easier-looking way as follows. Let us first define dimensionless versions of the position and momentum operators as

$$\hat{X} = \sqrt{\frac{2\omega m}{\hbar}} \hat{q} \quad \text{and} \quad \hat{Y} = \sqrt{\frac{2}{\hbar\omega m}} \hat{p}, \quad (2.6)$$

whose corresponding observables we will call the *X* and *Y quadratures* in the following, which satisfy the commutation relation $[\hat{X}, \hat{Y}] = 2i$. The Hamiltonian can be rewritten then as

$$\hat{H} = \frac{\hbar\omega}{4} (\hat{X}^2 + \hat{Y}^2). \quad (2.7)$$

Next, we decompose these quadratures as¹

$$\hat{X} = \hat{a}^\dagger + \hat{a} \quad \text{and} \quad \hat{Y} = i(\hat{a}^\dagger - \hat{a}), \quad (2.8)$$

where the operator \hat{a} and its adjoint \hat{a}^\dagger are called the *annihilation* and *creation* operators, respectively, and satisfy the commutation relations $[\hat{a}, \hat{a}^\dagger] = 1$, which we will denote by *canonical commutation relations* in the following; these

¹ Note that this kind of decompositions are always allowed for any self-adjoint operator; they are equivalent to write a real number as the addition of a complex number and its complex conjugate.

operators can be seen as the quantum counterparts of the normal variables of the classical oscillator. In terms of these operators the Hamiltonian takes the form²

$$\hat{H} = \hbar\omega \left(\hat{a}^\dagger \hat{a} + \frac{1}{2} \right), \quad (2.11)$$

and hence the problem is simplified to finding the eigensystem of the self-adjoint operator $\hat{n} = \hat{a}^\dagger \hat{a}$, which we will call the *number operator*.

Let us call n to a generic real number contained in the spectrum of \hat{n} , whose corresponding eigenvector we denote by $|n\rangle$, so that, $\hat{n}|n\rangle = n|n\rangle$. We normalize the vectors to one by definition, that is, $\langle n|n\rangle = 1 \forall n$. The eigensystem of \hat{n} is readily found from the following two properties:

- \hat{n} is a positive operator, as for any vector $|\psi\rangle$ it is satisfied $\langle \psi|\hat{n}|\psi\rangle = (\hat{a}|\psi\rangle, \hat{a}|\psi\rangle) \geq 0$. When applied to its eigenvectors, this property forbids the existence of negative eigenvalues, that is $n \geq 0$.
- Using the commutation relation³ $[\hat{n}, \hat{a}] = -\hat{a}$, it is trivial to show that the vector $\hat{a}|n\rangle$ is also an eigenvector of \hat{n} with eigenvalue $n - 1$. Similarly, from the commutation relation $[\hat{n}, \hat{a}^\dagger] = \hat{a}^\dagger$ it is found that the vector $\hat{a}^\dagger|n\rangle$ is an eigenvector of \hat{n} with eigenvalue $n + 1$.

These two properties imply that the spectrum of \hat{n} is the set of natural numbers $n \in \{0, 1, 2, \dots\} \equiv \mathbb{N}$, and that the eigenvector $|0\rangle$ corresponding to $n = 0$ must satisfy $\hat{a}|0\rangle = 0$; otherwise it would be possible to find negative eigenvalues, hence contradicting the positivity of \hat{n} . Thus, the set of eigenvectors $\{|n\rangle\}_{n \in \mathbb{N}}$ is an infinite, countable set. Moreover, using the property $\hat{a}|0\rangle = 0$ and the commutation relations, it is easy to prove that the eigenvectors corresponding to different eigenvalues are orthogonal, that is, $\langle n|m\rangle = \delta_{nm}$. Finally, according to the axioms of quantum mechanics only the vectors normalized to one are physically relevant. Hence, we conclude that the space generated by the eigenvectors of \hat{n} is isomorphic to $l^2(\infty)$, and hence it is an infinite-dimensional Hilbert space (see Section A.2.3).

Summarizing, we have been able to prove that the Hilbert space associated to the one-dimensional harmonic oscillator is infinite-dimensional. In the process, we have explicitly built an orthonormal basis of this space by using the eigenvectors $\{|n\rangle\}_{n \in \mathbb{N}}$ of the number operator \hat{n} , with the annihilation and creation operators $\{\hat{a}, \hat{a}^\dagger\}$ allowing us to move through this set as

$$\hat{a}|n\rangle = \sqrt{n}|n-1\rangle \quad \text{and} \quad \hat{a}^\dagger|n\rangle = \sqrt{n+1}|n+1\rangle, \quad (2.12)$$

the factors in the square roots being easily found from normalization requirements.

Let us now explain some physical consequences of this. The vectors $\{|n\rangle\}_{n \in \mathbb{N}}$ are eigenvectors of the energy (the Hamiltonian) with eigenvalues $\{E_n = \hbar\omega(n + 1/2)\}_{n \in \mathbb{N}}$, and hence quantum theory predicts that the energy of the oscillator is quantized: Only a discrete set of energies separated by $\hbar\omega$ can be measured in an experiment. The number of *quanta* or *excitations* is given by n , and that's why \hat{n} is called the “number” operator, it ‘counts’ the number of excitations. Similarly, the creation and annihilation operators receive their names because they add and subtract excitations. As these vectors have a well defined number of excitations, $\Delta n = 0$, we will call them *number states*. Consequently, $|0\rangle$ will be called the *vacuum state* of the oscillator, as it has no quanta.

On the other hand, while in classical mechanics the harmonic oscillator can have zero energy —what happens when it is in its equilibrium state—, quantum mechanics predicts that the minimum energy that the oscillator can have is $E_0 = \hbar\omega/2 > 0$. One way to understand where this *zero-point* energy comes from is by minimizing the expectation value of the Hamiltonian, which can be written as

$$\langle \hat{H} \rangle = \frac{\hbar\omega}{4} (\Delta X^2 + \Delta Y^2 + \langle X \rangle^2 + \langle Y \rangle^2), \quad (2.13)$$

subject to the constraint $\Delta X \Delta Y \geq 1$ imposed by the uncertainty principle. It is easy to argue that the minimum value of $\langle \hat{H} \rangle$ is obtained for the state satisfying $\Delta X = \Delta Y = 1$ and $\langle X \rangle = \langle Y \rangle = 0$, which corresponds, not surprisingly,

² Note that this Hamiltonian could have been obtained by following another quantization procedure based on the normal variables of the oscillator. In particular, we could symmetrize the classic Hamiltonian (2.4) respect to the normal variables, writing it then as

$$H = \frac{m\omega^2}{4} (\nu^* \nu + \nu \nu^*), \quad (2.9)$$

to then make the classical-to-quantum correspondences

$$\nu \rightarrow \sqrt{2\hbar/m\omega} \hat{a} \quad \text{and} \quad \nu^* \rightarrow \sqrt{2\hbar/m\omega} \hat{a}^\dagger, \quad (2.10)$$

replacing the Axiom III introduced in Section A.3.2 by $[\hat{a}, \hat{a}^\dagger] = 1$, $[\hat{a}, \hat{a}] = [\hat{a}^\dagger, \hat{a}^\dagger] = 0$. This quantization procedure offers an alternative to the procedure based on the generalized coordinates and momenta of a mechanical system.

³ This is straightforward to find by using the property $[\hat{A}\hat{B}, \hat{C}] = \hat{A}[\hat{B}, \hat{C}] + [\hat{A}, \hat{C}]\hat{B}$, valid for any three operators \hat{A} , \hat{B} , and \hat{C} .

to the vacuum state $|0\rangle$. Hence, the energy present in the ground state of the oscillator comes from the fact that the uncertainty principle does not allow its position and momentum to be exactly zero, they have some fluctuations even in the vacuum state, and this *vacuum fluctuations* contribute to the energy of the oscillator.

2.3 Coherent states

2.3.1 Connection to classical mechanics

Based on the previous sections, we see that the classical and quantum formalisms seem completely different in essence: While classically the oscillator can have any positive value of the energy and has a definite trajectory in phase space, quantum mechanics allows only for discrete values of the energy and introduces position and momentum uncertainties which prevent the existence of well defined trajectories. In this section we show that, despite their differences, both descriptions are compatible in some limit.

Let us first note that, instead of its position and momentum, from now on we take the X and Y quadratures of the oscillator as the observables defining the phase space. Using these variables, the classical phase space trajectory of the oscillator reads $(X, Y) = (X_0 \cos \omega t + Y_0 \sin \omega t, Y_0 \cos \omega t - X_0 \sin \omega t)$, which defines a circumference of radius $R = \sqrt{X_0^2 + Y_0^2}$, being $X_0 = X(0)$ and $Y_0 = Y(0)$.

Quantum mechanics is all about predicting the statistics of experiments, see Section A.3.2. Hence, a way of connecting it to classical mechanics is by finding the quantum state which predicts that the statistics obtained in the experiment will coincide with what is classically expected. The following two points explain the properties that such a state should have in the case of the harmonic oscillator:

- Classically, the energy is a continuous observable. On the hand, the ratio between the energies of two consecutive number states is $E_{n+1}/E_n = (n + 3/2)/(n + 1/2)$; hence, as the number of excitations increases, the discrete character of the energy becomes barely perceptible, that is, $E_{n+1}/E_n \sim 1$ if $n \gg 1$. Thus, the state should have a large number of excitations, that is, $\langle \hat{n} \rangle \gg 1$.
- The expectation value of the quadratures must describe the classical circular trajectory, while the uncertainties of both quadratures should be well below the radius of the circumference defined by it, that is, $(\langle \hat{X}(t) \rangle, \langle \hat{Y}(t) \rangle) = (X_0 \cos \omega t + Y_0 \sin \omega t, Y_0 \cos \omega t - X_0 \sin \omega t)$ with $\{\Delta X, \Delta Y\} \ll R$. Hence, at all effects the experimental outcomes predicted by quantum theory for the quadratures will coincide with those expected from classical mechanics. Note that the condition for the uncertainties requires $R \gg 1$, as we know that $\Delta X = \Delta Y = 1$ is the minimum simultaneous value that the variances can take.

Then, if states satisfying this properties exist, we see that it is indeed possible to reconcile quantum theory with classical mechanics at least on what concerns to physical observations.

Our starting point for obtaining these states are the Heisenberg evolution equations for the quadrature operators \hat{X} and \hat{Y} , which read

$$\frac{d}{dt} \hat{X} = \frac{1}{i\hbar} [\hat{X}, \hat{H}] = \omega \hat{Y}, \quad (2.14a)$$

$$\frac{d}{dt} \hat{Y} = \frac{1}{i\hbar} [\hat{Y}, \hat{H}] = -\omega \hat{X}, \quad (2.14b)$$

from which we obtain

$$\hat{X}(t) = \hat{X}(0) \cos \omega t + \hat{Y}(0) \sin \omega t, \quad (2.15a)$$

$$\hat{Y}(t) = \hat{Y}(0) \cos \omega t - \hat{X}(0) \sin \omega t. \quad (2.15b)$$

Hence, the expectation values of the quadratures describe the classical trajectories by construction, so that in order to reproduce a classical trajectory with initial quadratures (X_0, Y_0) , the state must satisfy $\langle \hat{X}(0) \rangle = X_0$ and $\langle \hat{Y}(0) \rangle = Y_0$. Writing now the quadratures in terms of the annihilation and creation operators (2.8) these last relations can be recasted as $\langle \hat{a} \rangle = (X_0 + iY_0)/2$; being (X_0, Y_0) arbitrary, this condition shows that the states we are looking for are the eigenvectors of the annihilation operator, that is, the states $|\alpha\rangle$ satisfying $\hat{a}|\alpha\rangle = \alpha|\alpha\rangle$ with $\alpha = (X_0 + iY_0)/2 \in \mathbb{C}$. We will call *coherent states* to the eigenvectors of the annihilation operator.

It is straightforward to show that, in addition, coherent states have $\langle \hat{n} \rangle = |\alpha|^2$, $R = 2|\alpha|$ and $\Delta X = \Delta Y = 1$, so that in the limit $|\alpha| \gg 1$ they satisfy all the requisites that we needed to make the connection with classical mechanics. Note that these properties hold at any time.

In the following we show that the eigenvectors of the annihilation operator exist by finding an explicit representation of them in the Hilbert space of the oscillator, and discuss some of their properties.

2.3.2 Properties of the coherent states

It is simple to find an explicit representation of the coherent states in terms of the basis of number states, that is, to find the coefficients c_n of the expansion $|\alpha\rangle = \sum_{n=0}^{\infty} c_n |n\rangle$. Introducing this expansion in the eigenvector equation⁴ $\hat{a}|\alpha\rangle = \alpha|\alpha\rangle$, we find the simple recurrence

$$c_n = \frac{\alpha}{\sqrt{n}} c_{n-1} \implies c_n = \frac{\alpha^n}{\sqrt{n!}} c_0. \quad (2.16)$$

On the other hand, the determination of c_0 comes from the normalization condition

$$\langle\alpha|\alpha\rangle = 1 = |c_0|^2 \sum_{n=0}^{\infty} |\alpha|^{2n}/n! \implies c_0 = \exp\left(-\frac{|\alpha|^2}{2}\right), \quad (2.17)$$

where we have chosen c_0 to be a positive real as the global phase of the state cannot play any physical role⁵. Hence, the coherent states are finally written as

$$|\alpha\rangle = \sum_{n=0}^{\infty} e^{-|\alpha|^2/2} \frac{\alpha^n}{\sqrt{n!}} |n\rangle. \quad (2.18)$$

Note that for $\alpha = 0$, coherent states are equivalent to the vacuum state, that is, $|\alpha = 0\rangle = |n = 0\rangle$. For any other value of α coherent states do not have a well defined number of excitations; instead, the number of *quanta* is distributed according to a Poissonian probability distribution

$$P_n(\alpha) = |\langle n|\alpha\rangle|^2 = e^{-|\alpha|^2} \frac{|\alpha|^{2n}}{n!}. \quad (2.19)$$

Let us now define the *displacement operator*

$$\hat{D}(\alpha) = \exp(\alpha\hat{a}^\dagger - \alpha^*\hat{a}); \quad (2.20)$$

the general formula $\exp(\hat{A} + \hat{B}) = \exp(-[\hat{A}, \hat{B}]/2) \exp(\hat{A}) \exp(\hat{B})$, valid for operators \hat{A} and \hat{B} which commute with their commutator, allows us to write it also as

$$\hat{D}^{(n)}(\alpha) = \exp(-|\alpha|^2/2) \exp(\alpha\hat{a}^\dagger) \exp(-\alpha^*\hat{a}), \quad (2.21)$$

or

$$\hat{D}^{(a)}(\alpha) = \exp(|\alpha|^2/2) \exp(-\alpha^*\hat{a}) \exp(\alpha\hat{a}^\dagger), \quad (2.22)$$

which we will refer to as its *normal* and *antinormal forms*, respectively⁶. Coherent states can then be obtained by *displacing* vacuum

$$|\alpha\rangle = \hat{D}(\alpha) |0\rangle, \quad (2.23)$$

what is trivially proved using the normal form of the displacement operator. This is interesting because the displacement operator is unitary by construction, that is, $\hat{D}^\dagger(\alpha) \hat{D}(\alpha) = \hat{D}(\alpha) \hat{D}^\dagger(\alpha) = \hat{I}$, and hence the coherent state $|\alpha\rangle$ can be created from a vacuum-state oscillator by making it evolve with a Hamiltonian $\hat{H}_D = i\hbar(\alpha\hat{a}^\dagger - \alpha^*\hat{a})/T$ during a time T . This is in contrast to the number states, which cannot be generated by unitary evolution of the oscillator in any way.

Note that when a displacement is applied to the annihilation and creation operators, we get⁷

$$\hat{D}^\dagger(\alpha) \hat{a} \hat{D}(\alpha) = \hat{a} + \alpha \quad \text{and} \quad \hat{D}^\dagger(\alpha) \hat{a}^\dagger \hat{D}(\alpha) = \hat{a}^\dagger + \alpha^*, \quad (2.25)$$

⁴ On a second thought, the existence of states satisfying this equation is kind of amazing: Consider for example a coherent state with $|\alpha|^2 \ll 1$, so that we are sure that the mean number of excitations is really below one; this equation states that we can still annihilate as many excitations as we want without altering the state!

⁵ This is evident since we have formulated quantum mechanics in terms of the density operator, which for all pure states $e^{i\phi}|\psi\rangle$ reads $\hat{\rho} = |\psi\rangle\langle\psi|$ irrespective of ϕ (see Section A.3.2).

⁶ With full generality, given an operator $\hat{A}(\hat{a}, \hat{a}^\dagger)$, we denote by $\hat{A}^{(n)}(\hat{a}, \hat{a}^\dagger)$ and $\hat{A}^{(a)}(\hat{a}, \hat{a}^\dagger)$ its *normal* and *antinormal forms*. $\hat{A}^{(n)}$ and $\hat{A}^{(a)}$ are obtained by writing $\hat{A}(\hat{a}, \hat{a}^\dagger)$ with all the creation operators to the left or to the right, respectively, with the help of the commutation relations. Hence, for example, the operator $\hat{A} = \hat{a}\hat{a}^\dagger\hat{a}$ has $\hat{A}^{(n)} = \hat{a}^\dagger\hat{a}^2 + \hat{a}$ and $\hat{A}^{(a)} = \hat{a}^2\hat{a}^\dagger - \hat{a}$ as normal and antinormal forms.

⁷ This is trivially proved by using the Baker–Campbell–Haussdorf lemma

$$e^{\hat{B}} \hat{A} e^{-\hat{B}} = \sum_{n=0}^{\infty} \frac{1}{n!} \underbrace{[\hat{B}, [\hat{B}, \dots [\hat{B}, \hat{A}] \dots]]}_n, \quad (2.24)$$

valid for two general operators \hat{A} and \hat{B} .

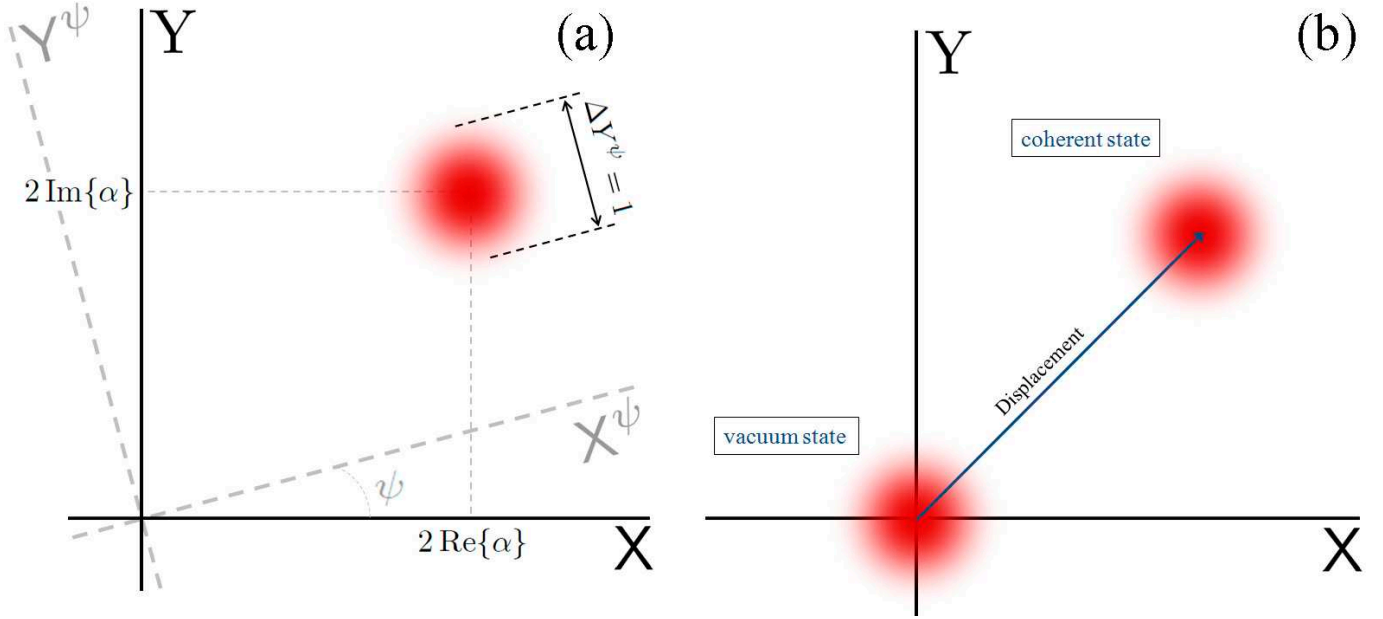


Fig. 2.2: (a) Phase space sketch of a coherent state. (b) A coherent state of arbitrary amplitude can be generated by applying a displacement to the vacuum state.

which shows where the name ‘displacement’ comes from. Hence, applied to the quadratures we get

$$\hat{D}^\dagger(\alpha) \hat{X} \hat{D}(\alpha) = \hat{X} + x \quad \text{and} \quad \hat{D}^\dagger(\alpha) \hat{Y} \hat{D}(\alpha) = \hat{Y} + y, \quad (2.26)$$

with $x + iy = 2\alpha$ and $\{x, y\} \in \mathbb{R}$. This transformation changes the mean of the quadratures but not its variance. Hence, a coherent state has the same uncertainty properties as the vacuum state.

Note finally that coherent states cannot form a true basis of the Hilbert space because they do not form a countable set. They cannot form a generalized continuous basis either (see Section A.2.3) because we have proved that they can be normalized in the usual sense, and hence, they are vectors defined inside the Hilbert space. Moreover, the inner product of two different coherent states $|\alpha\rangle$ and $|\beta\rangle$ reads

$$\langle \alpha | \beta \rangle = \exp\left(-\frac{|\alpha|^2}{2} + \alpha^* \beta - \frac{|\beta|^2}{2}\right), \quad (2.27)$$

and hence coherent states are not orthogonal. Despite all these, they do form a resolution of the identity, as it is easy to prove that

$$\int_{\mathbb{C}} d^2\alpha \frac{|\alpha\rangle\langle\alpha|}{\pi} = \sum_{n=0}^{\infty} |n\rangle\langle n| = \hat{I}, \quad (2.28)$$

where the integral covers the entire complex- α space. Hence, even though coherent states do not form a basis, they can still be used to represent any vector or operator: They form an *overcomplete basis*. Indeed, this overcompleteness can even be an advantage in some circumstances; for example, it is easy to show that any operator \hat{L} is completely determined from just its diagonal elements $\langle \alpha | \hat{L} | \alpha \rangle$ in the coherent basis, as

$$\begin{aligned} \langle \alpha | \hat{L} | \alpha \rangle &= \sum_{n,m=0}^{\infty} e^{-|\alpha|^2/2} \frac{\alpha^{*m} \alpha^n}{\sqrt{n!m!}} L_{mn} \\ &\Downarrow \\ L_{mn} &= \frac{1}{\sqrt{n!m!}} \left. \frac{\partial^{m+n}}{\partial \alpha^{*m} \partial \alpha^n} \langle \alpha | \hat{L} | \alpha \rangle e^{|\alpha|^2/2} \right|_{\alpha, \alpha^*=0}. \end{aligned} \quad (2.29)$$

We will use these *coherent representations* quite a lot during this thesis. We will come back to them in the last section of this chapter.

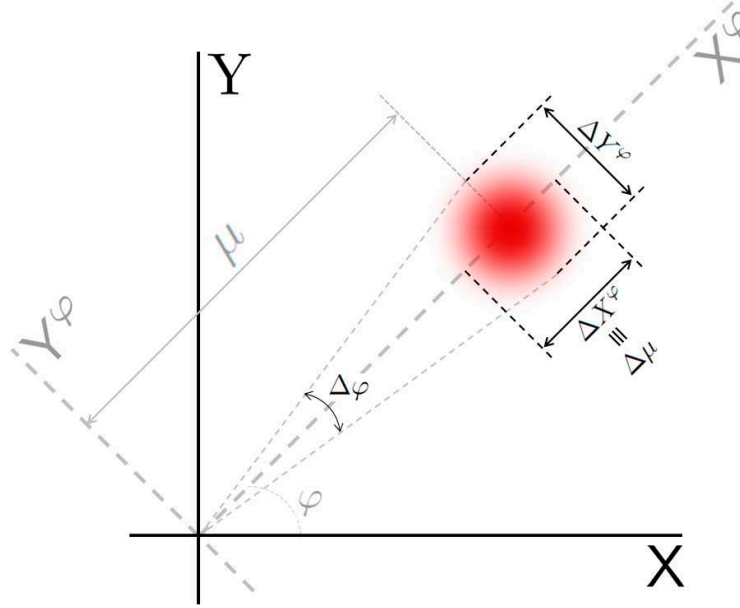


Fig. 2.3: Quantum amplitude–phase properties of a coherent state. $\Delta\mu$ and $\Delta\varphi$ represent the uncertainties in the amplitude and phase of the oscillator, which are obviously related to the uncertainties of the amplitude and phase quadratures, \hat{X}^ψ and \hat{Y}^ψ , respectively.

2.3.3 Phase space sketch of coherent states

Even though in quantum mechanics systems do not have a defined trajectory on phase space, it is useful to have some pictorial representation of their quantum states. The rigorous way of building such representations is discussed at the end of this chapter; here we just want to motivate this representation and build it for coherent states from an intuitive point of view. Among other things, this representation will allow us to understand the importance of squeezed states, which are described in the next section and are actually the basic theme of this thesis. It will also help us to understand the amplitude and phase properties of the quantum harmonic oscillator, two observables which still lack of a satisfactory description in terms of self-adjoint operators [23, 20].

Let us first build a *general quadrature* defined along an arbitrary direction ψ of phase space as

$$\hat{X}^\psi = \hat{X} \cos \psi + \hat{Y} \sin \psi = e^{-i\psi} \hat{a} + e^{i\psi} \hat{a}^\dagger. \quad (2.30)$$

We will denote the quadrature defined along its orthogonal direction by $\hat{Y}^\psi = \hat{X}^{\psi+\pi/2}$. These orthogonal quadratures define a new coordinate system in phase space rotated by an angle ψ respect to the original X–Y system (see Figure 2.2). They also satisfy the commutation relation $[\hat{X}^\psi, \hat{Y}^\psi] = 2i$, and hence must satisfy the uncertainty relation $\Delta X^\psi \Delta Y^\psi \geq 1$.

Coherent states $|\alpha\rangle$ admit a simple, descriptive representation in phase space (Figure 2.2). The idea for this sketch is to represent the statistics that would be obtained if a general quadrature is measured⁸. In the classical limit, a reasonable representation is then simply a point $(\langle \hat{X} \rangle, \langle \hat{Y} \rangle) = (2 \operatorname{Re}\{\alpha\}, 2 \operatorname{Im}\{\alpha\})$ in phase space. As quantum mechanics starts showing, uncertainties start playing a role. It is easy to see that the uncertainty of any quadrature \hat{X}^ψ in a coherent state is $\Delta X^\psi = 1$, irrespective of ψ , so that the statistics of a measurement of the quadratures will be spread around the mean equally in any direction of phase space. Hence, the classical representation can be generalized by drawing a circle of unit radius representing the quantum uncertainties associated to a measurement of these quadratures. This is shown in Figure 2.2a.

The special case $\alpha = 0$, the vacuum state, is represented in Figure 2.2b. Note that it is represented by the exact same circle (the uncertainty ΔX^ψ does not depend on α either), but now centered at the origin of phase space. The representation of any other coherent state is then obtained by displacing this uncertainty circle to the point $(2 \operatorname{Re}\{\alpha\}, 2 \operatorname{Im}\{\alpha\})$, and hence these states can be visualized as classical states carrying with the quantum vacuum uncertainties.

⁸ We will learn how to perform quadrature measurements in Chapter 6 for the case of light.

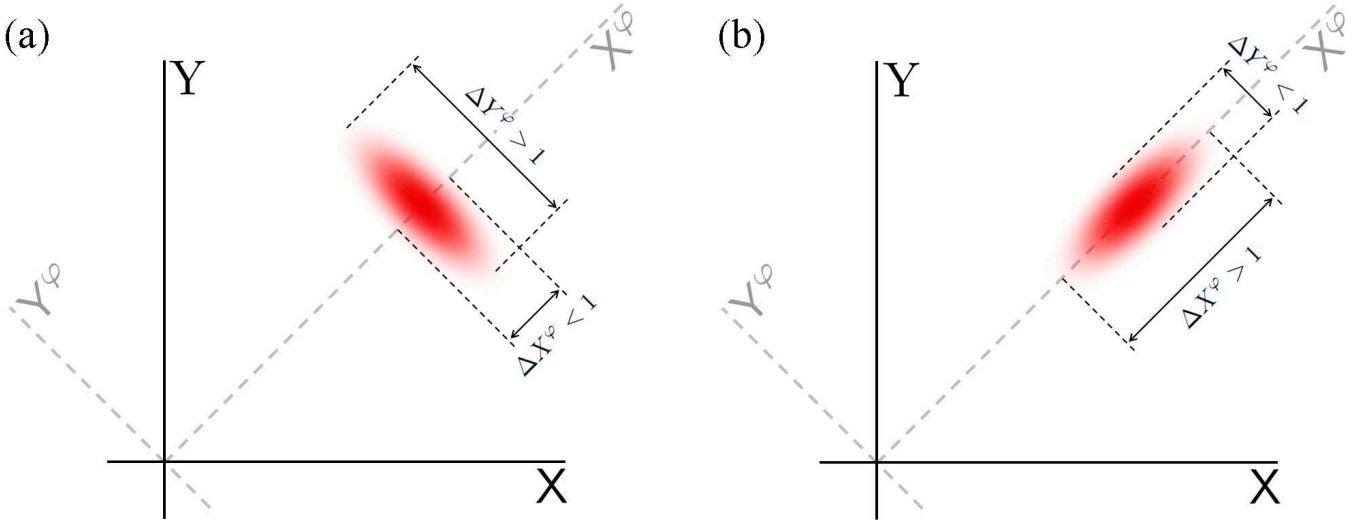


Fig. 2.4: Phase space sketches of the squeezed states. At (a) the uncertainty of the amplitude quadrature is reduced below the vacuum level at the expense of increasing the uncertainty of the phase quadrature. At (b), on the other hand, it is the phase quadrature the one which is squeezed, while the amplitude quadrature becomes more noisy.

This intuitive picture of coherent states allows us to understand its amplitude and phase properties (Figure 2.3). The mean values of the quadratures define a phase $\varphi = \arctan(\langle \hat{Y} \rangle / \langle \hat{X} \rangle)$ and an amplitude $\mu = \sqrt{\langle \hat{Y} \rangle^2 + \langle \hat{X} \rangle^2}$; in the classical limit these are exactly the phase and amplitude that would be measured for the oscillator. When quantum uncertainties in the quadratures cannot be neglected, it is reasonable to think that φ and μ will still be the mean values measured for the phase and amplitude of the oscillator, but now they will be also affected by some uncertainties. It seems obvious from Figure 2.3 that these amplitude and phase uncertainties are related to the uncertainties of the \hat{X}^φ and \hat{Y}^φ quadratures, which we shall consequently call the *amplitude* and *phase* quadratures. Hence, even if at the quantum level the phase and amplitude observables are not satisfactorily understood, one can somehow relate their properties to those of the amplitude and phase quadratures, at least for states with a well defined amplitude, that is, $\mu > \Delta X^\varphi$.

2.4 Squeezed states

2.4.1 Definition and relevance

An important application of harmonic oscillators is *sensing*: The oscillator is put in contact with a system that we want to test, and some information about this gets encoded as phase or amplitude modulations in the oscillator. We have seen in the previous section that when the oscillator is in a coherent state both its amplitude and phase suffer from uncertainties, and hence the encoded signal cannot be perfectly retrieved from measurements on the oscillator. When any other source of technical noise is removed, that is, when the measurement equipment behaves basically as ideal, this *quantum noise* becomes the main limitation; moreover, when the signal generated by the system that we want to study is tiny, it can even be disguised below quantum noise, so that it could not be distinguished at all. Note that this quantum noise appears even if the oscillator is in its vacuum state $|\alpha = 0\rangle$, as it has its roots in the *vacuum fluctuations* of the position and momentum of the oscillator.

Squeezed states are the solution to this problem; the idea is the following. Suppose that the signal is encoded in the amplitude of the oscillator. In a coherent state the amplitude and phase quadratures are affected of equal uncertainties $\Delta X^\varphi = \Delta Y^\varphi = 1$; however, we can conceive a state of the oscillator in which the uncertainty of the amplitude quadrature is reduced, while that of the phase quadrature is increased, say $\Delta X^\varphi \ll 1$ and $\Delta Y^\varphi \gg 1$, so that the product of uncertainties keeps lower bounded by one, $\Delta X^\varphi \Delta Y^\varphi \geq 1$. The phase space sketch of such state is depicted in Figure 2.4a. In this case the amplitude quadrature is well defined, and one can in principle monitor its modulations with arbitrary accuracy. Of course, this is accomplished at the expense of not being able to retrieve any information from the phase quadrature, but if we only care about the signal encoded in the amplitude quadrature that's not a problem.

We will define *squeezed states* as those in which some quadrature, say \hat{X}^ψ , has an uncertainty below the vacuum

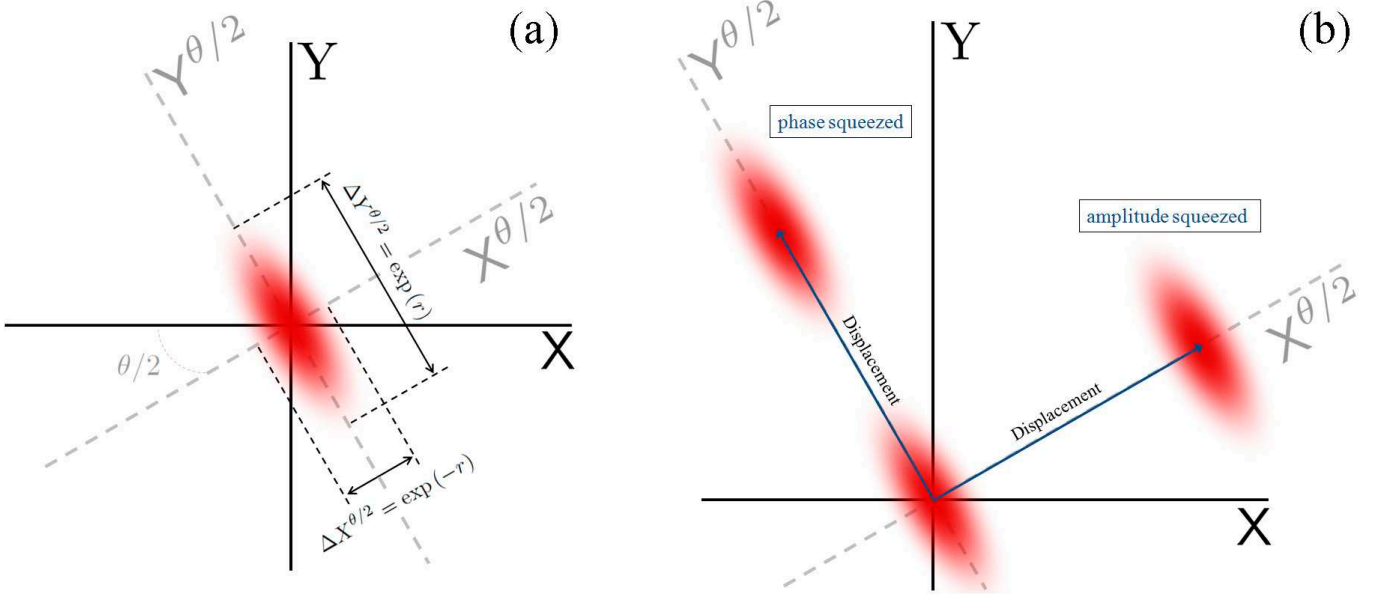


Fig. 2.5: (a) Phase space sketch of a squeezed vacuum state. (b) Applying displacements in the direction of the squeezed or antisqueezed quadratures, one obtains amplitude or phase squeezed states, respectively.

or coherent level, that is, $\Delta X^\psi < 1$. We then say that quadrature \hat{X}^ψ is *squeezed*. Together with the *amplitude squeezed state* already introduced (for which $\psi = \varphi$), we show the phase space sketch of a *phase squeezed state* (for which $\psi = \varphi + \pi/2$) in Figure 2.4. Let us now study one specially relevant type of squeezed states.

2.4.2 Minimum uncertainty squeezed states

Minimum uncertainty states are states which satisfy the lower bound of the quadrature uncertainty relation, that is, $\Delta X^\psi \Delta Y^\psi = 1 \forall \psi$. The simplest of these states is the vacuum state $|0\rangle$; any other number state $|n \neq 0\rangle$ is not contained in this class, as it is easily checked that it satisfies $\Delta X^\psi = 2n + 1$ for any ψ . Coherent states, on the other hand, are minimum uncertainty states, as they are obtained from vacuum by the displacement transformation, which does not change the quadrature variances.

It is possible to generate squeezed states of this kind by using the *squeezing operator*

$$\hat{S}(z) = \exp\left(\frac{z^*}{2}\hat{a}^2 - \frac{z}{2}\hat{a}^{\dagger 2}\right), \quad (2.31)$$

where $z \in \mathbb{C}$ is called the *squeezing parameter*. Similarly to the displacement operator, this operator is unitary; hence, it is generated by making the oscillator evolve with the Hamiltonian $\hat{H}_S = i\hbar(z^*\hat{a}^2 - z\hat{a}^{\dagger 2})/2T$ during a time T . In this thesis we will explain how this Hamiltonian can be generated in optical systems.

Applied to the annihilation operator this evolution gives

$$\hat{S}^\dagger(z)\hat{a}\hat{S}(z) = \hat{a} \cosh r - e^{i\theta}\hat{a}^\dagger \sinh r, \quad (2.32)$$

where we have written z in the polar form $z = r \exp(i\theta)$, and have used (2.24). In terms of quadratures, these expressions are easily rewritten as

$$\hat{S}^\dagger(z)\hat{X}^{\theta/2}\hat{S}(z) = e^{-r}\hat{X}^{\theta/2} \quad \text{and} \quad \hat{S}^\dagger(z)\hat{Y}^{\theta/2}\hat{S}(z) = e^r\hat{Y}^{\theta/2}. \quad (2.33)$$

Suppose now that before the *squeezing transformation* the state of the system was vacuum, which has the statistical properties $\langle \hat{X}^\psi \rangle = 0$ and $\Delta X^\psi = 1$ for all ψ as already seen. After the transformation (2.33) the mean of any quadrature is still zero, but the uncertainty of quadrature $\hat{X}^{\theta/2}$ has decreased to $\Delta X^{\theta/2} = \exp(-r)$, while that of quadrature $\hat{Y}^{\theta/2}$ has increased to $\Delta Y^{\theta/2} = \exp(r)$. Hence, the squeezing operator creates a *minimum uncertainty squeezed state*, that is, a state in which the uncertainty of one quadrature is reduced below the vacuum level, while the quadratures still satisfy the lower bound set by uncertainty relation.

The phase space sketch of this *squeezed vacuum state* is showed in Figure 2.5a. The uncertainty circle associated to the vacuum state has turned into an ellipse, showing that the quadrature uncertainty along the $\theta/2$ direction of phase space is reduced. An amplitude squeezed state can be then created by applying a subsequent displacement along the $\theta/2$ axis as shown in Figure 2.5b. If the displacement is applied along the $(\theta + \pi)/2$ direction, then a phase squeezed state is obtained. As displacements do not change the uncertainty properties of the state, these amplitude or phase squeezed states are still minimum uncertainty states.

2.5 Entangled states

2.5.1 The EPR argument and quantum non-locality

Even though Einstein is considered one of the founding fathers of quantum mechanics, he always felt uncomfortable with its probabilistic character. Fruit of this criticism, in 1935, and together with Podolsky and Rosen, he came out with an argument which was supposed to tumble down the foundations of quantum mechanics, showing in particular how the theory was both *incomplete* and *inconsistent with causality* [39]. Looking from our current perspective, it is quite ironic how the very same ideas they introduced, far from destroying the theory, are the power source for some of the most promising present applications of quantum physics.

Before introducing the EPR argument (standing for Einstein, Podolsky, and Rosen), let us explain the properties of the eigensystem of the quadrature operators. Consider the self-adjoint operator associated to the X quadrature, that is \hat{X} . It is easy to argue that this operator has a pure continuous spectrum⁹ $\{x\}_{x \in \mathbb{R}}$, with corresponding eigenvectors $\{|x\rangle\}_{x \in \mathbb{R}}$ which are Dirac-normalized, that is, $\langle x|x'\rangle = \delta(x - x')$. Of course, this vectors cannot describe a physical state of the harmonic oscillator, as they do not belong to its Hilbert space (they cannot be properly normalized, see Section A.2.3). In fact, an eigenstate $|x\rangle$ corresponds to the infinitely squeezed state $|x\rangle = \lim_{r \rightarrow \infty} \hat{D}(x/2) \hat{S}(r) |0\rangle$, which is unphysical as it leads to an infinite mean energy of the oscillator, see Eq. (2.13). Similar reasoning applies to the Y quadrature, whose associated self-adjoint operator \hat{Y} has a continuous spectrum $\{y\}_{y \in \mathbb{R}}$ with corresponding eigenvectors $\{|y\rangle\}_{y \in \mathbb{R}}$.

The EPR argument starts by considering two harmonic oscillators with Hilbert spaces \mathcal{H}_A and \mathcal{H}_B , which after interacting for a while are left in the state

$$|EPR\rangle = \int dx |x, x\rangle. \quad (2.35)$$

Note that this state can be written also as

$$|EPR\rangle = \int dy |y, -y\rangle, \quad (2.36)$$

in terms of the eigenstates of the Y quadratures of the oscillators. Note also that $|EPR\rangle$ cannot be a true state of the oscillators, as it cannot be normalized, but let us forget about this detail for the sake of the argument; we will deal later with a realistic situation. The oscillators *A* and *B* are then given, respectively, to *Alice* and *Bob*, two observers placed at distant locations, so that they are not able to interact anymore.

EPR argue then as follows. Imagine that Alice measures X and obtains the result¹⁰ x_0 ; according to quantum mechanics the state of oscillators collapses to $|x_0, x_0\rangle$, and hence, any subsequent measurement of X performed by Bob will reveal that his oscillator has a definite value of this quadrature, x_0 . However, Alice could have measured Y instead, obtaining for example the result y_0 ; in this case, quantum mechanics says that the state would have collapsed to $|y_0, -y_0\rangle$, after which Bob would have concluded that his oscillator had a definite value of its Y quadrature, $-y_0$. Now, and this is the center of all the argument, *assuming that nothing Alice may do can alter the physical state of Bob's oscillator* (the oscillators are separated, even *space-like* or *causally* during the life of Alice and Bob if we like!), one must conclude that the oscillator *B* must had well defined values of both its X and Y quadratures from the beginning, hence *violating the quantum mechanical uncertainty relation* $\Delta X \Delta Y \geq 1$, and showing that quantum mechanics is inconsistent.

Even though it seems a completely reasonable statement (specially at 1935, just a decade after the true birth of quantum mechanics), the center of their argument is actually its flaw. The reason is that the state of the system

⁹ Indeed, from the relation

$$\exp\left(\frac{i}{2}\xi\hat{Y}\right)\hat{X}\exp\left(-\frac{i}{2}\xi\hat{Y}\right) = \hat{X} + \xi, \quad (2.34)$$

with $\xi \in \mathbb{R}$, which is easily proved with the Baker–Campbell–Hausdorff lemma (2.24), it follows that if $|x\rangle$ is an eigenvector of \hat{X} with eigenvalue, then the vector $\exp(-i\xi\hat{Y}/2)|x\rangle$ is also an eigenvector of \hat{X} with eigenvalue $x + \xi$. Now, as this holds for any real ξ , we conclude that the spectrum of \hat{X} is the whole real line.

¹⁰ Again, this is an idealized situation used just for the sake of argumentation; this is because having a continuous spectrum, a measurement of \hat{X} cannot give a definite number x_0 .

is not an *element of reality* (in EPR's words), it is just a mathematically convenient object which describes the statistics that would be obtained if a physical observable is measured. Consequently, causality does not apply to it: *The actions of Alice can indeed alter Bob's state*, even if these are causally disconnected. Of course, a completely different matter is whether Alice and Bob can use this *spooky action at a distance* (in Einstein's words) to transmit information superluminally. Even though there is no rigorous proof for the negative answer to this question, such violation of causality has never been observed or predicted, even in the most sound and subtle applications of this *quantum non-local effects* (like *teleportation*), and hence, most physicists believe that despite non-local effects at the level of states, quantum mechanics cannot violate causality in any way.

2.5.2 Entanglement and the two-mode squeezing operator

The work of Einstein, Podolsky, and Rosen is the very best example of how one can make advances in a theory by trying to disprove it. Even if their motivation was based on wrong ideas, they were the first ones to realize that in quantum mechanics it is possible to create correlations between systems which go beyond those admitted in the classical world. Such states were coined *entangled states* by Schrödinger, which was actually supportive of the EPR ideas, and a strong believer of the incompleteness of quantum mechanics. After the 60's, physicists stopped looking at these states as the puzzle EPR suggested they were, and started searching for possible applications of them to various problems. Bell was the first one who realized the potential of such states, proving that they could be used to rule out the incompleteness of quantum mechanics [40] (exactly the opposite of what EPR created them for!), or, in other words, to prove that the probabilistic character of quantum mechanics does not come from some missing information we fail to account for, but from a probabilistic character of nature itself¹¹. Nowadays, entangled states have been shown to be a resource for remarkable applications such as the fast performance of computational tasks that would be impossible to perform classically (like factorization of large numbers [41], which is actually at the core of every present cryptographic system). This section is devoted to understand a little deeper these kind of states, as well as explaining how they can be generated in harmonic oscillator systems.

As in the previous section, consider two harmonic oscillators with joint Hilbert space $\mathcal{H}_A \otimes \mathcal{H}_B$. If the state of the joint system is of the type $\hat{\rho}_{AB}^{(t)} = \hat{\rho}_A \otimes \hat{\rho}_B$, that is, a tensor product of two arbitrary density operators, the actions performed by Alice on the A oscillator won't affect Bob's oscillator, the statistics of which are given by $\hat{\rho}_B$, no matter the actual state $\hat{\rho}_A$ (see Axiom V in Appendix A). In this case A and B are *uncorrelated*. For any other type of joint state, A and B will share some kind of correlation.

Correlations are not strange in classical systems; hence, the problem in quantum mechanics is to distinguish between correlations which can appear at a classical level, and correlations which are purely quantum, as only in the latter case one can expect to exploit them in applications requiring entanglement. Intuitively, a state will have only classical correlations if, starting from a state of the $\hat{\rho}_{AB}^{(t)}$ type, Alice and Bob can prepare it by making use only of *local operations* (such as local unitaries or measurements) and *classical communication* (such as phone calls). It is not difficult to convince oneself that the most general state that can be created by such means has the so-called *separable form*

$$\hat{\rho}_{AB}^{(s)} = \sum_k w_k \hat{\rho}_A^{(k)} \otimes \hat{\rho}_B^{(k)}, \quad (2.37)$$

where the $\hat{\rho}^{(k)}$'s are density operators and $\sum_k w_k = 1$. Any state which cannot be written as a convex mixture of tensor product states will induce quantum correlations between A and B , and will therefore be an entangled state in the spirit of *EPR*.

There is yet another way of justifying that states which cannot be written in the separable form (2.37) will make A and B share quantum correlations. The idea is that the fundamental difference between classical and quantum mechanics is the superposition principle. Hence, it is intuitive that correlations will have a quantum nature when the joint state of the oscillators exploits the concept of "superposition of joint states", that is, when it cannot be written as a tensor product of two independent states of the oscillators, or as a purely classical statistical mixture of these, which corresponds exactly to (2.37).

Given a general state $\hat{\rho}_{AB} \in \mathcal{H}_A \otimes \mathcal{H}_B$ it is hard to find out whether it is separable or not. However, for the class of so-called *Gaussian states* (to which the states to be discussed in this thesis belong), a *necessary and sufficient* criterion is known. This criterion was proposed independently by Duan et al. [42] and Simon [43], and it can be formulated as follows¹². Consider two orthogonal quadratures $\{\hat{X}_A^\varphi, \hat{Y}_A^\varphi\}$ and $\{\hat{X}_B^\varphi, \hat{Y}_B^\varphi\}$ for the oscillators A and B ,

¹¹ Strictly speaking, he proved that *no local hidden-variables theory* is consistent with the predictions of quantum mechanics.

¹² Even though this criterion is much simpler, it is worth remarking that for the ten years before its formulation, the only experimentally testable criterion for entanglement was that of Reid's [44]; this criterion was based on how much information one can infer about the quadratures of one of the oscillators by performing measurements on the other, and in a sense expanded the EPR ideas to entangled states with imperfect correlations.

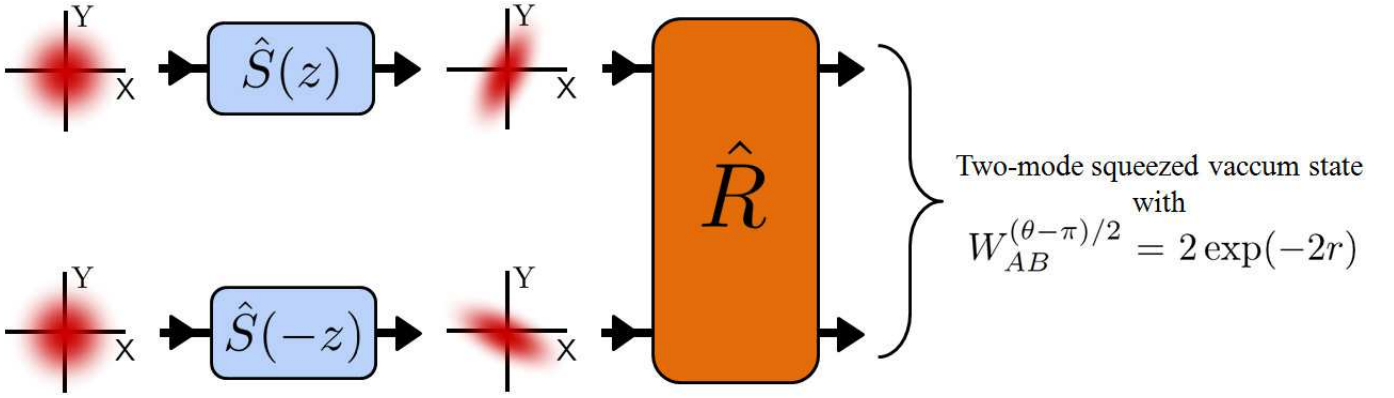


Fig. 2.6: Schematic relation between entanglement and squeezing: Two orthogonally squeezed vacua are connected to a two-mode squeezed vacuum state by the beam splitter transformation \hat{R} .

respectively; then their joint state is separable if and only if

$$W_{AB}^\varphi = V[(\hat{X}_A^\varphi - \hat{X}_B^\varphi)/\sqrt{2}] + V[(\hat{Y}_A^\varphi + \hat{Y}_B^\varphi)/\sqrt{2}] \geq 2, \quad (2.38)$$

for every φ . This criterion can be seen as a formalization of the ideas introduced in the EPR article; just note that a coherent state has $V[(\hat{X}_A^\varphi - \hat{X}_B^\varphi)/\sqrt{2}] = V[(\hat{Y}_A^\varphi + \hat{Y}_B^\varphi)/\sqrt{2}] = 1 \forall \varphi$, and hence if $W_{AB}^\varphi < 2$ one can be sure that two orthogonal quadratures of the oscillators are correlated above what is classically allowed. For example, a maximal violation of this inequality is obtained for the unphysical $|EPR\rangle$ state, which has $W_{AB}^0 = 0$, showing that there is a perfect correlation (anticorrelation) between the X (Y) quadratures of the oscillators. Note that this criterion does not quantify the amount of entanglement present in the state, it offers just a way to prove whether a state is separable or not (see the next section for quantitative entanglement). In practice, however, and incorrectly without further arguments, it customary to state that the lower W_{AB}^φ is, the larger the amount of entanglement is.

Let us now explain how to generate a class of pure entangled states which coincide with $|EPR\rangle$ in some (unphysical) limit. We will call *EPR-like states* to such states. To proceed, note that the conditions $V[(\hat{X}_A^\varphi - \hat{X}_B^\varphi)/\sqrt{2}] < 1$ and $V[(\hat{Y}_A^\varphi + \hat{Y}_B^\varphi)/\sqrt{2}] < 1$ are actually quite reminiscent of the quadrature squeezing that we introduced in the previous section, with the difference that now the squeezing is present in a joint quadrature. Let us call \hat{a} and \hat{b} to the annihilation operators for the A and B harmonic oscillators, respectively. Consider the unitary operator

$$\hat{S}_{AB}(z) = \exp(z^* \hat{a} \hat{b} - z \hat{a}^\dagger \hat{b}^\dagger), \quad (2.39)$$

which we will call the *two-mode squeezing operator*, which is easily proved to transform the annihilation operators as

$$\hat{S}_{AB}^\dagger(z) \hat{a} \hat{S}_{AB}(z) = \hat{a} \cosh r - e^{i\theta} \hat{b}^\dagger \sinh r, \quad (2.40a)$$

$$\hat{S}_{AB}^\dagger(z) \hat{b} \hat{S}_{AB}(z) = \hat{b} \cosh r - e^{i\theta} \hat{a}^\dagger \sinh r, \quad (2.40b)$$

where $z = r \exp(i\theta)$. Using these expressions and their conjugates, it is straightforward to prove that if the oscillators are initially in their vacuum state, then

$$V[(\hat{X}_A^{\theta/2} + \hat{X}_B^{\theta/2})/\sqrt{2}] = V[(\hat{Y}_A^{\theta/2} - \hat{Y}_B^{\theta/2})/\sqrt{2}] = \exp(-2r), \quad (2.41a)$$

$$V[(\hat{X}_A^{\theta/2} - \hat{X}_B^{\theta/2})/\sqrt{2}] = V[(\hat{Y}_A^{\theta/2} + \hat{Y}_B^{\theta/2})/\sqrt{2}] = \exp(2r). \quad (2.41b)$$

Hence, applied to the vacuum state of the oscillators, the two-mode squeezing operator generates an entangled state, the so-called *two-mode squeezed vacuum state*, as $W_{AB}^{(\theta-\pi)/2} = 2 \exp(-2r) < 2$. In particular, for $\theta = \pi$ and $r \rightarrow \infty$ we have $W_{AB}^0 \rightarrow 0$, and hence the $|EPR\rangle$ state is recovered. For a finite value of r we then get an EPR state with imperfect correlations between orthogonal quadratures of the oscillators, these correlations being always above what is classically permitted. In Chapter 6 we will learn how to generate this type of states.

The connection between squeezing and entanglement can be made even more explicit. To this aim, assume that we induce an evolution of the entangled oscillators A and B corresponding to the unitary operator

$$\hat{R} = \exp\left[\frac{\pi}{4}(\hat{a}\hat{b}^\dagger - \hat{a}^\dagger\hat{b})\right], \quad (2.42)$$

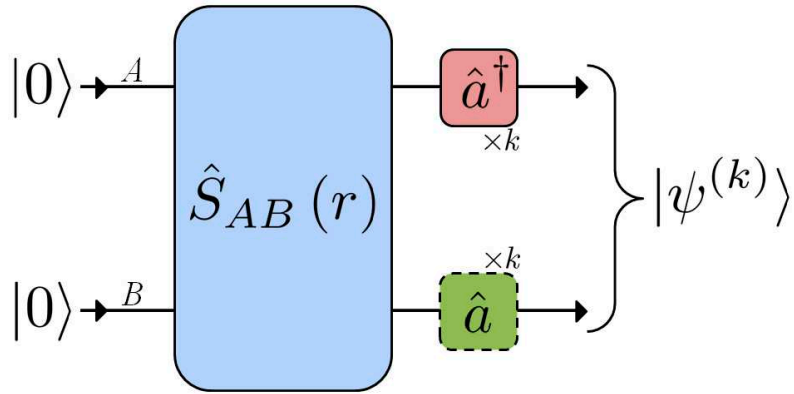


Fig. 2.7: Schematic representation of the example studied in this section. After the generation of the two-mode squeezed vacuum state, Alice adds k excitations to her oscillator (pink box with solid contour), or Bob subtracts k excitations out of his (green box with dashed contour); in either case the final state is $|\psi^{(k)}\rangle$, and what we have been able to prove is that the entanglement increases with the number of operations, k .

what in the Heisenberg picture means that the boson operators are transformed as

$$\hat{a}_1 = \hat{R}^\dagger \hat{a} \hat{R} = (\hat{b} + \hat{a})/\sqrt{2} \quad (2.43a)$$

$$\hat{a}_2 = \hat{R}^\dagger \hat{b} \hat{R} = (\hat{b} - \hat{a})/\sqrt{2}. \quad (2.43b)$$

In terms of the new, independent boson operators \hat{a}_1 and \hat{a}_2 , the two-mode squeezing operator is written as

$$\hat{S}_{AB}(z) = \exp\left(\frac{z^*}{2}\hat{a}_1^2 - \frac{z}{2}\hat{a}_1^{\dagger 2} - \frac{z^*}{2}\hat{a}_2^2 + \frac{z}{2}\hat{a}_2^{\dagger 2}\right) = \hat{S}_1(z)\hat{S}_2(-z), \quad (2.44)$$

that is, as two individual squeezing operators for each of the new modes. Read backwards, this shows that one can entangle two oscillators by squeezing them along two orthogonal directions of phase space, and then make them interact according to the unitary operator (2.42), see Figure 2.6. In the case of light we shall see that the unitary transformation (2.42) corresponds to a 50/50 beam splitter. This means that one can generate two entangled optical beams by mixing in a beam splitter two beams that have been previously squeezed; this is interesting because, as we shall see in Chapter 6, we are now in position to generate light with large levels of squeezing experimentally.

2.5.3 Enhancing entanglement by addition and subtraction of excitations

In this section we will introduce part of the work initiated during a three-month visit to the Massachusetts Institute of Technology by the author of this thesis [26]. In particular, we have been able to prove that Alice and Bob can enhance the entanglement of the two-mode squeezed vacuum state by annihilating or creating excitations on their corresponding oscillators¹³. Even though this result was known prior to our work, we offer a systematic analysis of such phenomenon, as well as prove it analytically for the very first time in a simple (but relevant) scheme that we introduce here.

Let us start by explaining how to quantify the entanglement present in a joint state of the oscillators. Even though we pretty much understand the conditions that a good entanglement measure $\mathcal{E}[\hat{\rho}_{AB}]$ must satisfy¹⁴, we haven't been able to build a satisfactory one for general bipartite states (the ones introduced so far either do not satisfy all the needed conditions, or can only be evaluated efficiently for restricted classes of states). Fortunately, when dealing only with pure states $\hat{\rho}_{AB} = |\psi\rangle_{AB}\langle\psi|$, it has been proved that there is a *unique* entanglement measure, the so-called

¹³ These operations correspond to the application of the annihilation or creation of excitations through the operators \hat{a} and \hat{a}^\dagger . Not being unitary, these operators cannot correspond to any Hamiltonian interaction; nevertheless, by using measurement-based techniques, they can be simulated probabilistically (that is, conditioned to a specific outcome in some measurement). Nowadays, it is possible to perform photon addition and subtraction from light beams [45, 46, 47, 48, 49]. In particular, photon subtraction is accomplished by making the beam pass through a beam splitter with very high transmittance; whenever a photon is detected in the reflected beam, it means that photon subtraction has been accomplished in the transmitted beam [45]. Photon addition is a little more involved [46]; in these case the beam acts as the seed of the signal mode in a down-conversion process, and whenever a photon is detected in the conjugate spatial mode (the idler mode), it means that a photon has been added to the beam. These operations have been used to make direct tests of things as fundamental as the bosonic commutation relations [48, 49].

¹⁴ Technically, it must be an *entanglement monotone*, see [50] for a clear and concise explanation.

entanglement entropy. Its definition is actually quite intuitive: One just needs to check how mixed the reduced state of one party is left when we trace the subspace corresponding to the other party. Operationally this means that, given the reduced states $\hat{\rho}_A = \text{tr}_B\{|\psi\rangle_{AB}\langle\psi|\}$ or $\hat{\rho}_B = \text{tr}_A\{|\psi\rangle_{AB}\langle\psi|\}$, this entanglement measure is given by

$$\mathcal{E}[|\psi\rangle_{AB}] \equiv \mathcal{S}[\hat{\rho}_A] = \mathcal{S}[\hat{\rho}_B], \quad (2.45)$$

where $\mathcal{S}[\hat{\rho}] = -\text{tr}\{\hat{\rho} \log \hat{\rho}\}$ is the so-called *von Neumann entropy*, which measures how mixed the state $\hat{\rho}$ is [51].

It is particularly simple to evaluate this entanglement measure when the state is given in its so-called Schmidt form¹⁵,

$$|\psi\rangle_{AB} = \sum_{j=1}^{\infty} \sqrt{p_j} |u_j\rangle \otimes |v_j\rangle, \quad (2.46)$$

being $\{p_j\}_{j=1,\dots,\infty}$ a probability distribution, and $\{|u_j\rangle\}_{j=1,\dots,\infty}$ and $\{|v_j\rangle\}_{j=1,\dots,\infty}$ two orthonormal bases. In this case, the reduced density operators are given by $\hat{\rho}_A = \sum_{j=1}^{\infty} p_j |u_j\rangle\langle u_j|$ and $\hat{\rho}_B = \sum_{j=1}^{\infty} p_j |v_j\rangle\langle v_j|$, which are already in their diagonal form, and hence we have

$$\mathcal{E}[|\psi\rangle_{AB}] = -\sum_{j=1}^{\infty} p_j \log p_j. \quad (2.47)$$

Now that we understand how to evaluate the amount of entanglement present in a pure bipartite state, we can pass to analyze the scheme depicted in Figure 2.7. The idea is that once the two oscillators (initialized in its vacuum state) go through the two-mode squeezer (with $\theta = 0$ for simplicity), Alice adds k excitations, that is, she applies k times the creation operator to her oscillator. It is not difficult to show that in the number state basis, the two-mode squeezed vacuum state reads [23]

$$|\text{TMSV}\rangle = \hat{S}_{AB}(r) |0,0\rangle = \sum_{n=0}^{\infty} \sqrt{1-\lambda^2} \lambda^n |n,n\rangle, \quad (2.48)$$

with $\lambda = \tanh r$. This state is already in Schmidt form with a distribution given by $p_n = (1-\lambda^2)\lambda^{2n}$, which plugged in (2.47) leads to the entanglement entropy

$$\mathcal{E}[|\text{TMSV}\rangle] = \log(1-\lambda^2) - \frac{2\lambda^2}{1-\lambda^2} \log \lambda. \quad (2.49)$$

It is very simple to check that this function is monotonically increasing with r , just as expected by the preceding section (quantum correlations are larger the larger is the squeezing, and hence the entanglement should increase with r).

Now we need to find the state after the k additions performed by Alice; it is completely straightforward to show by using (2.12), that the final state reads

$$|\psi^{(k)}\rangle = \sum_{n=0}^{\infty} \sqrt{p_n^{(k)}} |n+k, n\rangle, \quad (2.50)$$

with

$$p_n^{(k)} = (1-\lambda^2)^{k+1} \lambda^{2n} \binom{n+k}{n}. \quad (2.51)$$

It is worth noting that this is exactly the same state that is obtained when Bob performs k subtractions on his oscillator, that is, Alice adding excitations is the same as Bob subtracting them (see Figure 2.7).

Just as with the two-mode squeezed vacuum state, this state is already in Schmidt form (check that $p_n^{(k)}$ is a probability distribution in n), and hence the entanglement entropy is easily evaluated as $\mathcal{E}^{(k)} = -\sum_{n=0}^{\infty} p_n^{(k)} \log p_n^{(k)}$. Unfortunately, this sum is not analytical except for $k=0$; nevertheless, we can prove that it is an increasing function of k as follows. Using the pascal identity

$$\binom{n+k+1}{k+1} = \binom{n+k}{k+1} + \binom{n+k}{k}, \quad (2.52)$$

¹⁵ It is simple to prove that every pure bipartite state can be uniquely written in this form [51].

we can write

$$p_n^{(k+1)} = \lambda^2 p_{n-1}^{(k+1)} + (1 - \lambda^2) p_n^{(k)}, \quad (2.53)$$

where we set $p_{-n}^{(k)} = 0$ for $n > 0$ by definition. Now, because of the strict concavity of the function $h(x) = -x \log x$, we have

$$\sum_{n=0}^{\infty} h[p_n^{(k)}] \geq \lambda^2 \sum_{n=0}^{\infty} h[p_{n-1}^{(k+1)}] + (1 - \lambda^2) \sum_{n=0}^{\infty} h[p_n^{(k)}], \quad (2.54)$$

and since $\sum_{n=0}^{\infty} h[p_{n-1}^{(k+1)}] = \sum_{n=0}^{\infty} h[p_n^{(k+1)}]$, this expression is equivalent to

$$\mathcal{E}^{(k+1)} \geq \mathcal{E}^{(k)}. \quad (2.55)$$

Hence, we have been able to prove analytically that entanglement increases with the number of additions/subtractions when acting on one mode of the entangled pair. The (numerical) discussion concerning the case of Alice and Bob acting both simultaneously on their respective oscillators can be found in [26], but nothing qualitatively different is found.

In a second work [27] we apply similar ideas in an effort to prove the so-called *minimum entropy conjecture for bosonic channels* [52, 53], which states that input coherent states are the states which minimize the output entropy of the most relevant class of optical communication channels (*phase-insensitive Gaussian channels* [54, 55]), or, equivalently, that they maximize the capacity of those channels, that is, the number of bits per second that can be transmitted reliably through the channel.

2.6 The harmonic oscillator in phase space

2.6.1 Phase space distributions

In the previous sections we have been able to make phase space sketches of various quantum states of the harmonic oscillator, which in particular allow us to visualize the statistics that would be obtained when measuring its quadratures. In this section we show how these sketches can be made in a rigorous way, by making a correspondence between the quantum state of the oscillator and a distribution in phase space [22]. One can tend to think that this suggests that quantum mechanics can be formulated just as noise impregnating the classical phase space trajectories, but the situation is a lot more subtle as we will show: Either these distributions are not probability density functions in the usual sense (they can be negative or strongly divergent), or the way that averages are made with them is not the usual one.

In the following we consider that the oscillator is in some generic state $\hat{\rho}$, and review three natural ways of defining a phase space distribution associated to it.

The Wigner distribution. As we have already argued, the quadratures \hat{X}^ψ possess a continuous spectrum $\{x^\psi\}_{x^\psi \in \mathbb{R}}$ and hence a continuous set of generalized eigenvectors $\{|x^\psi\rangle\}_{x^\psi \in \mathbb{R}}$. Hence, quantum mechanics assigns a probability density function $\langle x^\psi | \hat{\rho} | x^\psi \rangle$ to any point $x^\psi = x \cos \psi + y \sin \psi$ of the phase space (x, y) , which completely describes the statistics of a measurement of the \hat{X}^ψ quadrature.

It follows that a natural way of defining a phase space distribution, say $W(x, y)$, is then as the one whose marginals $\int_{-\infty}^{+\infty} dy W(x, y)$ and $\int_{-\infty}^{+\infty} dx W(x, y)$ give, respectively, the probability density functions $\langle x | \hat{\rho} | x \rangle$ and $\langle y | \hat{\rho} | y \rangle$ corresponding to a measurement of the X and Y quadratures. It is possible to show that such a distribution, which is known as the *Wigner distribution* [56], can be uniquely defined as

$$W(x, y) = \frac{1}{4\pi} \int_{\mathbb{R}} d\xi \exp(-iy\xi/2) \langle x + \xi/2 | \hat{\rho} | x - \xi/2 \rangle. \quad (2.56)$$

It can also be shown that given an operator $\hat{A}(\hat{X}, \hat{Y})$, we can evaluate its expectation value as

$$\langle \hat{A} \rangle = \int_{\mathbb{R}^2} dx dy W(x, y) A^{(s)}(x, y), \quad (2.57)$$

where $A^{(s)}$ is obtained by writing $\hat{A}(\hat{X}, \hat{Y})$ as a symmetric function of \hat{X} and \hat{Y} with the help of the commutation relations, and then changing these operators by the real variables x and y , respectively.

This expression deserves some comments. Note that when discussing the axioms of quantum mechanics (Section A.3.2) we decided that a reasonable strategy to generate the self-adjoint operators associated to a given classical observable was to first symmetrize its associated classical phase space function and then change the position and

momenta by the corresponding self-adjoint operators; hence, it may look like Eq. (2.57) is telling us that quantum mechanics appears *just* as noise acting onto the classical picture of the system, that is, by introducing probability density function $W(x, y)$ in phase space to which every observable must be averaged. Even though this intuitive picture might be useful to understand certain quantum phenomena (like squeezing), this is far from the end of the story; quantum mechanics is a little more subtle: Even though $W(x, y)$ is normalized to one and is a real function of the phase space variables, it can take negative values [22], and hence it is not a true probability density function. In other words, in general quantum mechanics *cannot* be simulated by adding classical noise to the system. As an example, for coherent and squeezed states it is possible to show that the Wigner distribution is positive all over phase space [22], and hence the interpretation of quantum mechanics as quantum noise acting onto the classical trajectories is somehow correct; however, this interpretation breaks down for number states, as in that case the Wigner function takes negative values [22].

The Husimi distribution. Coherent states offer an alternative way of building a phase space distribution. We saw that they are specified by a complex parameter α , *coherent amplitude* in the following, and admit a simple representation in a phase space formed with the variables $(x, y) = (2 \operatorname{Re}\{\alpha\}, 2 \operatorname{Im}\{\alpha\})$. These suggests that we could define another phase space distribution, say $Q(x, y)$, by asking to the state $\hat{\rho}$ of the oscillator how much does it project onto the set of coherent states $\{|\alpha\rangle\}_{\alpha \in \mathbb{C}}$, that is,

$$Q(\alpha) = \frac{\langle \alpha | \hat{\rho} | \alpha \rangle}{\pi}, \quad (2.58)$$

where the factor π^{-1} appears to ensure that Q is normalized to one. This simple distribution is called the *Husimi Q distribution* [57], and has a very nice property: It is positive and finite for any state of the oscillator¹⁶, and hence it is a true phase space probability distribution.

It has however a drawback: Its marginals do not give the proper probability density functions for quadrature measurements. Nevertheless, we can still evaluate the expectation value of an operator $\hat{A}(\hat{a}, \hat{a}^\dagger)$ with it as

$$\langle \hat{A} \rangle = \int_{\mathbb{C}} d^2\alpha Q(\alpha) A^{(a)}(\alpha, \alpha^*), \quad (2.59)$$

where $A^{(a)}$ is obtained by writing $\hat{A}(\hat{a}, \hat{a}^\dagger)$ in anti-normal order with the help of the commutation relations, and then changing the annihilation and creation operators by α and α^* , respectively. Note that this expression cannot be seen as an average of the classical phase space function associated to the observable because of the antinormal order.

Note finally that it is possible to characterize the full state $\hat{\rho}$ by only the diagonal elements $\langle \alpha | \hat{\rho} | \alpha \rangle$ because coherent states form an overcomplete basis, as we already discussed in Section 2.3.2.

The Glauber–Sudarshan distribution. Instead of asking how much does our state project onto a coherent state, we can assign a phase space distribution in the complex- α plane with a different but equally reasonable question: How do we have to mix the set of coherent states $\{|\alpha\rangle\}_{\alpha \in \mathbb{C}}$ to generate the state $\hat{\rho}$ of the oscillator? In other words, we are asking for the distribution $P(\alpha)$ satisfying

$$\hat{\rho} = \int_{\mathbb{C}} d^2\alpha P(\alpha) |\alpha\rangle\langle\alpha|. \quad (2.60)$$

If the coherent states were orthogonal, the answer would be the Q distribution; however, as they are not, this $P(\alpha)$, known as the *Glauber–Sudarshan P distribution* [58, 59], is a completely different distribution. In fact, this distribution can be negative and has in general strong divergences such as derivatives of the delta function. As an example, here we show the P distribution associated to a coherent and a number state

$$P_{|\alpha_0\rangle}(\alpha) = \delta^2(\alpha - \alpha_0), \quad (2.61a)$$

$$P_{|n\rangle}(\alpha) = \frac{\exp(-|\alpha|^2)}{n!} (\partial_{\alpha\alpha^*}^2)^n \delta^2(\alpha), \quad (2.61b)$$

which are not difficult to find by using the general formula¹⁷

$$P(\alpha) = \int_{\mathbb{C}} \frac{d^2\beta}{\pi^2} \exp(|\beta|^2 + |\alpha|^2 + \beta^*\alpha - \beta\alpha^*) \langle -\beta | \hat{\rho} | \beta \rangle, \quad (2.63)$$

¹⁶ Note that, in particular, it is lower bounded by 0 and upper bounded by $1/\pi$, as follows from the positivity and the unit trace of $\hat{\rho}$, respectively

¹⁷ The identity

$$|n\rangle\langle n| = \frac{1}{n!} (\partial_{\alpha\alpha^*}^2)^n \left(e^{|\alpha|^2} |\alpha\rangle\langle\alpha| \right) \Big|_{\alpha=0}, \quad (2.62)$$

is also useful in the case of the number state. Note that this identity comes directly from the representation of coherent states in terms of number states (2.18).

which comes from inverting equation (2.60).

Despite these properties which make the P distribution being far from a true probability distribution, it turns out to be extremely useful to solve quantum optical problems. This is because we can evaluate the expectation value of an operator $\hat{A}(\hat{a}, \hat{a}^\dagger)$ as

$$\langle \hat{A} \rangle = \int_{\mathbb{C}} d^2\alpha P(\alpha) A^{(n)}(\alpha, \alpha^*), \quad (2.64)$$

where $A^{(n)}$ is obtained by writing $\hat{A}(\hat{a}, \hat{a}^\dagger)$ in normal order with the help of the commutation relations, and then changing $\{\hat{a}, \hat{a}^\dagger\}$ by $\{\alpha, \alpha^*\}$, and, as we shall see in Chapter 5, most of the theoretical predictions for experimental observations involving light detection are formulated ultimately as the expectation value of some operator written in normal order.

We will refer to these continuous representations of the density operator as *coherent representations*. It is possible to show that the three distributions W , Q , and P exist for any quantum state $\hat{\rho}$. This means that all the information concerning the state of the oscillator is completely contained in any of them, that is, the three of them are equivalent to the density operator $\hat{\rho}$. Hence, they provide a quantum mechanical description of the harmonic oscillator in phase space, but they cannot be regarded as probability distributions in the classical sense, showing that there are quantum states which cannot be understood within the framework of classical mechanics.

2.6.2 The positive P distribution

The three types of distributions that we have defined have both advantages and drawbacks: The marginals of the W distribution give the correct statistics for quadrature measurements, but the distribution itself can be negative; on the other hand, the Q distribution is a well behaved probability distribution, but it gives quantum expectation values of operators only in antinormal order; finally, the P distribution gives expectation values of operators in normal order (which turns out to be quite useful in quantum optics), but it usually has singularities beyond those of the Dirac–delta function.

In this section we develop a new probability distribution, the *positive P distribution*, which is always a well behaved probability distribution and gives expectation values of operators written in normal order. These are the properties that will be needed for the purposes of this thesis, but, as we will see, these are accomplished at the expense of working in a phase space with twice the usual dimensionality. Even so, we will sketch in the next section (and show explicitly along the next chapters) how this distribution allows us to make calculations which could be impossible to perform otherwise.

The positive P distribution was originally defined by Drummond and Gardiner [60] via the following non-diagonal coherent state representation of the density matrix

$$\hat{\rho} = \int_{\mathbb{C}^2} d^2\alpha d^2\alpha^+ P(\alpha, \alpha^+) \hat{\Lambda}(\alpha, \alpha^+), \quad (2.65)$$

where we have defined the so-called *non-diagonal projector*

$$\hat{\Lambda}(\alpha, \alpha^+) = \frac{|\alpha\rangle\langle(\alpha^+)^*|}{\langle(\alpha^+)^*|\alpha\rangle} = \exp(-\alpha^+\alpha) \exp(\alpha a^\dagger) |0\rangle\langle 0| \exp(\alpha^+ a). \quad (2.66)$$

We use the same notation for this distribution and for the Glauber–Sudarshan distribution because from now on we will make use of the positive P distribution only, and hence there will be no room for confusion. Note that as α and α^+ are complex, independent variables, $P(\alpha, \alpha^+)$ lives in what we will call an *extended phase space* (α, α^+) , the four-dimensional space formed by the real and imaginary parts of α and α^+ .

Even though the positive P distribution is not uniquely defined from (2.65), it can always be chosen as [60]

$$P(\alpha, \alpha^+) = \frac{1}{4\pi} \exp\left(-\frac{1}{4}|\alpha^* - \alpha^+|^2\right) Q\left[\frac{1}{2}(\alpha^* + \alpha^+)^*\right], \quad (2.67)$$

which shows explicitly that it is a well defined probability distribution in the extended phase space (α, α^+) .

Similarly to the Glauber–Sudarshan P distribution, it allows us to find the expectation value of an operator $\hat{A}(\hat{a}, \hat{a}^\dagger)$ as

$$\langle \hat{A} \rangle = \int_{\mathbb{C}^2} d^2\alpha d^2\alpha^+ P(\alpha, \alpha^+) A^{(n)}(\alpha, \alpha^+); \quad (2.68)$$

note that the correspondence $\hat{a}^\dagger \rightarrow \alpha^*$ in the normal form of the operator \hat{A} is replaced within this representation by $\hat{a}^\dagger \rightarrow \alpha^+$.

We would like to finally note that it is completely straightforward to prove that $\hat{\Lambda}(\alpha, \alpha^+)$ is an analytic function¹⁸ of the complex variables (α, α^+) , while the distribution $P(\alpha, \alpha^+)$ itself is not, as it has to depend on both (α, α^+) and their complex conjugates in order to be a real function. We will exploit the analyticity of $\hat{\Lambda}(\alpha, \alpha^+)$ in the next section and along the upcoming chapters.

2.6.3 Fokker–Planck and stochastic Langevin equations

As a taste of the usefulness of the positive P representation, consider the following evolution equation for the state of an oscillator:

$$\frac{d\hat{\rho}}{dt} = [-i\omega\hat{a}^\dagger\hat{a} + (\kappa\hat{a}^{\dagger 2} - \kappa^*\hat{a}^2) + (\mathcal{E}\hat{a}^\dagger - \mathcal{E}^*\hat{a}), \hat{\rho}] + \gamma(2\hat{a}\hat{\rho}\hat{a}^\dagger - \hat{a}^\dagger\hat{a}\hat{\rho} - \hat{\rho}\hat{a}^\dagger\hat{a}), \quad (2.71)$$

being ω , \mathcal{E} , κ , and γ some parameters (ω and γ are real). The first term includes the regular Hamiltonian evolution of the oscillator, an squeezing term, and a term corresponding to an external driving of the oscillator, while the second part cannot be written in Hamiltonian form, and describes damping on the ideal harmonic motion of the oscillator. In the forthcoming chapters we will see how these terms arise naturally in the evolution of light contained in an optical cavity. In any case, let us assume for the moment that the state of the harmonic oscillator is subject to this evolution equation. We are going to show that it can be reduced to a set of 2 complex differential equations with noise, that is, to a set of *stochastic equations* [61].

One way to solve these operator equation would be to project it onto a truncated number state basis $\{|0\rangle, |1\rangle, \dots, |N\rangle\}$, obtaining then a linear system with $N \times N$ variables (the independent elements of the representation of the density operator). This method, however, is usually of little help if we intend to deal with states having a large number of photons, so that the size of the linear system is too large. It is in this case when coherent representations can be useful. Let us explain this for the positive P distribution.

We would like to stress that even though we are using equation (2.71) as a guiding example, most of the derivations that we are going to perform are completely general.

Let us collect the coherent variables into a single vector $\alpha = \text{col}(\alpha, \alpha^+)$. It is very simple to prove that the nondiagonal projector $\hat{\Lambda}(\alpha)$ satisfies the following properties:

$$\hat{a}\hat{\Lambda}(\alpha) = \alpha\hat{\Lambda}(\alpha) \quad (2.72a)$$

$$\hat{\Lambda}(\alpha)\hat{a} = \left(\alpha + \frac{\partial}{\partial\alpha^+}\right)\hat{\Lambda}(\alpha) \quad (2.72b)$$

$$\hat{\Lambda}(\alpha)\hat{a}^\dagger = \alpha^+\hat{\Lambda}(\alpha) \quad (2.72c)$$

$$\hat{a}^\dagger\hat{\Lambda}(\alpha) = \left(\alpha^+ + \frac{\partial}{\partial\alpha}\right)\hat{\Lambda}(\alpha); \quad (2.72d)$$

therefore, introducing the expansion of the density operator in terms of the positive P distribution (2.65), these properties allow us to rewrite the evolution equation (2.71) as

$$\int_{\mathbb{C}^2} d^4\alpha \hat{\Lambda}(\alpha) \partial_t P(\alpha; t) = \int_{\mathbb{C}^2} d^4\alpha d^2\alpha^+ P(\alpha; t) \left[\sum_j A_j(\alpha) \partial_j + \frac{1}{2} \sum_{jl} D_{jl}(\alpha) \partial_j \partial_l \right] \hat{\Lambda}(\alpha), \quad (2.73)$$

¹⁸ Given the complex function $f(z) = f_{\text{R}}(z_{\text{R}}, z_{\text{I}}) + i f_{\text{I}}(z_{\text{R}}, z_{\text{I}})$ of a complex variable $z = z_{\text{R}} + iz_{\text{I}}$, where f_{R} , f_{I} , z_{R} , and z_{I} are all real, we say that it is analytic if the derivative of the function in the complex- z plane does not depend on the direction along which it is performed. A necessary and sufficient condition for this is that all the partial derivatives $\partial f_k / \partial z_l$ ($k, l = \text{R, I}$) are continuous and satisfy the *Cauchy–Riemann relations*

$$\frac{\partial f_{\text{R}}}{\partial z_{\text{R}}} = \frac{\partial f_{\text{I}}}{\partial z_{\text{I}}} \quad \text{and} \quad \frac{\partial f_{\text{R}}}{\partial z_{\text{I}}} = -\frac{\partial f_{\text{I}}}{\partial z_{\text{R}}}. \quad (2.69)$$

Note that this relations imply that $\partial f / \partial z^* = 0$, and hence, an analytical complex function can only depend on z_{R} and z_{I} through the combination $z_{\text{R}} + iz_{\text{I}}$, that is, it cannot depend on the complex conjugate of z . An important property of analytical complex functions is that the derivative respect to the complex variable can be made in two equivalent ways

$$\frac{df}{dz} = \frac{\partial f}{\partial z_{\text{R}}} = -i \frac{\partial f}{\partial z_{\text{I}}}. \quad (2.70)$$

All this discussion is generalized to a complex function of several complex variables in a natural straightforward manner.

where all the indices can take the values α or α^+ , and

$$A_\alpha(\boldsymbol{\alpha}) = \mathcal{E} - (\gamma + i\omega)\alpha + 2\kappa\alpha^+, \quad (2.74a)$$

$$A_{\alpha^+}(\boldsymbol{\alpha}) = \mathcal{E}^* - (\gamma - i\omega)\alpha^+ + 2\kappa^*\alpha, \quad (2.74b)$$

$$D_{\alpha\alpha}(\boldsymbol{\alpha}) = 2\kappa = D_{\alpha^+\alpha^+}(\boldsymbol{\alpha}), \quad (2.74c)$$

$$D_{\alpha\alpha^+}(\boldsymbol{\alpha}) = D_{\alpha^+\alpha}(\boldsymbol{\alpha}) = 0. \quad (2.74d)$$

The symmetric matrix D can always be decomposed as $D = BB^T$ for some matrix B , although this is not unique (note that it has to be a $2 \times d$ matrix, though, with d arbitrary). D being diagonal in this particular example, we could choose for example

$$B = \begin{bmatrix} \sqrt{2\kappa} & 0 \\ 0 & \sqrt{2\kappa^*} \end{bmatrix}. \quad (2.75)$$

Define now the real and imaginary parts of the coherent amplitudes $\alpha = \alpha_R + i\alpha_I$ and $\alpha^+ = \alpha_R^+ + i\alpha_I^+$, which we collect in the vectors $\boldsymbol{\alpha}_R = \text{col}(\alpha_R, \alpha_R^+)$ and $\boldsymbol{\alpha}_I = \text{col}(\alpha_I, \alpha_I^+)$. Define also the real and imaginary parts of the vector \mathbf{A} and the matrix B by

$$A_j(\boldsymbol{\alpha}) = A_R^j(\boldsymbol{\alpha}_R, \boldsymbol{\alpha}_I) + iA_I^j(\boldsymbol{\alpha}_R, \boldsymbol{\alpha}_I), \quad (2.76a)$$

$$B_{jl}(\boldsymbol{\alpha}) = B_R^{jl}(\boldsymbol{\alpha}_R, \boldsymbol{\alpha}_I) + iB_I^{jl}(\boldsymbol{\alpha}_R, \boldsymbol{\alpha}_I). \quad (2.76b)$$

The analyticity of $\hat{\Lambda}(\boldsymbol{\alpha})$ allows us to choose the derivatives ∂_j as ∂_j^R or $-i\partial_j^I$ at will, where we use the notation $\partial/\partial\alpha_R = \partial_\alpha^R$ and $\partial/\partial\alpha_I = \partial_\alpha^I$ (similarly for α^+), and we choose them so that the differential operator inside the square brackets reads

$$\sum_j \left(A_R^j \partial_j^R + A_I^j \partial_j^I \right) + \frac{1}{2} \sum_{jlm} \left(B_R^{jm} B_R^{lm} \partial_j^R \partial_l^R + 2B_R^{jm} B_I^{lm} \partial_j^R \partial_l^I + B_I^{jm} B_I^{lm} \partial_j^I \partial_l^I \right), \quad (2.77)$$

for future convenience.

The main result of the section is obtained by performing an integration by parts in (2.73) to make the derivatives act onto $P(\boldsymbol{\alpha}; t)$ instead of onto the projector $\hat{\Lambda}(\boldsymbol{\alpha})$, what leads to

$$\partial_t P(\boldsymbol{\alpha}; t) = \left[- \sum_j \left(\partial_j^R A_R^j + \partial_j^I A_I^j \right) + \frac{1}{2} \sum_{jlm} \left(\partial_j^R \partial_l^R B_R^{jm} B_R^{lm} + 2\partial_j^R \partial_l^I B_R^{jm} B_I^{lm} + \partial_j^I \partial_l^I B_I^{jm} B_I^{lm} \right) \right] P(\boldsymbol{\alpha}; t), \quad (2.78)$$

where we have used the fact that physical states must correspond to positive P distributions which decay to zero at infinity, so that we can get rid of the total derivative terms appearing upon integrating by parts. Hence, we have turned the operator equation (2.71) into a linear partial differential equation for the P distribution. Indeed, this equation is a very special one. By defining the vector $\vec{\mathcal{A}} = \text{col}(A_R^\alpha, A_R^{\alpha^+}, A_I^\alpha, A_I^{\alpha^+})$ and the matrix

$$\mathcal{D} = \begin{bmatrix} B_R B_R^T & B_R B_I^T \\ B_I B_R^T & B_I B_I^T \end{bmatrix} = \mathcal{B} \mathcal{B}^T \quad \text{with} \quad \mathcal{B} = \begin{bmatrix} B_R & 0_{2 \times 2} \\ B_I & 0_{2 \times 2} \end{bmatrix}, \quad (2.79)$$

we can write it in the more compact way

$$\partial_t P(\mathbf{x}; t) = \left[- \sum_{j=1}^4 \partial_j \mathcal{A}_j(\mathbf{x}) + \frac{1}{2} \sum_{jl=1}^4 \partial_j \partial_l \mathcal{D}_{jl}(\mathbf{x}) \right] P(\mathbf{x}; t), \quad (2.80)$$

where we have defined the vector $\mathbf{x} = \text{col}(\alpha_R, \alpha_R^+, \alpha_I, \alpha_I^+)$. When the matrix \mathcal{D} is positive semidefinite, as it is in our case, this is known as the *Fokker–Planck equation* [61]; this equation has been subject of study for a very long time, and we have a lot of different techniques available to solve it or extract information from it. $\vec{\mathcal{A}}$, \mathcal{D} , and \mathcal{B} , are known as the *drift vector*, the *diffusion matrix*, and the *noise matrix*, respectively.

For this thesis, the most important property of Fokker–Planck equations is its relation to stochastic equations. In particular, it can be proved that any Fokker–Planck equation written in the form (2.80) is equivalent to the following system of *stochastic equations* [61]

$$\dot{\mathbf{x}} = \vec{\mathcal{A}}(\mathbf{x}) + \mathcal{B}(\mathbf{x}) \boldsymbol{\eta}(t), \quad (2.81)$$

where $\boldsymbol{\eta}(t) = \text{col}[\eta_1(t), \eta_2(t), \eta_3(t), \eta_4(t)]$ is a vector whose elements are independent, real, Gaussian noises which satisfy the statistical properties

$$\langle \eta_j(t) \rangle = 0 \quad \text{and} \quad \langle \eta_j(t) \eta_l(t') \rangle = \delta_{jl} \delta(t - t'). \quad (2.82)$$

We will call *stochastic Langevin equations* to these equations. The equivalence between them and the original Fokker–Planck equation must be understood in the “average” sense, that is, given any function $F(\mathbf{x})$, we can find its average either by using the distribution $P(\mathbf{x}; t)$ or the solutions $\mathbf{x}[\boldsymbol{\eta}(t)]$ of the variables in terms of noise integrals as

$$\int_{\mathbb{R}^4} d^4 \mathbf{x} F(\mathbf{x}) P(\mathbf{x}; t) = \langle F\{\mathbf{x}[\boldsymbol{\eta}(t)]\} \rangle. \quad (2.83)$$

Given the simple structure of \mathcal{B} , see (2.79), we can rewrite the Langevin equations in the complex form

$$\dot{\boldsymbol{\alpha}} = \mathbf{A}(\boldsymbol{\alpha}) + B(\boldsymbol{\alpha}) \boldsymbol{\eta}(t), \quad (2.84)$$

where $\boldsymbol{\eta}(t) = \text{col}[\eta_1(t), \eta_2(t)]$ is in this case a two-dimensional vector. This is an amazingly simple final result: As complex stochastic variables, α and α^+ evolve according to a set of Langevin equations built with the original \mathbf{A} and $D = BB^T$. Then, whenever we are able to rewrite an arbitrary master equation in the form (2.73) by using the positive P representation, we can directly write down equations (2.84) for the coherent amplitudes of the system.

Applied to our purposes, this means that given the solution $\boldsymbol{\alpha} = \boldsymbol{\alpha}[\boldsymbol{\eta}(t)]$ of equation (2.84), we can evaluate the quantum expectation value of any operator $\hat{A}(\hat{a}, \hat{a}^\dagger)$ as

$$\langle \hat{A} \rangle = \langle A^{(n)}(\alpha, \alpha^+) \rangle_P, \quad (2.85)$$

where in the following we will denote by $\langle \dots \rangle_P$ to any stochastic average obtained from the Langevin equations within the positive P representation.

There is one subtlety that we have not mentioned though. Without entering into much detail (see [61] for a deep discussion), a stochastic equation can be interpreted in infinitely many inequivalent ways, which attend to how the integrals involving noise are defined in the Riemann sense, that is, as a limit of some series. The connection we made between the Fokker–Planck equation and the Langevin equations is only valid if the stochastic equations are interpreted in a very particular form first defined by Ito (the so-called *Ito interpretation*). The problem with this interpretation is that integration is defined in such a way that the rules of calculus as we know them no longer apply, and one needs to use a new form of calculus called *Ito calculus*. Integrals can be defined in a way which allows us to use the usual rules of calculus, arriving then to the so-called *Stratonovich interpretation* of stochastic equations. However, there is a price to pay: Interpreted in such way, the set of stochastic equations associated to the Fokker–Planck equation (2.80) is no longer (2.84), but the same type of equation with a different deterministic part given by

$$A_j^{(\text{St})}(\boldsymbol{\alpha}) = A_j(\boldsymbol{\alpha}) - \frac{1}{2} \sum_{lm} B_{lm}(\boldsymbol{\alpha}) \partial_l B_{jm}(\boldsymbol{\alpha}), \quad \text{with} \quad j, l, m = \alpha, \alpha^+, \quad (2.86)$$

that is, the deterministic part of the equations acquires an extra term which depends on the noise matrix. In this thesis we shall always use this Stratonovich form. Nevertheless, note that if the noise matrix does not depend on the coherent amplitudes $\boldsymbol{\alpha}$, both forms are the same, that is, Ito and Stratonovich interpretations differ only when noise is multiplicative, not additive. This is indeed the case in our simple example (2.74,2.75), whose associated set of complex Langevin equations are given by

$$\dot{\alpha} = \mathcal{E} - (\gamma + i\omega)\alpha + 2\kappa\alpha^+ + \sqrt{2\kappa}\eta_1(t), \quad (2.87a)$$

$$\dot{\alpha}^+ = \mathcal{E}^* - (\gamma - i\omega)\alpha^+ + 2\kappa^*\alpha + \sqrt{2\kappa^*}\eta_2(t), \quad (2.87b)$$

both within the Ito and Stratonovich interpretations.

3. QUANTIZATION OF THE ELECTROMAGNETIC FIELD IN AN OPTICAL CAVITY

The goal of this chapter is the quantization of the electromagnetic field inside an optical cavity with perfectly reflecting mirrors. We will follow a heuristic, but physically intuitive approach in which the electromagnetic field is put in correspondence with a collection of harmonic oscillators. Nevertheless, we would like to note that the quantization of the electromagnetic field can be carried out in a more rigorous fashion by generalizing the method that we described for mechanical systems in the previous chapter and in Appendix A; this procedure relies on a Lagrangian theory of fields, and is called *canonical quantization* [16].

In order to show how the heuristic procedure works, we will first apply the method to a simple, but highly relevant case: The quantization of the electromagnetic field in free space. This will allow us to introduce plane-waves as well as the concept of polarization. We then pass to describe optical beams within the paraxial approximation, and discuss the modal decomposition of such fields in terms of transverse modes. We finally consider the electromagnetic field inside a stable optical cavity and proceed to its quantization.

3.1 Light as an electromagnetic wave

Nowadays it feels quite natural to say that *light* is an *electromagnetic wave*. Arriving to this conclusion, however, was not trivial at all. The history of such a discovery starts in the first half of the XIX century with Faraday, who showed that the polarization of light can change when subject to a magnetic field; this was the first hint suggesting that there could be a connection between light and electromagnetism, and he was the first to propose that light could be an electromagnetic disturbance of some kind, able to propagate without the need of a reference medium. However, this qualitative idea did not find a rigorous mathematical formulation until the second half of the century, when Maxwell developed a consistent theory of electromagnetism, and showed how the theory was able to predict the existence of electromagnetic waves propagating at a speed which was in agreement with the speed measured for light at that time [62]. A couple of decades after his proposal, the existence of electromagnetic waves was experimentally demonstrated by Hertz [63], and the theory of light as an electromagnetic wave found its way towards being accepted.

Our starting point are Maxwell's equations formulated as partial differential equations for the *electric* and *magnetic*¹ vector fields $\mathbf{E}(\mathbf{r}, t)$ and $\mathbf{B}(\mathbf{r}, t)$, respectively, where $\mathbf{r}(t)$ is the position (time) where (when) the fields are observed. This formulation is due to Heaviside [64], as Maxwell originally proposed his theory in terms of *quaternions*. The theory consists of four equations; the first two are called the *homogeneous Maxwell equations* and read

$$\nabla \cdot \mathbf{B} = 0 \quad \text{and} \quad \nabla \times \mathbf{E} = -\partial_t \mathbf{B}, \quad (3.1)$$

where $\nabla = (\partial_x, \partial_y, \partial_z)$. The other two are called the *inhomogeneous Maxwell equations* and are written as

$$\nabla \cdot \mathbf{E} = \rho/\varepsilon_0 \quad \text{and} \quad \nabla \times \mathbf{B} = \mu_0 \varepsilon_0 \partial_t \mathbf{E} + \mu_0 \mathbf{j}, \quad (3.2)$$

where any electric or magnetic source is introduced in the theory by a *charge density* function $\rho(\mathbf{r}, t)$ and a *current distribution* vector $\mathbf{j}(\mathbf{r}, t)$, respectively; the parameters $\varepsilon_0 = 8.8 \times 10^{-12}$ F/m and $\mu_0 = 1.3 \times 10^{-6}$ H/m are the so-called *electric permittivity* and the *magnetic permeability* of vacuum, respectively.

We will show the process of quantization of the electromagnetic field in the absence of sources ($\rho = 0$ and $\mathbf{j} = \mathbf{0}$). Under these circumstances, the inhomogeneous equations are simplified to

$$\nabla \cdot \mathbf{E} = 0 \quad \text{and} \quad c^2 \nabla \times \mathbf{B} = \partial_t \mathbf{E}, \quad (3.3)$$

where $c = 1/\sqrt{\varepsilon_0 \mu_0} \simeq 3 \times 10^8$ m/s.

The homogeneous equations (3.1) allow us to derive the fields from a *scalar potential* $\phi(\mathbf{r}, t)$ and a *vector potential* $\mathbf{A}(\mathbf{r}, t)$ as

$$\mathbf{B} = \nabla \times \mathbf{A} \quad \text{and} \quad \mathbf{E} = -\nabla \phi - \partial_t \mathbf{A}, \quad (3.4)$$

¹ As we won't deal with materials sensitive to the magnetic field, we will use the term "magnetic field" for the \mathbf{B} -field, which is usually denoted by "magnetic induction field" when it needs to be distinguished from the \mathbf{H} -field (which we won't be using in this thesis).

hence reducing to four the degrees of freedom of the electromagnetic field. These potentials, however, are not unique; we can always use an arbitrary function $\Lambda(\mathbf{r}, t)$ to change them as

$$\mathbf{A} \rightarrow \mathbf{A} + \nabla\Lambda \quad \text{and} \quad \phi \rightarrow \phi - \partial_t\Lambda, \quad (3.5)$$

what is known as the *gauge invariance* of Maxwell's equations.

Introducing (3.4) into the inhomogeneous equations we get the equations satisfied by the potentials

$$(c^2\nabla^2 - \partial_t^2)\mathbf{A} = \partial_t\nabla\phi + c^2\nabla(\nabla\cdot\mathbf{A}) \quad (3.6a)$$

$$\nabla^2\phi + \partial_t\nabla\cdot\mathbf{A} = 0. \quad (3.6b)$$

The problem is highly simplified if we exploit the gauge invariance and choose $\nabla\cdot\mathbf{A} = 0$, as the second equation can be shown to further imply that $\phi = 0$ for physical fields vanishing at infinity, and hence the only equations left are

$$(c^2\nabla^2 - \partial_t^2)\mathbf{A} = \mathbf{0} \quad (3.7)$$

which are wave equations with speed c for the components of the vector potential. Note that the condition $\nabla\cdot\mathbf{A} = 0$ (known as the *Coulomb condition*) relates the three components of \mathbf{A} , and hence, only two degrees of freedom of the initial six (the electric and magnetic vector fields) remain.

It is finally important to note that the wave equation (3.7) has a unique solution inside a given spatio-temporal region only if both the vector potential and its derivative along the direction normal to the boundary of the region are specified at any point of the boundary [65]; these are known as *Dirichlet* and *Neumann* conditions, respectively. In general, however, physical problems do not impose all those constraints, and hence there coexist several solutions of the wave equation, which we will call *spatio-temporal modes* of the system.

In all the optical systems that we will treat, we will be able to write these solutions in the form $\varepsilon A(\mathbf{r}, t)$, with ε a constant unit vector and $A(\mathbf{r}, t)$ a function of space and time; this is called the *scalar approximation*, and can be made when the system looks the same for the two independent components of the vector potential (for example, both components must be subject to the same boundary conditions). In addition, it will be convenient to look for solutions separable in space and time, that is, $A(\mathbf{r}, t) = u(\mathbf{r})\mathcal{A}(t)$. We will see that the connection with the harmonic oscillator is made through the temporal part of the solutions. As for the spatial part, introducing the separable ansatz in the wave equation, we find that it must satisfy the equation

$$\nabla^2 u + k^2 u = 0, \quad (3.8)$$

where k^2 is a suitable *separation constant*. This is a Helmholtz equation, which yields a unique solution inside a given volume only if the Dirichlet or Neumann conditions are given for $u(\mathbf{r})$ [65]. If the boundary conditions are less restrictive than these, several solutions $\{u_n(\mathbf{r})\}$ appear corresponding to the eigenfunctions of the differential operator ∇^2 , which is a self-adjoint differential operator called *Laplacian*, whose corresponding eigenvalues $\{-k_n^2\}$ can be shown to be all negative. These solutions are known as the *spatial modes* of the system, and play a central role in the heuristic quantization procedure that we will follow.

3.2 Quantization in free space: Plane waves and polarization

3.2.1 Quantization in terms of plane waves

The scalar approximation works fine in free space, as by definition it has no boundaries. This also means that the Helmholtz equation (3.8) has to be solved in all \mathbb{R}^3 . In this case, the eigenfunctions of the Laplacian form a continuous set given by $\{\exp(i\mathbf{k}\cdot\mathbf{r})\}_{\mathbf{k}\in\mathbb{R}^3}$, with corresponding eigenvalues $\{-|\mathbf{k}|^2\}_{\mathbf{k}\in\mathbb{R}^3}$. Hence, the solutions of the wave equation will be of the type $\varepsilon(\mathbf{k})\mathcal{A}(\mathbf{k}, t)\exp(i\mathbf{k}\cdot\mathbf{r})$. Moreover, the Coulomb condition imposes that $\mathbf{k}\cdot\varepsilon(\mathbf{k}) = 0$, that is, the vector potential is orthogonal to the mode vectors \mathbf{k} ; this means that for any \mathbf{k} we can define two vectors $\varepsilon_1(\mathbf{k})$ and $\varepsilon_2(\mathbf{k})$, which are called the *polarization vectors*, satisfying the relations

$$\mathbf{k}\cdot\varepsilon_\sigma(\mathbf{k}) = 0, \quad (\sigma = 1, 2) \quad (3.9a)$$

$$\varepsilon_\sigma^*(\mathbf{k})\cdot\varepsilon_{\sigma'}(\mathbf{k}) = \delta_{\sigma\sigma'}, \quad (\sigma, \sigma' = 1, 2) \quad (3.9b)$$

$$\varepsilon_1^*(\mathbf{k})\times\varepsilon_2(\mathbf{k}) = \mathbf{k}/k \equiv \boldsymbol{\kappa}, \quad (3.9c)$$

with $k = |\mathbf{k}|$, so that we can make the following modal expansion of the vector potential:

$$\mathbf{A}(\mathbf{r}, t) = \sum_{\sigma=1,2} \int_{\mathbb{R}^3} d^3\mathbf{k} \varepsilon_\sigma(\mathbf{k}) \mathcal{A}_\sigma(\mathbf{k}, t) \exp(i\mathbf{k}\cdot\mathbf{r}). \quad (3.10)$$

Note that the reality of the vector potential imposes that

$$\varepsilon_\sigma^*(\mathbf{k}) \mathcal{A}_\sigma^*(\mathbf{k}, t) = \varepsilon_\sigma(-\mathbf{k}) \mathcal{A}_\sigma(-\mathbf{k}, t). \quad (3.11)$$

From the wave equation, we get that the temporal part of the vector potential satisfies the equation

$$\left[\frac{d^2}{dt^2} + \omega^2(\mathbf{k}) \right] \mathcal{A}_\sigma(\mathbf{k}, t) = 0, \quad (3.12)$$

with $\omega(\mathbf{k}) = ck$. Being this the equation of motion of a harmonic oscillator, one might be tempted to directly interpret the modal amplitudes $\mathcal{A}_\sigma(\mathbf{k}, t)$ as the positions of harmonic oscillators associated to the different modes; however, $\mathcal{A}_\sigma(\mathbf{k}, t)$ is not real in general, and hence we need another strategy to make the connection with the harmonic oscillator. The idea is to define

$$\nu_\sigma(\mathbf{k}, t) = \frac{1}{\Gamma} \left[\mathcal{A}_\sigma(\mathbf{k}, t) + \frac{i}{\omega_k} \dot{\mathcal{A}}_\sigma(\mathbf{k}, t) \right], \quad (3.13)$$

where Γ is a real parameter that will be chosen later, which satisfies the equation

$$\dot{\nu}_\sigma(\mathbf{k}, t) = -i\omega(\mathbf{k}) \nu_\sigma(\mathbf{k}, t) \implies \nu_\sigma(\mathbf{k}, t) = \nu_\sigma(\mathbf{k}) \exp[-i\omega(\mathbf{k})t], \quad (3.14)$$

where we denote $\nu_\sigma(\mathbf{k}, 0)$ simply by $\nu_\sigma(\mathbf{k})$; this expression shows that $\nu_\sigma(\mathbf{k}, t)$ and $\nu_\sigma^*(\mathbf{k}, t)$ are subject to the same evolution as that of the normal variables of a harmonic oscillator, see Section 2.1.

This approach shows that the modes of the electromagnetic field behave as harmonic oscillators of frequency $\omega(\mathbf{k})$ having $\{\nu_\sigma(\mathbf{k}, t), \nu_\sigma^*(\mathbf{k}, t)\}_{\mathbf{k} \in \mathbb{R}^3}$ as normal variables. Indeed, we can show that the electromagnetic energy, which is defined in vacuum as the integral

$$E_{\text{em}} = \frac{1}{2} \int d^3\mathbf{r} \left[\varepsilon_0 \mathbf{E}^2(\mathbf{r}, t) + \frac{1}{\mu_0} \mathbf{B}^2(\mathbf{r}, t) \right], \quad (3.15)$$

can be written as the Hamiltonian of this collection of harmonic oscillators. By using the modal expansion of the vector potential (3.10) and its relation with the electric and magnetic fields (3.4), it is straightforward to show that

$$E_{\text{em}} = 4\pi^3 \varepsilon_0 \sum_{\sigma=1,2} \int_{\mathbb{R}^3} d^3\mathbf{k} \left[|\dot{\mathcal{A}}_\sigma(\mathbf{k}, t)|^2 + \omega_k^2 |\mathcal{A}_\sigma(\mathbf{k}, t)|^2 \right]. \quad (3.16)$$

Now, inverting the relations (3.13) we get

$$\mathcal{A}_\sigma(\mathbf{k}, t) = \frac{\Gamma}{2} [\nu_\sigma(\mathbf{k}, t) + \nu_\sigma^*(-\mathbf{k}, t)], \quad (3.17a)$$

$$\dot{\mathcal{A}}_\sigma(\mathbf{k}, t) = \frac{\omega_k \Gamma}{2i} [\nu_\sigma(\mathbf{k}, t) - \nu_\sigma^*(-\mathbf{k}, t)], \quad (3.17b)$$

from which one trivially obtains

$$E_{\text{em}} = 4\pi^3 \varepsilon_0 \Gamma^2 \sum_{\sigma=1,2} \int_{\mathbb{R}^3} d^3\mathbf{k} \omega^2(\mathbf{k}) \nu_\sigma^*(\mathbf{k}, t) \nu_\sigma(\mathbf{k}, t). \quad (3.18)$$

Hence, by choosing $\Gamma = 1/\sqrt{8\pi^3 \varepsilon_0}$, the final expression for the electromagnetic energy reads

$$E_{\text{em}} = \sum_{\sigma=1,2} \int_{\mathbb{R}^3} d^3\mathbf{k} \frac{\omega^2(\mathbf{k})}{2} \nu_\sigma^*(\mathbf{k}) \nu_\sigma(\mathbf{k}), \quad (3.19)$$

which is exactly a sum of the Hamiltonians for each harmonic oscillator of frequency $\omega(\mathbf{k})$ with normal variables $\{\nu_\sigma(\mathbf{k}, t), \nu_\sigma^*(\mathbf{k}, t)\}_{\mathbf{k} \in \mathbb{R}^3}$ and unit mass.

These derivations suggest that we can treat the electromagnetic field as a mechanical system consisting of a (continuous) collection of harmonic oscillators, and quantize it accordingly, that is, by replacing the normal variables of each oscillator $\{\nu_\sigma(\mathbf{k}, t), \nu_\sigma^*(\mathbf{k}, t)\}_{\mathbf{k} \in \mathbb{R}^3}$ by the set $\sqrt{2\hbar/\omega(\mathbf{k})} \{\hat{a}_\sigma(\mathbf{k}, t), \hat{a}_\sigma^\dagger(\mathbf{k}, t)\}_{\mathbf{k} \in \mathbb{R}^3}$ of *boson operators*, where the annihilation and creation operators satisfy the commutation relations

$$[\hat{a}_\sigma(\mathbf{k}, t), \hat{a}_{\sigma'}^\dagger(\mathbf{k}', t)] = \delta_{\sigma\sigma'} \delta^3(\mathbf{k} - \mathbf{k}'), \quad (3.20a)$$

$$[\hat{a}_\sigma(\mathbf{k}, t), \hat{a}_{\sigma'}(\mathbf{k}', t)] = [\hat{a}_\sigma^\dagger(\mathbf{k}, t), \hat{a}_{\sigma'}^\dagger(\mathbf{k}', t)] = 0. \quad (3.20b)$$

Photons are then associated to the excitations of each electromagnetic oscillator (σ, \mathbf{k}) .

According to the quantization scheme that we used in the previous chapter for the harmonic oscillator, the Hamiltonian for the electromagnetic field in free space is then found from (3.19) as

$$\hat{H}_{\text{em}} = \sum_{\sigma=1,2} \int_{\mathbb{R}^3} d^3\mathbf{k} \frac{\hbar\omega(\mathbf{k})}{2} [\hat{a}_\sigma^\dagger(\mathbf{k}) \hat{a}_\sigma(\mathbf{k}) + \hat{a}_\sigma(\mathbf{k}) \hat{a}_\sigma^\dagger(\mathbf{k})]. \quad (3.21)$$

Using the commutation relations (3.20a) we can rewrite it in the following normal form

$$\hat{H}_{\text{em}} = \sum_{\sigma=1,2} \int_{\mathbb{R}^3} d^3\mathbf{k} \hbar\omega(\mathbf{k}) \hat{a}_\sigma^\dagger(\mathbf{k}) \hat{a}_\sigma(\mathbf{k}) + 4\pi\hbar\delta^3(\mathbf{0}) \int_0^\infty dk k^3 \equiv: \hat{H}_{\text{em}} : + E_\infty. \quad (3.22)$$

The first contribution is like \hat{H}_{em} but where the boson operators have been reordered in normal order as if they were usual numbers, that is, without making use of the commutation relations, an operation that we denote by $: \hat{A}(\hat{a}, \hat{a}^\dagger) :$ for any operator in the following. The second contribution, on the other hand, is a number, but an infinite one. Note however, that it contributes as a global phase to the time evolution operator, and it is therefore not observable, what allows us to redefine the origin of the energy such as this contribution is removed².

The vector potential becomes then an operator $\hat{\mathbf{A}}(\mathbf{r}, t) = \hat{\mathbf{A}}^{(+)}(\mathbf{r}, t) + \hat{\mathbf{A}}^{(-)}(\mathbf{r}, t)$, with

$$\hat{\mathbf{A}}^{(+)}(\mathbf{r}, t) = \sum_{\sigma=1,2} \int_{\mathbb{R}^3} d^3\mathbf{k} \sqrt{\frac{\hbar}{16\pi^3\epsilon_0\omega(\mathbf{k})}} \boldsymbol{\varepsilon}_\sigma(\mathbf{k}) \hat{a}_\sigma(\mathbf{k}) \exp[-i\omega(\mathbf{k})t + i\mathbf{k} \cdot \mathbf{r}] = [\hat{\mathbf{A}}^{(-)}(\mathbf{r}, t)]^\dagger. \quad (3.23)$$

This decomposition of the vector potential in terms of $\hat{\mathbf{A}}^{(\pm)}(\mathbf{r}, t)$, usually called its *positive-frequency* and *negative-frequency* parts, will be used for every field from now on; we will sometimes refer to either part by itself as “the field” The electric and magnetic fields are described then by the operators

$$\hat{\mathbf{E}}^{(+)}(\mathbf{r}, t) = i \int_{\mathbb{R}^3} d^3\mathbf{k} \sqrt{\frac{\hbar\omega(\mathbf{k})}{16\pi^3\epsilon_0}} \boldsymbol{\varepsilon}_\sigma(\mathbf{k}) \hat{a}_\sigma(\mathbf{k}) \exp[-i\omega(\mathbf{k})t + i\mathbf{k} \cdot \mathbf{r}], \quad (3.24a)$$

$$\hat{\mathbf{B}}^{(+)}(\mathbf{r}, t) = i \sum_{\sigma=1,2} \int_{\mathbb{R}^3} d^3\mathbf{k} \sqrt{\frac{\hbar}{16\pi^3\epsilon_0\omega(\mathbf{k})}} [\mathbf{k} \times \boldsymbol{\varepsilon}_\sigma(\mathbf{k})] \hat{a}_\sigma(\mathbf{k}) \exp[-i\omega(\mathbf{k})t + i\mathbf{k} \cdot \mathbf{r}]; \quad (3.24b)$$

this is consistent with quantum mechanics, as being observable quantities, the fields must correspond to self-adjoint operators. Note that all these expressions are given within the Heisenberg picture, as the operators evolve in time.

Note finally that the spatio-temporal modes of the problem have the functional form $\exp[-i\omega(\mathbf{k})t + i\mathbf{k} \cdot \mathbf{r}]$. These modes are called *plane-waves*. They are “plane” because all the points laying in the plane $\mathbf{k} \cdot \mathbf{r} = \text{const}$ take the same value of the mode; they are “waves” because the mode at the space time point (\mathbf{r}, t) has the same value that it had at $(\mathbf{r} - c\boldsymbol{\kappa}t, 0)$, and hence these modes can be visualized as a plane propagating at speed c along the direction of $\boldsymbol{\kappa}$. We will call *wave vector* to \mathbf{k} in the following. Our eyes are sensitive to electromagnetic waves having frequencies $\omega(\mathbf{k})$ between 2.5×10^{15} Hz (red) to 5×10^{15} Hz (violet), or equivalently *wavelengths* $\lambda = 2\pi/k$ between 760 nm and 380 nm, which are customarily called *light*; in this thesis we will focus on this region of the *electromagnetic spectrum* (which sometimes is extended to the near infrared or ultraviolet), which we will refer to as *optical domain*.

3.2.2 Vector character of the fields and polarization

Let us explain now a property of the electromagnetic field that we will be using in several parts of this thesis, the *polarization*. To this aim we come back to a classical description of the electromagnetic field.

Consider a Cartesian system defined by the triad $\{\mathbf{e}_x, \mathbf{e}_y, \mathbf{e}_z\}$ of unit length vectors. Consider now an electromagnetic field described by a plane-wave mode propagating along the \mathbf{e}_z direction, and having definite frequency ω and polarization vector $\boldsymbol{\varepsilon}$, whose vector potential is given by

$$\mathbf{A}(\mathbf{r}, t) = \frac{A_0}{2} \boldsymbol{\varepsilon} \exp(-i\omega t + ikz) + \text{c.c.}, \quad (3.25)$$

² There are certain situations (like the *Casimir effect* or the *Lamb shift*) in which this term has observable consequences, and the theory must be properly *renormalized*. We will however not find such situations in this thesis, and hence a direct removal of these infinite quantities leads to the proper results.

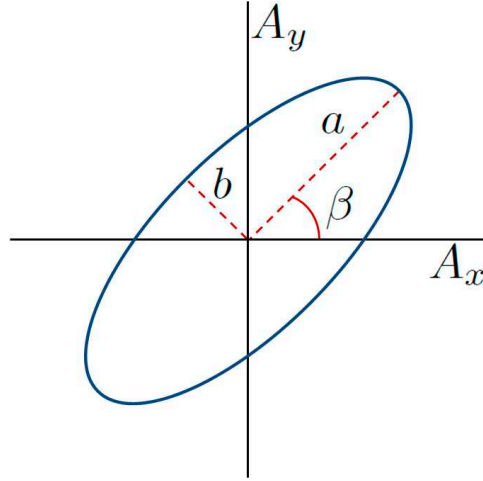


Fig. 3.1: Ellipse described by the components of the vector potential as they evolve.

with A_0 some amplitude that we take real and positive without loss of generality. The associated electric and magnetic fields are given by

$$\mathbf{E}(\mathbf{r}, t) = i \frac{\omega A_0}{2} \boldsymbol{\varepsilon} \exp(-i\omega t + ikz) + \text{c.c.}, \quad (3.26a)$$

$$\mathbf{B}(\mathbf{r}, t) = i \frac{k A_0}{2} [\mathbf{e}_z \times \boldsymbol{\varepsilon}] \exp(-i\omega t + ikz) + \text{c.c.}; \quad (3.26b)$$

the first interesting thing that we observe is that the electric and magnetic fields are not only orthogonal to the propagation direction (we say that they are *transverse fields*), but also to each other.

Suppose now that we observe the time evolution of the electric field at a given position which we take as $\mathbf{r} = \mathbf{0}$ to simplify the upcoming discussion. Let us parametrize with full generality the polarization vector as

$$\boldsymbol{\varepsilon}(\theta, \varphi) = \mathbf{e}_x \exp(-i\theta) \cos \varphi + \mathbf{e}_y \exp(i\theta) \sin \varphi, \quad (3.27)$$

with $\theta \in [0, \pi]$ and $\varphi \in [0, \pi/2]$. At the observation point, the vector potential takes the simple form

$$\mathbf{A}(t) = \begin{pmatrix} \cos \varphi \cos(\omega t + \theta) \\ \sin \varphi \cos(\omega t - \theta) \end{pmatrix}, \quad (3.28)$$

where we have taken $A_0 = 1$ for simplicity, and we have represented \mathbf{A} in our Cartesian system, but obviating the z component which is always zero given the transversality of the fields. It is not difficult to realize that, starting at the point $\mathbf{A}(0) = (\cos \varphi \cos \theta, \sin \varphi \cos \theta)$, this vector describes an ellipse in the $x - y$ plane as time increases, as shown in Figure 3.1. Let us call a and b to the *semi-major* and *semi-minor axes* of this ellipse (positive definite), and $\beta \in [-\pi/2, \pi/2]$ to its *orientation* (the angle that its major axis forms with the x axis). The orientation of this ellipse, called the *polarization ellipse*, is given by

$$\tan 2\beta = \tan 2\varphi \cos 2\theta, \quad (3.29)$$

while defining an auxiliary angle $\chi \in [-\pi/4, \pi/4]$ from $\sin 2\chi = \sin 2\varphi \sin 2\theta$, the semi-major and semi-minor axes are given by

$$a^2 = \frac{1}{1 + \tan^2 \chi} \quad \text{and} \quad b^2 = \frac{\tan^2 \chi}{1 + \tan^2 \chi}.$$

Hence, the eccentricity of the ellipse is

$$e = \sqrt{1 - \tan^2 \chi}, \quad (3.30)$$

for $e = 1$ ($\chi = 0$) the ellipse degenerates into a straight line, while for $e = 0$ ($\chi = \pm\pi/4$) the ellipse is a circumference. In the first (second) case we say that light has *linear* (*circular*) polarization. Of special interest for this thesis is the case $\varphi = \pi/4$. In this case, the orientation of the ellipse is $\beta = \pm\pi/4$, and the polarization changes from linear to circular (and from right to left, see below) depending on the angle θ as shown in Figure 3.2.

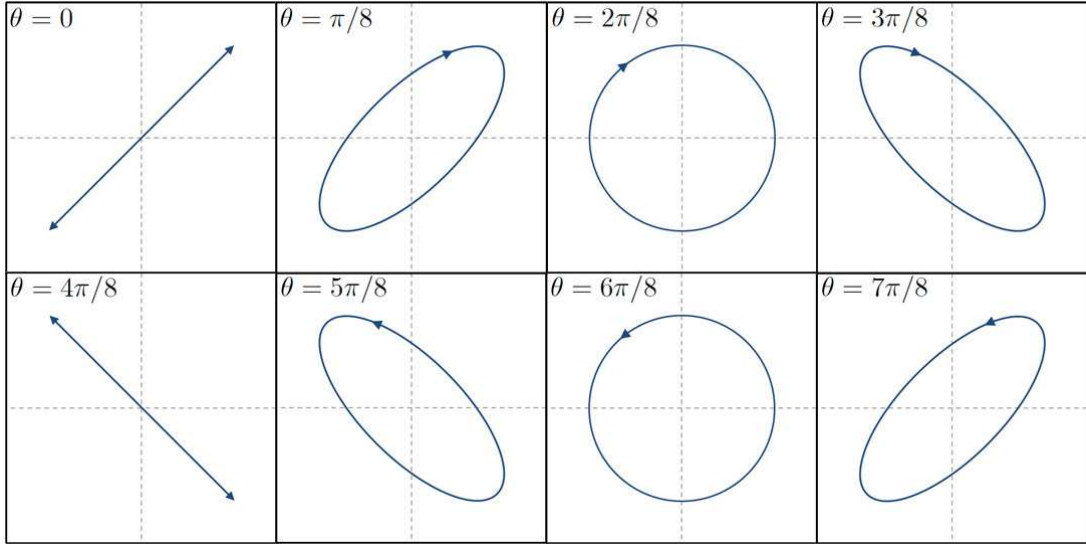


Fig. 3.2: Polarization ellipse for $\varphi = \pi/4$. Note how the polarization changes from linear to circular and from left to right as a function of θ , but the ellipse is always oriented along the $\pm\pi/4$ axes.

The vector potential can then be seen as a point in the polarization ellipse rotating around it with angular frequency ω *clockwise* or *anticlockwise* for $\sin 2\theta > 0$ and $\sin 2\theta < 0$, respectively. In the first (second) case we say that light has *right* (*left*) *elicity*.

3.3 Paraxial optics and transverse modes

In the previous section we have quantized the electromagnetic field by using a modal decomposition based on plane waves propagating in all possible directions. However, we have seen that plane waves have an infinite transverse size, and hence cannot describe real fields, which have a finite extent. In this section we are going to introduce another set of modes which are better adapted to the optical scenarios that we will treat along this thesis, and can even be generated in laboratories.

3.3.1 Optical beams and the paraxial approximation

In this thesis we will deal with the electromagnetic field in the form of *optical beams*, that is, light propagating nearly within a given direction, which we take as the z axis. The vector potential of any such beam can be written as

$$\mathbf{A}(\mathbf{r}, t) = \int_{\mathcal{O}} dk_z \tilde{\mathbf{A}}(k_z; \mathbf{r}_\perp, z, t) \exp(ik_z z), \quad (3.31)$$

where \mathcal{O} refers to wave vectors k_z such that $\lambda = 2\pi/|k_z|$ is in the optical domain, $\mathbf{r}_\perp = (x, y)$ are the *transverse coordinates*, and $\tilde{\mathbf{A}}(k_z; \mathbf{r}_\perp, z, t)$ is an amplitude which, compared to $|k_z|$, varies slowly both along the *longitudinal axis* and the *transverse plane* generated, respectively, by \mathbf{e}_z and $\{\mathbf{e}_x, \mathbf{e}_y\}$, that is,

$$|\partial_z^2 \tilde{\mathbf{A}}| \ll |k_z \partial_z \tilde{\mathbf{A}}| \ll k_z^2 |\tilde{\mathbf{A}}| \quad (3.32a)$$

$$|\nabla_\perp \cdot \tilde{\mathbf{A}}| \ll |k_z \tilde{\mathbf{A}}|, \quad (3.32b)$$

where $\nabla_\perp = (\partial_x, \partial_y)$. These generalizations of plane waves are called *paraxial waves*. It is easy to prove that the polarization properties of $\tilde{\mathbf{A}}(k_z; \mathbf{r}_\perp, z, t)$ are just as those of plane waves (we say that the *polarization degrees of freedom* decouple from the *spatio-temporal* ones), so that we can still work under the scalar approximation as in the previous section, and look for solutions of the wave equation of the type $\epsilon(k_z) \mathcal{A}(k_z, t) u(k_z; \mathbf{r}_\perp, z) \exp(ik_z z)$.

$u(k_z; \mathbf{r}_\perp, z)$ satisfies the slowly varying conditions (3.32), what allows us to rewrite the Helmholtz equation as

$$(2ik_z \partial_z + \nabla_\perp^2) u(k_z; \mathbf{r}_\perp, z) = 0. \quad (3.33)$$

The solution of this equation is unique provided that the transverse structure of $u(k_z; \mathbf{r}_\perp, z)$ is given at one plane $z = z_0$; indeed, this solution can be written in the integral form [66]

$$u(k_z; \mathbf{r}_\perp, z) = -\frac{ik_z}{2\pi(z-z_0)} \int_{\mathbb{R}^2} d^2\mathbf{r}'_\perp u(k_z; \mathbf{r}'_\perp, z_0) \exp\left[-\frac{ik_z}{2(z-z_0)} (\mathbf{r}_\perp - \mathbf{r}'_\perp)^2\right]. \quad (3.34)$$

Hence, an optical beam can be visualized as a *transverse pattern* propagating along the longitudinal axis, whose shape is changing owed to the *diffraction* term ∇_\perp^2 of equation (3.33).

3.3.2 Transverse modes

The paraxial equation has a very special set of solutions whose transverse shape is retained upon propagation except for variations of its scale and the acquisition of a phase, that is, mathematically they satisfy

$$u(k_z; \mathbf{r}_\perp, z) = \sigma(z) \exp[i\gamma(\mathbf{r}_\perp, z)] u[k_z; \sigma(z) \mathbf{r}_\perp, z_0], \quad (3.35)$$

for some real functions $\sigma(z)$ and $\gamma(\mathbf{r}_\perp, z)$. In a sense, these are eigenfunctions of the integral operator acting on $u(k_z; \mathbf{r}_\perp, z_0)$ in (3.34), the so-called *paraxial propagator*. These solutions are known as *transverse modes* and form an infinite, but countable set. Their explicit form depend on the transverse coordinate system that one uses to express the propagator. In the following we discuss the structure of such modes in *Cartesian* and *polar* coordinates.

Let us start by analyzing the propagation of the most simple transverse mode (which is the same in any coordinate system). The structure of the integral equation (3.34) invites us to try a Gaussian ansatz

$$u(k_z; \mathbf{r}_\perp, z_0) = u_0 \exp\left[i\frac{k_z \mathbf{r}_\perp^2}{2q(z_0)}\right], \quad (3.36)$$

where $q(z)$ is a complex parameter which we will call the *q-parameter* of the beam, and is usually written as

$$\frac{1}{q(z)} = \frac{1}{R(z)} + i\frac{2}{k_z w^2(z)}, \quad (3.37)$$

being $R(z)$ and $w(z)$ real functions called the *curvature radius* and *spot size* of the mode, respectively. Introducing this decomposition of the *q-parameter* in (3.36) we get

$$u(k_z; \mathbf{r}_\perp, z_0) \exp(ik_z z_0) = u_0 \exp\left[-\frac{\mathbf{r}_\perp^2}{w^2(z_0)}\right] \exp\left[ik_z \left(z_0 + \frac{\mathbf{r}_\perp^2}{2R(z_0)}\right)\right], \quad (3.38)$$

which has a very suggestive form: A spherical surface of curvature radius ρ centered at $\mathbf{r} = \mathbf{0}$ can be written within the paraxial approximation as

$$z = \rho \sqrt{1 - \frac{\mathbf{r}_\perp^2}{\rho^2}} \simeq \rho - \frac{\mathbf{r}_\perp^2}{2\rho}, \quad (3.39)$$

and hence the wavefront³ of our Gaussian ansatz is spherical and has a curvature radius $R(z_0)$. On the other hand, this *spherical wave* is modulated by a circular Gaussian distribution in the transverse plane of thickness $w(z_0)$. It is straightforward to prove that after the action of the paraxial propagator, this transverse pattern evolves to

$$u(k_z; \mathbf{r}_\perp, z) = \frac{u_0}{w(z)} \exp\left[i\frac{k_z \mathbf{r}_\perp^2}{2q(z)} + i\psi(z)\right], \quad (3.40)$$

where

$$q(z) = q(z_0) + z - z_0, \quad (3.41a)$$

$$\psi(z) = \arg\left\{1 + \frac{z - z_0}{q(z_0)}\right\}. \quad (3.41b)$$

³ The surface formed by the points of equal phase.

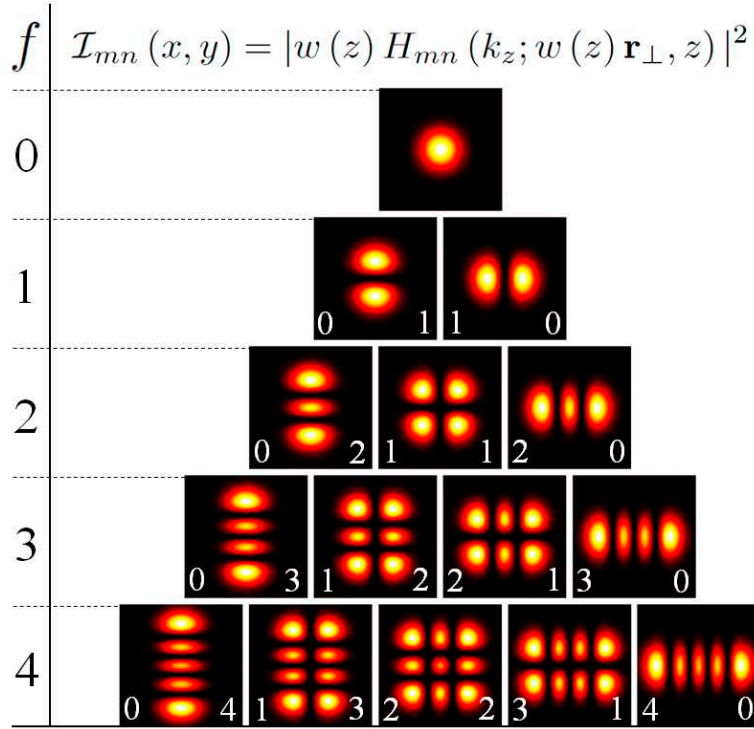


Fig. 3.3: Transverse distribution of the Hermite–Gauss modes.

It is customary to take the reference plane $z_0 = 0$ as that in which the wavefront is plane, that is, the plane in which $R(z_0 = 0) = \infty$, denoting $w(z_0 = 0)$ by w_0 . Particularized to this election, the previous expressions lead to

$$w^2(z) = w_0^2 \left[1 + \left(\frac{z}{z_R} \right)^2 \right], \quad (3.42a)$$

$$R(z) = z \left[1 + \left(\frac{z_R}{z} \right)^2 \right], \quad (3.42b)$$

$$\psi(z) = -\arctan \left(\frac{z}{z_R} \right) \in \left[-\frac{\pi}{2}, \frac{\pi}{2} \right], \quad (3.42c)$$

where we have defined the *Rayleigh length* $z_R = k_z w_0^2 / 2$ (note that it is not positive definite, it is negative when k_z is negative). $\psi(z)$ is known as the Gouy phase. Note that this pattern $u(k_z; \mathbf{r}_\perp, z)$ is related to $u(k_z; \mathbf{r}_\perp, z_0)$ in the form (3.35), and hence, it is indeed a transverse mode; it is called the *fundamental transverse mode*. The rest of transverse modes have a structure similar to this Gaussian mode, but modulated by additional transverse functions.

For Cartesian coordinates $\mathbf{r}_\perp = (x, y)$, the transverse modes are known as the *Hermite–Gauss* (HG) or TEM_{mn} modes $\{H_{mn}(k_z; \mathbf{r}_\perp, z)\}_{m,n \in \mathbb{N}}$, and have the form

$$H_{mn}(k_z; \mathbf{r}_\perp, z) = \frac{1}{\sqrt{2^{m+n-1} \pi m! n! w(z)}} H_m \left[\frac{\sqrt{2}x}{w(z)} \right] H_n \left[\frac{\sqrt{2}y}{w(z)} \right] \exp \left[ik_z \frac{x^2 + y^2}{2q(z)} + i(1 + m + n) \psi(z) \right], \quad (3.43)$$

where $H_m(x)$ denote the Hermite polynomials⁴. The indices m and n , called collectively the *transverse modal indices*, are called individually the *horizontal* and *vertical indices* of the mode, respectively. Note that these modes form an orthonormal set in the transverse plane, that is,

$$\int_{\mathbb{R}^2} d^2 \mathbf{r}_\perp H_{mn}^*(k_z; \mathbf{r}_\perp, z) H_{m'n'}(k_z; \mathbf{r}_\perp, z) = \delta_{mm'} \delta_{nn'} \quad \forall z. \quad (3.45)$$

⁴ The Hermite polynomial $H_m(x)$ can be found from the Rodrigues formula

$$H_m(x) = (-1)^m \exp(x^2) \frac{d^m}{dt^m} \exp(-x^2). \quad (3.44)$$

Hence, for example, $H_0(x) = 1$ and $H_1(x) = 2x$.

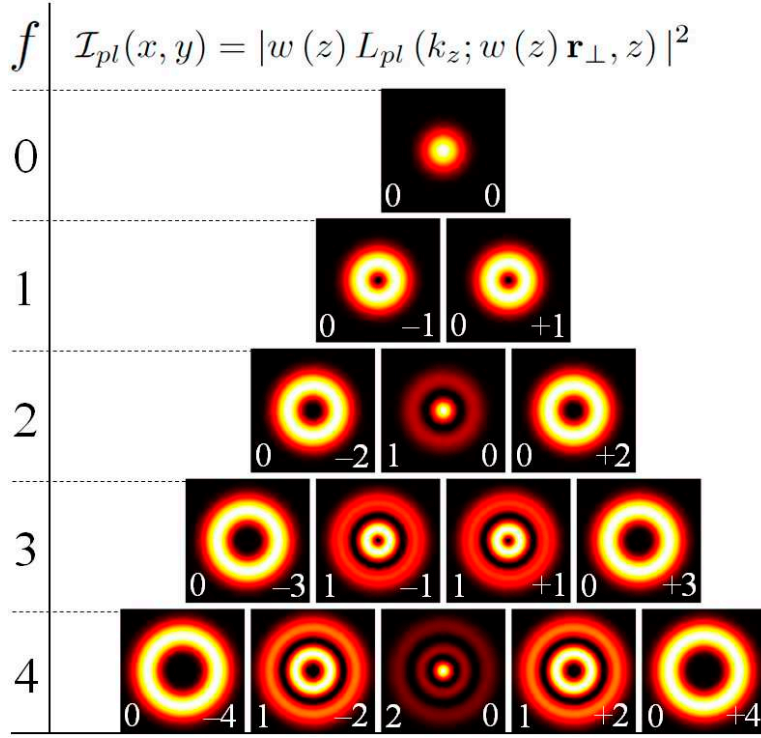


Fig. 3.4: Transverse distribution of the Laguerre–Gauss modes.

Indeed, it is possible to show that they also form a basis for any function contained in $L^2(\mathbf{r}_\perp)$, that is, for any square integrable function in \mathbb{R}^2 ; this *completeness* of the modes is expressed mathematically as

$$\sum_{m,n} H_{mn}^*(k_z; \mathbf{r}'_\perp, z) H_{mn}(k_z; \mathbf{r}_\perp, z) = \delta^2(\mathbf{r}_\perp - \mathbf{r}'_\perp) \quad \forall z. \quad (3.46)$$

Let us define the collective index $f = m + n$, which we will call *family index* for reasons that will become clear when dealing with optical cavities; we say that modes with the same family parameter f are contained in the f 'th *transverse family*. Note that family f contains $f + 1$ modes. In Figure 3.3 we plot the transverse distribution $\mathcal{I}_{mn}(\mathbf{r}_\perp) = |w(z) H_{mn}(k_z; w(z) \mathbf{r}_\perp, z)|^2$ of these modes. We see that the transverse indices m and n give the number of zeros present in the x and y directions respectively (the number of *nodal lines*).

On the other hand, for polar coordinates $\mathbf{r}_\perp = r(\cos \phi, \sin \phi)$, the set of transverse modes are known as the *Laguerre–Gauss (LG) modes* $\{L_{pl}(k_z; \mathbf{r}_\perp, z)\}_{p \in \mathbb{N}, l \in \mathbb{Z}}$, and have the form

$$L_{pl}(k_z; \mathbf{r}_\perp, z) = \sqrt{\frac{2p!}{\pi(p+|l|)!}} \frac{1}{w(z)} \left[\frac{\sqrt{2}r}{w(z)} \right]^{|l|} L_p^{(|l|)} \left[\frac{2r^2}{w^2(z)} \right] \exp \left[ik_z \frac{r^2}{2q(z)} + i(1+2p+|l|)\psi(z) + il\phi \right], \quad (3.47)$$

where $L_p^{(|l|)}(t)$ denote the modified Laguerre polynomials⁵. In this case p and l are known as the *radial* and *polar indices*, respectively. These modes form also an orthonormal basis of $L^2(\mathbf{r}_\perp)$.

For the LG modes the family index is defined as $f = 2p + |l|$. In Figure 3.4 we show $\mathcal{I}_{pl}(\mathbf{r}_\perp) = |w(z) L_{pl}(k_z; w(z) \mathbf{r}_\perp, z)|^2$ just as we did with the HG modes. Note that this intensity profiles are independent of the polar angle ϕ , and p gives us the number of zero-intensity circumferences (the number of *radial nodes*).

⁵ The modified Laguerre polynomial $L_p^{(|l|)}(t)$ can be found from the Rodrigues formula

$$L_p^{(|l|)}(t) = \frac{t^{-|l|} \exp(t)}{p!} \frac{d^p}{dt^p} \left[t^{p+|l|} \exp(-t) \right]. \quad (3.48)$$

Hence, for example, $L_0^{(|l|)}(t) = 1$ and $L_1^{(|l|)}(t) = -t + |l| + 1$.

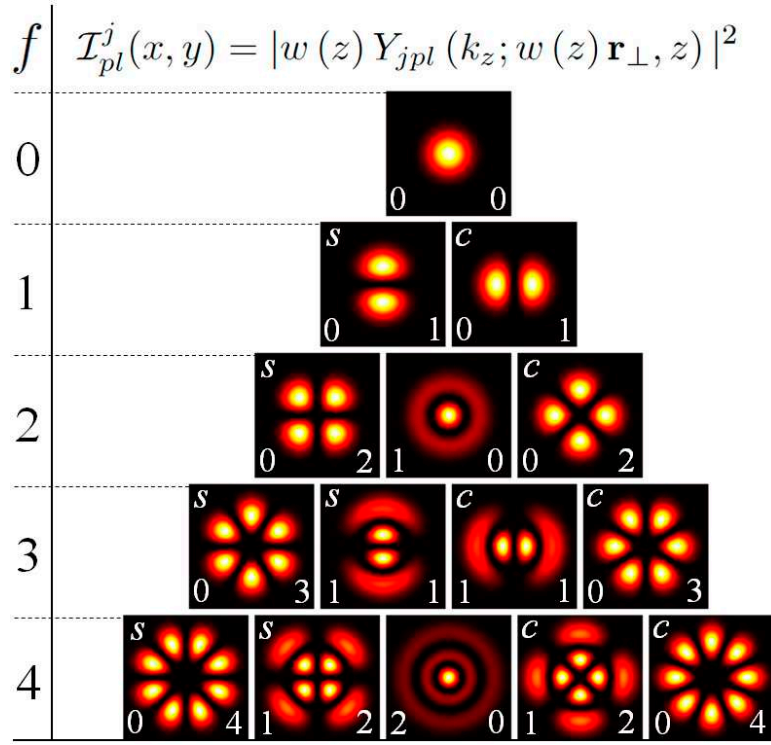


Fig. 3.5: Transverse distribution of the Hybrid Laguerre–Gauss modes. Note that the modes of its first family are the same as the corresponding Hermite–Gauss modes.

Instead of the LG modes which have a complex dependence $\exp(il\phi)$ on the polar angle, sometimes it is more convenient to use the *Hybrid Laguerre–Gauss* (HLG) modes $\{Y_{pl}^j(k_z; \mathbf{r}_\perp, z)\}_{p,l \in \mathbb{N}}^{j=c,s}$, which are defined as

$$Y_{cpl}(k_z; \mathbf{r}_\perp, z) = \frac{1}{\sqrt{2}} [L_{pl}(k_z; \mathbf{r}_\perp, z) + L_{p,-l}(k_z; \mathbf{r}_\perp, z)] \propto \cos(l\phi), \quad (3.49a)$$

$$Y_{spl}(k_z; \mathbf{r}_\perp, z) = \frac{1}{\sqrt{2}i} [L_{pl}(k_z; \mathbf{r}_\perp, z) - L_{p,-l}(k_z; \mathbf{r}_\perp, z)] \propto \sin(l\phi), \quad (3.49b)$$

and have a trigonometric dependence on ϕ . Of course, these relations are not valid for $l = 0$, where the polar dependence disappears and the convention is to define the Hybrid *cosine* mode as the LG mode and the Hybrid *sine* mode as zero, that is, $Y_{cp0}(k_z; \mathbf{r}_\perp, z) = L_{p0}(k_z; \mathbf{r}_\perp, z)$ and $Y_{sp0}(k_z; \mathbf{r}_\perp, z) = 0$. In Figure 3.5 we show the intensity of these modes. Note that they are like the LG modes, but modulated by a periodic function of the polar angle; in particular, given the dependence $\cos(l\phi)$ or $\sin(l\phi)$, $2l$ gives the number of zeros present in any circle around $r = 0$ (the number of *polar nodes*). This set of transverse modes is usually denoted by TEM_{pl}^* in the literature.

In the following, in order to make the next derivations general, we define an arbitrary set of transverse modes $\{T_{\mathbf{n}}(k_z; \mathbf{r}_\perp, z)\}_{\mathbf{n}}$ satisfying the orthonormality and completeness relations

$$\int_{\mathbb{R}^2} d^2\mathbf{r}_\perp T_{\mathbf{n}}^*(k_z; \mathbf{r}_\perp, z) T_{\mathbf{n}'}(k_z; \mathbf{r}_\perp, z) = \delta_{\mathbf{n}\mathbf{n}'}, \quad (3.50a)$$

$$\sum_{\mathbf{n}} T_{\mathbf{n}}^*(k_z; \mathbf{r}'_\perp, z) T_{\mathbf{n}}(k_z; \mathbf{r}_\perp, z) = \delta^2(\mathbf{r}_\perp - \mathbf{r}'_\perp) \quad \forall z; \quad (3.50b)$$

for example, when the modes are taken to be the HG, LG, or HLG, the set of transverse modal indices $\{\mathbf{n}\}$ is $\{n, m\}_{n,m \in \mathbb{N}}$, $\{p, l\}_{p \in \mathbb{N}}^{l \in \mathbb{Z}}$, and $\{j, p, l\}_{p,l \in \mathbb{N}}^{j=c,s}$, respectively.

As for arbitrary $q(z)$ and $\psi(z)$ parameters the transverse modes form a basis of $L^2(\mathbf{r}_\perp)$, which is the space of physical transverse patterns (they cannot extend to infinity or have singularities), the vector potential associated to any optical beam propagating along the z axis can be expanded as

$$\mathbf{A}(\mathbf{r}, t) = \sum_{\sigma=1,2} \sum_{\mathbf{n}} \int_{\mathcal{O}} dk_z \varepsilon_{\sigma\mathbf{n}}(k_z) \mathcal{A}_{\sigma\mathbf{n}}(k_z, t) T_{\mathbf{n}}(k_z; \mathbf{r}_\perp, z) \exp(ik_z z). \quad (3.51)$$

The HG, LG, and HLG modes satisfy the relations

$$H_{mn}^*(k_z; \mathbf{r}_\perp, z) = H_{mn}(-k_z; \mathbf{r}_\perp, z), \quad (3.52a)$$

$$L_{pl}^*(k_z; \mathbf{r}_\perp, z) = L_{p,-l}(-k_z; \mathbf{r}_\perp, z), \quad (3.52b)$$

$$Y_{jpl}^*(k_z; \mathbf{r}_\perp, z) = Y_{jpl}(-k_z; \mathbf{r}_\perp, z); \quad (3.52c)$$

hence, similarly to what happened with plane waves, the reality of the vector potential imposes the following restrictions on the polarization and temporal parts of the modes:

$$\varepsilon_{\sigma mn}^*(k_z) \mathcal{A}_{\sigma mn}^*(k_z, t) = \varepsilon_{\sigma mn}(-k_z) \mathcal{A}_{\sigma mn}(-k_z, t), \quad (3.53a)$$

$$\varepsilon_{\sigma pl}^*(k_z) \mathcal{A}_{\sigma pl}^*(k_z, t) = \varepsilon_{\sigma p,-l}(-k_z) \mathcal{A}_{\sigma p,-l}(-k_z, t), \quad (3.53b)$$

$$\varepsilon_{\sigma jpl}^*(k_z) \mathcal{A}_{\sigma jpl}^*(k_z, t) = \varepsilon_{\sigma jpl}(-k_z) \mathcal{A}_{\sigma jpl}(-k_z, t). \quad (3.53c)$$

Note finally that all these transverse bases have two free parameters, e.g., the spot size at the waist plane and the position of this plane; in free space we can choose these parameters as we feel more convenient, and hence this paraxial basis is actually a continuous family of bases. We will see that these transverse modes form also a basis for light contained in an optical cavity, but in this case the parameters of the basis get fixed by the cavity geometry.

3.4 Quantization in an optical cavity

3.4.1 Geometrical optics: Propagation through optical elements and stable optical cavities

Optical cavities are useful for their ability to trap light. In their most basic configuration, they consist on two spherical mirrors facing each other (*linear resonators*), so that when an optical beam enters the system, it stays bouncing back and forth between these. In this section we explain the conditions that any cavity must satisfy in order to truly confine light.

Consider an optical beam propagating nearly within the z axis. In the preceding section we studied the propagation of such a beam by taking into account the diffraction effects of the wave equation. There is yet another description of the beam which is very useful owed to its simplicity, but works only for large *Fresnel numbers* $F = d^2/\lambda l$, where d is the transverse size of the beam and l the distance that it has propagated along the z axis. This approach is known as *geometrical optics*, and it visualizes the beam as a collection of *collimated rays* propagating as straight lines (hence, it doesn't take into account the changes in transverse size or shape of the beam). Within this description, any ray is specified at a given longitudinal position z by a vector

$$\mathbf{v}(z) = \begin{bmatrix} r(z) \\ \theta(z) \end{bmatrix}, \quad (3.54)$$

being $r(z)$ its distance to the z axis and $\theta(z)$ the angle that it forms with the this axis as it propagates. We will call *transverse position* and *inclination* to these *ray coordinates*.

The effect of *optical elements* on the beam is described within this framework by a so-called ABCD matrix

$$M = \begin{bmatrix} A & B \\ C & D \end{bmatrix}, \quad (3.55)$$

which takes a ray $\mathbf{v}(z_{in}) = \text{col}(r, \theta)$ of the beam at its input and transforms it into the ray

$$\mathbf{v}(z_{out}) = M\mathbf{v}(z_{in}) = \begin{bmatrix} Ar + B\theta \\ Cr + D\theta \end{bmatrix}. \quad (3.56)$$

The most simple optical operation consists on allowing the beam to propagate in free space a distance l . The resulting ABCD matrix is trivially found to be

$$M_{\text{free}}(l) = \begin{bmatrix} 1 & l \\ 0 & 1 \end{bmatrix}, \quad (3.57)$$

that is, the inclination of the rays doesn't change, while their transverse positions are increased by $l\theta$. Another example consists in a spherical interface with curvature radius⁶ R separating two dielectric media with refractive indices⁷ n_L

⁶ Some comments on sign conventions are in order. First, optical elements are described as seen from the ray. The curvature radius of convex (concave) dielectric surfaces is then taken as positive (negative), and the opposite for reflecting surfaces.

⁷ The refractive index is rigorously introduced in Chapter 4.

and n_R (assumed propagation from *left* to *right*); by using Snell's law in paraxial form $n_L\theta_L = n_R\theta_R$ and simple geometrical arguments, it is straightforward to prove that its ABCD matrix is

$$M_{\text{interface}}(n_L, n_R, R) = \begin{bmatrix} 1 & 0 \\ \frac{n_L - n_R}{n_R} \frac{1}{R} & \frac{n_L}{n_R} \end{bmatrix}, \quad (3.58)$$

that is, in this case the transverse positions of the rays do not change, while their inclination does.

From these two fundamental ABCD systems (*propagation* and *refraction*) one can find the ABCD matrices of a whole family of useful optical elements such as *thin lenses* or *mirrors*, which have

$$M_{\text{lens}}(f) = \begin{bmatrix} 1 & 0 \\ -\frac{1}{f} & 1 \end{bmatrix} \quad \text{and} \quad M_{\text{mirror}}(R) = \begin{bmatrix} 1 & 0 \\ -\frac{2}{R} & 1 \end{bmatrix}, \quad (3.59)$$

where f is called the *focal length* of the lens and R is the curvature radius of the mirror.

Given a general ABCD matrix M connecting two planes with refractive indices n_{in} and n_{out} , one has $\det\{M\} = n_{in}/n_{out}$; to prove this just note that M can always be decomposed as a combination of propagation (3.57) and refraction (3.58) ABCD matrices, and that the determinant of a product of matrices equals the product of the individual determinants.

It is very interesting to note that the transverse modes that we just described in the previous section preserve their transverse shape upon propagation through an arbitrary ABCD system. In particular, it can be proved that if we take an arbitrary transverse mode with q -parameter $q(z_{in})$ and Gouy phase $\psi(z_{in})$ at the input face of the ABCD system, it is transformed at the output face of the optical system into the exact same mode but with new parameters

$$q(z_{out}) = \frac{Aq(z_{in}) + B}{Cq(z_{in}) + D}, \quad (3.60a)$$

$$\psi(z_{out}) = \psi(z_{in}) - \arg \left\{ A + \frac{|B|}{q(z_{in})} \right\}; \quad (3.60b)$$

these expressions are known as the *ABCD propagation laws*.

Let us now pass to describe optical cavities from this geometrical viewpoint. Consider a ray $\mathbf{v}(z_0) = \text{col}(r, \theta)$ at some reference plane $z = z_0$ of the cavity; after a roundtrip inside the cavity, it is transformed by an ABCD matrix that we will call

$$M_{\text{roundtrip}} = \begin{bmatrix} A_{rt} & B_{rt} \\ C_{rt} & D_{rt} \end{bmatrix}, \quad (3.61)$$

which consists in the composition of all the operations performed by the optical elements inside the cavity until the ray comes back to the reference plane $z = z_0$ with the same propagation direction (hence $\det\{M_{\text{roundtrip}}\} = 1$). After N roundtrips the ray coordinates will become

$$\mathbf{v}_N(z_0) = M_{\text{roundtrip}}^N \mathbf{v}(z_0) = \frac{1}{\sin \theta} \begin{bmatrix} A_{rt} \sin N\theta - \sin[(N-1)\theta] & B_{rt} \sin N\theta \\ C_{rt} \sin N\theta & D_{rt} \sin N\theta - \sin(N-1)\theta \end{bmatrix} \mathbf{v}(z_0), \quad (3.62)$$

with $\cos \theta = (A_{rt} + D_{rt})/2$, where the second equality comes from the *Sylvester theorem* applied to the N 'th power of a 2×2 matrix with determinant one. The ray will stay confined in the cavity only if θ is real, as otherwise the trigonometric functions become hyperbolic, and the ray coordinates diverge. This means that the condition for a resonator to confine optical beams is

$$-1 < \frac{A_{rt} + D_{rt}}{2} < 1 \quad (3.63)$$

An optical cavity satisfying this condition is said to be *stable*. Note that it looks like this condition may depend on the reference plane from which the roundtrip matrix is evaluated; however, it is possible to show that the trace of the roundtrip matrix does not depend on the reference plane.

As stated, in this thesis we assume that the optical cavity consists in two spherical mirrors with curvature radii R_1 and R_2 separated a distance L ; for reasons that will become clear in Chapter 6, we allow for the existence of a plane dielectric slab of length l_c and refractive index n_c . Taking the reference plane at mirror one with the rays propagating away from it, the roundtrip ABCD matrix of this simple cavity is easily found to be

$$M_{\text{roundtrip}} = \begin{bmatrix} 2g_2 - 1 & 2g_2 L_{\text{eff}} \\ 2(2g_1 g_2 - g_2 - g_1)/L_{\text{eff}} & 4g_1 g_2 - 2g_2 - 1 \end{bmatrix}, \quad (3.64)$$

where we have defined the g -parameters of the cavity

$$g_j = 1 - \frac{L_{\text{eff}}}{R_j} \quad (j = 1, 2), \quad (3.65)$$

as well as its *effective length*

$$L_{\text{eff}} = L - \left(1 - \frac{1}{n_c}\right) l_c. \quad (3.66)$$

This linear resonator is stable then only if

$$0 < g_1 g_2 < 1. \quad (3.67)$$

In this thesis we will only work with stable linear cavities.

3.4.2 Considerations at a non-reflecting interface

As stated, throughout the thesis we will work with a linear cavity having a dielectric medium inside. In this section we discuss some particularities that must be taken into account for the field due to the presence of this medium.

The details concerning how Maxwell's equations are modified in the presence of a medium with refractive index n_m will be explained in Chapter 6. Here, however, we just want to note that for a homogeneous, isotropic medium and reasonably weak fields, the only effect of the medium is to change the wave equation of the vector potential (3.7) as

$$\left(\frac{1}{n_m^2} \nabla^2 - \frac{1}{c^2} \partial_t^2\right) \mathbf{A} = \mathbf{0}. \quad (3.68)$$

Therefore, for field configurations of the type we have discussed, $\varepsilon u(\mathbf{r}) \mathcal{A}(t)$, the effect of the medium is to change the Helmholtz equation for the spatial part as

$$\nabla^2 u + n_m^2 k^2 u = 0, \quad (3.69)$$

that is, to multiply by a factor n_m the wave vector of the spatial modes of the system. Hence, except for this n_m factor, plane waves (or transverse modes within the paraxial approximation) can still be considered the spatial modes of a medium which fills the whole \mathbb{R}^3 space.

A different matter is what happens when the field crosses a plane interface separating two media with refractive indices n_L and n_R . The first interesting thing to note is that the shape of the transverse modes is not modified at all, what is not surprising by continuity arguments: It would make no sense that the thickness or the radius of the beam changed abruptly upon crossing the interface. To see this, just note that given the q and ψ parameters of the modes at both sides of the interface, denoted by (q_L, ψ_L) and (q_R, ψ_R) , the propagation laws (3.60) together with the refraction ABCD matrix (3.58) tells us that

$$\frac{n_R}{q_R} = \frac{n_L}{q_L} \quad \text{and} \quad \psi_R = \psi_L; \quad (3.70)$$

hence, the complex Gaussian profile of the modes match each other, that is

$$\exp\left[im_R k_z \frac{\mathbf{r}_\perp^2}{2q_R} + i(1+f)\psi_R\right] = \exp\left[im_L k_z \frac{\mathbf{r}_\perp^2}{2q_L} + i(1+f)\psi_L\right], \quad (3.71)$$

and therefore the modes are independent of the refractive index. Note though, that the spot size and the curvature radius of the modes in a medium with refractive index n_m are defined by

$$\frac{1}{q(z)} = \frac{1}{R(z)} + i \frac{2}{n_m k_z w^2(z)}. \quad (3.72)$$

Crossing an interface induces further relations between the vector potentials at both sides of the interface, say $\mathbf{A}_L(\mathbf{r}, t)$ and $\mathbf{A}_R(\mathbf{r}, t)$ with

$$\mathbf{A}_j(\mathbf{r}, t) = \varepsilon A_j(t) T(k; \mathbf{r}_\perp, z_I) \exp(-i\omega t + in_j k z_I) + \text{c.c.}, \quad (3.73)$$

for a single mode with polarization ε , frequency $\omega = ck$, and transverse profile $T(k; \mathbf{r}_\perp, z)$. z_I is the longitudinal position of the plane interface and $A_j(t)$ is a slowly varying envelope which remains almost unaltered after an optical cycle, that is,

$$\dot{A}_j(t) \ll 2\pi/\omega. \quad (3.74)$$

The corresponding electric and magnetic fields are given by

$$\mathbf{E}_j(\mathbf{r}, t) = i\omega\epsilon A_j(t)T(k; \mathbf{r}_\perp, z_1) \exp(-i\omega t + in_j k z_1) + \text{c.c.}, \quad (3.75a)$$

$$\mathbf{B}_j(\mathbf{r}, t) = i\frac{n_j\omega}{c}(\mathbf{e}_z \times \boldsymbol{\epsilon}) A_j(t)T(k; \mathbf{r}_\perp, z_1) \exp(-i\omega t + in_j k z_1) + \text{c.c.}, \quad (3.75b)$$

where we have made use of the paraxial approximations (3.32). The instantaneous power content in the transverse plane is given by

$$P_j(t) = \frac{1}{\mu_0} \frac{\omega}{2\pi} \int_{t-\pi/\omega}^{t+\pi/\omega} dt' \int_{\mathbb{R}^2} d^2\mathbf{r}_\perp |\mathbf{E}_j(\mathbf{r}, t') \times \mathbf{B}_j(\mathbf{r}, t')| = \frac{2n_j\omega^2}{c\mu_0} |A_j(t)|^2, \quad (3.76)$$

that is, by the absolute value of the time averaged Poynting vector, integrated in the transverse plane. Now, assume that the interface has some kind of anti-reflecting coating, so that the whole beam is transmitted from the left medium to the right one; as the power must be conserved, that is, $P_L = P_R$, this establishes the relation

$$\mathbf{A}_L(\mathbf{r}, t) = \sqrt{\frac{n_R}{n_L}} \mathbf{A}_R(\mathbf{r}, t). \quad (3.77)$$

Note that even though we have argued with a single mode, this relation holds for any field as follows from a trivial generalization of the argument.

All these relations will be important to perform a proper quantization of the field inside the cavity.

3.4.3 Modes of an optical resonator

As in the case of free space, the first step in order to quantize the electromagnetic field inside an optical resonator is to find the set of spatial modes satisfying the Helmholtz equation and the boundary conditions imposed by the cavity mirrors. We are going to work with paraxial optical beams whose transverse size is small compared with the transverse dimensions of the cavity; under these conditions, we know that any transverse structure of the field can be expanded in terms of the paraxial transverse modes (3.51) that we introduced in Section 3.3.2. On the other hand, the mirrors impose an additional boundary condition on these transverse modes: After a roundtrip in the cavity, they must exactly match themselves, that is, not only they need to be shape-preserving with propagation, but also *self-reproducing* after a roundtrip. This means that the modes of a general optical cavity can be found by imposing the condition

$$T_{\mathbf{n}}(k_z; \mathbf{r}_\perp, z_0) \exp(ik_z z_0) = T_{\mathbf{n}}(k_z; \mathbf{r}_\perp, z) \exp(ik_z z)|_{z_0 \oplus \text{r.t.}}, \quad (3.78)$$

where ‘ $z_0 \oplus \text{r.t.}$ ’ stands for ‘roundtrip propagation from the reference plane $z = z_0$ ’. Using the ABCD propagation laws (3.60), this condition is easily proved to be equivalent to

$$q(z_0) = \frac{A_{\text{rt}}q(z_0) + B_{\text{rt}}}{C_{\text{rt}}q(z_0) + D_{\text{rt}}}, \quad (3.79a)$$

$$2q\pi = -(1+f) \arg \left\{ A_{\text{rt}} + \frac{B_{\text{rt}}}{q(z_0)} \right\} + 2k_z L_{\text{opt}}, \quad (3.79b)$$

with $q \in \mathbb{N}$ the so-called *longitudinal index* (do not confuse it with the q -parameter of the modes, $q(z)$, which is always written with a label referring to the longitudinal position where it is evaluated). L_{opt} is the *optical length* of the cavity, that is, if rays propagate a longitudinal length l_j on the j 'th optical element with refractive index n_j , $L_{\text{opt}} = \sum_j n_j l_j$, where the sum extends to all the optical elements contained in the cavity (including free space propagation).

The first condition fixes the q -parameter of the modes at the reference plane to

$$\frac{1}{q(z_0)} = \frac{D_{\text{rt}} - A_{\text{rt}}}{2B_{\text{rt}}} + \frac{i}{|B_{\text{rt}}|} \sqrt{1 - \left(\frac{A_{\text{rt}} + D_{\text{rt}}}{2} \right)^2}. \quad (3.80)$$

Surprisingly, this expression leads to the condition $-1 < (A_{\text{rt}} + D_{\text{rt}})/2 < 1$ for these modes to exist in the resonator, which is exactly the stability condition (3.63) that we already found by geometrical means. On the other hand, the second condition discretizes the frequencies at which transverse modes can *resonate* inside the cavity; in particular, the modes exist at the cavity only at frequencies

$$\omega_{qf} = \Omega_{\text{FSR}} \left[q + \frac{1+f}{2\pi} \zeta \right], \quad (3.81)$$

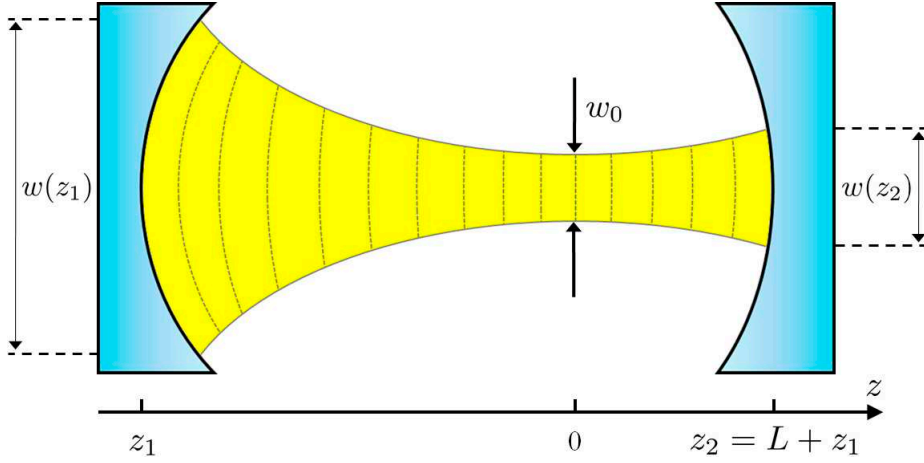


Fig. 3.6: Schematic representation of the wavefront and the thickness of the modes in a linear cavity with two concave mirrors. Note that in this case the waist plane is between the mirrors.

where

$$\zeta = \arg \left\{ \left(\frac{A_{\text{rt}} + D_{\text{rt}}}{2} \right) + i \sqrt{1 - \left(\frac{A_{\text{rt}} + D_{\text{rt}}}{2} \right)^2} \right\} \quad (3.82)$$

is the Gouy phase accumulated after the roundtrip, $\Omega_{\text{FSR}} = \pi c / L_{\text{opt}}$ is the so-called *free spectral range* of the resonator, and f is the family index that we defined in Section 3.3.2. Note that these frequencies are independent of the reference plane $z = z_0$ because they depend only on the trace of the roundtrip matrix. Note also that modes having the same family index f ‘live’ inside the cavity at the same frequencies, what gives sense to the name of this index.

For the particular case of the linear resonator that we introduced above, which has an optical length

$$L_{\text{opt}} = L + (n_c - 1) l_c, \quad (3.83)$$

we have

$$\zeta = 2 \arccos \pm \sqrt{g_1 g_2} \in [0, \pi], \quad (3.84)$$

where the ‘+’ and ‘-’ signs hold for $g_2 > 0$ and $g_2 < 0$, respectively. Hence the resonance distribution of the different families inside the cavity is fixed by the product $g_1 g_2$.

On other hand, calling z_1 to the longitudinal position of mirror 1, whose plane we took as the reference when evaluating the roundtrip matrix (3.64), we get

$$R(z_1) = -R_1, \quad (3.85a)$$

$$w_{qf}(z_1) = \left(\frac{L_{\text{eff}} \lambda_{qf}}{\pi} \right)^{1/2} \left[\frac{g_2}{g_1 (1 - g_1 g_2)} \right]^{1/4}, \quad (3.85b)$$

where $\lambda_{qf} = 2\pi c / \omega_{qf}$. Note that even though the spot size depends on the particular longitudinal and family indices (q, f) of the mode, the q -parameter is the same for all of them, as it depends on $k_z w^2$ which is independent of (q, f) . Note also that the spherical wavefront of the modes is adapted to mirror 1 (the sign just means that the wave is propagating away from the mirror). We could have taken the position $z = z_2$ of mirror 2 as the longitudinal reference and would have found that the wavefront is also adapted to mirror 2 at $z = z_2$. Hence, upon propagation from mirror 1 to mirror 2, the mode is reshaped as shown in Figures 3.6 and 3.7. For a cavity with two concave mirrors (Figure 3.6) the wavefront of the modes has to change the sign of its radius with the propagation, and hence it becomes plane at a longitudinal position inside the cavity. This is not the case if one of the mirrors is convex (Figure 3.7), a situation leading to a waist plane outside the cavity.

Having characterized the modes in the plane $z = z_1$, we can now find them at any other plane by using the ABCD propagation laws. In particular, we would like to refer the modes to the plane in which the wavefronts are plane, that is, $R(z = 0) = \infty$, which we take as the longitudinal origin $z = 0$; we will denote this plane by *beam waist* or *waist plane*, as it is the plane where the spot size of the modes is minimum. Let us denote by $w_{0,qf}$ the spot size of a mode with indices (q, f) at this plane, and by $z_{1,\text{eff}}$ the longitudinal position of mirror 1 (as we allow an intracavity

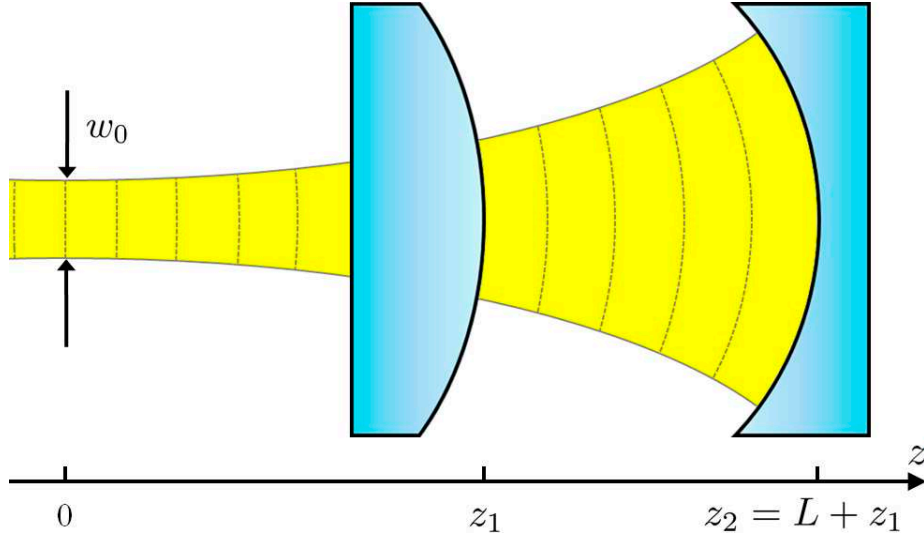


Fig. 3.7: Schematic representation of the wavefront and the thickness of the modes in a linear cavity having one convex mirror. In this case the waist plane is outside resonator.

plane dielectric slab, we have to use effective lengths, and then transform to geometric length depending on where the slab is placed). The ABCD propagation law (3.60a) allows us to write $q(z_0) = q(z_1) + z_{1,\text{eff}}$, which after imposing $q(z_0) = k_z w_0^2/2i$, leads us to

$$z_{1,\text{eff}} = L_{\text{eff}} \frac{(1 - g_1)|g_2|}{|g_1 + g_2 - 2g_1g_2|}, \quad (3.86a)$$

$$w_{0,qf} = \left(\frac{\lambda_{qf} L_{\text{eff}}}{\pi} \right)^{1/2} \left[\frac{g_1 g_2 (1 - g_1 g_2)}{(g_1 + g_2 - 2g_1 g_2)^2} \right]^{1/4}. \quad (3.86b)$$

The first thing to note is that the waist plane is the same for all the modes, even though they have different spot sizes in general. Taking this waist plane as our reference, the modes at any other plane (or even outside the cavity if it is allowed to leave, what we will do in the next section) are given by (3.42), but with z being an effective longitudinal coordinate when dielectric plane slabs are involved, that is,

$$w_{qf}^2(z) = w_{0,qf}^2 \left[1 + \left(\frac{z_{\text{eff}}}{z_R} \right)^2 \right], \quad (3.87a)$$

$$R(z) = z_{\text{eff}} \left[1 + \left(\frac{z_R}{z_{\text{eff}}} \right)^2 \right], \quad (3.87b)$$

$$\psi(z) = -\arctan \left(\frac{z_{\text{eff}}}{z_R} \right) \in \left[-\frac{\pi}{2}, \frac{\pi}{2} \right]. \quad (3.87c)$$

To fix ideas, let us consider the example an empty symmetric resonator, that is, a resonator satisfying $g_1 = g_2 \equiv g = 1 - L/R$, in which the cavity resonances and Rayleigh length read

$$\omega_{qf} = \Omega_{\text{FSR}} \left[q + \frac{1+f}{\pi} \arccos g \right], \quad (3.88a)$$

$$|z_R| = \frac{L}{2} \sqrt{\frac{1+g}{1-g}}. \quad (3.88b)$$

Consider now the following extreme situations:

- $R \rightarrow \infty$ (near-planar resonator). In this case the longitudinal frequencies of the different transverse families are $\omega_{qf} = \Omega_{\text{FSR}} q$. Hence, at every cavity resonance we can find all the transverse modes. In this case the Rayleigh length is by far larger than the cavity length, what means that the modes are basically plane waves.

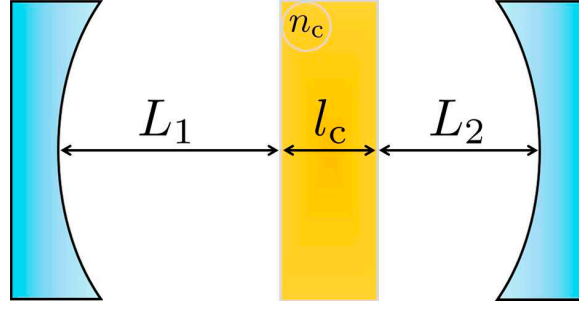


Fig. 3.8: We quantize the electromagnetic field inside a cavity containing a dielectric slab.

- $L = 2R$ (concentric resonator). In this case $\omega_{qf} = \Omega_{\text{FSR}}(q + f + 1)$, what means that $\omega_{qf} = \omega_{q-1, f+1} = \omega_{q-2, f+2} = \dots$, and hence, we find again all the transverse modes at a given resonance. In this case the Rayleigh length is zero, and hence the modes are point-like at the waist plane.
- $L = R$ (confocal resonator). In this case $\omega_{qf} = \Omega_{\text{FSR}}(q + f/2 + 1/2)$, which implies $\omega_{qf} = \omega_{q-1, f+2} = \omega_{q-2, f+4} = \dots$, and hence even and odd families are separated inside the cavity by half a free spectral range. As for the Rayleigh length, it is half the cavity's effective length.

To get an idea of the numbers, let us consider the example of an empty, confocal, symmetric resonator with lengths varying from 5 mm to 500 mm. The free spectral range varies then between 200 GHz and 2 GHz. On the other hand, the spot size at the waist varies from 20 μm to 205 μm at a wavelength of 532 nm (frequency of 3.5×10^{15} Hz).

3.4.4 Quantization of the electromagnetic field inside a cavity

In the previous discussion we have shown that the modes of the resonator are the transverse modes that we studied in the previous section, but with a q -parameter fixed by the cavity geometry. In addition, instead of a continuous set of optical wave vectors k_z only a discrete set $\{k_{z, qf} = \pm\omega_{qf}/c\}_{q \in \mathbb{Z}}$ can exist for the modes contained in a given family f . Hence, the vector potential inside the linear cavity depicted in Figure 3.8 can be written as

$$\mathbf{A}(\mathbf{r}, t) = \sum_{\sigma=1,2} \sum_{\mathbf{n}} \sum_{k_{z,qf} \in \mathcal{O}} \frac{1}{\sqrt{n(z)}} \boldsymbol{\varepsilon}_{\sigma\mathbf{n}}(k_{z,qf}) \mathcal{A}_{\sigma\mathbf{n}}(k_{z,qf}, t) T_{\mathbf{n}}(k_{z,qf}; \mathbf{r}_{\perp}, z) \times \exp[in(z)k_{z,qf}z], \quad (3.89)$$

where we have introduced the z -dependent refractive index

$$n(z) = \begin{cases} 1 & z_1 < z < z_1 + L_1 \quad \text{or} \quad z_1 + L_1 + l_c < z < z_1 + L \\ n_c & z_1 + L_1 < z < z_1 + L_1 + l_c \end{cases}. \quad (3.90)$$

Note that the refractive index does not appear in $\boldsymbol{\varepsilon}_{\sigma\mathbf{n}}(k_{z,qf})$ or $\mathcal{A}_{\sigma\mathbf{n}}(k_{z,qf}, t)$ because $k_{z,qf}$ acts in that case just as a mode label.

Quantization is made following exactly the same procedure as in free space (see Section 3.2.1) but with some particularities that we discuss now. We define first the electromagnetic normal variables for each mode

$$\nu_{\sigma\mathbf{n}}(k_{z,qf}, t) = \frac{1}{\Gamma} \left[\mathcal{A}_{\sigma\mathbf{n}}(k_{z,qf}, t) + \frac{i}{\omega_{qf}} \dot{\mathcal{A}}_{\sigma\mathbf{n}}(k_{z,qf}, t) \right], \quad (3.91)$$

which again evolve as the normal variables of harmonic oscillators (3.14) with the corresponding frequency. In this case the dielectric medium contributes to the electromagnetic energy contained in system, which cannot be written as (3.15) in its presence, but in the modified form [65, 67]

$$E_{\text{em}} = \frac{1}{2} \int d^3\mathbf{r} \left[\varepsilon_0 n^2(z) \mathbf{E}^2(\mathbf{r}, t) + \frac{1}{\mu_0} \mathbf{B}^2(\mathbf{r}, t) \right]. \quad (3.92)$$

In order to simplify this expression we use some approximations. First, the paraxial condition (3.32a) allow us to perform the approximation

$$\int_{z_0}^{z_0+l} dz \int_{\mathbb{R}^2} d^2\mathbf{r}_{\perp} T_{\mathbf{n}}(k_{z,qf}; \mathbf{r}_{\perp}, z) T_{\mathbf{n}'}(k'_{z,qf}; \mathbf{r}_{\perp}, z) \exp[in(z)(k_{z,qf} + k'_{z,qf})z] \simeq l \delta_{\mathbf{n}\mathbf{n}'} \delta_{k_{z,qf}, -k'_{z,qf}}, \quad (3.93)$$

valid for any reference plane $z = z_0$ as long as $l \gg \{|k_{z,qf}|^{-1}, |k'_{z,qf}|^{-1}\}$, that is, as long as light is able to undergo many cycles between $z = z_0$ and $z = z_0 + l$. Then, the second paraxial condition (3.32b) leads to the approximation

$$\nabla \{T_{\mathbf{n}}(k_{z,qf}; \mathbf{r}_{\perp}, z) \exp[in(z)k_{z,qf}z]\} \simeq in(z)k_{z,qf}\mathbf{e}_z T_{\mathbf{n}}(k_{z,qf}; \mathbf{r}_{\perp}, z) \exp[in(z)k_{z,qf}z]. \quad (3.94)$$

With this approximations at hand, it is straightforward to write the electromagnetic energy in terms of the normal variables as

$$E_{\text{em}} = \sum_{\sigma=1,2} \sum_{\mathbf{n}} \sum_{k_{z,qf} \in \mathcal{O}} \frac{\varepsilon_0 L_{\text{opt}} \Gamma^2 \omega_{qf}^2}{2} \nu_{\sigma\mathbf{n}}^*(k_{z,qf}) \nu_{\sigma\mathbf{n}}(k_{z,qf}). \quad (3.95)$$

The last particularity of optical cavities is that there is no sense in making a distinction between modes propagating to the right or to the left, because they cannot be excited separately. Hence, we just define collective normal variables $\nu_{\sigma q\mathbf{n}} = \nu_{\sigma\mathbf{n}}(\pm|k_{z,qf}|)$, so that the modes get completely specified inside the cavity by their polarization σ , and their longitudinal and transverse indices (q, \mathbf{n}) . Therefore, the electromagnetic energy can be finally written as

$$E_{\text{em}} = \sum_{\sigma q\mathbf{n}} \frac{\omega_{qf}^2}{2} \nu_{\sigma q\mathbf{n}}^* \nu_{\sigma q\mathbf{n}}, \quad (3.96)$$

where we have chosen $\Gamma = 1/\sqrt{2\varepsilon_0 L_{\text{opt}}}$ so that this expression coincides with that of a collection of harmonic oscillators as before. Quantization is therefore introduced by making a correspondence between the normal variables $\{\nu_{\sigma q\mathbf{n}}(t), \nu_{\sigma q\mathbf{n}}^*(t)\}$ and boson operators $\sqrt{2\hbar/\omega_{qf}}\{\hat{a}_{\sigma q\mathbf{n}}(t), \hat{a}_{\sigma q\mathbf{n}}^\dagger(t)\}$ satisfying the commutation relations

$$[\hat{a}_{\sigma q\mathbf{n}}(t), \hat{a}_{\sigma' q' \mathbf{n}'}^\dagger(t)] = \delta_{\sigma\sigma'} \delta_{qq'} \delta_{\mathbf{n}\mathbf{n}'}, \quad (3.97a)$$

$$[\hat{a}_{\sigma q\mathbf{n}}(t), \hat{a}_{\sigma' q' \mathbf{n}'}(t)] = [\hat{a}_{\sigma q\mathbf{n}}^\dagger(t), \hat{a}_{\sigma' q' \mathbf{n}'}^\dagger(t)] = 0. \quad (3.97b)$$

The Hamiltonian of the electromagnetic field inside the cavity is then written as

$$\hat{H}_{\text{em}} = \sum_{\sigma q\mathbf{n}} \hbar \omega_{qf} \hat{a}_{\sigma q\mathbf{n}}^\dagger \hat{a}_{\sigma q\mathbf{n}}, \quad (3.98)$$

where we have already removed the infinite contribution appearing when using the commutation relations to write it in normal order.

Finally, the vector potential inside the resonator is given by the operator

$$\hat{\mathbf{A}}^{(+)}(\mathbf{r}, t) = \sum_{\sigma q\mathbf{n}} \frac{1}{2} \sqrt{\frac{\hbar}{n(z)\varepsilon_0 L_{\text{opt}} \omega_{qf}}} \varepsilon_{\sigma q\mathbf{n}} \hat{a}_{\sigma q\mathbf{n}}(t) \{T_{\mathbf{n}}(k_{qf}; \mathbf{r}_{\perp}, z) \exp[in(z)k_{qf}z] + \text{c.c.}\}, \quad (3.99)$$

where we have defined the positive definite modal wave vector $k_{qf} = \omega_{qf}/c$, while the electric and magnetic fields correspond then to

$$\hat{\mathbf{E}}^{(+)}(\mathbf{r}, t) = i \sum_{\sigma q\mathbf{n}} \frac{1}{2} \sqrt{\frac{\hbar \omega_{qf}}{n(z)\varepsilon_0 L_{\text{opt}}}} \varepsilon_{\sigma q\mathbf{n}} \hat{a}_{\sigma q\mathbf{n}}(t) \{T_{\mathbf{n}}(k_{qf}; \mathbf{r}_{\perp}, z) \exp[in(z)k_{z,qf}z] + \text{c.c.}\}, \quad (3.100a)$$

$$\hat{\mathbf{B}}^{(+)}(\mathbf{r}, t) = i \sum_{\sigma q\mathbf{n}} \frac{1}{2} \sqrt{\frac{n(z)\hbar \omega_{qf}}{c^2 \varepsilon_0 L_{\text{opt}}}} \varepsilon_{\sigma q\mathbf{n}} \hat{a}_{\sigma q\mathbf{n}}(t) \{T_{\mathbf{n}}(k_{qf}; \mathbf{r}_{\perp}, z) \exp[in(z)k_{z,qf}z] - \text{c.c.}\}, \quad (3.100b)$$

where the expressions emphasize the parts of the fields propagating to the right and to the left, which will be of later convenience even if their associated boson operators are the same.

4. QUANTUM THEORY OF OPEN CAVITIES

In the previous chapter we have been able to quantize the electromagnetic inside an optical cavity formed by perfectly reflecting mirrors. However, in reality optical cavities must have at least one partially transmitting mirror allowing us to both inject light inside it and observe the intracavity processes by studying the light that comes out of it. In this section we explain how to deal with such an open cavity within the quantum formalism. To this aim we first build a model for an open cavity with only one partially transmitting mirror, and then proceed to derive the evolution equations satisfied by the intracavity field both in the Heisenberg and Schrödinger pictures.

In the last section, and as an example of another type of phenomenology that can be studied with the formalism of open quantum systems, we show how quantum–optical phenomena can be simulated with ultra–cold atoms trapped in optical lattices [68, 28] (a work developed by the author of the thesis at the Max–Planck Institute for Quantum Optics).

4.1 The open cavity model

For simplicity, we consider only one cavity mode with frequency ω_c , polarization $\boldsymbol{\varepsilon}$, and in the transverse mode $T(\omega_c/c; \mathbf{r}_\perp, z)$, whose boson operators we denote by $\{\hat{a}, \hat{a}^\dagger\}$. The following discussion is straightforwardly generalized to an arbitrary number of cavity modes.

We propose a model in which the cavity mode is coupled through the partially transmitting mirror to the external modes matching it in polarization and transverse shape. These external modes can be modeled as the modes of a second cavity which shares the partially transmitting mirror with the real cavity, but has the second mirror placed at infinity. According to the previous chapter, the field corresponding to such cavity can be written as

$$\hat{\mathbf{A}}(\mathbf{r}, t) = \lim_{L \rightarrow \infty} \sum_q \frac{\boldsymbol{\varepsilon}}{2} \sqrt{\frac{\hbar}{\varepsilon_0 L \omega_{qf}}} \hat{b}_q(t) \{T(\omega_q/c; \mathbf{r}_\perp, z) \exp[i\omega_q z/c] + T(-\omega_q/c; \mathbf{r}_\perp, z) \exp[-i\omega_q z/c]\} + \text{H.c.}, \quad (4.1)$$

where the boson operators satisfy the commutation relations $[\hat{b}_q(t), \hat{b}_{q'}(t)] = \delta_{qq'}$, and $\omega_q = (\pi c/L)q + \Delta\omega^\perp$, being $\Delta\omega^\perp$ a contribution coming from the transverse structure of the modes, which is the same for all the longitudinal modes. Now, as the length of this auxiliary cavity goes to infinity, the set of longitudinal modes becomes infinitely dense in frequency space, so that the sum over q can be replaced by the following integral:

$$\lim_{L \rightarrow \infty} \sum_q = \frac{L}{\pi c} \int_{\mathcal{O}} d\omega. \quad (4.2)$$

Accordingly, the Kronecker delta converges to a Dirac delta as

$$\lim_{L \rightarrow \infty} \delta_{qq'} = \frac{\pi c}{L} \delta(\omega - \omega'), \quad (4.3)$$

so that defining new continuous boson operators by

$$\hat{b}(\omega) = \sqrt{\frac{L}{\pi c}} \lim_{L \rightarrow \infty} \hat{b}_q, \quad (4.4)$$

which satisfy the commutation relations $[\hat{b}(\omega), \hat{b}^\dagger(\omega')] = \delta(\omega - \omega')$, we can finally write the vector potential of the field outside the cavity as

$$\hat{\mathbf{A}}(\mathbf{r}, t) = \int_{\mathcal{O}} d\omega \sqrt{\frac{\hbar}{4\pi c \varepsilon_0 \omega}} \boldsymbol{\varepsilon} \hat{b}(\omega; t) \{T(\omega/c; \mathbf{r}_\perp, z) \exp[i\omega z/c] + T(-\omega/c; \mathbf{r}_\perp, z) \exp[-i\omega z/c]\} + \text{H.c.} \quad (4.5)$$

From the previous sections, we know that the free evolution of the cavity mode and the external modes is ruled by the Hamiltonian $\hat{H}_0 = \hat{H}_{\text{cav}} + \hat{H}_{\text{ext}}$ with

$$\hat{H}_{\text{cav}} = \hbar\omega_c \hat{a}^\dagger \hat{a} + \hat{H}_c \quad \text{and} \quad \hat{H}_{\text{ext}} = \int_{\mathcal{O}} d\omega \hbar\omega \hat{b}^\dagger(\omega) \hat{b}(\omega), \quad (4.6)$$

where \hat{H}_c stands for any other intracavity process that we decide to introduce.

The cavity and external modes are coupled through the mirror via a beam-splitter Hamiltonian

$$\hat{H}_{\text{int}} = i\hbar \int_{\mathcal{O}} d\omega g(\omega) [\hat{b}^\dagger(\omega)\hat{a} - \hat{a}^\dagger\hat{b}(\omega)], \quad (4.7)$$

where the parameter $g(\omega)$ depends basically on the transmittivity of the mirror at the corresponding frequency, and satisfies $g^2(\omega) \ll \omega_c$ for optical frequencies. On the other hand, it is to be expected that only frequencies around the cavity frequency will contribute to the interaction (*resonant interaction*), what allows us to rewrite $g(\omega) = \sqrt{\gamma/\pi}$ in terms of a frequency-independent constant γ , as the transmittivity of mirrors is a slowly varying function of frequency at least within the interval $[\omega_c - \gamma, \omega_c + \gamma]$, as well as extend the integration limits to $[-\infty, +\infty]$, so that finally

$$\hat{H}_{\text{int}} = i\hbar \sqrt{\frac{\gamma}{\pi}} \int_{-\infty}^{+\infty} d\omega [\hat{b}^\dagger(\omega)\hat{a} - \hat{a}^\dagger\hat{b}(\omega)]. \quad (4.8)$$

This is the basic model that we will use to ‘open the cavity’. In the following we show how to deduce reduced evolution equations for the intracavity mode only both at the level of operators (Heisenberg picture) and states (Schrödinger picture).

4.2 Heisenberg picture approach: The quantum Langevin equation

The Heisenberg equations of motion of the annihilation operators are

$$\frac{d\hat{a}}{dt} = -i\omega_c\hat{a} + \left[\hat{a}, \frac{\hat{H}_c}{i\hbar} \right] - \sqrt{\frac{\gamma}{\pi}} \int_{-\infty}^{+\infty} d\omega \hat{b}(\omega), \quad (4.9a)$$

$$\frac{d\hat{b}(\omega)}{dt} = -i\omega\hat{b}(\omega) + \sqrt{\frac{\gamma}{\pi}}\hat{a}. \quad (4.9b)$$

We can formally integrate the second equation as

$$b(\omega; t) = b_0(\omega)e^{-i\omega t} + \sqrt{\frac{\gamma}{\pi}} \int_0^t dt' e^{i\omega(t'-t)} \hat{a}(t'), \quad (4.10)$$

where $b_0(\omega)$ are the external annihilation operators at the initial time. Introducing this solution into the evolution equation for \hat{a} , using $\int_{\tau_0}^{\tau_1} d\tau f(\tau)\delta(\tau - \tau_1) = f(\tau_1)/2$, and defining the *input operator*

$$\hat{b}_{\text{in}}(t) = -\frac{1}{\sqrt{2\pi}} \int_{-\infty}^{+\infty} d\omega e^{-i\omega t} \hat{b}_0(\omega), \quad (4.11)$$

which is easily shown to satisfy the commutation relations

$$[\hat{b}_{\text{in}}(t), \hat{b}_{\text{in}}^\dagger(t')] = \delta(t - t'), \quad (4.12a)$$

$$[\hat{b}_{\text{in}}(t), \hat{b}_{\text{in}}(t')] = [\hat{b}_{\text{in}}^\dagger(t), \hat{b}_{\text{in}}^\dagger(t')] = 0, \quad (4.12b)$$

we get

$$\frac{d\hat{a}}{dt} = -(\gamma + i\omega_c)\hat{a} + \left[\hat{a}, \frac{\hat{H}_c}{i\hbar} \right] + \sqrt{2\gamma}\hat{b}_{\text{in}}(t), \quad (4.13)$$

as the evolution equation for the intracavity mode.

This equation is known as the *quantum Langevin equation* for its similarity with the stochastic Langevin equation, the operator $b_{\text{in}}(t)$ playing the role of the stochastic noise. $b_{\text{in}}(t)$ is interpreted as the operator accounting for the input field driving the cavity at each instant (see Figure 4.1). Indeed, note that when the external modes are in the vacuum state initially, we have

$$\langle \hat{b}_{\text{in}}(t) \rangle = \langle \hat{b}_{\text{in}}^\dagger(t)\hat{b}_{\text{in}}(t') \rangle = 0 \quad \text{and} \quad \langle \hat{b}_{\text{in}}(t)\hat{b}_{\text{in}}^\dagger(t') \rangle = \delta(t - t'), \quad (4.14)$$

so much like complex, Gaussian noises in stochastic Langevin equations.

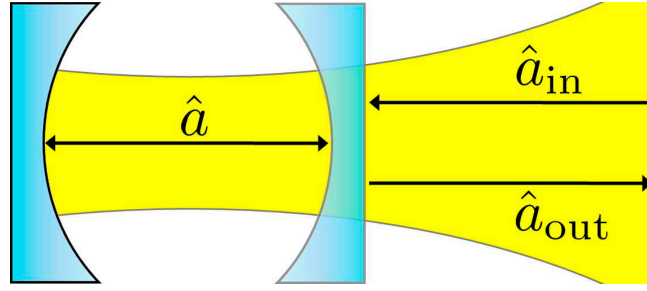


Fig. 4.1: Scheme of the open cavity model. One of the mirrors is not perfectly reflecting, what allows the external modes to drive the cavity via a collective operator \hat{a}_{in} . Similarly, the field coming out from the cavity can be described by a single annihilation operator \hat{a}_{out} , as we show in the next chapter.

In this thesis we will also consider injection of a (ideal) monochromatic laser at frequency ω_L , so that

$$\langle \hat{b}_0(\omega) \rangle = \alpha_L \delta(\omega - \omega_L) \quad \text{and} \quad \langle \hat{b}_0^\dagger(\omega) \hat{b}_0(\omega') \rangle = |\alpha_L|^2 \delta(\omega - \omega_L) \delta(\omega' - \omega_L), \quad (4.15)$$

being α_L the amplitude of the coherent injection. In this case, it is recommendable to define a new input operator

$$\hat{a}_{\text{in}}(t) = \hat{b}_{\text{in}}(t) - \langle \hat{b}_{\text{in}}(t) \rangle, \quad (4.16)$$

which can be shown to satisfy the vacuum correlations (4.14), in terms of which the quantum Langevin equation for the intracavity mode reads

$$\frac{d\hat{a}}{dt} = \mathcal{E} e^{-i\omega_L t} - (\gamma + i\omega_c) \hat{a} + \left[\hat{a}, \frac{\hat{H}_c}{i\hbar} \right] + \sqrt{2\gamma} \hat{a}_{\text{in}}(t), \quad (4.17)$$

with $\mathcal{E} = \alpha_L \sqrt{\gamma/\pi}$. Hence, the injection of a coherent, monochromatic field at frequency ω_L is equivalent to the addition of the following new time-dependent term in the Hamiltonian

$$\hat{H}_{\text{inj}}(t) = i\hbar (\mathcal{E} a^\dagger e^{-i\omega_L t} - \mathcal{E}^* a e^{i\omega_L t}), \quad (4.18)$$

while considering the external modes in vacuum.

Note finally that the solution of this quantum Langevin equation for the case of an empty cavity ($\hat{H}_c = 0$), reads

$$\hat{a}(t) = \hat{a}(t_0) e^{-(\gamma + i\omega_c)t} + \frac{\mathcal{E}}{\gamma + i(\omega_c - \omega_L)} \left[e^{-i\omega_L t} - e^{-(\gamma + i\omega_c)t} \right] + \sqrt{2\gamma} \int_0^t dt' \hat{a}_{\text{in}}(t') e^{(\gamma + i\omega_c)(t'-t)}, \quad (4.19)$$

which for $t \gg \gamma^{-1}$ is simplified to

$$\hat{a}(t) = \frac{\mathcal{E}}{\gamma + i(\omega_c - \omega_L)} e^{-i\omega_L t} + \sqrt{2\gamma} \int_0^t dt' \hat{a}_{\text{in}}(t') e^{(\gamma + i\omega_c)(t'-t)}. \quad (4.20)$$

This time limit is known as the *stationary limit*, as it is possible to show that (4.20) predicts the expectation value of any operator (or function of operators) to be invariant under translations of the time origin, what defines a quantum state as *stationary* [20]. It is possible to show that this condition is satisfied if and only if the density operator describing the state of the system commutes with the Hamiltonian in the Schrödinger picture.

4.3 Schrödinger picture approach: The master equation

Consider now the density operator $\hat{\rho}$ corresponding to the state of the whole system “cavity mode + external modes”, which evolves according to the von Neumann equation

$$i\hbar \frac{d\hat{\rho}}{dt} = [\hat{H}_0 + \hat{H}_{\text{int}} + \hat{H}_{\text{inj}}(t), \hat{\rho}]. \quad (4.21)$$

Note that following the discussion in the previous section, we have included the coherent injection in the Hamiltonian, so that the initial state of the external modes can be taken as vacuum, that is, $\hat{\rho}(t=0) = \hat{\rho}_c(t=0) \otimes \hat{\rho}_{\text{vac}}$, with

$$\langle \hat{b}(\omega) \rangle_{\text{vac}} = \langle \hat{b}^\dagger(\omega) \hat{b}(\omega') \rangle_{\text{vac}} = \langle \hat{b}(\omega) \hat{b}(\omega') \rangle_{\text{vac}} = 0, \quad (4.22)$$

where it is worth reminding that the expectation value of any external operator \hat{A}_{ext} is evaluated as $\langle \hat{A}_{\text{ext}} \rangle_{\text{vac}} = \text{tr}_{\text{ext}}\{\hat{\rho}_{\text{vac}}\hat{A}_{\text{ext}}\}$.

We are going to work in the interaction picture (see Section A.3.2) defined by the transformation operator $\hat{U}_1 = \hat{U}_1\hat{U}_2$, which is a sequence of two transformations defined as $\hat{U}_j = \exp[\hat{H}_j t/i\hbar]$ with

$$\hat{H}_1 = \hbar\omega_L \left[\hat{a}^\dagger \hat{a} + \int_{-\infty}^{+\infty} d\omega \hat{b}^\dagger(\omega) \hat{b}(\omega) \right], \quad (4.23)$$

and

$$\hat{H}_2 = \hat{U}_1^\dagger \left[\hat{H}_0 + \hat{H}_{\text{inj}}(t) \right] \hat{U}_1 - \hat{H}_1 = \hbar\Delta_c \hat{a}^\dagger \hat{a} + \hat{H}_c + \int_{-\infty}^{+\infty} d\omega \hbar\Delta(\omega) \hat{b}^\dagger(\omega) \hat{b}(\omega) + i\hbar(\mathcal{E}a^\dagger - \mathcal{E}^*a). \quad (4.24)$$

In this expression $\Delta_c = \omega_c - \omega_L$, $\Delta(\omega) = \omega - \omega_L$, and we have assumed that $[\hat{H}_c, \hat{U}_1] = 0$ (physically, this means that we consider only intracavity processes that conserve the number of photons). The first transformation rotates the modes to the laser frequency, and is performed in order to eliminate the time dependence of the Hamiltonian (of \hat{H}_{inj} in particular). The second one is made in order to remove all the pieces but \hat{H}_{int} from the Hamiltonian, as a crucial incoming approximation requires the Hamiltonian to be ‘small’.

In this new picture, the state $\rho_I = \hat{U}_2^\dagger \hat{U}_1^\dagger \hat{\rho} \hat{U}_1 \hat{U}_2$ evolves according to $i\hbar d\hat{\rho}_I/dt = [\hat{H}_I, \hat{\rho}_I]$, with $\hat{H}_I = \hat{U}_2^\dagger \hat{U}_1^\dagger \hat{H}_{\text{int}} \hat{U}_1 \hat{U}_2$. Let us define the interaction picture intracavity annihilation operator

$$\hat{a}_I(t) = \hat{U}_2^\dagger \hat{U}_1^\dagger \hat{a} \hat{U}_1 \hat{U}_2, \quad (4.25)$$

so that taking into account that

$$\hat{U}_2^\dagger \hat{U}_1^\dagger \hat{b}(\omega) \hat{U}_1 \hat{U}_2 = e^{-i\omega t} \hat{b}(\omega), \quad (4.26)$$

the interaction picture Hamiltonian can be rewritten as

$$\hat{H}_I(t) = i\hbar \sqrt{\frac{\gamma}{\pi}} \int_{-\infty}^{+\infty} d\omega \left[\hat{a}_I(t) \hat{b}^\dagger(\omega) e^{i\omega t} - \hat{a}_I^\dagger(t) \hat{b}(\omega) e^{-i\omega t} \right]. \quad (4.27)$$

We seek now for the evolution equation of the reduced state $\hat{\rho}_{\text{CI}} = \text{tr}_{\text{ext}}\{\hat{\rho}_I\}$ corresponding to the intracavity mode alone. To do so, we first integrate formally the von Neumann equation for the whole system as

$$\hat{\rho}_I(t) = \hat{\rho}_I(t_0) + \frac{1}{i\hbar} \int_{t_0}^t dt' [\hat{H}_I(t'), \hat{\rho}_I(t')]; \quad (4.28)$$

reintroducing this expression into the von Neumann equation, making the partial trace over the external modes taking into account that $\text{tr}_{\text{ext}}\{[\hat{H}_I(t), \hat{\rho}_I(0)]\} \sim \langle \hat{b} \rangle_{\text{vac}} = 0$, and making the variable change $t' = t - \tau$ in the time integral, we get the following integro-differential equation for the reduced density operator $\hat{\rho}_{\text{CI}}$:

$$\frac{d\hat{\rho}_{\text{CI}}(t)}{dt} = -\frac{1}{\hbar^2} \int_0^t d\tau \text{tr}_{\text{ext}}\{[\hat{H}_I(t), [\hat{H}_I(t-\tau), \hat{\rho}_I(t-\tau)]]\}. \quad (4.29)$$

This equation is exact, but now we are going to introduce two important approximations which lead to huge simplifications. The first is the *Born approximation*, which states that the external modes are basically unaffected by the intracavity dynamics, that is, $\hat{\rho}_I(t) = \hat{\rho}_{\text{CI}}(t) \otimes \hat{\rho}_{\text{vac}}$. Then we perform the *Markov approximation*, which states that memory effects can be neglected, that is, we can take $\hat{\rho}_I(t-\tau) = \hat{\rho}_I(t)$ in the integral kernel. It can be shown that this approximations are quite good in quantum optics thanks to the fact that $\gamma/\omega_c \ll 1$ [69].

Introducing these approximations in (4.29), and performing the partial traces using (4.22), it is completely straightforward to arrive to the following linear differential equation for the reduced intracavity state

$$\frac{d\hat{\rho}_{\text{CI}}}{dt} = 2\gamma \hat{a}_I \hat{\rho}_{\text{CI}} \hat{a}_I^\dagger - \gamma \hat{a}_I^\dagger \hat{a}_I \hat{\rho}_{\text{CI}} - \gamma \hat{\rho}_{\text{CI}} \hat{a}_I^\dagger \hat{a}_I, \quad (4.30)$$

where all the operators are evaluated at the same time. Finally, coming back to the Schrödinger picture, we finally arrive to

$$\frac{d\hat{\rho}_{\text{C}}}{dt} = \left[\frac{\hat{H}_{\text{cav}} + \hat{H}_{\text{inj}}(t)}{i\hbar}, \hat{\rho}_{\text{C}} \right] + \gamma (2\hat{a} \hat{\rho}_{\text{C}} \hat{a}^\dagger - \hat{a}^\dagger \hat{a} \hat{\rho}_{\text{C}} - \hat{\rho}_{\text{C}} \hat{a}^\dagger \hat{a}), \quad (4.31)$$

where $\hat{\rho}_{\text{C}} = \text{tr}_{\text{ext}}\{\hat{\rho}\}$ is the reduced state of the intracavity mode in the Schrödinger picture. This equation is known as the *master equation* of the intracavity mode.

In order to evaluate intracavity moments of observables, in this thesis we will choose this Schrödinger approach in general. The reason is that having a master equation for the intracavity state only, we can apply the positive P techniques that we introduced at the end of Chapter 2 for the harmonic oscillator, what will allow us to deal with stochastic equations instead of operator equations of the type (4.17).

4.4 Relation of the model parameters to physical parameters

In the previous sections we have introduced the basic model that we will use for the evolution of a light mode inside an open cavity. The model turned out to have two basic parameters, \mathcal{E} and γ , describing the rates at which coherent light is injected into the cavity and intracavity light is lost through the partially transmitting mirror, respectively. In this section we connect these model parameters to relevant physical parameters like the transmittivity of the mirror and the power of the injected laser beam.

This connection is easily done by following classical arguments. Consider the classical electromagnetic field associated to the intracavity mode, whose corresponding vector potential can be written as

$$\mathbf{A}(\mathbf{r}, t) = \frac{1}{2} \sqrt{\frac{1}{2n(z)\varepsilon_0 L_{\text{opt}}}} \varepsilon \nu(t) \{T(k_c; \mathbf{r}_\perp, z) \exp[in(z)k_c z] + T^*(k_c; \mathbf{r}_\perp, z) \exp[-in(z)k_c z]\} + \text{c.c.}, \quad (4.32)$$

in terms of the normal variable ν of the equivalent harmonic oscillator as we showed in Section 3.4.4. In this expression we have defined $k_c = \omega_c/c$. Now, remember that in Chapter 2 we learned that the mean values of quantum observables provide the behavior of their classical counterparts as long as quantum fluctuations can be neglected (see also the discussion at the beginning of Section 6.3.2). Applied to the cavity mode, this means that its classical normal variable evolves as $\nu(t) = \sqrt{2\hbar/\omega_c} \langle \hat{a}(t) \rangle$. Then, for an empty cavity ($\dot{H}_c = 0$) and injecting *on resonance* for simplicity, that is, $\omega_L = \omega_c$, we have

$$\nu(t) = \nu_0 e^{-(\gamma+i\omega_c)t} + \sqrt{\frac{2\hbar}{\omega_c}} \frac{\mathcal{E}}{\gamma} \left[e^{-i\omega_c t} - e^{-(\gamma+i\omega_c)t} \right], \quad (4.33)$$

with $\nu_0 = \nu(t=0)$, as follows from (4.19).

Loss rate. We can connect the damping rate γ with the mirror transmittivity \mathcal{T} (reflectivity $\mathcal{R} = 1 - \mathcal{T}$) by noting that in the absence of injection, $\mathcal{E} = 0$, a fraction $\mathcal{R}^{1/2}$ of the field amplitude is lost through the mirror at every roundtrip; hence, after $m \in \mathbb{N}$ roundtrips, we will have the relation

$$\mathbf{A}(\mathbf{r}_\perp, z \oplus_m \text{r.t.}, t_m) = \mathcal{R}^{m/2} \mathbf{A}(\mathbf{r}_\perp, z, t_m), \quad (4.34)$$

where ‘ $\oplus_m \text{r.t.}$ ’ stands for ‘plus m -roundtrips’ and $t_m = 2mL_{\text{opt}}/c$. Introducing the solution (4.33) for $\nu(t)$ in this expression, and taking into account the definition of the cavity modes (3.78), it is straightforward to get

$$\gamma = -\frac{c}{4L_{\text{opt}}} \ln \mathcal{R} \simeq \frac{c\mathcal{T}}{4L_{\text{opt}}}, \quad (4.35)$$

where in the last equality we have assumed that $\mathcal{R} \approx 1$. Hence, we see that for small mirror transmittivities, there exists a linear relation between the model parameter γ and the actual mirror transmittivity \mathcal{T} .

In order to understand the magnitude of this parameter let us consider a cavity with lengths varying between 5 mm to 500 mm as in the previous chapter; the damping rate γ varies then between 150 MHz and 1.5 MHz for $\mathcal{R} = 0.99$, and 1.5 GHz and 0.015 GHz for $\mathcal{R} = 0.9$, which are well below optical frequencies. It is customary to call *quality factor* to the ratio between the free spectral range and the damping rate, $Q = \Omega_{\text{FSR}}/\gamma$. This parameter is very important as it measures the ratio between the separation of the longitudinal resonances of a given transverse family and the width of these. In other words, when the quality factor is large one can distinguish the different longitudinal resonances, while when it is small the Lorentzians associated to different resonances overlap, and the resonances are no longer distinguishable. In this thesis we will always work with cavities having large enough quality factors as can be deduced from the numerical examples that we have introduced.

Injection parameter. Consider now the part of the intracavity vector potential propagating along the $-\mathbf{e}_z$ direction. According to (4.32) and (4.33), for a finite injection parameter \mathcal{E} and in the stationary limit $t \gg \gamma^{-1}$, we can write it as

$$\mathbf{A}_\leftarrow(\mathbf{r}, t) = \frac{1}{2} \sqrt{\frac{\hbar}{n(z)\varepsilon_0 L_{\text{opt}} \omega_c}} \frac{|\mathcal{E}|}{\gamma} \varepsilon T^*(k_c; \mathbf{r}_\perp, z) e^{-in(z)k_c z - i\omega_c t + i\varphi} + \text{c.c.}, \quad (4.36)$$

being φ the phase of the injected laser beam. On the other hand, based on (3.73) and (3.76), the vector potential associated to the laser inciding the cavity is written in terms of its power P_{inj} as

$$\mathbf{A}_{\text{inj}}(\mathbf{r}, t) = \sqrt{\frac{P_{\text{inj}}}{2\varepsilon_0 c \omega_c^2}} \varepsilon T^*(k_c; \mathbf{r}_\perp, z) \exp(-ik_c z - i\omega_c t + i\varphi) + \text{c.c.}, \quad (4.37)$$

We can obtain an expression of the field inside the cavity by looking at it as an interferometer: The part of the injection which is transmitted inside the cavity at a given time interferes with the fields that have been bouncing back and forth for several roundtrips. In this sense, the complete field will be a superposition of the fields

$$\mathbf{A}^{(0)}(\mathbf{r}, t) = \mathcal{T}^{1/2} \mathbf{A}_{\text{inj}}(\mathbf{r}, t), \quad (4.38a)$$

$$\mathbf{A}^{(1)}(\mathbf{r}, t) = \mathcal{T}^{1/2} \mathcal{R}^{1/2} \mathbf{A}_{\text{inj}}(\mathbf{r}_{\perp}, z \oplus \text{r.t.}, t), \quad (4.38b)$$

$$\mathbf{A}^{(2)}(\mathbf{r}, t) = \mathcal{T}^{1/2} \mathcal{R} \mathbf{A}_{\text{inj}}(\mathbf{r}_{\perp}, z \oplus_2 \text{r.t.}, t), \quad (4.38c)$$

⋮

$$\mathbf{A}^{(m)}(\mathbf{r}, t) = \mathcal{T}^{1/2} \mathcal{R}^{m/2} \mathbf{A}_{\text{inj}}(\mathbf{r}_{\perp}, z \oplus_m \text{r.t.}, t), \quad (4.38d)$$

and hence, assuming that the time is large enough as to take the $m \rightarrow \infty$ limit we get

$$\mathbf{A}_{\leftarrow}(\mathbf{r}, t) = \sqrt{\frac{P_{\text{inj}}}{2n(z)\varepsilon_0 c}} \mathcal{T}^{1/2} \left(\sum_{m=0}^{\infty} \mathcal{R}^{m/2} \right) \varepsilon T^*(k_c; \mathbf{r}_{\perp}, z) e^{-ik_c z - i\omega_c t + i\varphi} + \text{c.c.}, \quad (4.39)$$

where we have used again the definition of the cavity modes (3.78). Comparing (4.36) with this expression, and performing the geometric sum we finally get

$$|\mathcal{E}| = \gamma \sqrt{\frac{2LP_{\text{inj}}}{\hbar\omega_c c}} \frac{\mathcal{T}^{1/2}}{1 - \mathcal{R}^{1/2}} \simeq \sqrt{\frac{2\gamma}{\hbar\omega_c} P_{\text{inj}}}, \quad (4.40)$$

where in the last equality we have assumed that $\mathcal{R} \approx 1$ and have made use of (4.35).

4.5 Quantum–optical phenomena with optical lattices

In connection with the theory of open quantum systems that we have particularized to optical cavities in this chapter, we now introduce the work that the author of this thesis started at the Max–Planck–Institute for Quantum Optics during a three–months visit in 2008, and that ended up published at the beginning of 2011 [28].

Ultracold atoms trapped in optical lattices are well known as quite versatile simulators of a large class of many–body condensed–matter Hamiltonians¹ (see [72, 73, 74] for extensive reviews on this subject). In this work, and exploiting currently available technology only, we have been able to show that they can also be used to simulate phenomena traditionally linked to quantum–optical systems, that is, to light–matter interactions [68, 28]. In this brief exposition of the work, we explain in particular how to observe phenomena arising from the collective spontaneous emission of atomic and harmonic oscillator ensembles such as sub/superradiance, including some phenomena which still lack experimental observation.

The concept of superradiance was introduced by Dicke in 1954 when studying the spontaneous emission of a collection of two–level atoms [78] (see [79] for a review). He showed that certain collective states where the excitations are distributed symmetrically over the whole sample have enhanced emission rates. Probably the most stunning example is the single–excitation symmetric state (now known as the symmetric Dicke state), which instead of decaying with the single–atom decay rate Γ_0 , was shown to decay with $N\Gamma_0$, N being the number of atoms. He also suggested that the emission rate of the state having all the atoms excited should be enhanced at the initial steps of the decay process, which was a most interesting prediction from the experimental point of view, as this state is in general easier to prepare. However, Dicke used a very simplified model in which all the atoms interact with a common radiation field within the dipolar approximation; almost 15 years later, and motivated by the new atom–inversion techniques, several authors showed that dipolar interactions impose a threshold value for the atom density, that is, for the number of interacting atoms, in order for superradiance to appear [80, 81, 82].

It is worth noting that together with atomic ensembles, spontaneous emission of collections of harmonic oscillators were also studied at that time [81]. Two interesting features of this system were reported: (i) an initial state with all

¹ One of the first proposals in this direction was the article by Jacksch et al. [70], where it was proved that the dynamics of cold atoms trapped in optical lattices is described by the Bose–Hubbard Hamiltonian provided that certain conditions are satisfied; shortly after, the superfluid–to–Mott insulator phase transition characteristic of this Hamiltonian was observed in the laboratory [71]. Since then, the broad tunability of the lattice parameters, and the increasing ability to trap different kind of particles (like bosonic and fermionic atoms with arbitrary spin or polar molecules), has allowed theoreticians to propose optical lattices as promising simulators for different types of generalized Bose–Hubbard and spin models which are in close relation to important condensed–matter phenomena [72, 73, 74]. Recent experiments have shown that optical lattices can be used to address open problems in physics like, e.g., high– T_c superconductivity [75], to study phenomena in low dimensions such as the Berezinskii–Kosterlitz–Thouless transition [76], or to implement quantum computation schemes [77].

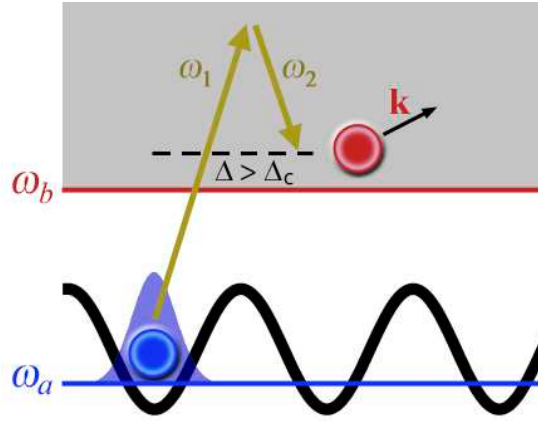


Fig. 4.2: Scheme of our proposed setup. Atoms in state a are trapped in an optical lattice, while atoms in state b are free, and can thus have any momentum. An external pair of Raman lasers connect the two levels with some detuning Δ . We will show that above some critical value $\Delta = \Delta_c$ the atoms in state b are able to leave the trap (left), and behave as the photons emitted in superradiant quantum-optical systems. The case $\Delta < \Delta_c$ and more quantum-optical phenomenology can be found in [28].

the harmonic oscillators excited does not show rate enhancement, on the contrary, most excitations remain within the sample in the steady state, while (ii) the state having all the oscillators in the same coherent state has a superradiant rate. This predictions have not been observed in the laboratory yet to our knowledge.

4.5.1 The basic idea

The basic setup that we introduce, and that was already presented in [68], is depicted in figure 4.2. Consider a collection of bosonic atoms with two relevant internal states labeled by a and b (which may correspond to hyperfine ground-state levels, see for example [72]). Atoms in state a are trapped by a deep optical lattice in which the localized wavefunction of traps at different lattice sites do not overlap (preventing hopping of atoms between sites), while atoms in state b are not affected by the lattice, and hence behave as free particles. A pair of lasers forming a Raman scheme drive the atoms from the trapped state to the free one [72], providing an effective interaction between the two types of particles. We consider the situation of having non-interacting bosons in the lattice [83], as well as hard-core bosons in the collisional blockade regime, where only one or zero atoms can be in a given lattice site [84]. In the first regime, the lattice consists of a collection of harmonic oscillators placed at the nodes of the lattice; in the second regime, two-level systems replace the harmonic oscillators, the two levels corresponding to the absence or presence of an atom in the lattice site. Therefore, it is apparent that this system is equivalent to a collection of independent emitters (harmonic oscillators or atoms) connected only through a common radiation field, the role of this radiation field being played by the free atoms. This system is therefore the cold-atom analog of the systems which are usually considered in the quantum description of light-matter interaction, with the difference that the radiated particles are massive, and hence have a different dispersion relation than that of photons in vacuum.

Let us introduce the model for such system. Our starting point is the Hamiltonian of the system in second quantization [85]. We will denote by $|a\rangle$ and $|b\rangle$ the trapped and free atomic states, respectively (having internal energies $\hbar\omega_a^0$ and $\hbar\omega_b^0$). Two-body interactions for the trapped atoms are included with the usual contact-like pseudopotential [74, 83], but we neglect the collisions for the free atoms. The Hamiltonian is then written as $\hat{H} = \hat{H}_0 + \hat{H}_{a-b}$, with

$$\hat{H}_0 = \sum_{j=a,b} \int d^3\mathbf{r} \hat{\Psi}_j^\dagger(\mathbf{r}) (H_j + \hbar\omega_j^0) \hat{\Psi}_j(\mathbf{r}) + \frac{g}{2} \int d^3\mathbf{r} \hat{\Psi}_a^\dagger{}^2(\mathbf{r}) \hat{\Psi}_a^2(\mathbf{r}), \quad (4.41a)$$

$$\hat{H}_{a-b} = \hbar\Omega \int d^3\mathbf{r} e^{i(\mathbf{k}_L \cdot \mathbf{r} - \omega_L t)} \hat{\Psi}_a(\mathbf{r}) \hat{\Psi}_b^\dagger(\mathbf{r}) + \text{H.c.}; \quad (4.41b)$$

\hat{H}_0 contains the individual dynamics of the atoms, H_j being the first-quantized motion Hamiltonian of the atom in the corresponding state, and $g = 4\pi\hbar^2 a_s/m$, where a_s is the s -wave scattering length of the trapped atoms (which have mass m). \hat{H}_{a-b} contains the Raman coupling between the atomic states, $\mathbf{k}_L = \mathbf{k}_1 - \mathbf{k}_2$ and $\omega_L = \omega_1 - \omega_2$ (laser wave vector and frequency in the following) being the relative wave vector and frequency of the two lasers involved in the Raman scheme (see figure 4.2), with Ω the corresponding two-photon Rabi frequency.

For atoms in state $|a\rangle$, $H_a = -(\hbar^2/2m)\nabla^2 + V_{\text{opt}}(\mathbf{r})$, where $V_{\text{opt}}(\mathbf{r})$ corresponds to a 3-dimensional optical lattice with cubic geometry and lattice period d_0 . We work with ultracold atoms under conditions such that their wavefunctions can be described by the set of first-band Wannier functions localized around the nodes of the lattice [72]. The traps of the optical lattice are approximated by isotropic harmonic potentials [72], what allows us to write the Wannier functions as

$$w_0(\mathbf{r} - \mathbf{r}_j) = \frac{1}{\pi^{3/4} X_0^{3/2}} \exp\left[-(\mathbf{r} - \mathbf{r}_j)^2 / 2X_0^2\right], \quad (4.42)$$

where $\mathbf{r}_j = d_0\mathbf{j}$ is the position of the $\mathbf{j} \in \mathbb{Z}^3$ lattice site (we consider M sites in each orthogonal direction defining the cubic lattice), and $X_0^2 = \hbar/m\omega_0$, being ω_0 the frequency of the harmonic trap. The energy associated to these wave functions is $E_0 = 3\hbar\omega_0/2$. We will assume that Wannier functions localized at different lattice sites do not overlap, hence preventing tunneling between sites.

On the other hand, atoms in state $|b\rangle$ can move freely in every direction of space according to $H_b = -(\hbar^2/2m)\nabla^2$, and hence the plane waves $\psi_{\mathbf{k}}(\mathbf{r}) = e^{i\mathbf{k}\cdot\mathbf{r}}/\sqrt{V}$, with energy $E_{\mathbf{k}} = \hbar^2 k^2/2m$, are their motion eigenfunctions (V is the total available volume for the free atoms, which we might take as infinite for calculations).

We consider two opposite regimes for the interaction between trapped atoms. The first limit consists in neglecting the interactions, which might be accomplished by, e.g., tuning the scattering length with an additional magnetic field through a Feshbach resonance [83]. Let us expand the quantum fields as

$$\hat{\Psi}_a(\mathbf{r}) = \sum_{\mathbf{j}} w_0(\mathbf{r} - \mathbf{r}_j) \hat{a}_{\mathbf{j}} \quad \text{and} \quad \hat{\Psi}_b(\mathbf{r}) = \sum_{\mathbf{k}} \psi_{\mathbf{k}}(\mathbf{r}) \hat{b}_{\mathbf{k}}, \quad (4.43)$$

where the operators $\{\hat{a}_{\mathbf{j}}, \hat{a}_{\mathbf{j}}^\dagger\}$ and $\{\hat{b}_{\mathbf{k}}, \hat{b}_{\mathbf{k}}^\dagger\}$ satisfy canonical bosonic commutation relations, and create or annihilate an atom at lattice site \mathbf{j} and a free atom with momentum \mathbf{k} , respectively. Working in the interaction picture defined by the transformation operator $\hat{U}_I = \exp[\hat{H}_0 t/i\hbar]$, we get the Hamiltonian

$$\hat{H}_I = \sum_{\mathbf{j}, \mathbf{k}} g_{\mathbf{k}} \exp[i\Delta_{\mathbf{k}} t - i(\mathbf{k} - \mathbf{k}_L) \cdot \mathbf{r}_j] \hat{a}_{\mathbf{j}} \hat{b}_{\mathbf{k}}^\dagger + \text{H.c.}, \quad (4.44)$$

with

$$g_{\mathbf{k}} = \hbar\Omega \sqrt{\frac{8\pi^{3/2} X_0^3}{V}} \exp\left[-\frac{1}{2} X_0^2 (\mathbf{k} - \mathbf{k}_L)^2\right], \quad \Delta_{\mathbf{k}} = \frac{\hbar k^2}{2m} - \Delta, \quad (4.45)$$

$\Delta = \omega_L - (\omega_b - \omega_a)$ being the detuning of the laser frequency respect to the $|a\rangle \rightleftharpoons |b\rangle$ transition ($\omega_a = \omega_a^0 + 3\omega_0/2$ and $\omega_b = \omega_b^0$).

As for the second limit, we assume that the on-site repulsive atom-atom interaction is the dominant energy scale, and hence the trapped atoms behave as hard-core bosons in the collisional blockade regime, what prevents the presence of two atoms in the same lattice site [84]; this means that the spectrum of $\hat{a}_{\mathbf{j}}^\dagger \hat{a}_{\mathbf{j}}$ can be restricted to the first two states $\{|0\rangle_{\mathbf{j}}, |1\rangle_{\mathbf{j}}\}$, having 0 or 1 atoms at site \mathbf{j} , and then the boson operators $\{\hat{a}_{\mathbf{j}}^\dagger, \hat{a}_{\mathbf{j}}\}$ can be changed by spin-like ladder operators $\{\hat{\sigma}_{\mathbf{j}}^\dagger, \hat{\sigma}_{\mathbf{j}}\} = \{|1\rangle_{\mathbf{j}}\langle 0|, |0\rangle_{\mathbf{j}}\langle 1|\}$. In this second limit the Hamiltonian reads

$$\hat{H}_I = \sum_{\mathbf{j}, \mathbf{k}} g_{\mathbf{k}} e^{i\Delta_{\mathbf{k}} t - i(\mathbf{k} - \mathbf{k}_L) \cdot \mathbf{r}_j} \hat{\sigma}_{\mathbf{j}} \hat{\sigma}_{\mathbf{k}}^\dagger + \text{H.c.} \quad (4.46)$$

Hamiltonians (4.44) and (4.46) show explicitly how this system mimics the dynamics of collections of harmonic oscillators or atoms, respectively, interacting with a common radiation field. Note finally that in order to satisfy that the trapped atoms are within the first Bloch band, it is required that $\omega_0 \gg \Delta, \Omega$.

We are going to analyze the system by considering the free atoms as an environment for the trapped atoms, similarly to the optical cavity, in which the external modes act as an environment for the intracavity modes. Following the same approach as that of Section 4.3, that is, assuming that the environment is in a non-evolving vacuum (Born-Markov approximation) and tracing out its associated Hilbert space, it is simple [28] to get the following master equation for the reduced density operator of the trapped atoms

$$\frac{d\hat{\rho}}{dt} = \sum_{\mathbf{j}, \mathbf{l}} \Gamma_{\mathbf{j}-\mathbf{l}} \hat{a}_{\mathbf{l}} \hat{\rho} \hat{a}_{\mathbf{j}}^\dagger - \Gamma_{\mathbf{j}-\mathbf{l}} \hat{a}_{\mathbf{j}}^\dagger \hat{a}_{\mathbf{l}} \hat{\rho} + \text{H.c.}; \quad (4.47)$$

a similar equation is obtained for the hard-core bosons but replacing the boson operators by the corresponding spin operators. Note the similarity between this equation, and the equation of the damped mode inside the cavity (4.30),

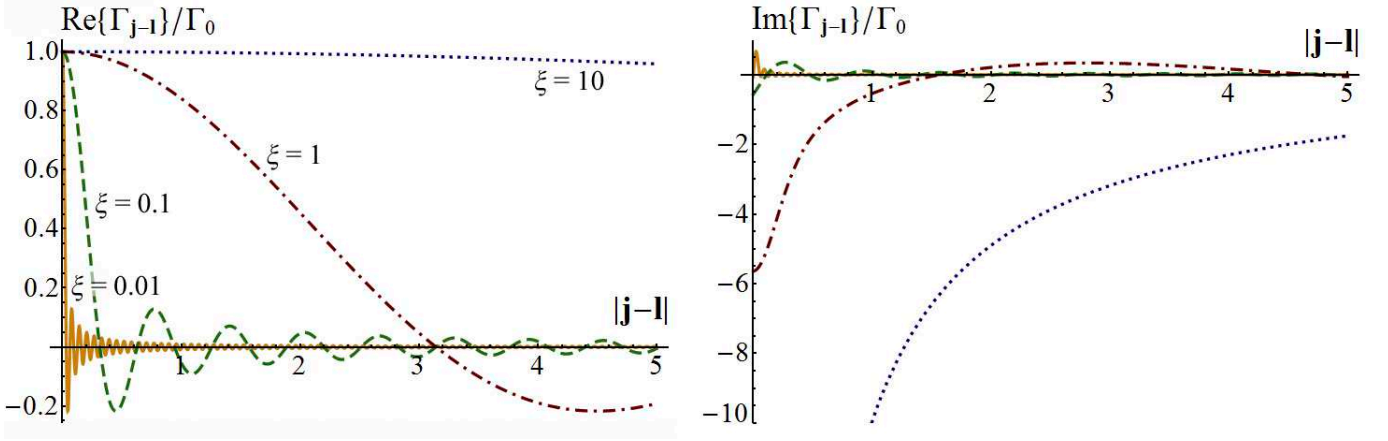


Fig. 4.3: We plot the Markov couplings (real and imaginary parts at left and right, respectively) as a function of the distance between sites for $\tilde{\Delta} > 0$. We have chosen $d_0/X_0 = 10$ and $\mathbf{k}_L = \mathbf{0}$, and plotted 4 different values of ξ . It can be appreciated that this parameter controls the spatial range of the interactions.

their main difference being that now the different modes of the system interact via the Markov couplings

$$\Gamma_{\mathbf{j}-\mathbf{l}} = i \exp(-i\mathbf{k}_L \cdot \mathbf{r}_{\mathbf{j}-\mathbf{l}}) \frac{\Gamma_0 \xi}{|\mathbf{j}-\mathbf{l}|} \left[1 - \operatorname{erf} \left(\frac{d_0}{2X_0} |\mathbf{j}-\mathbf{l}| \right) - \exp \left(-\nu \frac{|\mathbf{j}-\mathbf{l}|}{\xi} \right) \right], \quad (4.48)$$

where $\xi = 1/d_0 k_0$ with $k_0 = X_0^{-1} \sqrt{2|\tilde{\Delta}|/\omega_0}$ measures the ratio between the lattice spacing and the characteristic wavelength of the radiated atoms, $\tilde{\Delta} = \Delta - 4\Omega^2/\omega_0$, and $\nu = 1$ ($-i$) for $\tilde{\Delta} < 0$ ($\tilde{\Delta} > 0$). The error function is defined as $\operatorname{erf}(x) = (2/\sqrt{\pi}) \int_0^x du \exp(-u^2)$. Note that the term ‘ $1 - \operatorname{erf}(d_0 |\mathbf{j}-\mathbf{l}|/2X_0)$ ’ is basically zero for $\mathbf{j} \neq \mathbf{l}$, and therefore the ξ parameter dictates the spatial range of the interactions as can be appreciated in figure 4.3. Finally, $\Gamma_0 = 4\Omega^2 \sqrt{2\pi|\tilde{\Delta}|/\omega_0^3}$ is the single-emitter decay rate, that is, the rate at which the atoms are emitted by the lattice when the sites emit independently (see [28] for details).

4.5.2 Superradiant phenomenology

In order to prove that quantum–optical phenomena can be found in this system we now show that the superradiant phenomenology described at the beginning of the section appears on it. For $\mathbf{k}_L = 0$ and $\tilde{\Delta} > 0$, the Markov couplings are complex in general, and therefore the master equation of the system takes the form

$$\frac{d\hat{\rho}}{dt} = \frac{1}{i\hbar} [\hat{H}_d, \hat{\rho}] + \mathcal{D}[\hat{\rho}], \quad (4.49)$$

with a dissipation term given by

$$\mathcal{D}[\hat{\rho}] = \sum_{\mathbf{j}, \mathbf{l}} \gamma_{\mathbf{j}-\mathbf{l}} \left(2\hat{a}_1 \hat{\rho} \hat{a}_j^\dagger - \hat{a}_j^\dagger \hat{a}_1 \hat{\rho} - \hat{\rho} \hat{a}_1^\dagger \hat{a}_j \right), \quad (4.50)$$

having collective decay rates

$$\gamma_{\mathbf{j}-\mathbf{l}} = \operatorname{Re} \{ \Gamma_{\mathbf{j}-\mathbf{l}} \} = \Gamma_0 \operatorname{sinc} \left(\frac{|\mathbf{j}-\mathbf{l}|}{\xi} \right), \quad (4.51)$$

and a reversible term corresponding to inhomogeneous dephasing with Hamiltonian

$$\hat{H}_d = \sum_{\mathbf{j}, \mathbf{l}} \hbar \Lambda_{\mathbf{j}-\mathbf{l}} \hat{a}_j^\dagger \hat{a}_l, \quad (4.52)$$

being

$$\Lambda_{\mathbf{j}-\mathbf{l}} = \operatorname{Im} \{ \Gamma_{\mathbf{j}-\mathbf{l}} \} = \frac{\Gamma_0 \xi}{|\mathbf{j}-\mathbf{l}|} \left[1 - \operatorname{erf} \left(\frac{d_0}{2X_0} |\mathbf{j}-\mathbf{l}| \right) - \cos \left(\frac{|\mathbf{j}-\mathbf{l}|}{\xi} \right) \right]. \quad (4.53)$$

The same holds for hard-core bosons but replacing the boson operators by the corresponding spin operators.

For $\xi \ll 1$ the Markov couplings do not connect different lattice sites, that is $\Gamma_{j-1} \simeq \Gamma_0 \delta_{j,1}$, and the sites emit independently. On the other hand, when $\xi \gg M$ the collective decay rates become homogeneous, $\gamma_{j-1} \simeq \Gamma_0$, and we enter the Dicke regime. Hence, we expect to observe the superradiant phase-transition in our system by varying the parameter ξ .

Note that in the Dicke regime the dephasing term cannot be neglected and connects the sites inhomogeneously with $\Lambda_{j \neq 1} \simeq \Gamma_0 \xi / |j-1|$. This term appears in the optical case too, although it was inappropriately neglected in the original work by Dicke [78] when assuming the dipolar approximation in his initial Hamiltonian, and slightly changes his original predictions as pointed out in [86, 87] (see also [79]).

In the following we analyze the superradiant behavior of our system by studying the evolution of the total number of particles in the lattice $n_T = \sum_j \langle \hat{a}_j^\dagger \hat{a}_j \rangle$ and the rate of emitted atoms

$$\mathcal{R}(t) = \sum_{\mathbf{k}} \frac{d}{dt} \langle \hat{b}_{\mathbf{k}}^\dagger \hat{b}_{\mathbf{k}} \rangle = -\dot{n}_T; \quad (4.54)$$

in the last equality we have used that the total number operator $\sum_{\mathbf{k}} \hat{b}_{\mathbf{k}}^\dagger \hat{b}_{\mathbf{k}} + \sum_j \hat{a}_j^\dagger \hat{a}_j$ is a constant of motion.

Hard-core bosons: Atomic superradiance.

Let us start by analyzing the case of a lattice in an initial Mott phase having one atom per site in the collisional blockade regime, which is the analog of an ensemble of excited atoms [68]. As explained in the Introduction, Dicke predicted that superradiance should appear in this system as an enhancement of the emission rate at early times [78], although this was later proved to happen only if the effective number of interacting emitters exceeds some threshold value [80, 81, 82]: This is the superradiant phase transition.

In our system, the number of interacting spins is governed by the parameter ξ (see figure 4.3), and the simplest way to show that the superradiant phase transition appears by varying it, is by evaluating the initial slope of the rate which can be written as²

$$\left. \frac{d}{dt} \mathcal{R} \right|_{t=0} = -4M^3 \Gamma_0^2 \left[1 - \sum_{\mathbf{m} \neq \mathbf{j}} \frac{\text{sinc}^2(|\mathbf{j} - \mathbf{m}|/\xi)}{M^3} \right]. \quad (4.56)$$

This expression has a very suggestive form: The term corresponding to the rate associated to independent emitters is balanced by a collective contribution arising from the interactions between them. In figure 4.4a we show the dependence of this derivative with ξ for various values of the number of sites M^3 . It can be appreciated that there exists a critical value of ξ above which the sign of the derivative is reversed; hence, the rate increases at the initial time and we expect its maximum to be no longer at $t = 0$, which is a signature of superradiance.

The time evolution of the rate for a cubic lattice with $M^3 = 27$ sites is shown in figure 4.4b for different values of ξ . We can appreciate how above some critical ξ value the maximum rate of emission is delayed as expected. In order to find $\mathcal{R}(t)$ we have simulated the evolution equations for the coherences $c_{\mathbf{j}\mathbf{l}} = \langle \hat{\sigma}_{\mathbf{j}}^\dagger \hat{\sigma}_{\mathbf{l}} \rangle$ and the populations $s_{\mathbf{j}} = \langle \hat{\sigma}_{\mathbf{j}}^3 \rangle$, which we close by using the semiclassical approximation $\langle \hat{\sigma}_{\mathbf{m}}^\dagger \hat{\sigma}_{\mathbf{j}}^3 \hat{\sigma}_{\mathbf{l}} \rangle = \langle \hat{\sigma}_{\mathbf{m}}^\dagger \hat{\sigma}_{\mathbf{l}} \rangle \langle \hat{\sigma}_{\mathbf{j}}^3 \rangle - 2\delta_{\mathbf{j}\mathbf{l}} \langle \hat{\sigma}_{\mathbf{m}}^\dagger \hat{\sigma}_{\mathbf{l}} \rangle$; they read (4.55)

$$\dot{c}_{\mathbf{j}\mathbf{l}} = -4\Gamma_0 c_{\mathbf{j}\mathbf{l}} + \sum_{\mathbf{m}} \Gamma_{\mathbf{l}-\mathbf{m}} c_{\mathbf{j}\mathbf{m}} s_{\mathbf{l}} + \Gamma_{\mathbf{j}-\mathbf{m}}^* c_{\mathbf{m}\mathbf{l}} s_{\mathbf{j}}, \quad (4.57a)$$

$$\dot{s}_{\mathbf{j}} = -2 \sum_{\mathbf{l}} \Gamma_{\mathbf{j}-\mathbf{l}} c_{\mathbf{j}\mathbf{l}} + \Gamma_{\mathbf{j}-\mathbf{l}}^* c_{\mathbf{l}\mathbf{j}}. \quad (4.57b)$$

We have checked the validity of these semiclassical equations by comparing them with a direct simulation of the master equation for small number of sites in 1D and 2D geometries; except for small quantitative deviations, they offer the same results.

² Note that the evolution equation of the expectation value of any operator \hat{O} can be written as

$$\frac{d}{dt} \langle \hat{O}(t) \rangle = \text{tr} \left\{ \frac{d\hat{\rho}}{dt} \hat{O} \right\} = - \sum_{\mathbf{m}, \mathbf{l}} \left\{ \Gamma_{\mathbf{m}-\mathbf{l}} \langle [\hat{O}, \hat{a}_{\mathbf{m}}^\dagger] \hat{a}_{\mathbf{l}} \rangle + \Gamma_{\mathbf{m}-\mathbf{l}}^* \langle \hat{a}_{\mathbf{l}}^\dagger [\hat{a}_{\mathbf{m}}, \hat{O}] \rangle \right\}, \quad (4.55)$$

and similarly the hard-core bosons in terms of the spin ladder operators.

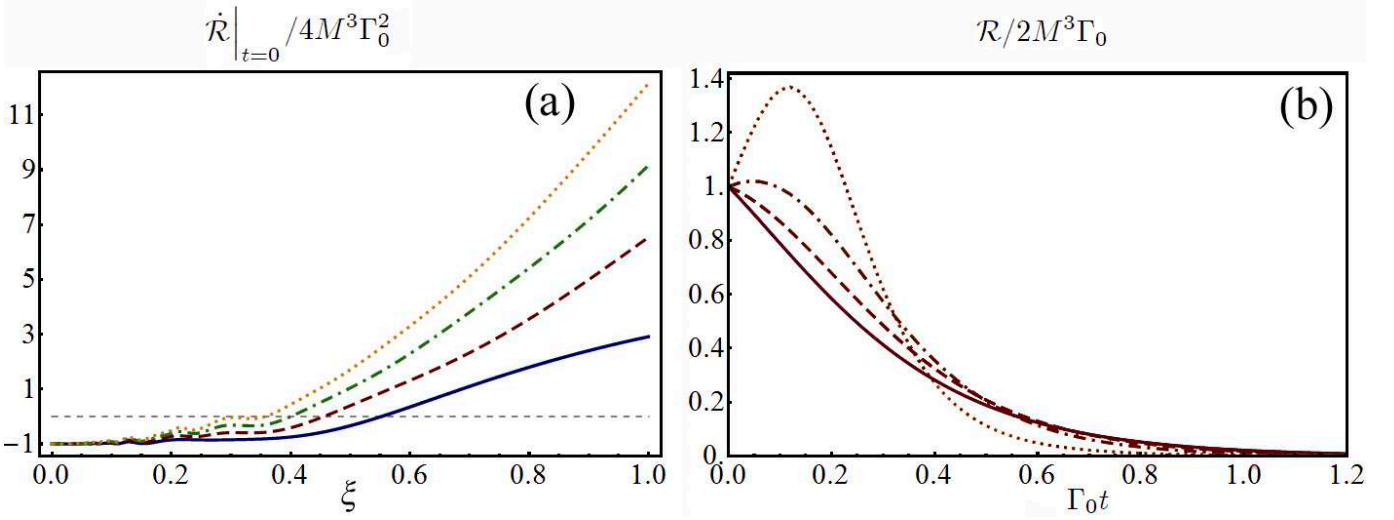


Fig. 4.4: Collective emission properties for an initial Mott state of hard-core bosons. (a) Time derivative of the rate at $t = 0$ as a function of the range of the interactions ξ , see (4.56). The values $M^3 = 8$ (solid, blue), 27 (dashed, red), 64 (dashed-dotted, green), and 125 (dotted, yellow) are considered. It can be appreciated that there exists a critical value of ξ above which the rate is enhanced at the initial times. (b) Rate as a function of time for $M^3 = 27$. The values $\xi = 0.01$ (solid), 0.5 (dashed), 1 (dashed-dotted), and 10 (dotted) are considered. As expected from (a), the maximum of the rate is delayed above some critical ξ value. Note that both the rate and its derivative have been normalized to the values expected for independent emitters, which are $4M^3\Gamma_0^2$ and $2M^3\Gamma_0$, respectively.

Non-interacting bosons: Harmonic oscillators superradiance.

Let us analyze now the case of having non-interacting bosons in the lattice, which is equivalent to a collection of harmonic oscillators as discussed before. In previous works on superradiance this system was studied in parallel to its atomic counterpart [81], and here we show how our system offers a physical realization of it. We will show that superradiant effects can be observed in the evolution of the total number of atoms in the lattice, both for initial Mott and superfluid phases³.

The evolution of the total number of atoms in the lattice is given by –see (4.55)–

$$\dot{n}_T = -2 \sum_{j,1} \gamma_{j-1} \text{Re} \left\{ \langle \hat{a}_j^\dagger \hat{a}_1 \rangle \right\}, \quad (4.59)$$

and hence depends only on the real part of the Markov couplings. Therefore, we restrict our analysis to the dissipative term $\mathcal{D}[\hat{\rho}]$ of the master equation (4.49).

By diagonalizing the real, symmetric collective decay rates with an orthogonal matrix S such that $\sum_{j,1} S_{\mathbf{p}j} \gamma_{j-1} S_{\mathbf{q}1} = \bar{\gamma}_{\mathbf{p}} \delta_{\mathbf{p}\mathbf{q}}$, one can find a set of modes $\{\hat{c}_{\mathbf{p}} = \sum_{j,1} S_{\mathbf{p}j} \hat{a}_j\}$ with definite decay properties. Then, it is completely straightforward to show that the total number of atoms can be written as a function of time as

$$n_T(t) = \sum_{\mathbf{p}} \langle \hat{c}_{\mathbf{p}}^\dagger \hat{c}_{\mathbf{p}}(0) \rangle \exp(-2\bar{\gamma}_{\mathbf{p}} t). \quad (4.60)$$

In general, γ_{j-1} requires numerical diagonalization. However, in the limiting cases $\xi \ll 1$ and $\xi \gg M$, its spectrum becomes quite simple. Following the discussion after (4.53), in the $\xi \ll 1$ limit $\gamma_{j-1} = \Gamma_0 \delta_{j1}$ is already diagonal and proportional to the identity. Hence, any orthogonal matrix S defines an equally suited set of modes all decaying with rate Γ_0 . Therefore, if the initial number of atoms in the lattice is N , this will evolve as

$$n_T(t) = N \exp(-2\Gamma_0 t), \quad (4.61)$$

³ Let us note that a superfluid state with N excitations distributed over the entire lattice is more easily defined in the discrete Fourier-transform basis

$$\hat{f}_{\mathbf{q}} = \frac{1}{M^{3/2}} \sum_{\mathbf{j}} \exp\left(\frac{2\pi i}{M} \mathbf{q} \cdot \mathbf{j}\right) \hat{a}_{\mathbf{j}}, \quad (4.58)$$

with $\mathbf{q} = (q_x, q_y, q_z)$ and $q_{x,y,z} = 0, 1, 2, \dots, M-1$, as the state having N excitations in the zero-momentum mode, that is, $|\text{SF}\rangle_N = (N!)^{-1/2} \hat{f}_0^\dagger{}^N |0\rangle$.

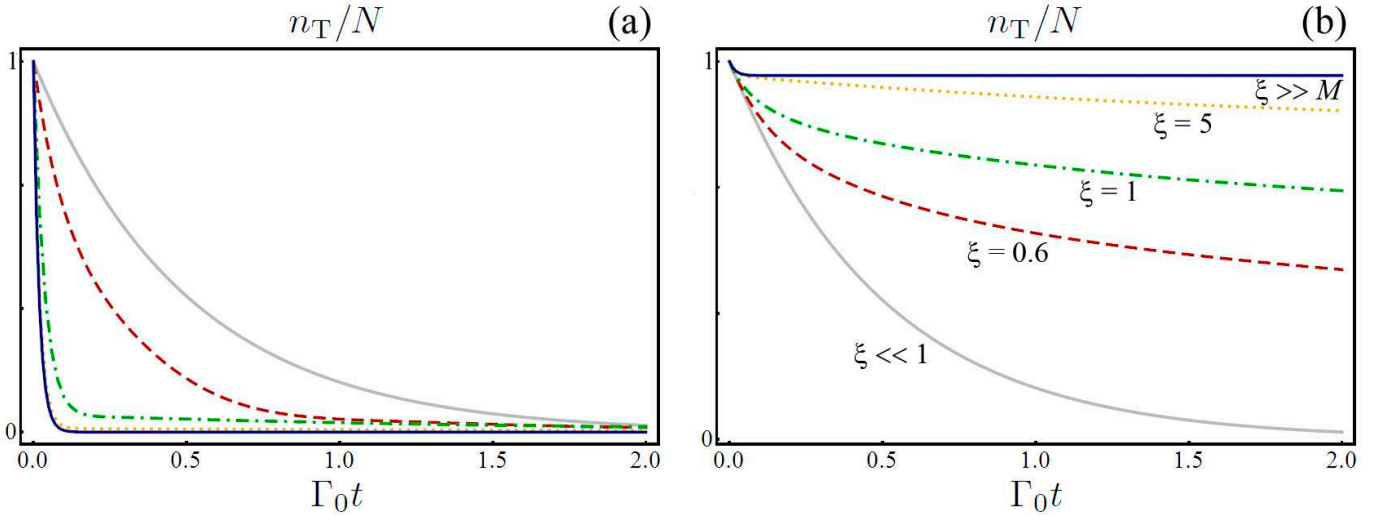


Fig. 4.5: Evolution of the total number of atoms in a lattice having $M^3 = 27$ sites for initial superfluid (a) and Mott (b) phases with N initial non-interacting atoms. The solid curves correspond to the limits $\xi \ll 1$ (grey) and $\xi \gg M$ (dark-blue). Note how the ‘evaporation time’ is reduced for the initial superfluid state as ξ increases (a). Equivalently, note how for an initial Mott state the atoms tend to stay in the lattice as ξ increases (b).

irrespective of the particular initial state of the lattice (e.g., Mott or superfluid). The emission rate $\mathcal{R} = 2\Gamma_0 N \exp(-2\Gamma_0 t)$, corresponds to the independent decay of the N atoms as expected in this regime having no interaction between the emitters.

Let us consider now the opposite limit $\xi \gg M$; in this case $\gamma_{\mathbf{j}-1} = \Gamma_0 \forall (\mathbf{j}, \mathbf{l})$, and the dissipative term can be written in terms of the symmetrical discrete Fourier-transform mode only as $\mathcal{D}[\hat{\rho}] = M^3 \Gamma_0 (2\hat{f}_0 \hat{\rho} \hat{f}_0^\dagger - \hat{f}_0^\dagger \hat{f}_0 \hat{\rho} - \hat{f}_0^\dagger \hat{f}_0 \hat{\rho})$, see (4.58). Hence, the discrete Fourier-transform basis diagonalizes the problem, and shows that all the modes have zero decay rate except the symmetrical one, which has an enhanced rate proportional to the number of emitters. Therefore, starting with a superfluid state, the N initial atoms will decay exponentially with initial rate $NM^3\Gamma_0$, that is

$$n_{\text{T}}(t) = N \exp(-2M^3\Gamma_0 t). \quad (4.62)$$

On the other hand, if the initial state corresponds to a Mott phase, most of the atoms will remain in the lattice, as only the component which projects onto the symmetric mode will be emitted; concretely, from (4.60) and (4.58) the number of atoms in the lattice will evolve for this particular initial state as

$$n_{\text{T}}(t) = \left(N - \frac{N}{M^3}\right) + \frac{N}{M^3} \exp(-2M^3\Gamma_0 t). \quad (4.63)$$

Hence, according to this picture, superradiant collective effects can be observed in our system by two different means. Calling t_0 the time needed to radiate the atoms in the absence of collective effects, one could start with a superfluid phase and measure this ‘evaporation time’ as a function of ξ ; this should go from t_0 for $\xi \ll 1$, to a much shorter time t_0/M^3 for $\xi \gg M$ (see figure 4.5a). Alternatively, one could start with a Mott phase, and measure the number of atoms left in the lattice in the steady state as a function of ξ ; in this case, it should go from $n_{\text{T,steady}} = 0$ after a time t_0 for $\xi \ll 1$, to $n_{\text{T,steady}} = N - N/M^3$ after a time t_0/M^3 for $\xi \gg M$ (see figure 4.5b).

In order to find the evolution of n_{T} we have simulated the equations satisfied by the coherences $c_{\mathbf{j}\mathbf{l}} = \langle \hat{a}_{\mathbf{j}}^\dagger \hat{a}_{\mathbf{l}} \rangle$, which read –see (4.55)–

$$\dot{c}_{\mathbf{j}\mathbf{l}} = - \sum_{\mathbf{m}} [\Gamma_{\mathbf{l}-\mathbf{m}} c_{\mathbf{j}\mathbf{m}} + \Gamma_{\mathbf{j}-\mathbf{m}}^* c_{\mathbf{m}\mathbf{l}}]. \quad (4.64)$$

Note that in this case the equations are closed without the need of a semiclassical approximation, and hence they are exact. Note that they reproduce the analytic evolution of n_{T} as given by (4.61), (4.63), and (4.62) in the corresponding limits (see figure 4.5).

Our results connect directly to those found by Agarwal some decades ago [81]. Working with a Dicke-like model, he showed that if all the oscillators start in the same coherent state $|\alpha\rangle$, the initial number of excitations, which in

that case is given by $N = M^3 |\alpha|^2$, decays following (4.62). This is not a coincidence, but rather a consequence that, if N is large enough, a multi-coherent state of that kind is a good approximation of a superfluid state with that number of excitations. He also predicted that if the oscillators start in a number state, most of the excitations would remain in the steady state as follows from (4.63).

5. DETECTION OF THE OUTPUT FIELD

In the previous chapter we developed a model to study the dynamics of the intracavity modes of an open cavity from a quantum viewpoint. However, it is the field coming out of the cavity the one which is customarily studied or used in applications, not the intracavity modes. The first part of this chapter is devoted to relate this output field with the intracavity field. We then explain the basic detection schemes which are used to characterize this output field, namely direct photodetection and balanced homodyne detection, which ideally give us access to the intensity (photon number) and the quadratures of light, respectively. Understanding how the field quadratures are analyzed in real experiments will allow us to reintroduce squeezing in an experimentally useful manner at the end of the chapter.

5.1 The output field

Using the expression of the vector potential outside the resonator (4.5), we see that the field coming out from the cavity can be written as

$$\hat{\mathbf{A}}_{\text{out}}^{(+)}(\mathbf{r}, t) = \int_{-\infty}^{+\infty} d\omega \sqrt{\frac{\hbar}{4\pi c \varepsilon_0 \omega}} \varepsilon T(\omega/c; \mathbf{r}_{\perp}, z) \hat{b}(\omega; t) \exp(i\omega z/c), \quad (5.1)$$

where the operator $\hat{b}(\omega; t)$ is given by (4.10) in terms of the initial operators $\hat{b}_0(\omega)$ and the intracavity mode \hat{a} . Now, given that only the frequencies around the cavity resonance contribute to the dynamics as we argued in the previous chapter, we can replace the slowly varying function of the frequency $T(\omega/c; \mathbf{r}_{\perp}, z) / \sqrt{\omega}$ by its value at ω_c , arriving to

$$\hat{\mathbf{A}}_{\text{out}}^{(+)}(\mathbf{r}, t) = \sqrt{\frac{\hbar}{4\pi c \varepsilon_0 \omega_c}} \varepsilon T(k_c; \mathbf{r}_{\perp}, z) \int_{-\infty}^{+\infty} d\omega \hat{b}(\omega; t) \exp(i\omega z/c). \quad (5.2)$$

Introducing the solution (4.10) for $\hat{b}(\omega; t)$ in this equation, we can write the output field as the sum of two terms, namely, $\hat{\mathbf{A}}_{\text{out}}^{(+)}(\mathbf{r}, t) = \hat{\mathbf{A}}_{\text{in}}^{(+)}(\mathbf{r}, t) + \hat{\mathbf{A}}_{\text{source}}^{(+)}(\mathbf{r}, t)$ with

$$\hat{\mathbf{A}}_{\text{in}}^{(+)}(\mathbf{r}, t) = \sqrt{\frac{\hbar}{4\pi c \varepsilon_0 \omega_c}} \varepsilon T(k_c; \mathbf{r}_{\perp}, z) \int_{-\infty}^{+\infty} d\omega \hat{b}_0(\omega) \exp[-i\omega(t_R - t_0)], \quad (5.3a)$$

$$\hat{\mathbf{A}}_{\text{source}}^{(+)}(\mathbf{r}, t) = \sqrt{\frac{\hbar \gamma}{4\pi^2 c \varepsilon_0 \omega_c}} \varepsilon T(k_c; \mathbf{r}_{\perp}, z) \int_{-\infty}^{+\infty} d\omega \int_0^t dt' \hat{a}(t') \exp[i\omega(t' - t_R)], \quad (5.3b)$$

where we have defined the *retarded time* $t_R = t - z/c$. Recalling the definition of the input operator (4.11), the first term can be rewritten as

$$\hat{\mathbf{A}}_{\text{in}}^{(+)}(\mathbf{r}, t) = -\sqrt{\frac{\hbar}{2c \varepsilon_0 \omega_c}} \varepsilon T(k_c; \mathbf{r}_{\perp}, z) \hat{a}_{\text{in}}(t_R), \quad (5.4)$$

and hence it is identified with a contribution coming from the input field driving the cavity. On the other hand, performing the frequency integral in the source term, we can rewrite it as

$$\hat{\mathbf{A}}_{\text{source}}^{(+)}(\mathbf{r}, t) = \begin{cases} \sqrt{\frac{\hbar \gamma}{c \varepsilon_0 \omega_c}} \varepsilon T(k_c; \mathbf{r}_{\perp}, z) \hat{a}(t_R) & z < ct \\ \sqrt{\frac{\hbar \gamma}{4c \varepsilon_0 \omega_c}} \varepsilon T(k_c; \mathbf{r}_{\perp}, z) \hat{a}(t_R) & z = ct \\ 0 & z > ct \end{cases}, \quad (5.5)$$

which is therefore identified with a contribution of the intracavity field, hence the name “source”. We will always work in the stationary limit $t \gg \gamma^{-1}$, and near the cavity, so that z will always be smaller than ct , what allows us to even neglect the z/c delay in the retarded time, that is, $t_R \simeq t$ (in any case, this doesn't have any fundamental relevance, it will just simplify future derivations).

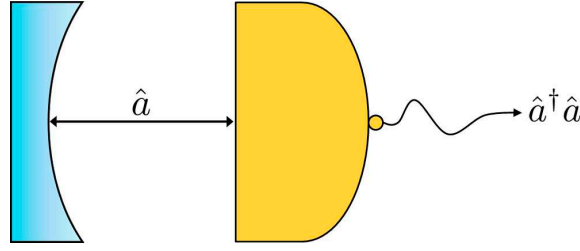


Fig. 5.1: Schematic representation of Mollow's ideal single-mode detection.

Hence, defining the *output operator*

$$\hat{a}_{\text{out}}(t) = \sqrt{2\gamma}\hat{a}(t) - \hat{a}_{\text{in}}(t), \quad (5.6)$$

the output field is finally written as

$$\hat{\mathbf{A}}_{\text{out}}^{(+)}(\mathbf{r}, t) = \sqrt{\frac{\hbar}{2c\varepsilon_0\omega_c}} \varepsilon T(k_c; \mathbf{r}_\perp, z) \hat{a}_{\text{out}}(t). \quad (5.7)$$

Hence the field coming out from the cavity is a superposition of the intracavity field leaking through the partially transmitting mirror and the part of the input field which is reflected, just as expected by the classical boundary conditions at the mirror (see Figure 4.1).

It is interesting for future purposes to generalize this expression to the case of several modes resonating at the same frequency inside the cavity. The corresponding output field can be written in this case as

$$\hat{\mathbf{A}}_{\text{out}}^{(+)}(\mathbf{r}, t) = \sqrt{\frac{\hbar}{2c\varepsilon_0\omega_c}} \sum_{\sigma\mathbf{n}} \varepsilon_{\sigma\mathbf{n}} T_{\mathbf{n}}(k_c; \mathbf{r}_\perp, z) \hat{a}_{\sigma\mathbf{n},\text{out}}(t), \quad (5.8)$$

where each cavity mode with annihilation operator $\hat{a}_{\sigma\mathbf{n}}$ is driven by an independent input operator $\hat{a}_{\sigma\mathbf{n},\text{in}}$ so that

$$\hat{a}_{\sigma\mathbf{n},\text{out}}(t) = \sqrt{2\gamma_{\sigma\mathbf{n}}}\hat{a}_{\sigma\mathbf{n}}(t) - \hat{a}_{\sigma\mathbf{n},\text{in}}(t), \quad (5.9)$$

being $\gamma_{\sigma\mathbf{n}}$ the cavity loss rate for each mode.

In the case of an empty cavity, it is straightforward to prove that this operators satisfy the commutation relations

$$[\hat{a}_{\sigma\mathbf{n},\text{out}}(t), \hat{a}_{\sigma'\mathbf{n}',\text{out}}^\dagger(t')] = \delta_{\sigma\sigma'} \delta_{\mathbf{n}\mathbf{n}'} \delta(t - t'), \quad (5.10a)$$

$$[\hat{a}_{\sigma\mathbf{n},\text{out}}(t), \hat{a}_{\sigma'\mathbf{n}',\text{out}}(t')] = [\hat{a}_{\sigma\mathbf{n},\text{out}}^\dagger(t), \hat{a}_{\sigma'\mathbf{n}',\text{out}}^\dagger(t')] = 0. \quad (5.10b)$$

When other intracavity processes are included one has in general to check how this commutation relations are modified.

5.2 Ideal detection: An intuitive picture of photo- and homodyne detection

Photodetection is the most fundamental measurement technique for light. As we shall see with a particular example (homodyne detection), any other scheme used for measuring different properties of light makes use of photodetection as a part of it.

This technique is based on the photoelectric effect or variations of it. The idea is that when the light beam that we want to detect impinges a metallic surface, it is able to release some of the bound electrons of the metal, which are then collected by an anode. The same happens if light incides on a semiconductor surface, though in this case instead of becoming free, valence electrons are promoted to the conduction band. The most widely used metallic photodetectors are known as *photo-multiplier tubes*, while those based on semiconducting films are the so-called *avalanche photo diodes*. In both cases, each photon is able to create one single electron, whose associated current would be equally difficult to measure by electronic means; for this reason, each photoelectron is accelerated towards a series of metallic plates at increasing positive voltages, releasing then more electrons which contribute to generate a measurable electric pulse, the *photopulse*.

It is customarily said that counting photopulses is equivalent to counting photons, and hence, photodetection is equivalent to a measurement of the number of photons of the light field. This is a highly idealized situation, valid only in some limits which are actually not the ones in which we usually work in the field of squeezing. Nevertheless,

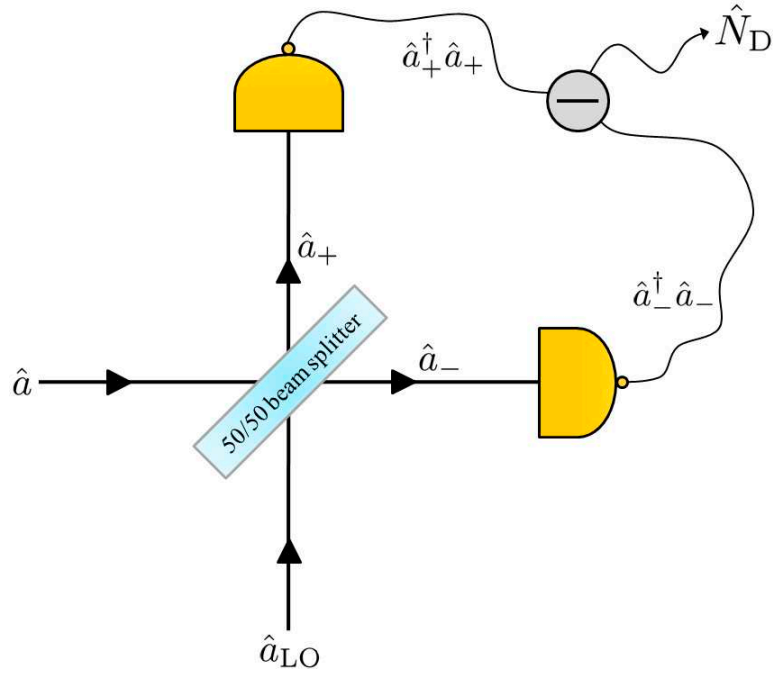


Fig. 5.2: Homodyne detection scheme with ideal photodetectors. When the local oscillator is in a strong coherent state, this setup gives access to the quadratures of light.

it is interesting to analyze this ideal limit first to gain some intuition about the photodetection process, and this is what we will do in this section. Using this idealized picture of photodetectors, we will study a detection scheme called homodyne detection, which will be shown to be equivalent to a measurement of the quadratures of light.

Consider the following model for a perfectly efficient detection scheme. A single-mode field with boson operators $\{\hat{a}, \hat{a}^\dagger\}$ initially in some state $\hat{\rho}$ is kept in continuous interaction with a photodetector during a time interval T . The intuitive picture of such a scenario is shown in Figure 5.1: A cavity formed by the photodetector itself and an extra perfectly reflecting mirror contains a single mode. By developing a microscopic model of the detector and its interaction with the light mode, Mollow was able to show that the probability of generating n photoelectrons (equivalently, the probability of observing n photopulses) during the time interval T is given by [88]

$$p_n = \left\langle : \frac{(1 - e^{-\kappa T})^n \hat{a}^\dagger n \hat{a}^n}{n!} \exp[-(1 - e^{-\kappa T}) \hat{a}^\dagger \hat{a}] : \right\rangle, \quad (5.11)$$

where the expectation value has to be evaluated in the initial state $\hat{\rho}$ of the light mode, and κ is some parameter accounting for the light-detector interaction. Using the operator identity $:\exp[-(1 - e^{-\lambda}) \hat{a}^\dagger \hat{a}]: = \exp(-\lambda \hat{a}^\dagger \hat{a})$ [15], and the help of the number state basis $\{|n\rangle\}_{n \in \mathbb{N}}$, it is straightforward to get

$$p_n = \sum_{m=n}^{\infty} \langle n | \hat{\rho} | n \rangle \frac{m!}{n!(m-n)!} (1 - e^{-\kappa T})^n (e^{-\kappa T})^{m-n} \xrightarrow{T \gg \kappa^{-1}} \langle n | \hat{\rho} | n \rangle, \quad (5.12)$$

and hence, for large enough detection times the number of observed pulses follows the statistics of the number of photons. In other words, this ideal photodetection scheme is equivalent to measuring the number operator $\hat{a}^\dagger \hat{a}$ as already commented.

Even though the output of the photodetectors can take only integer values (number of recorded photopulses), they can be arranged to approximately measure the quadratures of light, which we remind are continuous observables. This arrangement is called homodyne detection. The basic scheme is shown in Figure 5.2. The mode we want to measure is mixed in a beam splitter with another mode, called the *local oscillator*, which is in a coherent state $|\alpha_{LO}\rangle$. When the beam splitter is 50/50 the homodyne scheme is said to be *balanced*, and the annihilation operators of the modes leaving its output ports are given by

$$\hat{a}_\pm = \frac{1}{\sqrt{2}} (\hat{a} \pm \hat{a}_{LO}), \quad (5.13)$$

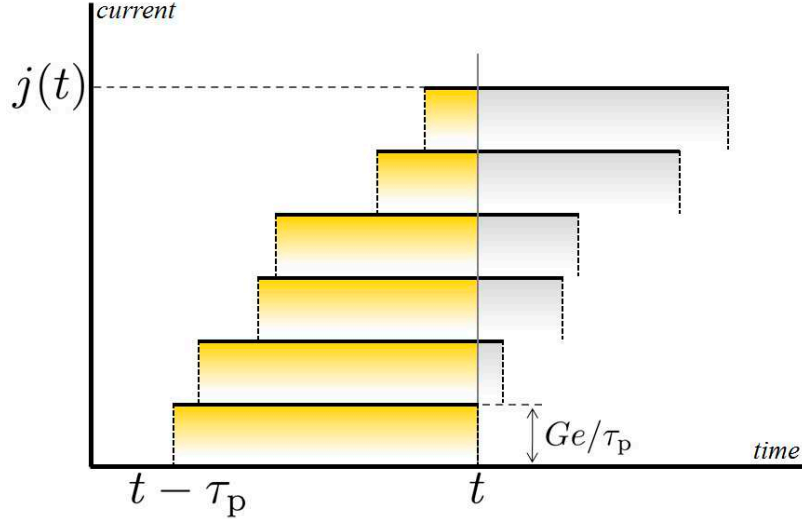


Fig. 5.3: Carmichael's picture of how the continuous photocurrent is built up from the individual photopulses.

being \hat{a}_{LO} the annihilation operator of the local oscillator mode. These modes are measured with independent photodetectors, and then the corresponding signals are subtracted. Based on the idealized photodetection picture, this scheme is analogous to a measurement of the photon number difference

$$\hat{N}_{\text{D}} = \hat{a}_{+}^{\dagger} \hat{a}_{+} - \hat{a}_{-}^{\dagger} \hat{a}_{-} = \hat{a}_{\text{LO}}^{\dagger} \hat{a} + \hat{a}_{\text{LO}} \hat{a}^{\dagger}. \quad (5.14)$$

Taking into account that the local oscillator is in a coherent state with amplitude $\alpha_{\text{LO}} = |\alpha_{\text{LO}}| \exp(i\varphi)$, and is not correlated with our measured mode, it is not difficult to show that the first moments of this operator can be written as

$$\langle \hat{N}_{\text{D}} \rangle = |\alpha_{\text{LO}}| \langle \hat{X}^{\varphi} \rangle \quad (5.15a)$$

$$\langle \hat{N}_{\text{D}}^2 \rangle = |\alpha_{\text{LO}}|^2 \left[\langle \hat{X}^{\varphi 2} \rangle + \frac{\langle \hat{a}^{\dagger} \hat{a} \rangle}{|\alpha_{\text{LO}}|^2} \right]. \quad (5.15b)$$

Hence, in the *strong local oscillator limit* $|\alpha_{\text{LO}}|^2 \gg \langle \hat{a}^{\dagger} \hat{a} \rangle$, the output signal of the homodyne scheme has the mean of a quadrature \hat{X}^{φ} of the analyzed mode (the one selected by the phase of the local oscillator), as well as its same quantum statistics.

Even though this picture offers all the basic ingredients that one has to understand about light detection, it is in a sense far from how light is observed in real experiments. In the following sections we discuss photodetection and homodyne detection scenarios which are closer to the experimental ones.

5.3 Real photodetection: The photocurrent and its power spectrum

In the detection schemes that we will consider throughout this thesis, the photodetectors will be measuring light beams with a high flux of photons (for example, in homodyne detection we have seen that the local oscillator is a strong coherent field). Under these circumstances several photopulses can be created during a time interval comparable to the width of a single pulse, so that it is not possible to count pulses anymore. Instead, one sees the signal coming out from the detector basically as a continuous current; it is the goal of this section to model the statistics of this *photocurrent* and explain the way in which it is analyzed experimentally.

For simplicity¹, let us assume that the pulses generated after the amplification stage of each photoelectron are square like and have a temporal width τ_{p} . This width is equivalent to the time response of the detector, which we will consider to be instantaneous eventually, that is, $\tau_{\text{p}} \rightarrow 0$. As shown in Figure 5.3, the photocurrent $j(t)$ detected at time t is a superposition of all the pulses generated in the time interval $[t - \tau_{\text{p}}, t]$, that is,

$$j(t) = \frac{Ge}{\tau_{\text{p}}} n(t - \tau_{\text{p}}, t), \quad (5.16)$$

¹ In the next sections we follow closely the treatment of photodetection and homodyne detection proposed by Carmichael [89, 17, 19]

where e is the electron charge, G is the number of electrons generated in the amplification stage from the initial photoelectron, and $n(t - \tau_p, t)$ is the number of photoelectrons generated in the interval $[t - \tau_p, t]$. As shown by Kelley and Kleiner [90], who generalized the semiclassical formula previously obtained by Mandel [91, 92], for a field such as the one coming out from a cavity (5.8), the statistics of the number of pulses $n(t - \tau_p, t)$ are dictated by the distribution [20]

$$p_n(t - \tau_p, t) = \left\langle : \frac{\hat{J}^n(t, \tau_p) \exp[-\hat{J}(t, \tau_p)]}{n!} : \right\rangle, \quad (5.17)$$

where “: :” must be understood from now on as normal order and *time order* (time increases to the right for products of creation operators and to the right for products of annihilation operators), and we have defined the *photocurrent operator*

$$\hat{J}(t, \tau_p) = \eta \frac{2c\epsilon_0\omega_c}{\hbar} \int_{t-\tau_p}^t dt' \int_{\mathbb{R}^2} d^2\mathbf{r}_\perp \hat{\mathbf{A}}_{\text{out}}^{(-)}(\mathbf{r}_\perp, z_d, t') \hat{\mathbf{A}}_{\text{out}}^{(+)}(\mathbf{r}_\perp, z_d, t') \simeq \eta\tau_p \sum_{\sigma\mathbf{n}} \hat{n}_{\sigma\mathbf{n},\text{out}}(t), \quad (5.18)$$

being $\hat{n}_{\sigma\mathbf{n},\text{out}} = \hat{a}_{\sigma\mathbf{n},\text{out}}^\dagger \hat{a}_{\sigma\mathbf{n},\text{out}}$, $\eta \in [0, 1]$ the photon–photoelectron conversion factor, and z_d the longitudinal position of the photodetector. In loose terms, the operator $\hat{n}_{\sigma\mathbf{n},\text{out}}$ ‘counts’ the total number of output photons detected during the time that a photopulse lasts. Note that we have assumed that the transverse size of the detector is larger than the transverse thickness of the output beam, and the last equality follows from assuming that $\hat{n}_{\sigma\mathbf{n},\text{out}}(t)$ doesn’t change too much in the brief interval $[t - \tau_p, t]$.

Let us evaluate the mean and the second factorial moment of the number of pulses $n(t - \tau_p, t)$:

$$\overline{n(t - \tau_p, t)} = \sum_{n=0}^{\infty} n p_n(t - \tau_p, t) = \left\langle : \hat{J}(t, \tau_p) \sum_{n=1}^{\infty} \frac{\hat{J}^{n-1}(t, \tau_p)}{(n-1)!} e^{-\hat{J}(t, \tau_p)} : \right\rangle = \left\langle : \hat{J}(t, \tau_p) : \right\rangle \quad (5.19a)$$

$$\overline{n(t - \tau_p, t) [n(t - \tau_p, t) - 1]} = \sum_{n=0}^{\infty} n(n-1) p_n(t - \tau_p, t) = \left\langle : \hat{J}^2(t, \tau_p) \sum_{n=2}^{\infty} \frac{\hat{J}^{n-2}(t, \tau_p)}{(n-2)!} e^{-\hat{J}(t, \tau_p)} : \right\rangle = \left\langle : \hat{J}^2(t, \tau_p) : \right\rangle, \quad (5.19b)$$

where we use the overbar to stress the difference between quantum averages and averages concerning the random electric signal coming out from the experiment. These expressions allow us to write the first moments of the photocurrent as

$$\overline{j(t)} = \frac{Ge}{\tau_p} \left\langle : \hat{J}(t, \tau_p) : \right\rangle = \eta Ge \sum_{\sigma\mathbf{n}} \langle \hat{n}_{\sigma\mathbf{n},\text{out}}(t) \rangle \quad (5.20a)$$

$$\begin{aligned} \overline{j^2(t)} &= \frac{G^2 e^2}{\tau_p^2} \left[\left\langle : \hat{J}^2(t, \tau_p) : \right\rangle + \left\langle : \hat{J}(t, \tau_p) : \right\rangle \right] \quad (5.20b) \\ &= \eta^2 G^2 e^2 \left[\sum_{\sigma\sigma'\mathbf{nn}'} \left\langle \hat{a}_{\sigma\mathbf{n},\text{out}}^\dagger \hat{a}_{\sigma'\mathbf{n}',\text{out}}^\dagger \hat{a}_{\sigma\mathbf{n},\text{out}} \hat{a}_{\sigma'\mathbf{n}',\text{out}} \right\rangle + \frac{1}{\eta\tau_p} \sum_{\sigma\mathbf{n}} \langle \hat{n}_{\sigma\mathbf{n},\text{out}}(t) \rangle \right], \end{aligned}$$

Note that any mode in a vacuum state does not contribute to the statistics of the photocurrent. This is due to the normal ordering appearing in $p_n(t - \tau_p, t)$.

To gain some insight, consider the output of an empty single–mode cavity in the stationary limit, which can be obtained from (5.6), with $\hat{a}(t)$ given by (4.19) and the input operator $\hat{a}_{\text{in}}(t)$ satisfying

$$\left\langle \hat{a}_{\text{in}}^\dagger(t_1) \hat{a}_{\text{in}}^\dagger(t_2) \dots \hat{a}_{\text{in}}^\dagger(t_j) \hat{a}_{\text{in}}(t'_1) \hat{a}_{\text{in}}(t'_2) \dots \hat{a}_{\text{in}}(t'_l) \right\rangle = 0 \quad \forall (j, l), \quad (5.21)$$

because the external modes are assumed to be in vacuum initially. This property allows us to relate moments of the output operators with intracavity moments in a very simple way:

$$\left\langle \hat{a}_{\text{out}}^\dagger(t_1) \hat{a}_{\text{out}}^\dagger(t_2) \dots \hat{a}_{\text{out}}^\dagger(t_j) \hat{a}_{\text{out}}(t'_1) \hat{a}_{\text{out}}(t'_2) \dots \hat{a}_{\text{out}}(t'_l) \right\rangle = (2\gamma)^{(j+l)/2} \langle \hat{a}^\dagger(t_1) \hat{a}^\dagger(t_2) \dots \hat{a}^\dagger(t_j) \hat{a}(t'_1) \hat{a}(t'_2) \dots \hat{a}(t'_l) \rangle \quad \forall (j, l) \quad (5.22)$$

Then, in terms of the intracavity operators, the photocurrent moments can be written as

$$\overline{j(t)} = 2\gamma\eta Ge \langle \hat{n}(t) \rangle = 2\pi\eta Ge |\mathcal{E}|^2 \frac{\gamma/\pi}{\gamma^2 + (\omega_c - \omega_L)^2} \equiv \overline{j_0} \quad (5.23a)$$

$$\overline{j^2(t)} = 4\gamma^2 \eta^2 G^2 e^2 \langle \hat{n}^2(t) \rangle + \frac{2\gamma\eta G^2 e^2}{\tau_p} (1 - 2\gamma\eta\tau_p) \langle \hat{n}(t) \rangle, \quad (5.23b)$$

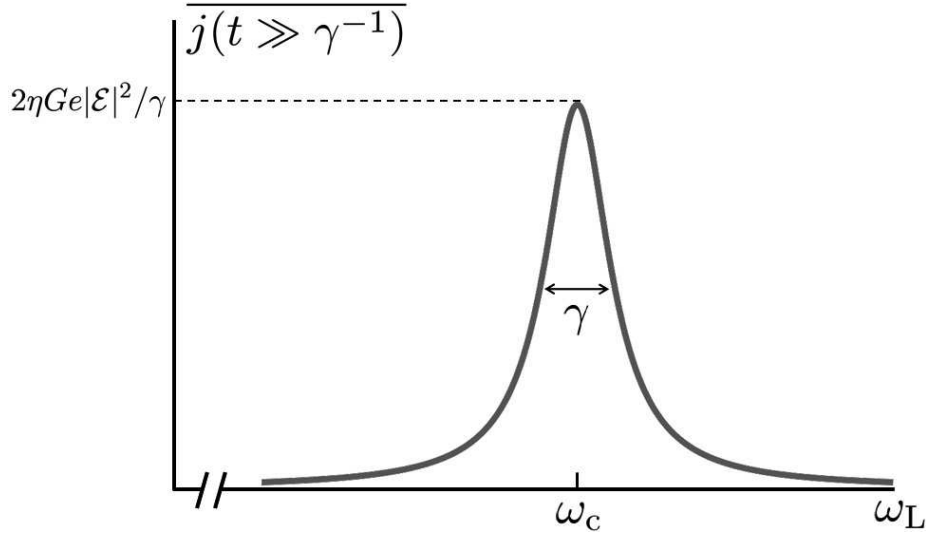


Fig. 5.4: Mean of the photocurrent measured for a single-mode field coming out from an empty cavity as a function of the frequency of the laser which drives it. Maximum transmission is obtained when the laser is tuned to the cavity resonance.

where $\hat{n} = \hat{a}^\dagger \hat{a}$ is the number operator for the photons inside the cavity. The mean of the photocurrent is proportional to the mean of the number of photons inside the cavity, similarly to the idealized photodetection description discussed in the previous section. However, the second moment of the photocurrent is not directly proportional to the second moment of \hat{n} , it has a deviation proportional to the mean, that is, an additional Poissonian contribution which shows that the photocurrent signal is affected by extra noise, and hence does not offer 100% truthful information about the intracavity number fluctuations. The situation is even more subtle as we show now.

Note that as a function of the frequency ω_L of the laser which ‘scans’ the cavity, the mean photocurrent (or the mean intracavity photon number) is a Lorentzian of width γ centered at the cavity resonance ω_c (see Figure 5.4), which read in reverse shows that only external modes within the interval $[\omega_c - \gamma, \omega_c + \gamma]$ can be excited as we explained in the previous chapter. However, the variance associated to this photocurrent can be written as

$$V[j(t)] = \overline{j^2(t)} - \overline{j(t)}^2 = \frac{Ge}{\tau_p} \overline{j_0}, \quad (5.24)$$

showing that the noise in the photocurrent dominates the output signal when the photodetector has a fast response, that is, $\tau_p \rightarrow 0$. Hence, instantaneous photocurrent signals cannot be usually studied in experiments. Instead, one studies the *power spectrum* of the photocurrent, which can be obtained at real time by introducing the electric signal coming out from the photodetector into a *spectrum analyzer*. The scheme of a spectrum analyzer is shown in Figure 5.5; the mean of the new output signal is then

$$P(\Omega) = \frac{1}{T} \left[\overline{\int_0^T dt j(t) \cos \Omega t} \right]^2 + \left[\overline{\int_0^T dt j(t) \sin \Omega t} \right]^2, \quad (5.25)$$

which can be easily rewritten as

$$P(\Omega) = \frac{1}{T} \int_0^T dt \int_0^T dt' \cos[\Omega(t-t')] \overline{j(t)j(t')}, \quad (5.26)$$

in terms of the two-time correlation function of the photocurrent. When this correlation depends solely on the time difference $|t-t'|$, that is, when $\overline{j(t)j(t')} = \mathcal{J}(|t-t'|)$, this expression can be simplified even further as

$$P(\Omega) = \int_{-\infty}^{+\infty} d\tau \mathcal{J}(|\tau|) e^{-i\Omega\tau}, \quad (5.27)$$

in the $T \rightarrow \infty$ limit. In such case we say that $j(t)$ corresponds to a *stationary process* [20].

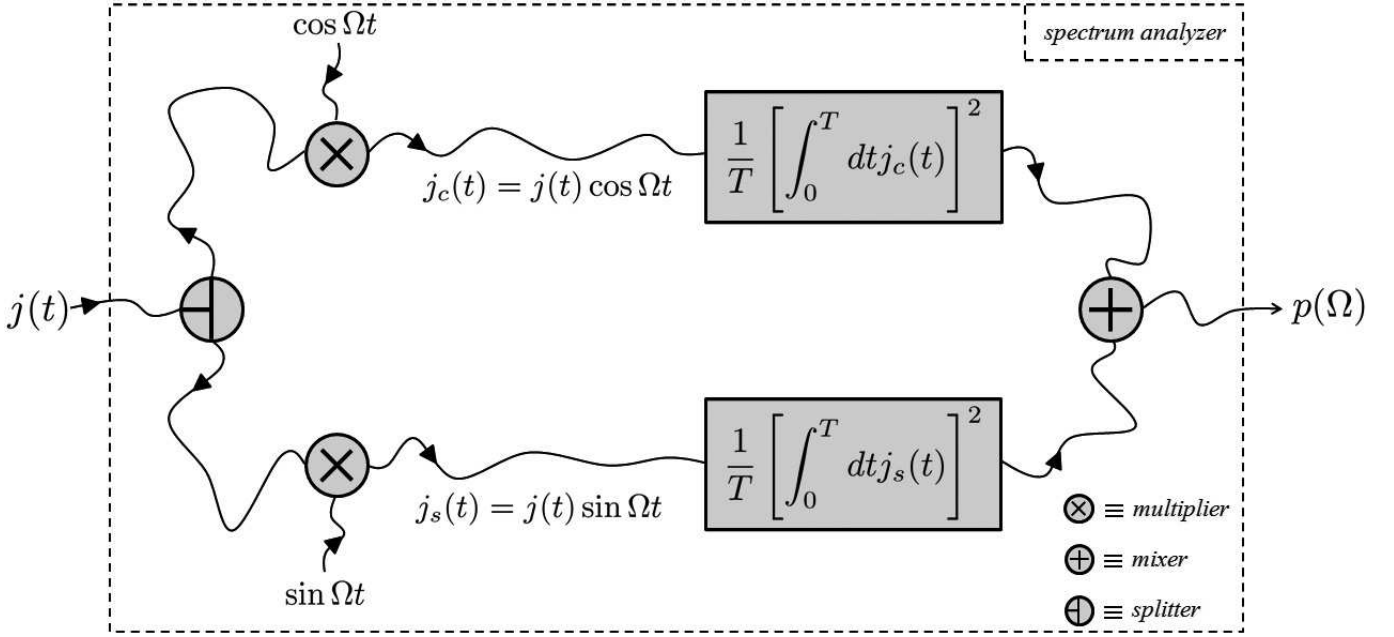


Fig. 5.5: Schematic representation of the action of a spectrum analyzer onto an incoming electric current. After dividing it and multiply the separated currents by a sine and a cosine oscillating at frequency Ω , the signals are accumulated during a time T (detection time); the squares of these quantities (normalized to T) are added, finally building the spectral signal $p(\Omega)$.

Using similar techniques as in the previous derivations, it is lengthy but simple to show that the correlation function of the photocurrent can be written in terms of the photocurrent operator as

$$\overline{j(t)j(t')} = \frac{G^2 e^2}{\tau_p^2} \left[\langle : \hat{J}(t, \tau_p) \hat{J}(t', \tau_p) : \rangle + H(\tau_p - |t' - t|) \langle : \hat{J}(\min\{t, t'\}, \tau_p - |t' - t|) : \rangle \right] \quad (5.28)$$

where

$$H(x) = \begin{cases} 1 & x > 0 \\ 0 & x \leq 0 \end{cases}, \quad (5.29)$$

is a step function. Particularizing this expression for the empty single-mode cavity in the stationary limit, it is straightforward to show that its associated power spectrum reads

$$P(\Omega) = 2\pi j_0^{-2} \left[\delta(\Omega) + \frac{Ge^{-2}}{2\pi j_0^2} \right], \quad (5.30)$$

where we have assumed a large detection time and a fast time response of the photodetector, that is, $T \rightarrow \infty$ and $\tau_p \rightarrow 0$. This shows that the massive noise masking the signal $j(t)$ at all times is concentrated in frequency space at $\Omega = 0$. For any other frequency (technically for $\Omega \gg T^{-1}$) the power spectrum is finite.

5.4 Real homodyne detection: Squeezing and the noise spectrum

Now that we understand how to treat the signal coming out of a real photodetector, we can analyze as well the signal coming out from a homodyne detection scheme as is usually done in experiments. This will allow us to introduce squeezing in a manner which is useful for experimental matters through the so-called squeezing spectrum.

The situation is depicted in Figure 5.6. Our output multi-mode field (5.8) is mixed in a 50/50 beam splitter with a *local oscillator field* coming out from a laser whose central frequency ω_{LO} is close to ω_c , and is assumed to emit in a well defined mode with polarization ε_Λ and transverse profile $T_\Lambda(k_c; \mathbf{r}_\perp, z)$, that is,

$$\hat{\mathbf{A}}_{LO}^{(+)}(\mathbf{r}, t) = \sqrt{\frac{\hbar}{2c\varepsilon_0\omega_c}} \varepsilon_\Lambda T_\Lambda(k_c; \mathbf{r}_\perp, z) \hat{a}_{LO}(t); \quad (5.31)$$

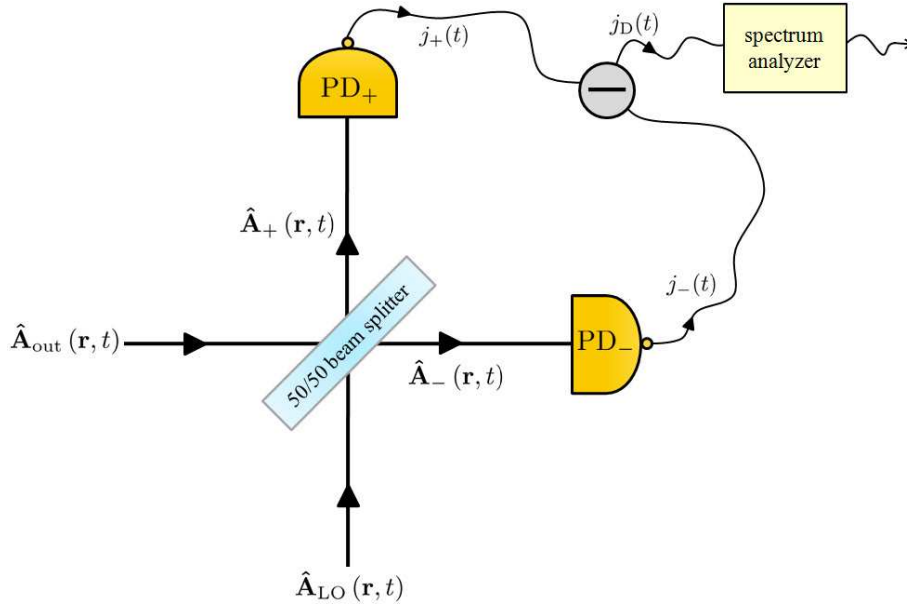


Fig. 5.6: Balanced homodyne detection scheme. The idea is exactly as in Figure 5.2, but now the setup is analyzed for a field coming out from a cavity, and considering the realistic picture of photodetection introduced in the previous section.

the state of this laser field is modelled as a stationary coherent state, and hence its associated output operator $\hat{a}_{\text{LO}}(t)$ satisfies

$$\langle \hat{a}_{\text{LO}}^\dagger(t_1) \hat{a}_{\text{LO}}^\dagger(t_2) \dots \hat{a}_{\text{LO}}^\dagger(t_j) \hat{a}_{\text{LO}}(t'_1) \hat{a}_{\text{LO}}(t'_2) \dots \hat{a}_{\text{LO}}(t'_l) \rangle = e^{i\omega_{\text{LO}}(t_1+t_2+\dots+t_j-t'_1-t'_2-\dots-t'_l)} \alpha_{\text{LO}}^{*j} \alpha_{\text{LO}}^l \quad \forall(j, l), \quad (5.32)$$

where we will write $\alpha_{\text{LO}} = |\alpha_{\text{LO}}| \exp(i\varphi)$.

On the other hand, the fields coming out from the beam splitter $\hat{\mathbf{A}}_\pm^{(+)} = [\hat{\mathbf{A}}_{\text{out}}^{(+)} \pm \hat{\mathbf{A}}_{\text{LO}}^{(+)}] / \sqrt{2}$ can be written as

$$\hat{\mathbf{A}}_\pm^{(+)}(\mathbf{r}, t) = \sqrt{\frac{\hbar}{2c\epsilon_0\omega_c}} \left\{ \frac{1}{\sqrt{2}} \epsilon_\Lambda T_\Lambda(k_c; \mathbf{r}_\perp, z) [\hat{a}_{\Lambda, \text{out}}(t) + \hat{a}_{\text{LO}}(t)] + \sum_{\sigma \mathbf{n} \neq \Lambda} \epsilon_{\sigma \mathbf{n}} T_\mathbf{n}(k_c; \mathbf{r}_\perp, z) \hat{a}_{\sigma \mathbf{n}, \text{out}}(t) \right\}. \quad (5.33)$$

The photodetectors PD_\pm are statistically independent, and hence, based on the previous section, the probability of observing n_+ and n_- photopulses in the time intervals $[t_+ - \tau_p, t_+]$ and $[t_- - \tau_p, t_-]$, respectively, is given by

$$p(n_+, t_+ - \tau_p, t_+; n_-, t_- - \tau_p, t_-) = p_{n_+}(t_+ - \tau_p, t_+) p_{n_-}(t_- - \tau_p, t_-), \quad (5.34)$$

where the photocurrent operators associated to the photodetectors can be written as

$$\hat{J}_\pm(t, \tau_p) = \frac{\eta \tau_p}{2} \left[\hat{n}_{\text{LO}}(t) + \hat{n}_{\Lambda, \text{out}}(t) \pm \hat{\chi}(t) + 2 \sum_{\sigma \mathbf{n} \neq \Lambda} \hat{n}_{\sigma \mathbf{n}, \text{out}}(t) \right], \quad (5.35)$$

and we have defined the operator

$$\hat{\chi}(t) = \hat{a}_{\text{LO}}^\dagger(t) \hat{a}_{\Lambda, \text{out}}(t) + \hat{a}_{\text{LO}}(t) \hat{a}_{\Lambda, \text{out}}^\dagger(t). \quad (5.36)$$

Note that the mean and two-time correlation functions of this operator are proportional to the ones of the *output quadrature operator* selected by the local oscillator

$$\hat{X}_{\Lambda, \text{out}}^{\varphi - \omega_{\text{LO}} t}(t) = e^{-i\varphi + i\omega_{\text{LO}} t} \hat{a}_{\Lambda, \text{out}}(t) + e^{i\varphi - i\omega_{\text{LO}} t} \hat{a}_{\Lambda, \text{out}}^\dagger(t), \quad (5.37)$$

that is,

$$\langle \hat{\chi}(t) \rangle = |\alpha_{\text{LO}}| \langle \hat{X}_{\Lambda, \text{out}}^{\varphi - \omega_{\text{LO}} t}(t) \rangle \quad (5.38a)$$

$$\langle \hat{\chi}(t) \hat{\chi}(t') \rangle = |\alpha_{\text{LO}}|^2 \langle \hat{X}_{\Lambda, \text{out}}^{\varphi - \omega_{\text{LO}} t}(t) \hat{X}_{\Lambda, \text{out}}^{\varphi - \omega_{\text{LO}} t'}(t') \rangle. \quad (5.38b)$$

The fast optical oscillations of the $\hat{a}_{\Lambda,\text{out}}(t)$ operator are canceled by the rapidly oscillating function $\exp(i\omega_{\text{LO}}t)$ added by the local oscillator. In order to simplify the derivations, it is then customary to move to an interaction picture defined by the transformation operator $\hat{U}_0 = \exp[\hat{H}_0 t/i\hbar]$ with

$$\hat{H}_0 = \sum_{\sigma\mathbf{n}} \hbar\omega_{\text{LO}} \left[\hat{a}_{\sigma\mathbf{n}}^\dagger \hat{a}_{\sigma\mathbf{n}} + \int_{-\infty}^{+\infty} d\omega \hat{b}_{\sigma\mathbf{n}}^\dagger(\omega) \hat{b}_{\sigma\mathbf{n}}(\omega) \right], \quad (5.39)$$

so that

$$\hat{U}_0^\dagger \hat{X}_{\Lambda,\text{out}}^{\varphi-\omega_{\text{LO}}t} \hat{U}_0 = \hat{X}_{\Lambda,\text{out}}^{\varphi}, \quad (5.40)$$

that is, the fast linear variation of the quadrature's phase is removed. From now on, we assume to work in this picture, that is, quantum expectation values are to be taken with the interaction picture state $\hat{\rho}_I(t) = \hat{U}_0^\dagger \hat{\rho}(t) \hat{U}_0$. We shall see how useful this picture is in the next chapter, when analyzing the squeezing properties of optical parametric oscillators.

It is not difficult to prove that in the strong local oscillator regime, the difference photocurrent $j_{\text{D}}(t) = j_+(t) - j_-(t)$ carries information about the $\hat{\chi}(t)$ operator only; any other possible contribution to this photocurrent is balanced out thanks to the 50/50 beam splitter. To this aim we evaluate the first moments of the difference photocurrent, which, given the statistical independency of the photodetectors, can be written in terms of the moments of $j_{\pm}(t)$ as

$$\overline{j_{\text{D}}(t)} = \overline{j_+(t)} - \overline{j_-(t)} \quad \text{and} \quad \overline{j_{\text{D}}^2(t)} = \overline{j_+^2(t)} + \overline{j_-^2(t)} - 2\overline{j_+(t)} \times \overline{j_-(t)}. \quad (5.41)$$

Making use of the relation (5.20) between the moments of $j_{\pm}(t)$ and the quantum expectation values of their corresponding photocurrent operators (5.35), it is straightforward to show after some algebra that the mean and variance of the difference photocurrent are given by

$$\overline{j_{\text{D}}(t)} = \eta G e |\alpha_{\text{LO}}| \langle \hat{X}_{\Lambda,\text{out}}^{\varphi} \rangle, \quad (5.42a)$$

$$V[j_{\text{D}}(t)] = \frac{\eta^2 G^2 e^2 |\alpha_{\text{LO}}|^2}{\tau_{\text{p}}} \left(1 + \sum_{\sigma\mathbf{n}} \frac{\langle \hat{n}_{\sigma\mathbf{n},\text{out}} \rangle}{|\alpha_{\text{LO}}|^2} \right) + \eta^3 G^2 e^2 |\alpha_{\text{LO}}|^2 \left[\langle : (\delta \hat{X}_{\Lambda,\text{out}}^{\varphi})^2 : \rangle + \sum_{\sigma\mathbf{n}} \frac{\langle : \delta \hat{n}_{\sigma\mathbf{n},\text{out}}^2 : \rangle}{|\alpha_{\text{LO}}|^2} \right], \quad (5.42b)$$

where we remind that we make use of the notation $\delta \hat{B} = \hat{B} - \langle \hat{B} \rangle$. Taking the strong local oscillator limit

$$|\alpha_{\text{LO}}|^2 \gg \{ \langle \hat{n}_{\sigma\mathbf{n},\text{out}} \rangle, \langle : \delta \hat{n}_{\sigma\mathbf{n},\text{out}}^2 : \rangle \} \quad \forall (\sigma\mathbf{n}), \quad (5.43)$$

the variance of the difference photocurrent is written as

$$V[j_{\text{D}}(t)] = \eta^2 G^2 e^2 |\alpha_{\text{LO}}|^2 \left\{ \frac{1}{\tau_{\text{p}}} + \eta \langle : [\delta \hat{X}_{\Lambda,\text{out}}^{\varphi}(t)]^2 : \rangle \right\}. \quad (5.44)$$

Expression (5.42a) shows that the mean of $j_{\text{D}}(t)$ carries information about the quadrature of the mode selected by the local oscillator, but similarly to the direct detection case, in the fast response limit $\tau_{\text{p}} \rightarrow 0$ this signal is masked by massive noise at all times.

Hence, also in homodyne detection one is forced to consider the power spectrum of the difference photocurrent. As there are no contributions from any of the modes with $(\sigma, \mathbf{n}) \neq \Lambda$, we will remove the local oscillator mode index Λ from now on. Using again the statistical independency of the signals coming out from the photodetectors PD_{\pm} , one can write the two-time correlation function of $j_{\text{D}}(t)$ as

$$\overline{j_{\text{D}}(t) j_{\text{D}}(t')} = \overline{j_+(t) j_+(t')} + \overline{j_-(t) j_-(t')} - \overline{j_+(t)} \times \overline{j_-(t')} - \overline{j_+(t')} \times \overline{j_-(t)}. \quad (5.45)$$

Using now the general expression (5.28) for the two-time correlation function of a photocurrent, it is lengthy but trivial to arrive to the following expression for the power spectrum of $j_{\text{D}}(t)$

$$P_{\text{D}}(\Omega) = \frac{1}{T} \int_0^T dt \int_0^T dt' \cos[\Omega(t-t')] \overline{j_{\text{D}}(t) j_{\text{D}}(t')} = P_{\text{shot}} + P(\Omega), \quad (5.46)$$

being

$$P_{\text{shot}} = \eta^2 G^2 e^2 |\alpha_{\text{LO}}|^2, \quad (5.47)$$

a contribution to the spectrum which does not depend either on the state of the system or in the frequency (the so-called *shot noise* contribution), and

$$P(\Omega) = \frac{\eta^2 G^2 e^2}{T} \int_0^T dt \int_0^T dt' \cos[\Omega(t-t')] \langle : \delta \hat{X}_{\text{out}}^{\varphi}(t) \delta \hat{X}_{\text{out}}^{\varphi}(t') : \rangle \quad (5.48)$$

a contribution which does depend on these.

It is customary to define a normalized version of this quantity called the *noise spectrum*

$$V^{\text{out}}(\hat{X}^\varphi; \Omega) = \frac{P_{\text{D}}(\Omega)}{P_{\text{shot}}} = 1 + S^{\text{out}}(\hat{X}^\varphi; \Omega) \quad (5.49)$$

where

$$S^{\text{out}}(\hat{X}^\varphi; \Omega) = \frac{\eta}{T} \int_0^T dt \int_0^T dt' \cos[\Omega(t-t')] \langle : \delta\hat{X}_{\text{out}}^\varphi(t) \delta\hat{X}_{\text{out}}^\varphi(t') : \rangle, \quad (5.50)$$

is the so-called *squeezing spectrum*, which, when $\langle : \delta\hat{X}_{\text{out}}^\varphi(t) \delta\hat{X}_{\text{out}}^\varphi(t') : \rangle$ depends only on $|t-t'|$, that is, for stationary states, can be written as

$$S^{\text{out}}(\hat{X}^\varphi; \Omega) = \eta \int_{-\infty}^{+\infty} dt' \langle : \delta\hat{X}_{\text{out}}^\varphi(t) \delta\hat{X}_{\text{out}}^\varphi(t+t') : \rangle e^{-i\Omega t'}. \quad (5.51)$$

Accordingly, we will call *noise frequency* to Ω , which needs not to be confused with the optical frequencies.

Note that the multi-time moments of the output operators still satisfy (5.22), and hence, in terms of the quadratures of the intracavity mode the squeezing spectrum reads

$$S^{\text{out}}(\hat{X}^\varphi; \Omega) = \frac{2\gamma\eta}{T} \int_0^T dt \int_0^T dt' \cos[\Omega(t-t')] \langle : \delta\hat{X}^\varphi(t) \delta\hat{X}^\varphi(t') : \rangle, \quad (5.52)$$

and similarly for the stationary expression. Hence, knowing the state of the intracavity mode, we can evaluate the noise spectrum measured for the field coming out from the cavity. In the upcoming chapters we will assume unit conversion efficiency², that is, $\eta = 1$.

In Chapter 2 we introduced squeezed states of a single harmonic oscillator as those in which one of its quadratures had an uncertainty below that of vacuum or a coherent state. However, we have seen that this simple intuitive object (the uncertainty of a single-mode quadrature) is not the relevant quantity in real experiments designed to measure the quadratures of light, and hence we need to come back a little bit and redefine the concept of squeezing in a way which is interesting from the experimental point of view.

To this aim, let us proceed similarly to how we did in Chapter 2. Consider a quasiperiodic modulation of frequency Ω_{signal} encoded in some quadrature of a cavity mode. It is to be expected that such modulation will appear in the noise spectrum of the corresponding output mode as a peak centered at the $\Omega = \Omega_{\text{signal}}$. The problem is that if this modulation is very small, the corresponding peak in the spectrum can be disguised by the basal shot noise contribution, and it will be impossible to observe it. This is indeed the case when the state of the light mode is coherent (like vacuum), as then the squeezing spectrum is zero for any quadrature and at any noise frequency, so that the noise spectrum has only the flat $V^{\text{out}}(\hat{X}^\varphi; \Omega) = 1$ shot noise contribution. We can then define squeezed states of light in an experimentally useful manner as those states in which $V^{\text{out}}(\hat{X}^\varphi; \Omega) < 1$ for some quadrature and some frequency.

It is not difficult to show that the noise spectra associated to two orthogonal quadratures satisfy the Heisenberg uncertainty relation

$$V^{\text{out}}(\hat{X}^\varphi; \Omega) V^{\text{out}}(\hat{X}^{\varphi+\pi/2}; \Omega) \geq 1. \quad (5.53)$$

Hence, if the shot noise contribution is balanced out for some quadrature, it will be increased accordingly for its orthogonal quadrature, similarly to what happened with the uncertainty of single-mode quadratures in the discussion of Chapter 2.

² Real experiments are not that far from this situation, arriving to efficiencies above 90%.

6. QUANTUM DESCRIPTION AND BASIC PROPERTIES OF OPTICAL PARAMETRIC OSCILLATORS

In the previous chapters we have developed the basic tools which allow us to study within the quantum formalism the light generated in optical cavities. It is now time to apply these to a specific system, optical parametric oscillators, which will be shown to be ideal candidates for the generation of squeezed and entangled light.

Such systems belong to the class of so-called nonlinear optical cavities, that is, resonators containing a nonlinear optical medium. For this reason, the first section of the chapter contains a brief introduction to the optics of dielectric media, with special emphasis on nonlinear uniaxial crystals and the three-wave mixing processes that occur inside them. We then introduce the model for optical parametric oscillators that will be used all along this thesis, and study the quantum properties of the light generated by them in different regimes.

6.1 Dielectric media and nonlinear optics

Roughly speaking [65, 67], from the point of view of their electromagnetic properties most materials fit either into the class of *conductors* or the class of *dielectrics*. A conducting material has charges which are free to move through it, and hence the application of an electromagnetic field can induce an electric current on it. On the other hand, in dielectric media every charge is strongly bounded to one specific atom or molecule fixed in some position of the material, and hence these can be seen as *insulators*. However, when an electromagnetic field is applied to a dielectric, the electron cloud surrounding each nucleus can be slightly displaced, what means that the center of mass of the positive and negative charge distributions of the atoms or molecules get slightly separated, and then the medium acquires a *polarization*, that is, a dipole moment per unit volume. In this section we briefly introduce the description of the electromagnetic field in such media from a classical viewpoint. We will work only with dielectrics which are sensitive to the electric field, but not to the magnetic field.

In principle, in order to describe the effects appearing in the field when propagating in the dielectric material one needs to develop a microscopic model for the medium, introduce it in the inhomogeneous Maxwell's equations via a charge distribution $\rho(\mathbf{r}, t)$ and a current distribution $\mathbf{j}(\mathbf{r}, t)$, and then solve the resulting field-medium coupled equations. However, for the type of media we will work with and for weak enough electromagnetic fields, one can assume that the polarization $\mathbf{P}(\mathbf{r}, t)$ acquired by the medium is a low order polynomial of the applied electric field, say¹

$$P_j(\mathbf{r}, t) = \varepsilon_0 \chi_{jk}^{(1)} E_k(\mathbf{r}, t) + \varepsilon_0 \chi_{jkl}^{(2)} E_k(\mathbf{r}, t) E_l(\mathbf{r}, t) + \dots, \quad (6.1)$$

so that the medium can be treated as a non-dynamical system whose information is all contained the $\overleftrightarrow{\chi}^{(n)}$ coefficients (*tensors* of order $n + 1$ technically²), called the *n-order susceptibilities*. In such circumstances one can define a *displacement field*

$$\mathbf{D}(\mathbf{r}, t) = \varepsilon_0 \mathbf{E}(\mathbf{r}, t) + \mathbf{P}(\mathbf{r}, t), \quad (6.2)$$

and replace the inhomogeneous Maxwell's equations in vacuum (3.2) by the so-called *macroscopic Maxwell's equations* [65, 67]

$$\nabla \cdot \mathbf{D} = 0 \quad \text{and} \quad \nabla \times \mathbf{B} = \mu_0 \partial_t \mathbf{D}. \quad (6.3)$$

Note that we assume to work with homogeneous media, as the susceptibilities are independent of the position vector. Moreover, it is simple to show that materials with an inversion symmetry have null second-order susceptibility. These include any isotropic medium, as well as 11 of the 32 classes of crystals [93], whose lowest-order nonlinear susceptibility is then $\overleftrightarrow{\chi}^{(3)}$.

In the following we discuss the effects of the linear and quadratic polarizations separately.

¹ To lighten the notation of the sections to come, we use the convention that summation over repeated indices is understood.

² In the following, we denote a tensor of order k with components $T_{j_1 j_2 \dots j_k}$ by \overleftrightarrow{T} .

6.1.1 Linear dielectrics and the refractive index

Let us consider only the linear term in the polarization (6.1), and define the *permittivity tensor*

$$\overleftrightarrow{\varepsilon} = \varepsilon_0(1 + \overleftrightarrow{\chi}^{(1)}). \quad (6.4)$$

As in vacuum, Maxwell's equations can be highly simplified with the help of the scalar and vector potentials (3.4). Choosing now the gauge condition $\nabla \cdot \overleftrightarrow{\varepsilon} \mathbf{A} = 0$, it is simple to prove that we can still select $\phi = 0$, and that the vector potential satisfies the modified wave equation

$$[\nabla^2 - (\mu_0 \overleftrightarrow{\varepsilon}) \partial_t^2] \mathbf{A} = \mathbf{0}, \quad (6.5)$$

where we have neglected a $\nabla(\nabla \cdot \mathbf{A})$ term, what can be safely done within the paraxial approximation as is easily proved.

When the medium is isotropic we have $\overleftrightarrow{\chi}^{(1)} = \chi^{(1)} \overleftrightarrow{I}$, being \overleftrightarrow{I} the identity matrix and $\chi^{(1)} \geq 0$, and hence we recover the wave equation that we introduced in (3.68),

$$\left[\frac{c^2}{n^2} \nabla^2 - \partial_t^2 \right] \mathbf{A} = \mathbf{0}, \quad (6.6)$$

being $n = \sqrt{1 + \chi^{(1)}}$ the so called *refractive index* of the medium. Note that the speed of the waves is no longer c but c/n , and hence, light slows down in a dielectric medium.

As this thesis will focus on second-order nonlinearities, we won't be working with isotropic media though; we will consider instead dielectric crystals having an intrinsic coordinate system defined by the orthonormal triad of real vectors $\{\mathbf{e}_e, \mathbf{e}_o, \mathbf{e}'_o\}$ in which the linear susceptibility tensor takes the diagonal form

$$\overleftrightarrow{\chi}^{(1)} = \begin{bmatrix} \chi_e & 0 & 0 \\ 0 & \chi_o & 0 \\ 0 & 0 & \chi_o \end{bmatrix}; \quad (6.7)$$

such birefringent crystals are called *uniaxial* because the refractive index is $n_e = \sqrt{1 + \chi_e}$ along the *extraordinary* direction \mathbf{e}_e , while it is $n_o = \sqrt{1 + \chi_o}$ along the *ordinary* directions $\{\mathbf{e}_o, \mathbf{e}'_o\}$ [93]. In the following, we will assume that the orientation of the crystal is always such that one of the ordinary axes coincides with the z -axis, say $\mathbf{e}'_o \equiv \mathbf{e}_z$, so that the extraordinary and ordinary linear polarization components of the field propagating along the z -axis feel different refractive indices inside the crystal. To see this, just note that writing the vector potential as

$$\mathbf{A}(\mathbf{r}, t) = A_e(\mathbf{r}, t) \mathbf{e}_e + A_o(\mathbf{r}, t) \mathbf{e}_o, \quad (6.8)$$

the components $A_j(\mathbf{r}, t)$ satisfy the wave equations

$$\left[\frac{c^2}{n_e^2} \nabla^2 - \partial_t^2 \right] A_e = 0, \quad \text{and} \quad \left[\frac{c^2}{n_o^2} \nabla^2 - \partial_t^2 \right] A_o = 0, \quad (6.9)$$

according to (6.5)³.

An important property of dielectric materials is called *dispersion*. To see what this is, note that when writing (6.1) we have assumed that the response of the medium to the electric field is instantaneous. Specially in the case of the linear term, this assumption is wrong for most materials, and one has to write more generally

$$P_j(\mathbf{r}, t) = \varepsilon_0 \int_0^\infty d\tau \chi_{jk}^{(1)}(\tau) E_k(\mathbf{r}, t - \tau), \quad (6.10)$$

where the temporal shape of the first-order susceptibility determines exactly how the polarization at a given time depends on the history of the electric field. Defining a spectral decomposition for a general vector field $\mathbf{F}(\mathbf{r}, t)$ as⁴

$$\tilde{\mathbf{F}}(\mathbf{r}, t) = \int_{-\infty}^{+\infty} d\omega \tilde{\mathbf{F}}(\mathbf{r}, \omega) \exp(-i\omega t), \quad (6.11)$$

³ Note that when quantizing the electromagnetic field in Chapter 2 we have assumed the dielectric slab inside the cavity to be isotropic. The procedure there showed is naturally generalized to the case of working with an uniaxial medium: One just needs to take the two allowed polarization vectors $\{\varepsilon_{\sigma q n}\}_{\sigma=1,2}$ along the ordinary and extraordinary directions for all the modes, and replace the refractive indices accompanying those components of the fields by the corresponding ones.

⁴ We choose to introduce the results of this section and the next one in terms of continuous spectral decompositions just because the notation is more compact. Exactly the same expressions apply when only a discrete set of frequencies exists for the fields, as happens inside an optical cavity.

with $\mathbf{F}(\mathbf{r}, -\omega) = \mathbf{F}^*(\mathbf{r}, \omega)$, one can write the previous expression as

$$\tilde{P}_j(\mathbf{r}, \omega) = \varepsilon_0 \chi_{jk}^{(1)}(\omega; \omega) \tilde{E}_k(\mathbf{r}, \omega), \quad (6.12)$$

where

$$\chi_{jk}^{(1)}(\omega; \omega) = \int_0^\infty d\tau \chi_{jk}^{(1)}(\tau) \exp(-i\omega\tau). \quad (6.13)$$

Hence, a non-instantaneous response of the medium is translated into a frequency dependence of the refractive index, which is the phenomenon known as dispersion. Note that while $\overleftrightarrow{\chi}^{(1)}(\tau)$ is real, $\overleftrightarrow{\chi}^{(1)}(\omega; \omega)$ can be complex, although it has to satisfy $\overleftrightarrow{\chi}^{(1)}(-\omega; -\omega) = [\overleftrightarrow{\chi}^{(1)}(\omega; \omega)]^*$ because of the reality of the fields. In this thesis we will ignore any light absorption by the dielectric medium; under such circumstances one can prove that the $\chi_{jk}^{(1)}(\omega; \omega)$ coefficients are real, and furthermore, that the refractive index is a monotonically increasing function of the frequency [93] (what is known as *normal dispersion*).

It is interesting to analyze how the anisotropy and dispersion of the crystal affects the structure of the resonances inside an optical cavity. In Figure 6.1 we show the longitudinal resonances associated to a given transverse mode polarized along \mathbf{e}_e or \mathbf{e}_o . As we showed in Section 3.4.3, without considering anisotropy or dispersion effects, the longitudinal modes are separated by the free spectral range Ω_{FSR} , being this the same for every polarization (Figure 6.1a). An uniaxial crystal introduces different refractive indices for the ordinary and extraordinary polarization components of the field; accordingly, the free spectral range associated to modes polarized along the ordinary and extraordinary directions will no longer be same, as it is inversely proportional to the optical length and hence to the refractive index (Figure 6.1b). On the other hand, the normal dispersion of the crystal makes the refractive index increase with frequency, and hence, the free spectral range will decrease as the frequency increases (Figure 6.1c). Nevertheless, this last effect can be compensated for when needed by adding further dispersive elements inside the cavity such as prisms.

6.1.2 Second order nonlinear dielectrics and frequency conversion

In a sense, the linear term of the polarization contributes to the dynamics of the field in a trivial way: It just modifies the speed of the electromagnetic waves propagating inside it. We are going to show now that, on the other hand, the nonlinear terms of the polarization induce nontrivial phenomena such as the excitation of frequencies not present in the field prior to its interaction with the dielectric [93]. In this thesis we are concerned only with second-order effects, and hence, we will forget about nonlinear terms other than

$$\varepsilon_0 \chi_{jkl}^{(2)} E_k(\mathbf{r}, t) E_l(\mathbf{r}, t) \equiv P_j^{(2)}(\mathbf{r}, t), \quad (6.14)$$

in (6.1). In the following we will simply denote $\mathbf{P}^{(2)}(\mathbf{r}, t)$ and $\overleftrightarrow{\chi}^{(2)}$ by *nonlinear polarization* and *nonlinear susceptibility tensor*, respectively, as no other nonlinear contribution will ever appear. Again, this expression assumes an instantaneous response of the medium, and it must be generalized as

$$P_j^{(2)}(\mathbf{r}, t) = \varepsilon_0 \int_0^\infty d\tau_1 \int_0^\infty d\tau_2 \chi_{jkl}^{(2)}(\tau_1, \tau_2) E_k(\mathbf{r}, t - \tau_1) E_l(\mathbf{r}, t - \tau_2), \quad (6.15)$$

or in frequency space as

$$\tilde{P}_j^{(2)}(\mathbf{r}, \omega) = \varepsilon_0 \int_{-\infty}^{+\infty} d\omega_1 \int_{-\infty}^{+\infty} d\omega_2 \chi_{jkl}^{(2)}(\omega; \omega_1, \omega_2) \tilde{E}_k(\mathbf{r}, \omega_1) \tilde{E}_l(\mathbf{r}, \omega_2), \quad (6.16)$$

where we have defined

$$\chi_{jkl}^{(2)}(\omega; \omega_1, \omega_2) = \delta(\omega - \omega_1 - \omega_2) \int_0^\infty d\tau \int_0^\infty d\tau' \chi_{jkl}^{(2)}(\tau, \tau') \exp[i(\omega_1\tau_1 + \omega_2\tau_2)]. \quad (6.17)$$

Because of the delta-function, this expression states that the ω frequency component of the nonlinear polarization receives contributions from any pair (ω_1, ω_2) of frequency components of the electric field satisfying $\omega_1 + \omega_2 = \omega$; this delta-function in $\overleftrightarrow{\chi}^{(2)}(\omega; \omega_1, \omega_2)$ appears even in the instantaneous case (6.14), and hence it is not a consequence of the dependence of $\mathbf{P}^{(2)}(\mathbf{r}, t)$ on the history of the electric field. Actually, the effect that this has on $\overleftrightarrow{\chi}^{(2)}$ is that, for example, given two pairs (ω_1, ω_2) and (Ω_1, Ω_2) satisfying $\omega = \omega_1 + \omega_2 = \Omega_1 + \Omega_2$, one has in general

$$\chi_{jkl}^{(2)}(\omega; \omega_1, \omega_2) \neq \chi_{jkl}^{(2)}(\omega; \Omega_1, \Omega_2), \quad (6.18)$$

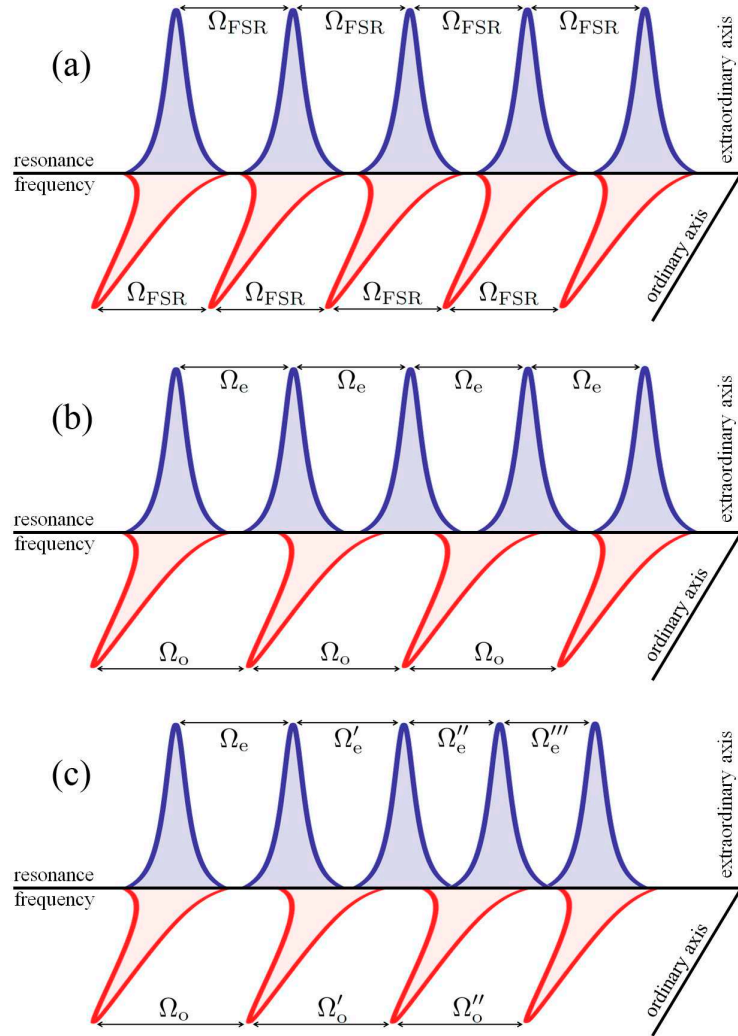


Fig. 6.1: Longitudinal resonances of a given transverse mode inside an optical cavity. (a) Without taking into account anisotropy and dispersion, the separation between resonances is given by Ω_{FSR} for any polarization of the modes. (b) The birefringence of the crystal introduces different refractive indices for the ordinary and extraordinary polarization components, and therefore these have no longer the same free spectral range. (c) The normal dispersion of the crystal introduces further corrections; in particular it increases the optical length of the cavity as frequency increases, making the free spectral range decrease accordingly, that is, $\Omega_j > \Omega'_j > \Omega''_j > \Omega'''_j > \dots$ ($j = e, o$).

which is the generalization of the linear dispersion that we introduced in the previous section. We note, however, that this *nonlinear dispersion* is not as relevant as the normal dispersion appearing in the linear case, and one can safely ignore it within a fairly broad spectral region [94].

Similarly to the linear susceptibility, $\overleftrightarrow{\chi}^{(2)}(\omega; \omega_1, \omega_2)$ might be complex, although it also has to satisfy

$$\overleftrightarrow{\chi}^{(2)}(-\omega; -\omega_1, -\omega_2) = [\overleftrightarrow{\chi}^{(2)}(\omega; \omega_1, \omega_2)]^*. \quad (6.19)$$

In any case, when absorption is neglected it can be proved to be real [93]. A number of general properties of the $\chi_{jkl}^{(2)}(\omega; \omega_1, \omega_2)$ coefficients upon permutation of its Cartesian or frequency arguments can also be proved [93]. For the case of a lossless medium that we will consider, the most general of these is the one called *full permutation symmetry*, which states that $\chi_{jkl}^{(2)}(\omega; \omega_1, \omega_2)$ is left unchanged upon permutation of two frequency arguments, as long as the Cartesian indices are permuted accordingly, that is,

$$\chi_{jkl}^{(2)}(\omega; \omega_1, \omega_2) = \chi_{jlk}^{(2)}(\omega; \omega_2, \omega_1) = \chi_{lkj}^{(2)}(\omega_2; \omega_1, -\omega) = \dots; \quad (6.20)$$

these relations will be useful in the next section.

It is time now to see how the phenomenon of frequency conversion appears. To this aim, let us build now the wave equation satisfied by the electric field, which is easily found to be

$$[\nabla^2 - \mu_0 \overleftrightarrow{\varepsilon} \partial_t^2] \mathbf{E}(\mathbf{r}, t) = -\mu_0 \partial_t^2 \mathbf{P}^{(2)}(\mathbf{r}, t), \quad (6.21)$$

from the “rotational Maxwell’s equations” (the equations involving $\nabla \times \mathbf{E}$ and $\nabla \times \mathbf{B}$). Imagine that we introduce a wave of frequency ω_0 in the medium. As we have shown, this wave induces a nonlinear polarization $P_j^{(2)}(\mathbf{r}, 2\omega_0) = \varepsilon_0 \chi_{jkl}^{(2)}(2\omega_0; \omega_0, \omega_0) E_k(\mathbf{r}, \omega_0) E_l(\mathbf{r}, \omega_0)$ in the medium oscillating at frequency $2\omega_0$, and hence the wave equation for the field component oscillating at that frequency will be

$$[\nabla^2 + 4\omega_0^2 \mu_0 \overleftrightarrow{\varepsilon}] E_j(\mathbf{r}, 2\omega_0) = 4\omega_0^2 \mu_0 \tilde{P}_j^{(2)}(\mathbf{r}, 2\omega_0); \quad (6.22)$$

this clearly shows that $\tilde{\mathbf{P}}^{(2)}(\mathbf{r}, 2\omega_0)$ acts as a source for a new wave which will oscillate at frequency $2\omega_0$. This phenomenon is known as *second harmonic generation*. It is a particular case of the phenomenon known as *frequency sum generation*, in which the wave oscillating at frequency $2\omega_0$ is generated from two waves of frequencies ω_1 and ω_2 satisfying $\omega_1 + \omega_2 = 2\omega_0$. All these effects are known as *up-conversion*, as the generated wave has a frequency larger than the initial ones.

One can think about the opposite kind of process, *down-conversion*, in which a wave of frequency ω_0 is generated from an initial wave oscillating at frequency $2\omega_0$. Note however, that this process is mediated by the nonlinear polarization term $\tilde{P}_j^{(2)}(\mathbf{r}, \omega_0) = \varepsilon_0 \chi_{jkl}^{(2)}(\omega_0; 2\omega_0, -\omega_0) \tilde{E}_k(\mathbf{r}, 2\omega_0) \tilde{E}_l^*(\mathbf{r}, \omega_0)$, which is zero if the ω_0 wave $\tilde{\mathbf{E}}(\mathbf{r}, \omega_0)$ is zero initially. Hence, the phenomenon of down-conversion cannot happen without some kind of initial seed. When this initial seed is not an externally injected wave, but rather some initial fluctuations in the system (e.g., some small amount of thermal photons), the process is known as *spontaneous parametric down-conversion* (the term “parametric” has a rather obscure origin that we won’t worry about).

In general, the down-conversion process might not be frequency degenerate, and hence two waves oscillating at frequencies ω_1 and ω_2 are spontaneously generated from the initial wave of frequency $2\omega_0 = \omega_1 + \omega_2$. In a down-conversion context, it is customary to call *signal* and *idler* to these two waves⁵, and *pump* to the $2\omega_0$ wave. We will stick with this nomenclature, as most of the thesis (and certainly this chapter) deals with down-conversion processes.

As we will see when we develop their quantum theory, all this processes (collectively known as *three-wave mixing processes*) can be intuitively understood as a conversion of a pair of photons of frequencies $\{\omega_s, \omega_i\}$ into one photon of frequency $\omega_p = \omega_s + \omega_i$, or vice versa. The dielectric medium acts just as a host, it doesn’t take any active involvement in the conversion process; hence, the energy and momentum of the photons must be conserved. Conservation of the energy is granted by the delta-function appearing in (6.17). On the other hand, conservation of the linear momentum requires one further condition, namely

$$n_p k_p = n_s k_s + n_i k_i, \quad (6.23)$$

being n_j the refractive index of the medium for the corresponding wave and $k_j = \omega_j/c$ its wave vector (in the following we assume that the three waves propagate in the same direction, what is known as *collinear three-wave mixing*, but

⁵ Which one is the signal or idler is not relevant. This nomenclature comes from the case in which one of the waves, say that of frequency ω_1 , is injected as a seed, and hence the other is generated through the *frequency-difference generation* process $2\omega_0 - \omega_1 \rightarrow \omega_2$. In this case, the injected wave is the *signal*, while the nonlinearly generated one is the *idler*.

everything we say applies for any other scheme). This condition is known as the *phase-matching condition*, and we will show how it appears rigorously in the quantum description of the process (next section).

Consider a situation in which the three waves (pump, signal, and idler) have the same polarization, or in which the nonlinear medium does not show birefringence⁶, so that all the different polarization components of the field feel the same refractive index; in such cases the phase-matching condition can be recasted as

$$\frac{\omega_i}{\omega_s} = -\frac{n(\omega_p) - n(\omega_s)}{n(\omega_p) - n(\omega_i)}. \quad (6.24)$$

The right hand side of this expression is always negative because, as follows from the normal dispersion commented above, $n(\omega_p) > \{n(\omega_s), n(\omega_i)\}$; hence in order to conserve linear momentum the three waves involved in the down-conversion process cannot have the same polarization, and the medium must show birefringence.

As commented above, we will work with uniaxial media, although the phase-matching condition can also be satisfied in biaxial media too. For definiteness, and without loss of generalization, let us assume that $\omega_s > \omega_i$ (we choose the higher frequency wave of the signal-idler pair as the signal), and that the extraordinary refractive index is larger than the ordinary one⁷, that is, $n_e(\omega) > n_o(\omega)$; in this case the pump (signal) wave has to be polarized along the ordinary (extraordinary) axis so that the numerator on the right hand side of (6.24) can become positive, that is, the phase-matching condition becomes

$$\frac{n_e(\omega_s) - n_o(\omega_p)}{n_o(\omega_p) - n_i} = \frac{\omega_i}{\omega_s}. \quad (6.25)$$

We can distinguish then two types of processes. In a *type I* process both signal and idler have the same polarization (extraordinary with our conventions), while in a *type II* process they have orthogonal polarizations (extraordinary the signal and ordinary the idler with our conventions).

Note that when signal and idler are frequency degenerate, the phase matching conditions are reduced to

$$\text{[type I]} \quad n_e(\omega_0) = n_o(2\omega_0), \quad (6.26a)$$

$$\text{[type II]} \quad n_e(\omega_0) = 2n_o(2\omega_0) - n_o(\omega_0). \quad (6.26b)$$

Hence, we see that the conditions for frequency degenerate processes are quite critical, they require a fine tuning of the crystal parameters (as well as a proper stabilization of the cavity resonances in the case of working inside an optical resonator, as we will).

Note finally that it may seem that the frequencies of the signal and idler waves are completely fixed by the frequency we choose for the pump wave and the refractive indices of the crystal, so that in order to change to different down-conversion frequencies we may need to change either the pump frequency, or the crystal we are working with. Fortunately, the conditions (6.25) and (6.26) are much more flexible than they look, because the refractive indices of the crystal depend on the temperature in a known (or at least tabulated) way. Hence, even for a fixed pump frequency, one can still achieve the phase-matching condition for a desired signal-idler frequency pair by tuning the refractive indices of the crystal⁸ via *temperature tuning*.

6.2 Quantum model for a general optical parametric oscillator

In order to optimize the frequency conversion process, it is customary to embed the nonlinear crystal in an optical cavity, so that, e.g. for down-conversion, if one pump photon is not transformed into a signal-idler pair when it first crosses the crystal, it is reflected back in order to have one more chance to be down-converted. This system consisting of a $\chi^{(2)}$ -crystal inside a resonator is known as *optical parametric oscillator* (OPO).

From the previous chapters we know how to treat quantum mechanically an optical cavity. The only question left in order to analyze OPOs within that framework is which intracavity Hamiltonian \hat{H}_c (in the notation of Chapter 4)

⁶ Actually, there is only one example of a crystalline class which does not have an inversion center (and hence, has second-order susceptibility), but does not show birefringence: the class $\bar{4}2m$ [93], to which for example Gallium arsenide belongs.

⁷ In general, an uniaxial crystal is called *positive* if $n_e > n_o$, and *negative* in the opposite case. Although we assume to work with positive uniaxial crystals, everything that we say is readily generalized to the negative case.

⁸ Another well known method to tune the phase-matching condition is by making a rotation θ of the crystal around the ordinary direction \mathbf{e}_o . Under these circumstances, the polarization component of the field parallel to this direction will still feel a refractive index n_o . However, the polarization component orthogonal to this direction won't be parallel to the extraordinary direction anymore, and hence it will feel an effective refractive index n'_e given by [93]

$$\frac{1}{n'_e} = \frac{\cos^2 \theta}{n_e} + \frac{\sin^2 \theta}{n_o}$$

For reasons that will become obvious along the next chapters, we will assume during most of this thesis that no *angular tuning* is needed.

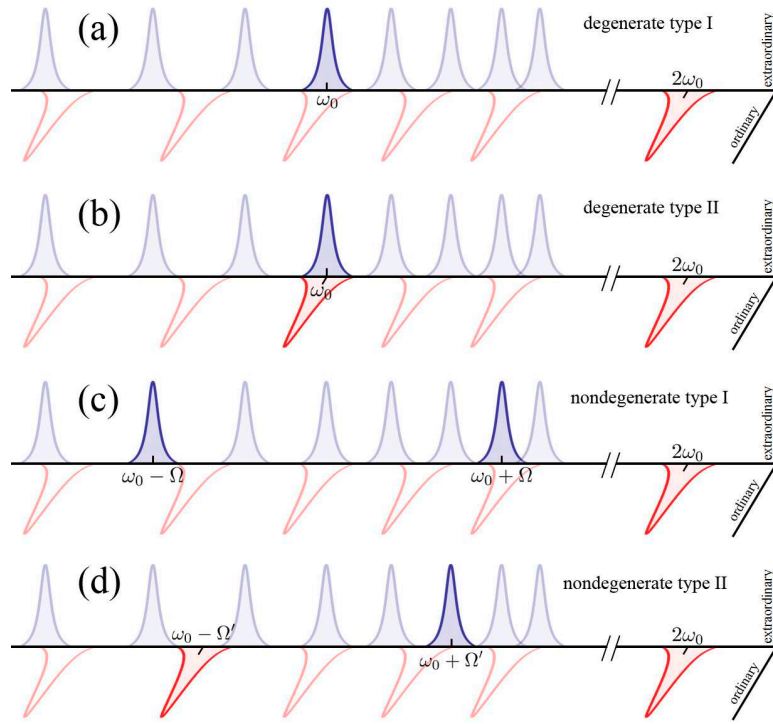


Fig. 6.2: Three-wave mixing processes inside an optical cavity. In this example the structure of the resonances inside the cavity is such that the 4 types of processes are can appear, as they are all energy conserving. Hence, when the pump field has frequency $2\omega_0$ signal and idler can be indistinguishable (a), or distinguishable in polarization (b), in frequency (c), or in them both (d).

accounts for the three-wave mixing processes occurring inside the nonlinear crystal. An intuitive way to proceed is as follows.

The energy associated to an electromagnetic field interacting with an electric (point-like) dipole \mathbf{d} is given by $-\mathbf{d} \cdot \mathbf{E}(\mathbf{r}_d)$, being \mathbf{r}_d the position of the dipole. Now, assume for a moment that the cavity field and the nonlinear polarization appearing in the crystal are independent; then, one would assign the Hamiltonian

$$\hat{H}_c = - \int_{\text{crystal}} d^3\mathbf{r} \hat{\mathbf{P}}^{(2)}(\mathbf{r}) \cdot \hat{\mathbf{E}}(\mathbf{r}), \quad (6.27)$$

to account for their interaction. Of course, the field and the nonlinear polarization are not independent at all (the former is indeed induced by the later!), but keeping in mind that the nonlinear polarization is rather small, the three-wave mixing Hamiltonian will be small compared to the free Hamiltonian, and hence this rude approximation can be justified as the first term of a perturbative expansion of the true Hamiltonian⁹. We would like to stress that, even though rigorous canonical quantization procedures are known for the Maxwell equations in nonlinear dielectric media [95, 3, 96], such intuitive perturbative expansion leading to (6.27) has not been performed to our knowledge, and hence, rigorously, (6.27) cannot be regarded other than as a phenomenological, albeit very successful model.

Let us evaluate now this Hamiltonian for the different three-wave mixing processes that can occur inside the resonator. Consider the cavity resonances depicted in Figure 6.2. In the previous section we showed that one can distinguish between four types of three-wave mixing processes attending to the degeneracies that signal and idler may have in frequency and polarization. If we choose some cavity resonance $2\omega_0$ as the pump mode (with ordinary polarization according to the conventions of the previous section), then one can operate the OPO in four different regimes: *degenerate type I OPO*, in which the signal and idler are indistinguishable and we talk then about a single mode, the signal mode, having frequency ω_0 and extraordinary polarization (Figure 6.2a); *degenerate type II OPO*, in which the signal and idler have orthogonal polarizations but the same frequency (Figure 6.2b); *non-degenerate type I*, in which the signal and idler have the same polarization but correspond to two opposite frequency sidebands around

⁹ Note that this is not true for the linear part of the induced polarization, that is, the refractive index, which is not small at all, and hence one needs to take it into account when developing the quantum theory of the electromagnetic field of the corresponding system. Note also that this is exactly what we did when quantizing the field inside a cavity containing a dielectric medium.

ω_0 (Figure 6.2c); and *non-degenerate type II*, in which the signal and idler are distinguishable both in frequency and polarization (Figure 6.2d).

We can evaluate the Hamiltonian (6.27) for the four processes altogether. To do so, let us write the electric field as

$$\hat{\mathbf{E}}(\mathbf{r}) = \hat{\mathbf{E}}_p^{(+)}(\mathbf{r}) + (1 - \delta_{si}/2)\hat{\mathbf{E}}_s^{(+)}(\mathbf{r}) + (1 - \delta_{si}/2)\hat{\mathbf{E}}_i^{(+)}(\mathbf{r}) + \text{H.c.}, \quad (6.28)$$

where $\hat{\mathbf{E}}_{p,s,i}^{(+)}(\mathbf{r})$ are the (Schrödinger picture) electric fields associated to the pump, signal, and idler cavity modes involved in the three-wave mixing process, and the factors $(1 - \delta_{si}/2)$ are introduced to include also the case in which signal and idler are indistinguishable (in which case $\delta_{si} = 1$), that is, the degenerate type I process.

The pump field has always $\omega_p = 2\omega_0$ and ordinary polarization (with the conventions of the previous section); on the other hand, the signal field has always extraordinary polarization, but its frequency is different for the degenerate (Figures 6.2a and 6.2b) and non-degenerate (Figures 6.2c and 6.2d) schemes; finally, the polarization and frequency of the idler field depend on the particular three-wave mixing scheme. Hence, based on (3.100a) we can write the different frequency components of the field as

$$\hat{\mathbf{E}}_p^{(+)}(\mathbf{r}) = i\sqrt{\frac{\hbar\omega_p}{4\varepsilon_0 n_p L_p}} \mathbf{e}_o \hat{a}_p [G(k_p; \mathbf{r}_\perp, z)e^{in_p k_p z} + \text{c.c.}], \quad (6.29a)$$

$$\hat{\mathbf{E}}_s^{(+)}(\mathbf{r}) = i\sqrt{\frac{\hbar\omega_s}{4\varepsilon_0 n_s L_s}} \mathbf{e}_e \sum_{\mathbf{n}} \hat{a}_{s,\mathbf{n}} [T_{\mathbf{n}}(k_s; \mathbf{r}_\perp, z)e^{in_s k_s z} + \text{c.c.}], \quad (6.29b)$$

$$\hat{\mathbf{E}}_i^{(+)}(\mathbf{r}) = i\sqrt{\frac{\hbar\omega_i}{4\varepsilon_0 n_i L_i}} \boldsymbol{\varepsilon}_i \sum_{\mathbf{n}} \hat{a}_{i,\mathbf{n}} [T_{\mathbf{n}}(k_i; \mathbf{r}_\perp, z)e^{in_i k_i z} + \text{c.c.}], \quad (6.29c)$$

where L_j is the optical length of the cavity evaluated for the refractive index seen by the corresponding mode, and the polarization of the idler mode $\boldsymbol{\varepsilon}_i$ is left unspecified. Note that we have assumed that at the cavity resonance $2\omega_0$ there exists only a TEM₀₀ mode, which is denoted by $G(k; \mathbf{r}_\perp, z)$, while several transverse modes $\{T_{\mathbf{n}}(k; \mathbf{r}_\perp, z)\}_{\mathbf{n}}$ can resonate at the signal and idler frequencies (the same for both, as this is the situation that we will find along this thesis). We denote by \hat{a}_p , $\hat{a}_{s,\mathbf{n}}$, and $\hat{a}_{i,\mathbf{n}}$, the intracavity annihilation operators for pump, signal, and idler photons, respectively.

As for the nonlinear polarization, we can also write it as

$$\hat{\mathbf{P}}^{(2)}(\mathbf{r}, t) = \hat{\mathbf{P}}_p^{(+)}(\mathbf{r}) + (1 - \delta_{si}/2)\hat{\mathbf{P}}_s^{(+)}(\mathbf{r}) + (1 - \delta_{si}/2)\hat{\mathbf{P}}_i^{(+)}(\mathbf{r}) + \text{H.c.}, \quad (6.30)$$

where, based on the previous section, we have¹⁰

$$\hat{\mathbf{P}}_p^{(+)}(\mathbf{r}) = (2 - \delta_{\omega_s, \omega_i}) \varepsilon_0 \chi_{jlm}^{(2)}(\omega_p; \omega_s, \omega_i) \mathbf{e}_j [\hat{\mathbf{E}}_s^{(+)}(\mathbf{r})]_l [\hat{\mathbf{E}}_i^{(+)}(\mathbf{r})]_m, \quad (6.31a)$$

$$\hat{\mathbf{P}}_s^{(+)}(\mathbf{r}) = 2\varepsilon_0 \chi_{jlm}^{(2)}(\omega_s; \omega_p, -\omega_i) \mathbf{e}_j [\hat{\mathbf{E}}_p^{(+)}(\mathbf{r})]_l [\hat{\mathbf{E}}_i^{(-)}(\mathbf{r})]_m, \quad (6.31b)$$

$$\hat{\mathbf{P}}_i^{(+)}(\mathbf{r}) = 2\varepsilon_0 \chi_{jlm}^{(2)}(\omega_i; \omega_p, -\omega_s) \mathbf{e}_j [\hat{\mathbf{E}}_p^{(+)}(\mathbf{r})]_l [\hat{\mathbf{E}}_s^{(-)}(\mathbf{r})]_m, \quad (6.31c)$$

or in terms of the boson operators

$$\hat{\mathbf{P}}_p^{(+)}(\mathbf{r}) = -(2 - \delta_{\omega_s, \omega_i}) \sqrt{\frac{\hbar^2 \omega_s \omega_i}{16 n_s n_i L_s L_i}} \varepsilon_0 \chi_{jem}^{(2)}(\omega_p; \omega_s, \omega_i) \mathbf{e}_j [\boldsymbol{\varepsilon}_i]_m \sum_{\mathbf{nm}} \hat{a}_{s,\mathbf{n}} \hat{a}_{i,\mathbf{m}} \quad (6.32a)$$

$$\times [T_{\mathbf{n}}(k_s; \mathbf{r}_\perp, z) T_{\mathbf{m}}(k_i; \mathbf{r}_\perp, z) e^{i(n_s k_s + n_i k_i)z} + T_{\mathbf{n}}(k_s; \mathbf{r}_\perp, z) T_{\mathbf{m}}^*(k_i; \mathbf{r}_\perp, z) e^{i(n_s k_s - n_i k_i)z} + \text{c.c.}],$$

$$\hat{\mathbf{P}}_s^{(+)}(\mathbf{r}) = 2\sqrt{\frac{\hbar^2 \omega_p \omega_i}{16 n_p n_i L_p L_i}} \varepsilon_0 \chi_{jom}^{(2)}(\omega_s; \omega_p, -\omega_i) \mathbf{e}_j [\boldsymbol{\varepsilon}_i]_m \sum_{\mathbf{n}} \hat{a}_p \hat{a}_{i,\mathbf{n}}^\dagger \quad (6.32b)$$

$$\times [G(k_p; \mathbf{r}_\perp, z) T_{\mathbf{n}}^*(k_i; \mathbf{r}_\perp, z) e^{i(n_p k_p - n_i k_i)z} + G(k_p; \mathbf{r}_\perp, z) T_{\mathbf{n}}(k_i; \mathbf{r}_\perp, z) e^{i(n_p k_p + n_i k_i)z} + \text{c.c.}],$$

$$\hat{\mathbf{P}}_i^{(+)}(\mathbf{r}) = 2\sqrt{\frac{\hbar^2 \omega_p \omega_s}{16 n_p n_s L_p L_s}} \varepsilon_0 \chi_{joe}^{(2)}(\omega_i; \omega_p, -\omega_s) \mathbf{e}_j \sum_{\mathbf{n}} \hat{a}_p \hat{a}_{s,\mathbf{n}}^\dagger \quad (6.32c)$$

$$\times [G(k_p; \mathbf{r}_\perp, z) T_{\mathbf{n}}^*(k_s; \mathbf{r}_\perp, z) e^{i(n_p k_p - n_s k_s)z} + G(k_p; \mathbf{r}_\perp, z) T_{\mathbf{n}}(k_s; \mathbf{r}_\perp, z) e^{i(n_p k_p + n_s k_s)z} + \text{c.c.}].$$

¹⁰ The factors 2 come because, for example $\hat{\mathbf{P}}_s^{(+)}(\mathbf{r})$, receives contributions both from $\chi_{jlm}^{(2)}(\omega_s; \omega_p, -\omega_i)$ and $\chi_{jlm}^{(2)}(\omega_s; -\omega_i, \omega_p)$; this contributions are easily shown to be the same by making use of full permutation symmetry.

Neglecting counter-rotating terms such as $\hat{\mathbf{P}}_j^{(+)}(\mathbf{r}) \cdot \hat{\mathbf{E}}_l^{(+)}(\mathbf{r})$ or $\hat{\mathbf{P}}_p^{(-)}(\mathbf{r}) \cdot \hat{\mathbf{E}}_s^{(+)}(\mathbf{r})$, and taking into account that by full permutation symmetry

$$\chi_{oej}^{(2)}(\omega_p; \omega_s, \omega_i) = \chi_{eoj}^{(2)}(-\omega_s; -\omega_p, \omega_i) = \chi_{joe}^{(2)}(-\omega_i; -\omega_p, \omega_s), \quad (6.33)$$

it is not difficult to write the Hamiltonian as

$$\hat{H}_c = i\hbar \sum_{\mathbf{nm}} \chi_{\mathbf{nm}} \hat{a}_p \hat{a}_{s,\mathbf{n}}^\dagger \hat{a}_{i,\mathbf{m}}^\dagger + \text{H.c.}, \quad (6.34)$$

where the coupling parameters are given by

$$\chi_{\mathbf{nm}} = \chi_{oej}^{(2)}(\omega_p; \omega_s, \omega_i) [\boldsymbol{\varepsilon}_i]_j \sqrt{\frac{\hbar \omega_p \omega_s \omega_i}{16 \varepsilon_0 n_p n_s n_i L_p L_s L_i}} (3 - \delta_{si} - \delta_{\omega_s, \omega_i} / 2) I_{\mathbf{nm}}, \quad (6.35)$$

and we have defined the *three-mode overlapping integral*

$$I_{\mathbf{nm}} = \int_{\text{crystal}} d^3\mathbf{r} \left[G(k_p; \mathbf{r}_\perp, z) T_{\mathbf{n}}^*(k_s; \mathbf{r}_\perp, z) T_{\mathbf{m}}^*(k_i; \mathbf{r}_\perp, z) e^{i\Delta k z} + G(k_p; \mathbf{r}_\perp, z) T_{\mathbf{n}}^*(k_s; \mathbf{r}_\perp, z) T_{\mathbf{m}}(k_i; \mathbf{r}_\perp, z) e^{i\Delta k_1 z} \right. \\ \left. + G^*(k_p; \mathbf{r}_\perp, z) T_{\mathbf{n}}^*(k_s; \mathbf{r}_\perp, z) T_{\mathbf{m}}(k_i; \mathbf{r}_\perp, z) e^{i\Delta k_2 z} + G^*(k_p; \mathbf{r}_\perp, z) T_{\mathbf{n}}^*(k_s; \mathbf{r}_\perp, z) T_{\mathbf{m}}^*(k_i; \mathbf{r}_\perp, z) e^{i\Delta k_3 z} \right] + \text{c.c.}, \quad (6.36)$$

with

$$\begin{aligned} \Delta k &= n_p k_p - n_s k_s - n_i k_i, & \Delta k_1 &= n_p k_p - n_s k_s + n_i k_i, \\ \Delta k_2 &= -n_p k_p - n_s k_s + n_i k_i, & \Delta k_3 &= -n_p k_p - n_s k_s - n_i k_i. \end{aligned} \quad (6.37)$$

Just as we stated in the previous section, this Hamiltonian shows how the three-wave mixing process is described from a quantum viewpoint as the annihilation of a pump photon and the simultaneous creation of a signal-idler pair, or vice versa. In order for the process to be efficient, we need the three-mode-overlapping integral to be as large as possible; let us now simplify the model a little bit in order to understand under which conditions $I_{\mathbf{nm}}$ is maximized.

Assume that the center of the crystal coincides with the cavity's waist plane, and that its length l_c is much smaller than the Rayleigh length of the resonator, that is, $l_c \ll z_R$, see after (3.42). Under these circumstances, the longitudinal variation of the transverse modes can be neglected inside the crystal, see (3.87), and therefore all the longitudinal integrals in $I_{\mathbf{nm}}$ are of the form

$$\int_{-l_c/2}^{l_c/2} dz e^{i\Delta k_j z} = l_c \text{sinc} \left(\frac{\Delta k_j l_c}{2} \right); \quad (6.38)$$

hence, we see that in order to maximize the conversion process, some of the Δk_j 's must satisfy $|\Delta k_j| \ll l_c^{-1}$. On the other hand, $\Delta k = 0$ is precisely the phase matching condition that we introduced in the previous section using linear momentum conservation arguments, and hence, we assume now that $\Delta k \ll l_c^{-1}$; under these conditions, it is completely trivial to show that the rest of Δk_j 's are all well above l_c^{-1} , so that their contribution to $I_{\mathbf{nm}}$ can be neglected.

The Hamiltonian can be even more simplified if we choose the Laguerre-Gauss basis for the transverse modes (3.47), which are written in the cavity waist as

$$L_{pl}(k; \mathbf{r}_\perp, z=0) = \mathcal{R}_p^{|l|}(k; r) \exp[i l \phi], \quad (6.39)$$

with

$$\mathcal{R}_p^{|l|}(k; r) = \sqrt{\frac{2p!}{\pi (p+|l|)!}} \frac{1}{w} \left(\frac{\sqrt{2}r}{w} \right)^{|l|} L_p^{|l|} \left(\frac{2r^2}{w^2} \right) \exp\left(-\frac{r^2}{w^2}\right), \quad (6.40)$$

being w the spot size of the modes at the cavity waist. The interesting thing about these modes is that they are eigenfunctions of the orbital angular momentum operator, that is, $-i\partial_\phi L_{pl}(k; \mathbf{r}_\perp, z) = l L_{pl}(k; \mathbf{r}_\perp, z)$, and hence conservation of this quantity in the conversion process should appear explicitly in this basis. In particular, taking into account the phase matching condition $\Delta k \ll l_c^{-1}$ that we have already selected, in the Laguerre-Gauss basis the three-mode overlapping integral reads

$$I_{pl,p'l'} = 2l_c \delta_{-ll'} \int_0^{+\infty} r dr G(k_p; r) \mathcal{R}_p^{|l|}(k_s; r) \mathcal{R}_{p'}^{|l'|}(k_i; r), \quad (6.41)$$

and hence the three-wave mixing Hamiltonian takes the final form

$$\hat{H}_c = i\hbar \sum_{pp', l \geq 0} \chi_{pp'}^l \hat{a}_p \hat{a}_{s,p,l}^\dagger \hat{a}_{i,p',-l}^\dagger + \text{H.c.}, \quad (6.42)$$

where the sum extend over all the opposite orbital angular momentum pairs present at the signal-idler cavity resonances, and

$$\chi_{pp'}^l = \frac{3 - \delta_{si} - \delta_{\omega_s, \omega_i}/2}{1 + \delta_{l,0}} l_c \chi_{\text{oe}j}^{(2)}(\omega_p; \omega_s, \omega_i) [\epsilon_i]_j \sqrt{\frac{\hbar \omega_p \omega_s \omega_i}{\epsilon_0 n_p n_s n_i L_p L_s L_i}} \int_0^{+\infty} r dr G(k_p; r) \mathcal{R}_p^l(k_s; r) \mathcal{R}_{p'}^l(k_i; r). \quad (6.43)$$

Let us remark at this point that, ideally, we can decide which of the possible intracavity three-wave mixing processes is selected by operating the OPO in the corresponding phase matching condition. In most of the thesis we will assume that this is the case. In practice, however, one can select between type I and II at will, but additional care must be taken in order to ensure working with a desired pair of signal-idler frequencies around ω_0 , or the degenerate frequency ω_0 itself. We shall come back to this issue in the next chapter.

We have now at our disposal a quantum model for a general OPO. Note that in the case of indistinguishable signal and idler, \hat{H}_c is similar to the Hamiltonian that we used to generate squeezed states of the harmonic oscillator, see (2.31). Similarly, when signal and idler are distinguishable, the Hamiltonian resembles the one which produced entangled states (2.39). Hence, the OPO seems a perfect candidate for the generation of squeezed and entangled states of light. The rest of the chapter is devoted to analyze these properties of the light generated by the OPO.

6.3 Squeezing properties of the DOPO

In this section we study the squeezing properties of degenerate type I OPOs (*DOPOs*). To this purpose, let us work with the simplest transverse mode configuration, in which we consider only a TEM₀₀ mode resonating at the signal frequency. Squeezing in OPOs was originally predicted by using this *single-mode DOPO* model [97]¹¹, and throughout this thesis we will learn under which conditions it is valid.

The analysis performed in this section is of major importance for this thesis, as any other OPO configuration will be analyzed with simple adaptations of it.

6.3.1 The DOPO within the positive P representation

The single-mode DOPO deals then with two cavity modes only: The pump mode, which resonates at frequency $\omega_p = 2\omega_0$ and has ordinary polarization, and the signal mode, which resonates at frequency $\omega_s = \omega_0$ and has extraordinary polarization (Figure 6.2a). Both are in a TEM₀₀ transverse mode. The pump mode is driven by an external laser beam of frequency $2\omega_L$ close to $2\omega_0$, while no injection is used for the signal mode; hence, signal photons are expected to appear from the pump field via spontaneous parametric down-conversion.

In Figure 6.3 it is shown the basic experimental scheme used to pump and detect the DOPO. Note that the same laser is used both as the injection for the cavity (after doubling its frequency) and as the local oscillator field, which ensures that all the phases of the system are more or less locked. Based on the analysis of homodyne detection introduced in the previous chapter, we move then to the interaction picture defined by the transformation operator

$$\hat{U}_0 = \exp[\hat{H}_0 t / i\hbar] \quad \text{with} \quad \hat{H}_0 = \hbar\omega_L (2\hat{a}_p^\dagger \hat{a}_p + \hat{a}_s^\dagger \hat{a}_s), \quad (6.44)$$

that is, we “rotate” the system to the local oscillator (or injection) frequency. The state $\hat{\rho}$ of the intracavity modes is written as $\hat{\rho}_I = \hat{U}_0^\dagger \hat{\rho} \hat{U}_0$ in this picture, and satisfies the master equation

$$\frac{d\hat{\rho}_I}{dt} = \left[-2i\Delta \hat{a}_p^\dagger \hat{a}_p - i\Delta \hat{a}_s^\dagger \hat{a}_s + \frac{\chi}{2} \hat{a}_p \hat{a}_s^{\dagger 2} + \mathcal{E}_p a_p^\dagger + \text{H.c.}, \hat{\rho}_I \right] + \sum_{j=p,s} \gamma_j (2\hat{a}_j \hat{\rho}_I \hat{a}_j^\dagger - \hat{a}_j^\dagger \hat{a}_j \hat{\rho}_I - \hat{\rho}_I \hat{a}_j^\dagger \hat{a}_j), \quad (6.45)$$

¹¹ The story of such prediction was actually quite intricate [1]. The problem was that the first analyses of squeezing in OPOs were performed not in terms of the noise spectrum of the field coming out from the cavity, but in terms of the uncertainties of the intracavity modes, which showed only a 50% noise reduction even in the most ideal situation [98, 99]. Hence, these initial predictions were a little disappointing, since such small levels of squeezing couldn’t help much for the applications of squeezing proposed at that time [100, 101, 102, 103]. The puzzle was finally solved by Collet and Gardiner [97], who applied the input-output formalism previously introduced by Yurke and Denker in electronic circuits [104], to analyze the field coming out from the parametric oscillator in terms of its squeezing spectrum.

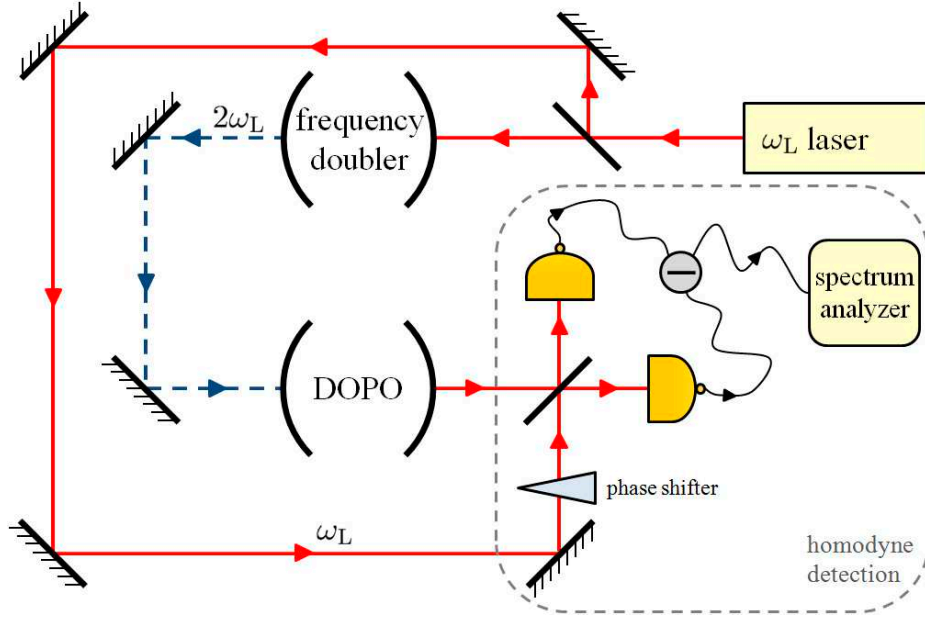


Fig. 6.3: Schematic representation of a typical DOPO experiment. Note that the same laser is used both as pump injection (after doubling its frequency) and as local oscillator of the homodyne detection with which the signal field is studied. This is a very convenient scheme, as the phases of all the involved fields are more or less locked to the initial laser phase.

where $\Delta = \omega_0 - \omega_L$ is the detuning of the laser field with respect to the cavity resonance. We take \mathcal{E}_p as a positive real, which is as taking the phase of the injected laser beam as the reference for any other phase of the system. The nonlinear coupling parameter χ is found from (6.1.2) particularized to the configuration that we are treating; taking into account that

$$\int_0^{+\infty} r dr G(k_p; r) G^2(k_s; r) = \left(\frac{2}{\pi}\right)^{3/2} \int_0^{+\infty} dr \frac{r}{w_p w_s^2} \exp\left[-\left(\frac{1}{w_p^2} + \frac{2}{w_s^2}\right) r^2\right] = \frac{1}{2\pi^{3/2} w_s}, \quad (6.46)$$

where we have used that $w_p^2/w_s^2 = \lambda_p/\lambda_s = 1/2$, see (3.86b), we get

$$\chi = 3 \frac{l_c}{w_s} \chi_{\text{oeo}}^{(2)}(2\omega_0; \omega_0, \omega_0) \sqrt{\frac{\hbar \omega_0^3}{8\pi^3 \epsilon_0 n_c^3 L_{\text{opt}}^3}}, \quad (6.47)$$

where pump and signal feel the same refractive index $n_c = n_e(\omega_0) = n_o(2\omega_0)$, as follows from the phase-matching condition (6.26a).

Our goal is to evaluate the noise spectrum of the field coming out from the cavity, which was shown in the previous chapter to be given by

$$V^{\text{out}}(\hat{X}_s^\varphi; \Omega) = 1 + S(\hat{X}_s^\varphi; \Omega), \quad (6.48)$$

with

$$S(\hat{X}_s^\varphi; \Omega) = 2\gamma_s \int_{-\infty}^{+\infty} dt' \exp(-i\Omega t') \langle: \delta \hat{X}_s^\varphi(t) \delta \hat{X}_s^\varphi(t+t') : \rangle, \quad (6.49)$$

when the state of the system is stationary, what will be shown to happen in the DOPO for $t \gg \gamma_s^{-1}$. Recall that the expectation value in this expression is to be evaluated within the interaction picture, that is, via the density operator $\hat{\rho}_I$ satisfying the master equation (6.45).

We use the positive P representation in order to evaluate the squeezing spectrum (6.49). In particular, following the same steps as those described in Section 2.6.3, it is completely straightforward to show that the stochastic Langevin

equations associated to the master equation (6.45) are

$$\dot{\alpha}_p = \mathcal{E}_p - (\gamma_p + i\Delta)\alpha_p - \frac{\chi}{2}\alpha_s^2, \quad (6.50a)$$

$$\dot{\alpha}_p^+ = \mathcal{E}_p - (\gamma_p - i\Delta)\alpha_p^+ - \frac{\chi}{2}\alpha_s^{+2}, \quad (6.50b)$$

$$\dot{\alpha}_s = -(\gamma_s + i\Delta)\alpha_s + \chi\alpha_p\alpha_s^+ + \sqrt{\chi\alpha_p}\eta(t), \quad (6.50c)$$

$$\dot{\alpha}_s^+ = -(\gamma_s - i\Delta)\alpha_s^+ + \chi\alpha_p^+\alpha_s + \sqrt{\chi\alpha_p^+}\eta^+(t), \quad (6.50d)$$

where $\eta(t)$ and $\eta^+(t)$ are independent real Gaussian noises which satisfy the usual statistical properties (2.82). Even though noise is multiplicative in these equations, it is easy to show that they have the same form both within the Ito and Stratonovich interpretations, and hence we can directly use the usual rules of calculus to analyze them.

In order to better appreciate the parameters needed to model the system, we will make the following variable change

$$\tau = \gamma_s t, \quad \beta_m(\tau) = \frac{\chi}{\gamma_s \sqrt{\gamma_p/\gamma_m}} \alpha_m(t), \quad \zeta_m(\tau) = \frac{1}{\sqrt{\gamma_s}} \eta_m(t), \quad (6.51)$$

where with these definitions the new noises $\zeta(\tau)$ and $\zeta^+(\tau)$ satisfy the same statistical properties as $\eta(t)$ and $\eta^+(t)$, but now with respect to the dimensionless time τ . In terms of these *scaled variables*, the Langevin equations (6.50) read (derivatives with respect to τ are understood)

$$\dot{\beta}_p = \kappa[\sigma - (1 + i\tilde{\Delta})\beta_p - \beta_s^2/2] \quad (6.52a)$$

$$\dot{\beta}_p^+ = \kappa[\sigma - (1 - i\tilde{\Delta})\beta_p^+ - \beta_s^{+2}/2] \quad (6.52b)$$

$$\dot{\beta}_s = -(1 + i\tilde{\Delta})\beta_s + \beta_p\beta_s^+ + g\sqrt{\beta_p}\zeta(\tau) \quad (6.52c)$$

$$\dot{\beta}_s^+ = -(1 - i\tilde{\Delta})\beta_s^+ + \beta_p^+\beta_s + g\sqrt{\beta_p^+}\zeta^+(\tau), \quad (6.52d)$$

which have only four dimensionless parameters

$$\kappa = \gamma_p/\gamma_s, \quad \tilde{\Delta} = \Delta/\gamma_s, \quad \sigma = \chi\mathcal{E}_p/\gamma_p\gamma_s, \quad g = \chi/\sqrt{\gamma_p\gamma_s}, \quad (6.53)$$

which are, respectively, normalized versions of the pump's damping rate, the detuning, the pump injection parameter, and the nonlinear coupling. In the following we will set $\Delta = 0$ for simplicity; we will analyze the effects of detuning in Section 6.3.4.

These equations allow us to evaluate the squeezing spectrum as

$$S(\hat{X}_s^\varphi; \Omega) = \frac{2}{g^2} \int_{-\infty}^{+\infty} d\tau' \exp(-i\tilde{\Omega}\tau') \langle \delta x_s^\varphi(\tau) \delta x_s^\varphi(\tau + \tau') \rangle_P, \quad (6.54)$$

where we have defined normalized versions of the noise frequency $\tilde{\Omega} = \Omega/\gamma_s$ and the quadratures within the positive P phase representation

$$x_s^\varphi(\tau) = e^{-i\varphi}\beta_s(\tau) + e^{i\varphi}\beta_s^+(\tau). \quad (6.55)$$

Hence, in order to evaluate the squeezing spectrum we need the solutions $\beta_m(\tau)$ of (6.52) in terms of the noises, so that from them we can evaluate the corresponding stochastic averages. However, these equations are a set of coupled nonlinear stochastic equations, and hence it is impossible to perform this task analytically without introducing further approximations. Let us first show the behavior of the DOPO in the classical limit, and then we will come back to the problem of solving (6.52).

6.3.2 Classical analysis of the DOPO

Before studying the quantum properties of any OPO, it is convenient to analyze what classical optics has to say about its dynamics. In the next section we will see that this is not only convenient, but also mandatory in order to extract analytic information from its quantum model. Moreover, along the thesis, and starting in the next section, we will learn how to predict the quantum properties of OPOs just from a qualitative understanding of their classical behavior.

In principle, the classical behavior of the field inside an OPO must be studied by using the nonlinear wave equation of the electric field (6.21) with appropriate boundary conditions accounting for the (open) cavity. There is a simpler route though. From the chapter where we studied the harmonic oscillator, we learned that quantum predictions

become equivalent to the classical description of the system in a certain limit. We introduced the coherent states of the oscillator as those which allowed for these quantum-to-classical transition; the interesting thing to note about coherent states is that there are no quantum correlations on them, that is, given two oscillators with annihilation operators \hat{a}_1 and \hat{a}_2 both in some coherent state, it is satisfied

$$\langle \hat{a}_1^2 \rangle = \langle \hat{a}_1 \rangle \langle \hat{a}_1 \rangle \quad \text{and} \quad \langle \hat{a}_1 \hat{a}_2 \rangle = \langle \hat{a}_1 \rangle \langle \hat{a}_2 \rangle, \quad (6.56)$$

for example. Hence, one way to retrieve the classical equations from the evolution equations for the operators of the system is to take expectation values, and decorrelate any product of operators following (6.56), which is as using a coherent ansatz for the state of the system. The quantities $\nu_j = \sqrt{2\hbar/\omega_j} \langle \hat{a}_j \rangle$ are then identified with the normal variables of the various harmonic oscillators that form the system, being ω_j their natural oscillation frequency. This procedure is called the *mean field limit*.

Equipped with an stochastic quantum model for the system, the classical limit is even simpler to devise. The idea now is that the classical behavior of the system (its classical phase-space trajectory) should be recovered when quantum noise is negligible. Hence, the classical equations of an OPO should be recovered by neglecting the noise terms on its corresponding Langevin equations, and identifying $\nu_j = \sqrt{2\hbar/\omega_j} \alpha_j$ with the normal variables of the cavity modes. When using the positive P representation there is one more prescription though: In order to come back to a classical phase space, the variables α_j^+ of the extended phase space have to be identified with α_j^* . This procedure is in agreement with (and completely equivalent to) the mean field scenario discussed above.

Applying these ideas to our DOPO model (6.52), we get the following classical equations

$$\dot{\beta}_p = \kappa (\sigma - \beta_p - \beta_s^2/2), \quad (6.57a)$$

$$\dot{\beta}_s = -\beta_s + \beta_p \beta_s^*. \quad (6.57b)$$

This is a set of first-order nonlinear differential equations, which, again, cannot be solved analytically. Fortunately, there is actually no need for doing so for our purposes. One is usually interested only on the long time term solutions that these equations predict for the system. In particular, the first type of solutions that one needs to look for are the so-called *stationary* or *steady state* solutions, in which the variables do not depend on time. These solutions are found by setting $\dot{\beta}_p = \dot{\beta}_s = 0$, then arriving to a simple algebraic system

$$\sigma = \beta_p + \beta_s^2/2, \quad (6.58a)$$

$$\beta_s = \beta_p \beta_s^*. \quad (6.58b)$$

This system admits two types of such solutions. In the first type the signal mode is *switched off*, and hence we have

$$\bar{\beta}_p = \sigma \quad \text{and} \quad \bar{\beta}_s = 0, \quad (6.59)$$

where the overbar is used to denote “classical long time term solution”. In the second type, the signal mode is *switched on*, and in order to find the explicit form of the solution we use the following amplitude-phase representation of the variables: $\beta_j = \rho_j \exp(i\varphi_j)$. From the second equation we trivially get $\rho_p = 1$ and $\exp(i\varphi_p) = \exp(2i\varphi_s)$, which introduced in the first equation leads to $\rho_s = \sqrt{\sigma - 1}$ and $\varphi_s = \{0, \pi\}$, that is,

$$\bar{\beta}_p = 1 \quad \text{and} \quad \bar{\beta}_s = \pm \sqrt{2(\sigma - 1)}. \quad (6.60)$$

Note that this second solution only exists for $\sigma \geq 1$; we say that the *domain of existence* of the solutions are all the parameter space $\{\sigma, \kappa\}$ and the region $\{\sigma \geq 1, \kappa\}$ for the first and second solutions, respectively. Note also that at $\sigma = 1$ both solutions coincide.

Knowing the possible solutions of (6.58) in the long time term is not enough. It can happen that a solution exists but is *unstable*, that is, an arbitrarily small perturbation can make the system move out from that solution and fall into another solution. It is not difficult to analyze the stability of a solution. With full generality, consider the equation

$$\dot{\boldsymbol{\beta}} = \mathbf{f}(\boldsymbol{\beta}), \quad (6.61)$$

where all the complex variables of the system are collected as

$$\boldsymbol{\beta} = (\beta_1, \beta_1^*, \beta_2, \beta_2^*, \dots, \beta_N, \beta_N^*), \quad (6.62)$$

and one stationary solution $\bar{\boldsymbol{\beta}}$ satisfying $\mathbf{f}(\bar{\boldsymbol{\beta}}) = \mathbf{0}$. In order to see whether this solution is stable or not, we just introduce a small perturbation $\mathbf{b}(\tau)$ in the system and analyze how it grows. Writing $\boldsymbol{\beta}(\tau) = \bar{\boldsymbol{\beta}} + \mathbf{b}(\tau)$, and making

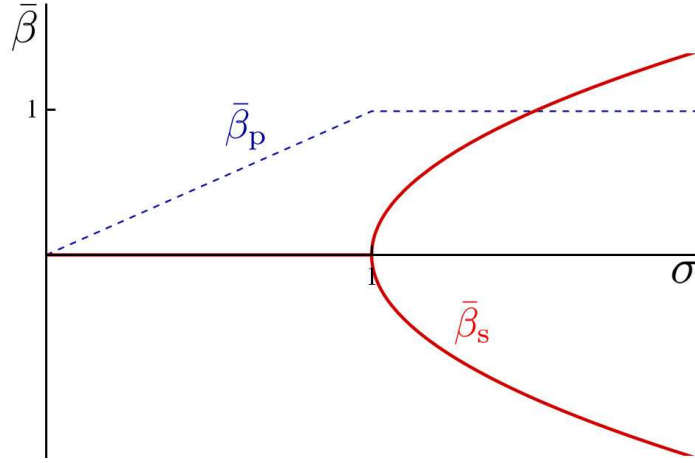


Fig. 6.4: Classical *bifurcation diagram* of the DOPO, that is, the amplitude of the different fields as a function of the system parameters. Below threshold ($\sigma < 1$) the pump amplitude (blue, dashed line) increases linearly with the pump parameter σ , and the signal field is off (red, solid line). Above this threshold the pump gets ‘frozen’ to a given value, and the signal field is switched on and can take any of two opposite phases (0 or π) owed to the symmetry $\alpha_s \rightarrow -\alpha_s$ of equations (6.57). Hence the system shows bistability above threshold.

a series expansion of $\mathbf{f}(\boldsymbol{\beta})$ up to linear order in \mathbf{b} , it is straightforward to show that the evolution equation of the perturbations is

$$\dot{\mathbf{b}} = \mathcal{L}\mathbf{b} \quad \text{with} \quad \mathcal{L}_{jl} = \left. \frac{\partial f_j}{\partial \beta_l} \right|_{\bar{\boldsymbol{\beta}}}, \quad (6.63)$$

and hence the linear evolution of the perturbations is governed by matrix \mathcal{L} , which we will call the *stability matrix*. Being a simple linear system, the growth of this perturbation is easily analyzed. Suppose that we diagonalize \mathcal{L} , so that we know the set $\{\lambda_j, \mathbf{w}_j\}_{j=1, \dots, 2N}$ satisfying $\mathbf{w}_j^* \mathcal{L} = \lambda_j \mathbf{w}_j^*$; projecting the linear system (6.63) onto the \mathbf{w}_j vectors, and defining the projections $c_j(t) = \mathbf{w}_j^* \cdot \mathbf{b}(t)$, we get the simple solutions

$$c_j(t) = c_j(0) \exp(\lambda_j \tau). \quad (6.64)$$

Hence, the growth of the perturbations is characterized by the real part of the eigenvalues λ_j . In particular, if *all* of them have negative real part, the perturbations will tend to decay, and after a time $\tau \gg \max[|\text{Re}\{\lambda_j\}|^{-1}]_{j=1, \dots, 2N}$ the stationary solution $\bar{\boldsymbol{\beta}}$ will be restored; on the other hand, if *any* of them has a positive real part, it will mean that perturbations tend to grow in some direction of phase space, and then the system won’t come back to $\bar{\boldsymbol{\beta}}$. Accordingly, we say in the first case that $\bar{\boldsymbol{\beta}}$ is a stable, stationary solution, while it is unstable in the second case.

We can apply these *stability analysis* to our DOPO equations (6.57) and the corresponding stationary solutions (6.59,6.60). Ordering the different amplitudes as $\boldsymbol{\beta} = (\beta_p, \beta_p^*, \beta_s, \beta_s^*)$, the general stability matrix associated to equations (6.57) is

$$\mathcal{L} = \begin{bmatrix} -\kappa & 0 & -\kappa \bar{\beta}_s & 0 \\ 0 & -\kappa & 0 & -\kappa \bar{\beta}_s^* \\ \bar{\beta}_s^* & 0 & -1 & \bar{\beta}_p \\ 0 & \bar{\beta}_s & \bar{\beta}_p^* & -1 \end{bmatrix}, \quad (6.65)$$

which has eigenvalues

$$\lambda_{\pm}^{(1)} = \frac{1}{2} \left[\bar{\rho}_p - \kappa - 1 \pm \sqrt{(\bar{\rho}_p + \kappa - 1)^2 - 4\kappa \bar{\rho}_s^2} \right], \quad (6.66a)$$

$$\lambda_{\pm}^{(2)} = \frac{1}{2} \left[-\bar{\rho}_p - \kappa - 1 \pm \sqrt{(\bar{\rho}_p - \kappa + 1)^2 - 4\kappa \bar{\rho}_s^2} \right]. \quad (6.66b)$$

Particularizing these eigenvalues to the first solution (6.59) it is simple to see that $\lambda_+^{(1)} = \sigma - 1$, and hence this solution becomes unstable when $\sigma > 1$. On the other hand, it is simple to check that all the eigenvalues have negative real part when particularized to the second solution (6.60) in all its domain of existence.

This allows us to understand the classical behavior of the system in the following way (see Figure 6.4): while the pump injection increases from $\sigma = 0$ to $\sigma = 1$, the signal mode remains switched off, and all the injection is used to excite the pump mode as $\bar{\beta}_p = \sigma$; on the other hand, when the point $\sigma = 1$ is crossed the pump mode gets “frozen” to a fix value $\bar{\beta}_p = 1$, while the signal mode starts oscillating inside the DOPO as $\bar{\beta}_s = \sqrt{\sigma - 1}$. The point $\sigma = 1$ is called a *bifurcation* of the system, because the system changes from one long time term stable solution to another. Physically, this means that the DOPO is a *threshold system*: The injected laser must be above some threshold power in order for the signal field to start oscillating inside the cavity. According to this picture, the solutions with the signal mode switched off (6.59) and on (6.60) are denoted by *below* and *above threshold solutions*, respectively.

6.3.3 Quantum analysis of the DOPO: linearization and noise spectrum

How does knowing the classical behavior of the DOPO help us to solve the nonlinear stochastic equations (6.52)? The idea is that the noise term is multiplied by g , which is a very small quantity¹² in usual OPOs, that is, $g \ll 1$, and hence, for most values of the system parameters quantum fluctuations act just as a small perturbation around the classical solution. One can then solve the Langevin equations perturbatively [3, 105, 106], that is, by writing the stochastic amplitudes as

$$\beta_j = \bar{\beta}_j + g\beta_j^{(1)} + g^2\beta_j^{(2)} + \dots, \quad (6.67a)$$

$$\beta_j^+ = \bar{\beta}_j^* + g\beta_j^{+(1)} + g^2\beta_j^{+(2)} + \dots, \quad (6.67b)$$

where the $\beta_j^{(k)}$ amplitudes are quantities of order g^k , and then solve iteratively order by order the Langevin equation. For the purposes of this thesis it will be enough to consider the first quantum correction, that is, the order g , although we will explain the effect of further quantum corrections. Let us then write

$$\boldsymbol{\beta}(\tau) = \bar{\boldsymbol{\beta}} + \mathbf{b}(\tau) \quad (6.68)$$

being $\bar{\boldsymbol{\beta}} = \text{col}(\bar{\beta}_p, \bar{\beta}_p^*, \bar{\beta}_s, \bar{\beta}_s^*)$ a vector containing the classical steady state solution of the DOPO and $\mathbf{b}(\tau) = \text{col}[b_p(\tau), b_p^+(\tau), b_s(\tau), b_s^+(\tau)]$ a vector with the corresponding quantum fluctuations, which we assume to be order g as explained. Retaining up to order g terms in the Langevin equation, we get

$$\dot{\mathbf{b}} = \mathcal{L}\mathbf{b} + g\boldsymbol{\zeta}(\tau), \quad (6.69)$$

where \mathcal{L} is the stability matrix already defined in the previous section, and $\boldsymbol{\zeta}(\tau) = \text{col}[0, 0, \sqrt{\bar{\beta}_p}\zeta(\tau), \sqrt{\bar{\beta}_p^*}\zeta^+(\tau)]$. We will call the *linearized Langevin equations* of the DOPO to this linear system. These can be solved easily by diagonalizing the stability matrix, after what the solution can be used to find the squeezing spectrum (6.54). Let us show this process below and above the DOPO’s threshold separately.

Quantum properties of the DOPO below threshold. Particularized to the below threshold solution (6.59), the stability matrix reads

$$\mathcal{L} = \begin{bmatrix} -\kappa & 0 & 0 & 0 \\ 0 & -\kappa & 0 & 0 \\ 0 & 0 & -1 & \sigma \\ 0 & 0 & \sigma & -1 \end{bmatrix}, \quad (6.70)$$

whose block-diagonal form shows that the (linear) properties of pump and signal are independent. We will learn throughout the thesis that this decoupling of the classically unexcited modes is a rather general property of OPOs. As the linearized Langevin equations for the pump modes have no noise terms, the pump stays in a coherent state. We can focus then on the quantum properties of the signal mode, which are given by the simple linear system

$$\dot{\mathbf{b}}_s = \mathcal{L}_s\mathbf{b}_s + g\sqrt{\sigma}\boldsymbol{\zeta}_s(\tau), \quad (6.71)$$

¹² For example, considering a symmetric, confocal cavity, and using the expressions we have given for the different model parameters in terms of physical parameters, it is easy to write

$$g = \frac{12\chi^{(2)}l_c}{\lambda_0^2} \sqrt{\frac{2\pi\hbar c}{L_{\text{eff}}L_{\text{opt}}\mathcal{T}_p\mathcal{T}_s\epsilon_0 n_c}}, \quad (6.66c)$$

where λ_0 is the wavelength of the signal mode, $\chi^{(2)}$ is the relevant nonlinear susceptibility, and $\mathcal{T}_p = \mathcal{T}(\lambda_0/2)$ and $\mathcal{T}_s = \mathcal{T}(\lambda_0)$ are the transmittivities of the output mirror at the pump and signal wavelengths, respectively. If we consider the numerical values (typical of OPO experiments)

$$n_c = 2, \quad \lambda_0 = 1064\text{nm}, \quad \mathcal{T}_p = 0.1, \\ \chi^{(2)} = 2.5\text{pm/V}, \quad l_c = L/10, \quad \mathcal{T}_s = 0.01, \quad (6.66d)$$

we get $g \approx 4 \times 10^{-6}$.

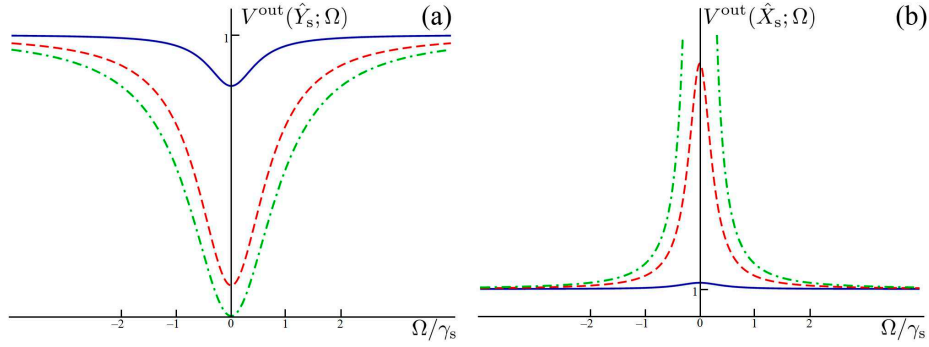


Fig. 6.5: Noise spectrum of the Y (a) and X (b) quadratures of the signal mode as a function of the noise frequency for $\sigma = 0.05$ (blue, solid), 0.5 (red, dashed), and 0.8 (green, dotted-dashed).

with $\mathbf{b}_s(\tau) = \text{col}[b_s(\tau), b_s^+(\tau)]$, $\zeta_s(\tau) = \text{col}[\zeta(\tau), \zeta^+(\tau)]$, being

$$\mathcal{L}_s = \begin{bmatrix} -1 & \sigma \\ \sigma & -1 \end{bmatrix}, \quad (6.72)$$

a symmetric, real matrix with orthonormal eigensystem

$$\left\{ \lambda_{\pm} = -(1 \mp \sigma), \mathbf{v}_{\pm} = \frac{1}{\sqrt{2}} \text{col}(1, \pm 1) \right\}. \quad (6.73)$$

Projecting the linear system onto this eigenvectors and defining the projections $c_{\pm} = \mathbf{v}_{\pm} \cdot \mathbf{b}_s$, we get

$$\dot{c}_j = \lambda_j c_j + g\sqrt{\sigma} \zeta_j(\tau), \quad (6.74)$$

where $\zeta_{\pm}(\tau) = [\zeta(\tau) \pm \zeta^+(\tau)]/\sqrt{2}$ are new independent real noises satisfying the usual statistical properties. This type of one-variable, linear stochastic equations with additive noise will be appearing all along the rest of the thesis, and we have included an appendix (Appendix B) in order to explain how to find their solutions $c_j(\tau)$. We also explain there how to evaluate their associated two-time correlation function $\langle c_j(\tau)c_j(\tau+\tau') \rangle$, which are shown to depend only on $|\tau'|$ in the stationary limit $\tau \gg |\text{Re}\{\lambda_j\}|^{-1}$, and their corresponding spectrum $\tilde{C}_j(\tilde{\Omega}) = \int_{-\infty}^{+\infty} d\tau' \langle c_j(\tau)c_j(\tau+\tau') \rangle_P \exp(-i\tilde{\Omega}\tau')$.

Note that by writing the projections in terms of the fluctuations we get

$$c_+(\tau) = [b_s(\tau) + b_s^+(\tau)]/\sqrt{2} = \delta x_s(\tau)/\sqrt{2}, \quad (6.75a)$$

$$c_-(\tau) = [b_s(\tau) - b_s^+(\tau)]/\sqrt{2} = i\delta y_s(\tau)/\sqrt{2}, \quad (6.75b)$$

and hence the properties of the X and Y quadratures of the signal field are linked to c_{\pm} , respectively. Hence, we can evaluate the noise spectrum of these quadratures as

$$V^{\text{out}}(\hat{X}_s; \Omega) = 1 + \frac{4}{g^2} \tilde{C}_+(\tilde{\Omega}) = \frac{(1+\sigma)^2 + \tilde{\Omega}^2}{(1-\sigma)^2 + \tilde{\Omega}^2}, \quad (6.76a)$$

$$V^{\text{out}}(\hat{Y}_s; \Omega) = 1 - \frac{4}{g^2} \tilde{C}_-(\tilde{\Omega}) = \frac{(1-\sigma)^2 + \tilde{\Omega}^2}{(1+\sigma)^2 + \tilde{\Omega}^2}, \quad (6.76b)$$

where we have made use of the results in Appendix B. These expressions are plotted in Figure 6.5 as a function of the dimensionless noise frequency $\tilde{\Omega}$ for different values of the pump parameter σ . Note first that they predict that the state of the signal modes is a minimum uncertainty state, because

$$V^{\text{out}}(\hat{X}_s; \Omega)V^{\text{out}}(\hat{Y}_s; \Omega) = 1. \quad (6.77)$$

As expected, for $\sigma = 0$ (no injection) $V^{\text{out}}(\Omega) = 1$ for both quadratures, that is, the external modes are in a vacuum state. On the other hand, as σ increases, quantum noise gets reduced in the Y quadrature (and correspondingly increased in the X quadrature), and hence the signal mode is in a squeezed state. Note that maximum squeezing is obtained at zero noise frequency, while at $|\Omega| = (1+\sigma)\gamma_s$ the squeezing level is reduced by a factor two, that is,

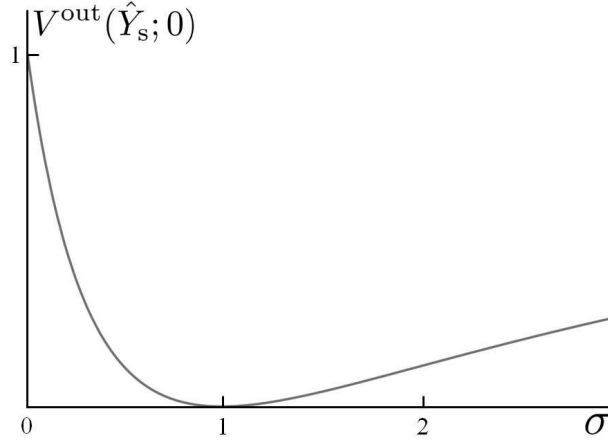


Fig. 6.6: Zero frequency noise spectrum for the Y quadrature of the signal mode as a function of the pump parameter. As explained in the text, the linearized theory predicts perfect squeezing only at threshold.

$S^{\text{out}}[\hat{Y}_s; \pm(1 + \sigma)\gamma_s] = S^{\text{out}}(\hat{Y}_s; 0)/2$; hence, the Lorentzian shape sets a bandwidth to the noise frequencies for which squeezing is obtained (see the end of Section 5.4).

Complete noise reduction is predicted at zero noise frequency exactly at threshold, that is, $V_{\sigma \rightarrow 1}^{\text{out}}(\hat{Y}_s; 0) = 0$ (see Figure 6.6). This is an unphysical result (as stressed in Chapter 2, perfect squeezing requires infinite energy) which shows that the linearization procedure that we have carried breaks down very close to threshold. Indeed, by going further in the perturbative expansion of the Langevin equations, one can show that as the system approaches $\sigma = 1$, the different orders in g kick in, and the noise spectrum becomes finite. In any case, all these contributions are rather small (e.g., $V^{\text{out}}(\hat{Y}_s; 0) = 3g^{4/3}/4$ for $\sigma = 1 - g^{2/3}$ and $\kappa \gg g^{2/3}$), and in practice one can argue as if squeezing would be perfect at threshold [3, 105, 106].

Quantum properties of the DOPO above threshold. We have proved that large levels of squeezing can be obtained in the signal field coming out from the DOPO as we approach its threshold $\sigma = 1$ from below. Now we are going to show that above threshold the situation is similar, that is, squeezing in the signal field decreases as one moves away from threshold.

The situation in this case is, however, much more complicated, because above threshold the stability matrix involves both the pump and the signal modes, and even more, not being symmetric, it does not possess a simple orthonormal eigensystem, though it can be seen to be diagonalizable. In order to avoid all these complications, let us first work in the $\kappa \gg 1$ limit, where the pump can be adiabatically eliminated, as its time scale γ_p^{-1} is much shorter than that of the signal, γ_s^{-1} .

Was (6.52) a simple differential equation, the procedure to adiabatically eliminate the pump variables would be clear: One just sets the corresponding time derivatives to zero, that is,

$$\dot{\beta}_p = 0 \implies \beta_p = \sigma - \beta_s^2/2, \quad (6.78a)$$

$$\dot{\beta}_p^+ = 0 \implies \beta_p^+ = \sigma - \beta_s^{+2}/2, \quad (6.78b)$$

and then substitutes the resulting expressions for the pump variables as a function of the signal variables in the remaining equations, arriving to

$$\dot{\beta}_s = -\beta_s + (\sigma - \beta_s^2/2) \beta_s^+ + g\sqrt{\sigma - \beta_s^2/2}\zeta(\tau) \quad (6.79a)$$

$$\dot{\beta}_s^+ = -\beta_s^+ + (\sigma - \beta_s^{+2}/2) \beta_s + g\sqrt{\sigma - \beta_s^{+2}/2}\zeta^+(\tau). \quad (6.79b)$$

Unfortunately, when dealing with stochastic equations there appears a subtle complication: While the original set of stochastic equations (6.52) is the same either in the Ito or the Stratonovich forms, the resulting equations (6.79) after applying this naïve procedure are not. To see this, just note that the noise matrix associated to these equations is

$$B(\boldsymbol{\alpha}) = g \begin{bmatrix} \sqrt{\sigma - \beta_s^2/2} & 0 \\ 0 & \sqrt{\sigma - \beta_s^{+2}/2} \end{bmatrix}, \quad (6.80)$$

so that the terms which connect the Ito and Stratonovich forms (2.86) read

$$\frac{1}{2} \sum_{lm} B_{lm}(\beta_s) \partial_l B_{\beta_s m}(\beta_s) = \frac{1}{2} B_{\beta_s \beta_s}(\beta_s) \partial_{\beta_s} B_{\beta_s \beta_s}(\beta_s) = -\frac{g^2}{4} \beta_s, \quad (6.81a)$$

$$\frac{1}{2} \sum_{lm} B_{lm}(\beta_s) \partial_l B_{\beta_s^+ m}(\beta_s) = \frac{1}{2} B_{\beta_s^+ \beta_s^+}(\beta_s) \partial_{\beta_s^+} B_{\beta_s^+ \beta_s^+}(\beta_s) = -\frac{g^2}{4} \beta_s^+, \quad (6.81b)$$

which are different from zero. Hence it is fair to ask within which interpretation is this “deterministic” procedure correct, if it is correct at all. Using the techniques explained in [61] to perform the adiabatic elimination in the Fokker–Planck equation (where there are no problems of interpretation), it is possible to show that this procedure is indeed correct within Ito’s interpretation. Hence, the corresponding Stratonovich equations have additional terms in the deterministic part, and in particular they read

$$\dot{\beta}_s = -(1 - g^2/4)\beta_s + (\sigma - \beta_s^2/2)\beta_s^+ + g\sqrt{\sigma - \beta_s^2/2}\zeta(\tau), \quad (6.82a)$$

$$\dot{\beta}_s^+ = -(1 - g^2/4)\beta_s^+ + (\sigma - \beta_s^{+2}/2)\beta_s + g\sqrt{\sigma - \beta_s^{+2}/2}\zeta^+(\tau). \quad (6.82b)$$

Note that the difference between the Ito and Stratonovich forms of the equations is of order g^2 , and then disappears when making the linearization procedure; in particular, the linearized equations read in this case

$$\dot{\mathbf{b}}_s = \mathcal{L}_s \mathbf{b}_s + g\boldsymbol{\zeta}_s(\tau), \quad (6.83)$$

with $\mathbf{b}_s(\tau) = \text{col}[b_s(\tau), b_s^+(\tau)]$, $\boldsymbol{\zeta}_s(\tau) = \text{col}[\zeta(\tau), \zeta^+(\tau)]$, being

$$\mathcal{L}_s = \begin{bmatrix} 1 - 2\sigma & 1 \\ 1 & 1 - 2\sigma \end{bmatrix}, \quad (6.84)$$

a symmetric, real matrix with orthonormal eigensystem

$$\lambda_+ = -2(\sigma - 1), \quad \mathbf{v}_+ = \frac{1}{\sqrt{2}} \text{col}(1, 1), \quad (6.85a)$$

$$\lambda_- = -2\sigma, \quad \mathbf{v}_- = \frac{1}{\sqrt{2}} \text{col}(1, -1). \quad (6.85b)$$

Note also that the eigenvectors are the same as the ones below threshold, and hence they have the same relation to the quadrature fluctuations of the signal modes (7.12). Then, by following the same procedure as before, that is, by projecting the linear system (6.83) onto the eigensystem of \mathcal{L}_s and evaluating the correlation spectrum of the projections $c_{\pm} = \mathbf{v}_{\pm} \cdot \mathbf{b}_s$, it is straightforward to find the following expressions for the noise spectrum of the X and Y quadratures of the signal field

$$V^{\text{out}}(\hat{X}_s; \Omega) = 1 + \frac{1}{(\sigma - 1)^2 + \Omega^2/4}, \quad (6.86a)$$

$$V^{\text{out}}(\hat{Y}_s; \Omega) = 1 - \frac{1}{\sigma^2 + \Omega^2/4}. \quad (6.86b)$$

These have again a Lorentzian shape, and, as already stated at the beginning of the present section, they predict perfect squeezing in the Y quadrature at zero noise frequency only at threshold (as before, the complete noise reduction comes from the linearization, and nonlinear corrections in the g parameter give rise to finite squeezing levels [106]). As σ increases this squeezing is lost (see Figure 6.6), with the particularity that now the state of the signal is no longer a minimum uncertainty state, because

$$V^{\text{out}}(\hat{X}_s; \Omega) V^{\text{out}}(\hat{Y}_s; \Omega) > 1, \quad (6.87)$$

for $\sigma > 1$.

6.3.4 Effect of signal detuning

In the previous sections we have analyzed the classical and quantum behavior of the DOPO when everything is on resonance, that is, the frequency ω_L of the external laser and its second harmonic coincide with the phase-matched cavity resonances ω_0 and $2\omega_0$, the signal and pump frequencies. Here we just want to show the effect that detuning

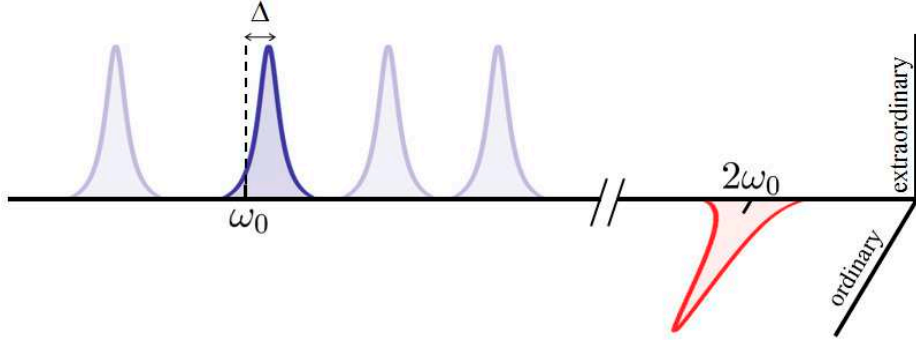


Fig. 6.7: This scheme shows a configuration of the cavity resonances leading to a DOPO with some detuning in the signal field.

has on the different properties of the DOPO by considering the simple scheme shown in Figure 6.7: The signal field does not resonate at frequency ω_0 but at a slightly shifted frequency $\omega_0 + \Delta$. In this conditions one can still drive the pump mode with an external laser at resonance, but then the signal mode will feel a detuning Δ , leading to the following Langevin equations for the system

$$\dot{\beta}_p = \kappa[\sigma - \beta_p - \beta_s^2/2] \quad (6.88a)$$

$$\dot{\beta}_p^+ = \kappa[\sigma - \beta_p^+ - \beta_s^{+2}/2] \quad (6.88b)$$

$$\dot{\beta}_s = -(1 + i\tilde{\Delta})\beta_s + \beta_p\beta_s^+ + g\sqrt{\beta_p}\zeta(\tau) \quad (6.88c)$$

$$\dot{\beta}_s^+ = -(1 - i\tilde{\Delta})\beta_s^+ + \beta_p^+\beta_s + g\sqrt{\beta_p^+}\zeta^+(\tau), \quad (6.88d)$$

where $\tilde{\Delta} = \Delta/\gamma_s$.

The fundamental difference between this case and the resonant one appears at the classical level. Just as before, the classical equations admit two types of stationary solutions, one with the signal field switched off, and one with the signal field switched on. As for the first type, it has exactly the same form as before (6.59), and has an associated stability matrix

$$\mathcal{L} = \begin{bmatrix} -\kappa & 0 & 0 & 0 \\ 0 & -\kappa & 0 & 0 \\ 0 & 0 & -(1 + i\tilde{\Delta}) & \sigma \\ 0 & 0 & \sigma & -(1 - i\tilde{\Delta}) \end{bmatrix}. \quad (6.89)$$

Amongst the eigensystem of this matrix, one can find three negative definite eigenvalues, plus the following one: $\lambda = -1 + \sqrt{\sigma^2 - \tilde{\Delta}^2}$. Hence, this solution becomes unstable when $\sigma > \sqrt{1 + \tilde{\Delta}^2}$. The solution with the signal field switched on is slightly different than before; with the notation $\beta_j = \rho_j \exp(i\varphi_j)$ it is easy to show after some algebra that it is given by

$$\rho_p = \sqrt{1 + \tilde{\Delta}^2}, \quad \sin \varphi_p = \frac{\tilde{\Delta}}{\sigma} \left[1 - (\sigma^2 - \tilde{\Delta}^2)^{-1/2} \right], \quad (6.90a)$$

$$\rho_s^2 = 2 \left(\sqrt{\sigma^2 - \tilde{\Delta}^2} - 1 \right), \quad \varphi_s = (\varphi_p - \psi_\Delta)/2, \quad (6.90b)$$

with $\psi_\Delta = \arctan \tilde{\Delta}$ defined in the interval $[-\pi/2, \pi/2]$. The stability of this solution is much more difficult to analyze than in the previous case; here, however, we are just interested in one simple fact: The solution only exists for $\sigma > \sqrt{1 + \tilde{\Delta}^2}$, which is exactly the point where the previous solution with the signal mode switched off becomes unstable. It is possible to show that indeed this solution is stable in all its domain of existence¹³ [107]. Hence, the only real difference between this case and the resonant one is the fact the threshold is increased to $\sigma = \sqrt{1 + \tilde{\Delta}^2}$, and the pump mode, whose phase was locked to that of the external laser when no detuning was present, gains now a phase that depends on the system parameters—as does the signal mode through the relation (6.90b)—.

¹³ When also the pump mode has some detuning, the situation is much more complicated. One can find regions of the parameter space where two stable solutions coexist at the same time (bistable behavior), or new instabilities where the solution becomes unstable via an eigenvalue with non-zero imaginary part (typical of the so-called Hopf bifurcations) what signals that the new stable solution to be born at that point will be no longer stationary, but time-dependent. The details can be found in [107].

As for the squeezing properties of the signal field, nothing is fundamentally changed: It is simple to show by following the procedure developed in the previous sections that there exists a squeezed quadrature which shows perfect noise reduction exactly at threshold, the squeezing level degrading as one moves away from this point [107]. The only subtlety which appears is that phase of the squeezed quadrature is no longer $\pi/2$, but depends on the σ and $\bar{\Delta}$ parameters [107].

6.4 Entanglement properties of the OPO

We study now the quantum properties of an OPO having distinguishable signal and idler modes (in polarization or/and frequency); from now on we will call OPO (in contrast to DOPO) to any such configuration. To this aim, let us work again with the simplest situation: only a fundamental TEM₀₀ transverse mode is present at the signal and idler resonances, so we are dealing with a so-called *two-mode OPO*.

We will see that, similarly to the DOPO, the OPO is also a threshold system. Quantum properties can then be divided in two classes:

- (i) Below threshold the signal and idler modes are in an EPR-like entangled state. Although below threshold OPOs were studied before (see [99, 108] for example), Reid and Drummond were the first ones to notice that the EPR *gedanken* experiment could actually be implemented with such devices [109, 44, 110]. The first experiment along this line was performed shortly after their proposal [111], and of course confirmed the quantum mechanical predictions.
- (ii) Above threshold the signal and idler modes leak out of the cavity as two bright beams with (ideally) perfectly correlated intensities, usually referred to as *twin beams*. Such intensity correlations between macroscopically occupied beams were first predicted [112] and experimentally observed [113] by Fabre et al. in Paris. Together with the intensity correlations, and in order to preserve the corresponding Heisenberg uncertainty principle, the phase difference between the twin beams is diffusing. In many articles concerning above threshold OPOs such phase diffusion is neglected; its effects on various properties of OPOs were first studied by Lane, Reid, and Walls [114] and by Reid and Drummond [109, 115]. In order to introduce twin beams in simple terms, we will not consider phase diffusion in this chapter; such effect will be treated rigorously in Chapter 8¹⁴.

6.4.1 The OPO within the positive P representation

Let us choose degenerate type II operation, as this is the ideal situation from the experimental viewpoint, because then the signal and idler fields can be analyzed using the same local oscillator field. In any case, the results that we are going to show are independent of the particular type of OPO. The two-mode OPO we are considering deals then with three cavity modes: The pump mode which resonates at frequency $\omega_p = 2\omega_0$ and has ordinary polarization, and the signal and idler modes which resonate at frequency $\omega_s = \omega_i = \omega_0$ and have extraordinary and ordinary polarization, respectively (Figure 6.2b). Every mode is assumed to be in a TEM₀₀ transverse mode. The pump mode is driven by an external, resonant laser beam, while no injection is used for the signal and idler modes, whose associated photons are then generated via spontaneous parametric down-conversion.

Similarly to the degenerate case, we move to the interaction picture defined by the transformation operator

$$\hat{U}_0 = \exp[\hat{H}_0 t / i\hbar] \quad \text{with} \quad \hat{H}_0 = \hbar\omega_L(2\hat{a}_p^\dagger \hat{a}_p + \hat{a}_s^\dagger \hat{a}_s + \hat{a}_i^\dagger \hat{a}_i). \quad (6.91)$$

In this picture, the state $\hat{\rho}$ of the intracavity modes is written as $\hat{\rho}_I = \hat{U}_0^\dagger \hat{\rho} \hat{U}_0$, and satisfies the master equation

$$\frac{d\hat{\rho}_I}{dt} = \left[\chi \hat{a}_p \hat{a}_s^\dagger \hat{a}_i^\dagger + \mathcal{E}_p a_p^\dagger + \text{H.c.}, \hat{\rho}_I \right] + \sum_{j=p,s,i} \gamma_j (2\hat{a}_j \hat{\rho}_I \hat{a}_j^\dagger - \hat{a}_j^\dagger \hat{a}_j \hat{\rho}_I - \hat{\rho}_I \hat{a}_j^\dagger \hat{a}_j), \quad (6.92)$$

where we take $\gamma_s = \gamma_i$, what is a reasonable approximation from the experimental viewpoint. We take \mathcal{E}_p as a positive real as before. Once again, the nonlinear coupling parameter χ is found from (6.1.2) particularized to the configuration that we are treating, which do not write explicitly because no real simplifications are obtained in this case.

¹⁴ Indeed, this phenomenon offers the perfect example of the usefulness of positive P techniques based on the master equation of the system (see Sections 2.6.3 and 4.3), as it cannot be studied by dealing with operator techniques such as that introduced in Section 4.2 because an operator corresponding to the phase of the cavity modes is not available [23, 20].

We use the positive P representation for the density operator, what in this case leads to the stochastic Langevin equations

$$\dot{\alpha}_p = \mathcal{E}_p - \gamma_p \alpha_p - \chi \alpha_s \alpha_i, \quad (6.93a)$$

$$\dot{\alpha}_p^+ = \mathcal{E}_p - \gamma_p \alpha_p^+ - \chi \alpha_s^+ \alpha_i^+, \quad (6.93b)$$

$$\dot{\alpha}_s = -\gamma_s \alpha_s + \chi \alpha_p \alpha_i^+ + \sqrt{\chi \alpha_p} \xi(t), \quad (6.93c)$$

$$\dot{\alpha}_s^+ = -\gamma_s \alpha_s^+ + \chi \alpha_p^+ \alpha_i + \sqrt{\chi \alpha_p^+} \xi^+(t), \quad (6.93d)$$

$$\dot{\alpha}_i = -\gamma_s \alpha_i + \chi \alpha_p \alpha_s^+ + \sqrt{\chi \alpha_p} \xi^*(t), \quad (6.93e)$$

$$\dot{\alpha}_i^+ = -\gamma_s \alpha_i^+ + \chi \alpha_p^+ \alpha_s + \sqrt{\chi \alpha_p^+} [\xi^+(t)]^*, \quad (6.93f)$$

where now $\xi(t)$ and $\xi^+(t)$ are independent complex Gaussian noises with zero mean and non-zero correlations

$$\langle \xi(t), \xi^*(t') \rangle_P = \langle \xi^+(t), [\xi^+(t')]^* \rangle_P = \delta(t - t'). \quad (6.94)$$

Once again, it is easy to show that these equations have the same form both within the Ito and Stratonovich interpretations, and hence we can directly use the usual rules of calculus to analyze them.

In order to simplify the equations, we will make the same variable change as in the DOPO,

$$\tau = \gamma_s t, \quad \beta_m(\tau) = \frac{\chi}{\gamma_s \sqrt{\gamma_p / \gamma_m}} \alpha_m(t), \quad \zeta_m(\tau) = \frac{1}{\sqrt{\gamma_s}} \xi_m(t), \quad (6.95)$$

where with these definitions the new noises $\zeta(\tau)$ and $\zeta^+(\tau)$ satisfy the same statistical properties as $\xi(t)$ and $\xi^+(t)$, but now with respect to the dimensionless time τ . In terms of these normalized variables, the Langevin equations (6.93) read (derivatives with respect to τ are understood)

$$\dot{\beta}_p = \kappa[\sigma - \beta_p - \beta_s \beta_i], \quad (6.96a)$$

$$\dot{\beta}_p^+ = \kappa[\sigma - \beta_p^+ - \beta_s^+ \beta_i^+], \quad (6.96b)$$

$$\dot{\beta}_s = -\beta_s + \beta_p \beta_i^+ + g \sqrt{\beta_p} \zeta(\tau), \quad (6.96c)$$

$$\dot{\beta}_s^+ = -\beta_s^+ + \beta_p^+ \beta_i + g \sqrt{\beta_p^+} \zeta^+(\tau), \quad (6.96d)$$

$$\dot{\beta}_i = -\beta_i + \beta_p \beta_s^+ + g \sqrt{\beta_p} \zeta^*(\tau), \quad (6.96e)$$

$$\dot{\beta}_i^+ = -\beta_i^+ + \beta_p^+ \beta_s + g \sqrt{\beta_p^+} [\zeta^+(\tau)]^*, \quad (6.96f)$$

where the σ , κ , and g parameters have the same definition as before (6.53).

In order to extract information from these equations we will proceed as before, that is, by linearizing them around the classical stable solution.

6.4.2 Classical analysis of the OPO

Using the same procedure as in Section (6.3.2), we retrieve the classical evolution equations of the OPO, which read

$$\dot{\beta}_p = \kappa[\sigma - \beta_p - \beta_s \beta_i], \quad (6.97a)$$

$$\dot{\beta}_s = -\beta_s + \beta_p \beta_i^*, \quad (6.97b)$$

$$\dot{\beta}_i = -\beta_i + \beta_p \beta_s^*. \quad (6.97c)$$

Similarly to (6.57), these equations admit two types of solutions, one with the signal–idler modes switched off, and another with all the modes switched on. Again, the first type exists for all the parameters, but becomes unstable for $\sigma > 1$, while the second type exists only for $\sigma \geq 1$ and is stable in all its domain of existence. Note however, that in this case these equations have the continuous symmetry $\{\beta_s \rightarrow \exp(-i\theta)\beta_s, \beta_i \rightarrow \exp(i\theta)\beta_i\}$, and hence the phase difference between the signal and idler modes is not fixed by the classical equations (a result of paramount importance for the results we derive later).

Explicitly, the stationary solution below threshold is

$$\bar{\beta}_p = \sigma, \quad \bar{\beta}_{s,i} = 0, \quad (6.98)$$

while now the above threshold stationary solution reads

$$\bar{\beta}_p = 1, \quad \bar{\beta}_{s,i} = \sqrt{\sigma - 1} \exp(\mp i\theta), \quad (6.99)$$

being θ arbitrary. The stability of these solutions is easily analyzed following the same steps as in (6.3.2), that is, analyzing the sign of the real part of the eigenvalues of the stability matrix, and leads to the scenario already commented above.

Let us finally discuss one point regarding what we could expect in real experiments. Assume that we operate the OPO above threshold. Bright signal and idler beams are then expected to start oscillating inside the cavity, their relative phase θ chosen randomly according to the particular fluctuations from which the beams are built up. We say then that θ is chosen by *spontaneous symmetry breaking*. In this chapter we assume that after this spontaneous symmetry breaking process, the value of θ remains fixed; in reality, any source of noise (thermal, electronic, etc...) can make it drift. We can assume all the classical sources of noise to be properly stabilized (at least within the time-scale of the experiment), but even then, quantum noise will remain. Nevertheless, for the purposes of this introduction to the properties of OPOs we will neglect this *quantum phase diffusion* phenomenon, which will be properly addressed along the next chapters.

6.4.3 The OPO below threshold: Signal–idler entanglement

Linearizing now the Langevin equations (6.96) around the below threshold classical solution (6.98) we can prove that the quadratures of the signal and idler modes have correlations of the EPR type. In particular, we will prove that for $\sigma > 0$ these modes satisfy

$$V^{\text{out}}[(\hat{X}_s - \hat{X}_i)/\sqrt{2}; \Omega] < 1 \quad \text{and} \quad V^{\text{out}}[(\hat{Y}_s + \hat{Y}_i)/\sqrt{2}; \Omega] < 1, \quad (6.100)$$

which is to be regarded as the generalization of the entanglement criterion (2.38) to the free-space fields leaking out of the cavity. Moreover, we will show that these EPR like correlations become perfect exactly at threshold.

To this aim, let us expand the stochastic amplitudes of the modes as (6.68); it is straightforward to see that the linear evolution of the signal/idler fluctuations is decoupled from the pump fluctuations, and obey the linear system

$$\dot{\mathbf{b}}_{si} = \mathcal{L}_{si} \mathbf{b}_{si} + g\sqrt{\sigma} \zeta_{si}(\tau), \quad (6.101)$$

with

$$\mathbf{b}_{si}(\tau) = \text{col}[b_s(\tau), b_s^+(\tau), b_i(\tau), b_i^+(\tau)], \quad (6.102a)$$

$$\zeta_{si}(\tau) = \text{col}\{\zeta(\tau), \zeta^+(\tau), \zeta^*(\tau), [\zeta^+(\tau)]^*\}, \quad (6.102b)$$

being

$$\mathcal{L}_s = \begin{bmatrix} -1 & 0 & 0 & \sigma \\ 0 & -1 & \sigma & 0 \\ 0 & \sigma & -1 & 0 \\ \sigma & 0 & 0 & -1 \end{bmatrix}, \quad (6.103)$$

a symmetric, real matrix with orthonormal eigensystem

$$\lambda_1 = -1 - \sigma, \quad \mathbf{v}_1 = \frac{1}{2} \text{col}(1, 1, -1, -1), \quad (6.104a)$$

$$\lambda_2 = -1 - \sigma, \quad \mathbf{v}_2 = \frac{1}{2} \text{col}(1, -1, 1, -1), \quad (6.104b)$$

$$\lambda_3 = 1 - \sigma, \quad \mathbf{v}_3 = \frac{1}{2} \text{col}(1, 1, 1, 1), \quad (6.104c)$$

$$\lambda_4 = 1 - \sigma, \quad \mathbf{v}_4 = \frac{1}{2} \text{col}(1, -1, -1, 1). \quad (6.104d)$$

Once again, this linear system is solved by defining the projections $c_j(\tau) = \mathbf{v}_j \cdot \mathbf{b}_{si}(\tau)$, which obey the following simple linear stochastic equation with additive noise

$$\dot{c}_{1,4} = \lambda_{1,4} c_{1,4} + ig\sqrt{\sigma} \zeta_{1,4}(\tau) \quad (6.105a)$$

$$\dot{c}_{2,3} = \lambda_{2,3} c_{2,3} + g\sqrt{\sigma} \zeta_{2,3}(\tau), \quad (6.105b)$$

where the new real noises $\{\zeta_j(\tau)\}_{j=1,2,3,4}$ satisfy the standard statistical properties (2.82); the correlation spectrum associated to each projection can be found then by particularizing the corresponding expression in Appendix B.

In this case, the relation between the quadrature fluctuations of the signal and idler modes, and the projections are easily found to be

$$c_1(\tau) = (\delta x_s - \delta x_i)/2, \quad (6.106a)$$

$$c_2(\tau) = i(\delta y_s + \delta y_i)/2, \quad (6.106b)$$

$$c_3(\tau) = (\delta x_s + \delta x_i)/2, \quad (6.106c)$$

$$c_4(\tau) = i(\delta y_s - \delta y_i)/2, \quad (6.106d)$$

where the normalized quadratures are defined as in (6.55). Hence, we can evaluate the noise spectra of the different combinations of signal–idler quadratures as

$$V^{\text{out}}[(\hat{X}_s - \hat{X}_i)/\sqrt{2}; \Omega] = 1 + \frac{4}{g^2} \tilde{C}_1(\tilde{\Omega}) = \frac{(1 - \sigma)^2 + \tilde{\Omega}^2}{(1 + \sigma)^2 + \tilde{\Omega}^2}, \quad (6.107a)$$

$$V^{\text{out}}[(\hat{Y}_s + \hat{Y}_i)/\sqrt{2}; \Omega] = 1 - \frac{4}{g^2} \tilde{C}_2(\tilde{\Omega}) = \frac{(1 - \sigma)^2 + \tilde{\Omega}^2}{(1 + \sigma)^2 + \tilde{\Omega}^2}, \quad (6.107b)$$

$$V^{\text{out}}[(\hat{X}_s + \hat{X}_i)/\sqrt{2}; \Omega] = 1 + \frac{4}{g^2} \tilde{C}_3(\tilde{\Omega}) = \frac{(1 + \sigma)^2 + \tilde{\Omega}^2}{(1 - \sigma)^2 + \tilde{\Omega}^2}, \quad (6.107c)$$

$$V^{\text{out}}[(\hat{Y}_s - \hat{Y}_i)/\sqrt{2}; \Omega] = 1 - \frac{4}{g^2} \tilde{C}_4(\tilde{\Omega}) = \frac{(1 + \sigma)^2 + \tilde{\Omega}^2}{(1 - \sigma)^2 + \tilde{\Omega}^2}. \quad (6.107d)$$

Note that the two first (last) expressions coincide with the noise spectrum of the squeezed (anti–squeezed) quadrature of the DOPO below threshold, see (6.76). Hence, we have proved exactly what we promised (6.100): Below threshold, the signal and idler fields have correlated X quadratures, and anticorrelated Y quadratures. This correlations become perfect at zero noise frequency when working exactly at threshold. Once again, it can be proved that this is a flaw of the linearization procedure, and nonlinear corrections in the g parameter make them become finite [116].

6.4.4 The OPO above threshold: Twin beams

Consider now the OPO operating above threshold. We are going to prove that the signal and idler beams, which have now a non-zero mean field, have perfectly correlated intensities; they are what we will call twin beams. In Figure 6.8 we show the scheme of a typical experiment designed to look for such intensity correlations. The signal and idler beams are first separated by a polarizing beam splitter, and then measured with independent photodetectors; the corresponding electric signals are then subtracted, and the power spectrum of this *difference photocurrent* is finally analyzed.

Using the approach that we developed in Section 5.3, it is not difficult to show that, similarly to the homodyne detection spectrum (5.46), in this case the power spectrum of the difference photocurrent is also formed by a shot noise contribution, plus a part which depends on the state of the system (and goes to zero for vacuum or coherent states). In particular, assuming the state of the system to be stationary, one easily gets

$$\frac{P_D(\Omega)}{P_{\text{shot}}} = 1 + \frac{1}{\langle \hat{n}_{s,\text{out}} \rangle + \langle \hat{n}_{i,\text{out}} \rangle} \int_{-\infty}^{+\infty} dt' \langle : \delta \hat{n}_{D,\text{out}}(t) \delta \hat{n}_{D,\text{out}}(t+t') : \rangle e^{-i\Omega t'}, \quad (6.108)$$

where we have defined the number–difference operator

$$\hat{n}_{D,\text{out}} = \hat{n}_{s,\text{out}} - \hat{n}_{i,\text{out}}. \quad (6.109)$$

We can rewrite this expression in terms of intracavity operators by using relations (5.22). After doing this, and given that all the expectation values are in normal order, we can directly use the positive P representation to evaluate them, just as we did in the previous sections. Taking also into account the definition of the normalized variables (6.95), this leads to

$$\frac{P_D(\Omega)}{P_{\text{shot}}} = 1 + \frac{2}{g^2(\langle n_s \rangle + \langle n_i \rangle)} \int_{-\infty}^{+\infty} dt' \langle \delta n_D(t) \delta n_D(t+t') \rangle_P e^{-i\Omega t'}, \quad (6.110)$$

where we have defined the normalized versions of the different operators within the positive P representation:

$$n_s = \beta_s^+ \beta_s, \quad n_i = \beta_i^+ \beta_i, \quad \text{and} \quad n_D = \beta_s^+ \beta_s - \beta_i^+ \beta_i. \quad (6.111)$$

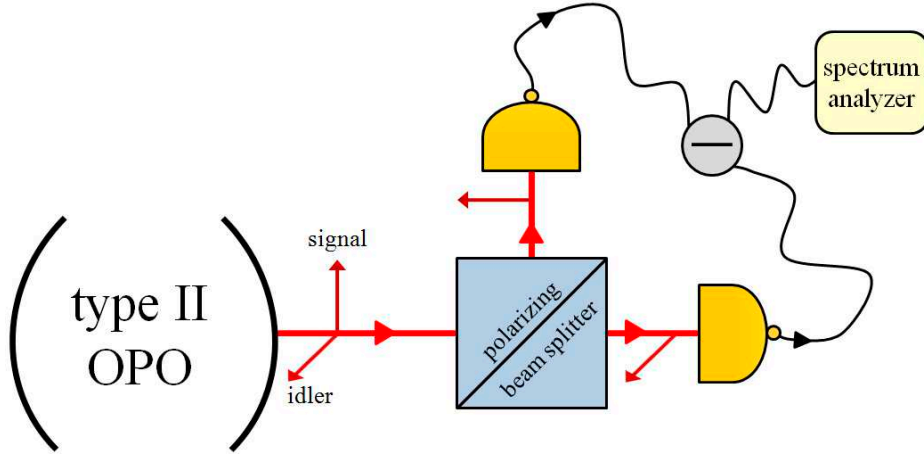


Fig. 6.8: Detection scheme designed for the observation of the intensity correlations between the signal and idler beams coming out from a type II OPO above threshold.

The last manipulation that we need is to consider the linearized version of this expression. To this aim, we can expand the coherent amplitudes as usual (6.68), that is, as some quantum fluctuations around the classical stationary solution (6.99), and then expand the spectrum (6.110) up to the lowest order in the fluctuations. The final result is actually very intuitive:

$$\frac{P_D(\Omega)}{P_{\text{shot}}} = V^{\text{out}}[(\hat{X}_s^{-\theta} - \hat{X}_i^\theta)/\sqrt{2}; \Omega], \quad (6.112)$$

that is, the linearized version of the spectrum (6.108) corresponds to the noise spectrum of the difference between the amplitude quadratures of the signal and idler modes. This result comes from the fact that the linearized version of the number–difference fluctuations itself is proportional to such quadrature–difference fluctuations, that is,

$$\delta n_D \simeq \bar{\beta}_s^* b_s + \bar{\beta}_s b_s^+ - \bar{\beta}_i^* b_i - \bar{\beta}_i b_i^+ = \sqrt{\sigma - 1}(\delta x_s^{-\theta} - \delta x_i^\theta); \quad (6.113)$$

this actually makes sense, as we already saw in Chapter 2 that the number and phase fluctuations of the harmonic oscillator are related to the fluctuations of its amplitude and phase quadratures, provided that the mean value of the oscillator’s amplitude is large enough (large enough σ in this case).

Hence, proving that the joint quadrature $(\hat{X}_s^{-\theta} - \hat{X}_i^\theta)/\sqrt{2}$ is squeezed is equivalent to proving intensity correlations. To do so we follow the procedure of the previous sections. First, we write the linear system obeyed by the quantum fluctuations, which for the above threshold OPO reads

$$\dot{\mathbf{b}} = \mathcal{L}\mathbf{b} + g\zeta(\tau), \quad (6.114)$$

where $\mathbf{b} = \text{col}(b_p, b_p^+, b_s, b_s^+, b_i, b_i^+)$, $\zeta(\tau) = \text{col}\{0, 0, \zeta(\tau), \zeta^+(\tau), \zeta^*(\tau), [\zeta^+(\tau)]^*\}$, and the linear stability matrix reads in this case

$$\mathcal{L} = \begin{bmatrix} -\kappa & 0 & -\kappa\rho e^{i\theta} & 0 & -\kappa\rho e^{-i\theta} & 0 \\ 0 & -\kappa & 0 & -\kappa\rho e^{-i\theta} & 0 & -\kappa\rho e^{i\theta} \\ \rho e^{-i\theta} & 0 & -1 & 0 & 0 & 1 \\ 0 & \rho e^{i\theta} & 0 & -1 & 1 & 0 \\ \rho e^{i\theta} & 0 & 0 & 1 & -1 & 0 \\ 0 & \rho e^{-i\theta} & 1 & 0 & 0 & -1 \end{bmatrix}, \quad (6.115)$$

where $\rho = \sqrt{\sigma - 1}$. Even though this matrix is not Hermitian, it is simple to check that the vector

$$\mathbf{v} = \frac{1}{2} \text{col}(0, 0, e^{-i\theta}, e^{i\theta}, -e^{i\theta}, -e^{-i\theta}), \quad (6.116)$$

is an eigenvector of it with eigenvalue $\lambda = -2$ irrespective of the system parameters, that is, $\mathbf{v}^* \mathcal{L} = -2\mathbf{v}^*$. On the other hand, the projection of the fluctuations \mathbf{b} onto this eigenvector is

$$c(\tau) = \mathbf{v}^* \cdot \mathbf{b}(\tau) = [\delta x_s^{-\theta}(\tau) - \delta x_i^\theta(\tau)]/2; \quad (6.117)$$

then, by projecting the linear system (6.114) onto \mathbf{v} we get the evolution equation for this projection, which reads

$$\dot{c} = -2c + i\eta(t), \quad (6.118)$$

where $\eta(t)$ is a real noise which satisfies the usual statistics (2.82). As usual this is a linear stochastic equation with additive noise, see Appendix B. Hence, the noise spectrum we are looking for can be finally written as

$$V^{\text{out}}[(\hat{X}_s^{-\theta} - \hat{X}_i^{\theta})/\sqrt{2}; \Omega] = 1 + \frac{4}{g^2} \tilde{C}(\tilde{\Omega}) = \frac{\tilde{\Omega}^2}{4 + \tilde{\Omega}^2}, \quad (6.119)$$

where once again we have used the results of Appendix B for the correlation spectrum of $c(\tau)$.

As stated, the signal and idler modes have perfect amplitude quadrature correlations above threshold (for any value of the system parameters) and at zero noise frequency, what is equivalent to perfect intensity correlations as explained above. The shape of the spectrum is the usual Lorentzian that we have found for all the previous perfectly squeezed quadratures; however, as we show in Section ..., in this case this shape is not an unrealistic artifact of the linearization: the intensities (or amplitude quadratures) of the generated twin beams can be indeed perfectly correlated.

Let us finally remark that the vector (6.116) is not the only one with a definite eigenvalue in all parameter space; it is simple to check that the vector

$$\mathbf{v}_0 = \frac{i}{2} \text{col}(0, 0, e^{-i\theta}, -e^{i\theta}, -e^{i\theta}, e^{-i\theta}), \quad (6.120)$$

satisfies $\mathbf{v}_0^* \mathcal{L} = 0$, and hence has zero eigenvalue. This zero eigenvalue is an indicator that there is a direction of phase space along which quantum noise can act freely. It is actually easy to realize which is the corresponding variable of the system affected by this undamped quantum noise; one just needs to evaluate the projection of the quantum fluctuations \mathbf{b} onto \mathbf{v}_0 , what leads to

$$c_0(\tau) = \mathbf{v}_0^* \cdot \mathbf{b}(\tau) = [\delta y_s^{-\theta}(\tau) - \delta y_i^{\theta}(\tau)]/2, \quad (6.121)$$

that is, the difference between the phase quadratures of the signal and idler modes is the variable we are looking for. In other words, as within the linearized description the fluctuations of the phase quadrature are related to the fluctuations of the actual phase of the mode, the phase difference θ that we have taken as a fixed quantity of the above threshold solution, is actually dynamical, it should diffuse with time owed to quantum noise (as already advanced above). Fortunately, it can be proved that adding this phase diffusion doesn't change the results we have shown concerning intensity correlations [114]; it however affects other aspects of above threshold OPOs that we haven't tackled in this introduction, and we will need to treat the phase diffusion in depth in the next chapters.

7. BASIC PHENOMENA IN MULTI-MODE OPTICAL PARAMETRIC OSCILLATORS

In the previous chapter we developed the quantum model of an optical parametric oscillator, showing that it is a threshold system capable of generating squeezed and entangled states of light. In order to prove so, we simplified the system as much as possible, particularly assuming that only a single three-wave mixing process is selected, that is, that pump photons can only be “broken” into one particular signal-idler pair (an extraordinary, frequency degenerate, TEM₀₀ pair of photons in the case of the DOPO, for example). This is however not general enough, as pump photons may have many different “decay channels”. We will call *multi-mode OPOs* to such OPOs in which pump photons have not a single decay channel.

The first type of multi-mode OPOs that were ever studied were DOPOs in which several transverse modes could resonate at the signal frequency, just as we allowed in the derivation of the three-wave mixing Hamiltonian in Section 6.2. In this case, the different decay channels available for the pump photons correspond to opposite orbital angular momentum signal-idler pairs, as can be appreciated in expression (6.42). The study of these *spatial multi-mode OPOs* was first motivated either by the desire to understand the spatial correlations of the signal beam [117, 118, 119], to model real experiments [120], or to describe quantum mechanically the phenomenon of pattern formation [121]. Shortly after these preliminary studies, Lugiato and collaborators [122, 123, 124, 125] came to realize that the phenomenology appearing in this system was far more rich than that of their single-mode counterpart, and their seminal ideas gave rise to the field of *quantum imaging*.

A different type of multi-mode OPOs are the so-called *temporal multi-mode OPOs*. In order to understand which are the different decay channels in this case, let us consider the following example. Assume that the OPO is tuned so that the frequency degenerate type I process (Figure 6.2a) is the one with optimal phase matching, that is $c\Delta k_{\text{D-I}} = 2\omega_0 [n_o(2\omega_0) - n_e(\omega_0)] = 0$. We can evaluate the *phase mismatch* associated to the nondegenerate process (Figure 6.2c) as

$$c\Delta k_{\text{ND-I}} = 2\omega_0 n_o(2\omega_0) - (\omega_0 + \Omega)n_e(\omega_0 + \Omega) - (\omega_0 - \Omega)n_e(\omega_0 - \Omega) \simeq -2\Omega^2 \left. \frac{dn_e}{d\omega} \right|_{\omega=\omega_0}, \quad (7.1)$$

where we have assumed $\Omega \ll \omega_0$ and made a series expansion of the refractive indices around $\omega = \omega_0$. It is not difficult to show that for typical values of the dispersion $dn_e/d\omega|_{\omega=\omega_0}$ and taking into account that Ω can be of the order of the free spectral range of the cavity, $\Delta k_{\text{ND-I}}^{-1}$ is usually much larger than the typical lengths of nonlinear crystals. In other words, even though not optimally, the phase matching condition $\Delta k_{\text{ND-I}} \ll l_c^{-1}$ can still be satisfied by nondegenerate processes, and hence pump photons have many decay channels open: The degenerate and all the nondegenerate ones allowed by energy and momentum (phase-matching) conservation. Even though temporal multi-mode parametric down-conversion was studied in free space a long time ago [126, 127, 128], it wasn't until a few years ago that these kind of processes were considered in cavity systems [129, 130, 131].

This thesis is devoted to the study of multi-mode OPOs. Throughout the rest of the thesis we will show that both their quantum and classical properties can be understood in terms of two basic phenomena: *pump clamping* and *spontaneous symmetry breaking*. In this Chapter we shall introduce these two phenomena in a general, intuitive way by making use of simple examples.

7.1 Pump clamping as a resource for noncritically squeezed light

In this section we would like to introduce the phenomenon of pump clamping which was first predicted in [29].

7.1.1 Introducing the phenomenon through the simplest model

In order to introduce the phenomenon of pump clamping we will consider the most simple multi-mode scenario: Pump photons can decay through two degenerate type I channels. As we will argue at the end, the results are trivially generalized to any other combination of decay channels. Hence, consider three intracavity modes: The pump mode,

with annihilation operator denoted by \hat{a}_0 , and two signal modes whose annihilation operators we denote by \hat{a}_1 and \hat{a}_2 ; these are connected via the Hamiltonian

$$\hat{H}_c = i\hbar(\chi_1\hat{a}_0\hat{a}_1^{\dagger 2} + \chi_2\hat{a}_0\hat{a}_2^{\dagger 2}) + \text{H.c.} \quad (7.2)$$

The dependence of the coupling parameters χ_j on the system parameters depends on the particular processes underlying this basic scheme¹; we will assume here that $\chi_1 > \chi_2$ for definiteness, that is, that the decay channel corresponding to mode 1 is favoured. Moreover, we will assume that the decay rates for the signal modes are the same, that is, $\gamma_1 = \gamma_2 = \gamma_s$, and that the system is pumped by the external laser exactly at resonance. Working in the interaction picture defined in the previous chapter, and scaling the variables as we did there (see Section 6.3.1), it is simple to show that the positive P Langevin equations associated to this system read

$$\dot{\beta}_0 = \kappa[\sigma - \beta_0 - \beta_1^2/2 - r\beta_2^2/2], \quad (7.3a)$$

$$\dot{\beta}_0^+ = \kappa[\sigma - \beta_0^+ - \beta_1^{+2}/2 - r\beta_2^{+2}/2], \quad (7.3b)$$

$$\dot{\beta}_1 = -\beta_1 + \beta_0\beta_1^+ + g\sqrt{\beta_0}\zeta_1(\tau), \quad (7.3c)$$

$$\dot{\beta}_1^+ = -\beta_1^+ + \beta_0^+\beta_1 + g\sqrt{\beta_0^+}\zeta_1^+(\tau), \quad (7.3d)$$

$$\dot{\beta}_2 = -\beta_2 + r\beta_0\beta_2^+ + g\sqrt{r\beta_0}\zeta_2(\tau), \quad (7.3e)$$

$$\dot{\beta}_2^+ = -\beta_2^+ + r\beta_0^+\beta_2 + g\sqrt{r\beta_0^+}\zeta_2^+(\tau), \quad (7.3f)$$

where we have defined the parameter $r = \chi_2/\chi_1 < 1$, and all the noises are real, independent, and satisfy the usual statistical properties (2.82).

Classical emission

Let's first analyze the classical emission properties of the system. In particular, let us study its classical stationary solutions. As we argued in Section 6.3.2, the classical equations corresponding to the Langevin equations (7.3) are

$$\dot{\beta}_0 = \kappa[\sigma - \beta_0 - \beta_1^2/2 - r\beta_2^2/2], \quad (7.4a)$$

$$\dot{\beta}_1 = -\beta_1 + \beta_0\beta_1^*, \quad (7.4b)$$

$$\dot{\beta}_2 = -\beta_2 + r\beta_0\beta_2^*. \quad (7.4c)$$

Just as the single-mode DOPO, these equations possess a stationary solution with the signal modes switched off which is given by

$$\bar{\beta}_0 = \sigma, \quad \beta_1 = \beta_2 = 0. \quad (7.5)$$

On the other hand, the first particularity that we can see in this case is that a stationary solution with the modes 1 and 2 switched on at the same time does not exist, as it would imply $|\bar{\beta}_0| = 1$ and $|\bar{\beta}_0| = r$ simultaneously, what is not possible (the pump amplitude cannot take two different values at the same time!). Hence, we are left with two different stationary solutions, one given by

$$\bar{\beta}_0 = 1, \quad \bar{\beta}_1 = \sqrt{2(\sigma - 1)}, \quad \bar{\beta}_2 = 0, \quad (7.6)$$

which has the second mode switched off, and another given by

$$\bar{\beta}_0 = r^{-1}, \quad \bar{\beta}_2 = \sqrt{2(\sigma - r^{-1})}, \quad \bar{\beta}_1 = 0, \quad (7.7)$$

which has the first mode switched off. Note that these solutions have thresholds located at $\sigma = 1$ and $\sigma = r^{-1} > 1$, respectively, and hence the lower threshold corresponds to the solution with mode 1 switched on.

On the other hand, the stability matrix associated to equations (7.4) is given by

$$\mathcal{L} = \begin{bmatrix} -\kappa & 0 & -\kappa\bar{\beta}_1 & 0 & -\kappa r\bar{\beta}_2 & 0 \\ 0 & -\kappa & 0 & -\kappa\bar{\beta}_1^* & 0 & -\kappa r\bar{\beta}_2^* \\ \bar{\beta}_1^* & 0 & -1 & \bar{\beta}_0 & 0 & 0 \\ 0 & \bar{\beta}_1 & \bar{\beta}_0^* & -1 & 0 & 0 \\ r\bar{\beta}_2^* & 0 & 0 & 0 & -1 & r\bar{\beta}_0 \\ 0 & r\bar{\beta}_2 & 0 & 0 & r\bar{\beta}_0^* & -1 \end{bmatrix}. \quad (7.8)$$

¹ For example, if the cavity is confocal, so that even and odd families are spectrally separated by half the free spectral range inside the cavity, we could assume that the even families resonate at the signal frequency, and modes 1 and 2 would correspond then to the $L_{00}(k_s; \mathbf{r}_\perp, z)$ and the $L_{10}(k_s; \mathbf{r}_\perp, z)$ transverse modes, as long as we could forget about the rest of the transverse modes.

It is then trivial to show that the eigenvalues of this matrix particularized to the trivial solution (7.5) are all real and negative except for the following two: $\lambda_1 = -1 + \sigma$ and $\lambda_2 = -1 + r\sigma$. Hence, for $\sigma > 1$ this solution becomes unstable, just as expected from the previous chapter: (7.5) is the so-called below threshold solution. Similarly, it is very simple to check that all the eigenvalues of \mathcal{L} particularized to the solution (7.6) have negative real part for $\sigma > 1$, and hence, this solution is stable in all its domain of existence. Finally, it is straightforward to find that the solution (7.7) is always unstable, as \mathcal{L} has in this case the eigenvalue $\lambda = -1 + r^{-1}$ which is always positive.

Hence, we arrive to the conclusion that only one of the two modes can be switched on by increasing the external pump injection, the one with the largest coupling to the pump mode. In other words, the nonlinear competition is won by the mode with the lowest threshold. Indeed, there is a simple physical explanation for this. The fluctuations of the signal modes are not fed directly through the injection parameter σ , but through the pump amplitude $\bar{\beta}_0$, as can be appreciated in (7.4b,7.4c). Now, once we get to $\sigma = 1$ —the threshold of mode 1— the pump mode gets clamped to $\bar{\beta}_0 = 1$ no matter how much we increase σ (all the remaining pump injection is used to make the signal mode oscillate). Hence, as mode 2 feels changes in the system only through the pump mode, it will feel as if the system is frozen to $\sigma = 1$, no matter how much we increase the actual σ . Hence, the instability point leading to its activation, which requires $\bar{\beta}_0 = r^{-1}$, cannot be reached, and hence it will stay switched off forever.

Quantum properties

Classically, the pump mode and mode 1 behave, respectively, as the pump and signal modes of the single-mode DOPO (see Section 6.3.2). Following the analysis of Section 6.3.3, it is straightforward to show that the quantum properties of these modes are also just like those that we found for the single-mode DOPO, that is, the pump mode is always in a coherent state, while mode 1 is squeezed only when working near to the threshold $\sigma = 1$. Hence we focus on the quantum properties of the non-amplified mode, which is indeed the one showing the new phenomenon appearing in the multi-mode case: No matter how much we increase σ , from the point of view of mode 2 the system is frozen to its state at $\sigma = 1$. As we are about to see, this is a very interesting effect from the quantum point of view.

In order to study the quantum properties of mode 2, we use the linearization procedure that we introduced in the previous chapter, that is, we expand all the stochastic amplitudes as $\beta_j(\tau) = \bar{\beta}_j + b_j(\tau)$ and $\beta_j^+(\tau) = \bar{\beta}_j^* + b_j^+(\tau)$, and assume that the b 's are order g quantities. Then, given that $\bar{\beta}_2 = 0$ irrespective of the system parameters, the stability matrix (7.8) shows that the fluctuations of mode 2 get decoupled from the rest of the modes; in particular, and taking into account that $\bar{\beta}_0$ is real and positive for all the system parameters, they satisfy the linear system

$$\dot{\mathbf{b}}_2 = \mathcal{L}_2 \mathbf{b}_2 + g\sqrt{r\bar{\beta}_0} \boldsymbol{\zeta}_2(\tau), \quad (7.9)$$

with $\mathbf{b}_2(\tau) = \text{col}[b_2(\tau), b_2^+(\tau)]$, $\boldsymbol{\zeta}_2(\tau) = \text{col}[\zeta_2(\tau), \zeta_2^+(\tau)]$, being

$$\mathcal{L}_2 = \begin{bmatrix} -1 & r\bar{\beta}_0 \\ r\bar{\beta}_0 & -1 \end{bmatrix}, \quad (7.10)$$

a real, symmetric matrix with orthonormal eigensystem

$$\left\{ \lambda_{\pm} = -(1 \mp r\bar{\beta}_0), \mathbf{v}_{\pm} = \frac{1}{\sqrt{2}} \text{col}(1, \pm 1) \right\}. \quad (7.11)$$

Note that, as commented, the evolution of the fluctuations of mode 2 does not depend directly on σ , but on the stationary value of the pump mode $\bar{\beta}_0$. Also, note that the eigenvectors \mathbf{v}_{\pm} are exactly the same as those which appeared in the single-mode DOPO below threshold (6.73), and hence the projections $c_{\pm} = \mathbf{v}_{\pm} \cdot \mathbf{b}_2$ are related to the quadratures of mode 2 by

$$c_+(\tau) = [b_2(\tau) + b_2^+(\tau)] / \sqrt{2} = \delta x_2(\tau) / \sqrt{2}, \quad (7.12a)$$

$$c_-(\tau) = [b_2(\tau) - b_2^+(\tau)] / \sqrt{2} = i\delta y_2(\tau) / \sqrt{2}, \quad (7.12b)$$

so that the noise spectrum of the X and Y quadratures of mode 2 can be evaluated as

$$V^{\text{out}}(\hat{X}_2; \Omega) = 1 + \frac{4}{g^2} \tilde{C}_+(\tilde{\Omega}), \quad (7.13a)$$

$$V^{\text{out}}(\hat{Y}_2; \Omega) = 1 - \frac{4}{g^2} \tilde{C}_-(\tilde{\Omega}). \quad (7.13b)$$

On the other hand, projecting the linear system (7.9) onto the eigenvectors \mathbf{v}_\pm we get the following evolution equations for the projections:

$$\dot{c}_j = \lambda_j c_j + g\sqrt{r\bar{\beta}_0}\zeta_j(\tau), \quad (7.14)$$

where $\zeta_\pm(\tau) = [\zeta_2(\tau) \pm \zeta_2^+(\tau)]/\sqrt{2}$ are new independent real noises satisfying the usual statistical properties. The general treatment of this type of equations can be found in Appendix B. Taking in particular the expression of their associated correlation spectrum (B.6), we can finally write

$$V^{\text{out}}(\hat{X}_2; \Omega) = \frac{(1+r\bar{\beta}_0)^2 + \tilde{\Omega}^2}{(1-r\bar{\beta}_0)^2 + \tilde{\Omega}^2}, \quad (7.15a)$$

$$V^{\text{out}}(\hat{Y}_2; \Omega) = \frac{(1-r\bar{\beta}_0)^2 + \tilde{\Omega}^2}{(1+r\bar{\beta}_0)^2 + \tilde{\Omega}^2}. \quad (7.15b)$$

Note first that mode 2 is in a minimum uncertainty state as

$$V^{\text{out}}(\hat{X}_2; \Omega)V^{\text{out}}(\hat{Y}_2; \Omega) = 1 \quad (7.16)$$

. On the other hand, for $\sigma < 1$ we have $\bar{\beta}_0 = \sigma$, while for $\sigma > 1$ the pump mode is clamped to $\bar{\beta}_0 = 1$. Hence, as σ increases, quantum noise gets reduced in the Y quadrature (and correspondingly increased in the X quadrature), so that mode 2 is in a squeezed state. Maximum squeezing is obtained at zero noise frequency and for $\sigma > 1$, where we have

$$V^{\text{out}}(\hat{Y}_2; 0) = (1-r)^2/(1+r)^2 < 1. \quad (7.17)$$

The interesting feature about this squeezing is that, owed to the fact that the system is frozen from the point of view of mode 2, it is independent of the system parameters (above threshold), a reason why we call it *noncritical squeezing*; this is in contrast to the squeezing appearing in the single-mode DOPO, which needs a fine tuning of the system parameters, in particular to the instability point $\sigma = 1$. It is interesting to note that the squeezing levels predicted by (7.17) are above 90% as long as $r < 0.5$; this is actually very good news, as it means that even if mode 2 has its threshold two times above the threshold of mode 1, it will still be highly squeezed.

7.1.2 Generalization to many down-conversion channels: The OPO output as a multi-mode non-classical field

The results we have just found for the simple situation of having two degenerate type I decay channels are trivially generalized to an arbitrary number of decay channels of any kind.

The idea is that when pumped at frequency $2\omega_0$, the OPO can have many available down-conversion channels (corresponding to degenerate or non-degenerate, type I or type II processes, and even channels having some detuning), but one of them will have the lowest threshold, say $\sigma = \sigma_0$. Classically, this channel, and only this, is the one that will be amplified above threshold, while the rest of the channels will remain switched off irrespective of the injection σ .

As for the quantum properties, from the point of view of the non-amplified channels the OPO will stay frozen at an injection parameter $\sigma = \sigma_0$, and they will show the levels of squeezing or entanglement predicted for that parameter. In particular, all the channels with indistinguishable (distinguishable) signal and idler modes will show squeezing (entanglement), the level of which will depend on the distance between σ_0 and their corresponding thresholds.

Hence, we predict that a general OPO with a single pump will emit an intrinsically non-classical field formed by a superposition of various squeezed or entangled vacua plus the bright amplified mode above threshold. This prediction was first introduced in [29] and it has been checked experimentally very recently [132].

7.2 Noncritically squeezed light via spontaneous symmetry breaking

We introduce now the phenomenon of noncritically squeezed light generation through spontaneous symmetry breaking, which will occupy indeed most of the original research to be found in this thesis.

7.2.1 The basic idea

The idea behind this phenomenon can be put in an abstract way as follows. Suppose that we work with an OPO which is invariant under changes of some continuous degree of freedom of the down-converted field, say ϵ , which we might call *free parameter* (FP) in the following (we already found an example of such system, the frequency degenerate type II OPO, in which the phase difference between signal and idler was a symmetry of the system). Above threshold the classical or mean field value of the down-converted field, say $\bar{\mathbf{E}}_\epsilon(\mathbf{r}, t)$ —we explicitly introduce the FP in the field—, is

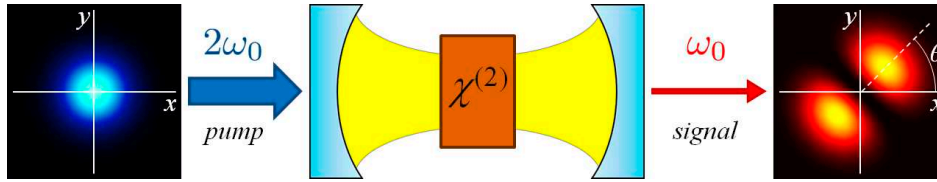


Fig. 7.1: Schematic representation of a DOPO tuned to the first family of transverse modes at the signal frequency. When pumped above threshold it emits a TEM_{10} mode whose orientation θ respect to the x axis is arbitrary. This is one of the simplest examples of spontaneous symmetry breaking, and it is actually the one that we will be using to study this phenomenon in depth.

not zero, and when the OPO starts emitting it, a particular value of the FP is chosen through spontaneous symmetry breaking, as commented in Section 6.4.2.

Let's think now about what quantum theory might introduce to this classical scenario. First, as variations of the FP do not affect the system, quantum fluctuations can be expected to make it fluctuate without opposition, eventually making it become completely undetermined. Then, invoking now the uncertainty principle, the complete indetermination of a system's variable allows for the perfect determination of its corresponding momentum, meaning this that we could expect perfect squeezing in the quadrature selected by the local oscillator $-i\partial_\epsilon \bar{\mathbf{E}}_\epsilon(\mathbf{r}, t)$ in an homodyne detection scheme.

The first proof of such an intuitive reasoning was offered through the study of a DOPO with plane mirrors [30, 31], where transverse patterns as well as cavity solitons have been predicted to appear above threshold [133, 134, 135, 136, 137, 138], hence breaking the translational symmetry of the system. The main difficulty of this model was that it is not too close to current experimental setups and such transverse structures have not even been observed yet in DOPOs. This was one of the main motivations to study the phenomenon with a simpler, more realistic system, consisting on a DOPO with spherical mirrors tuned to the first family of transverse modes at the subharmonic [32, 33] (see Figure 7.1). We will introduce in this section the phenomenon through this example, which was actually the first original work originated from this thesis [32]; we will show that it is the rotational symmetry in the transverse plane the one which is broken in this case, a symmetry that was also exploited later in another type of nonlinear cavities which make use of $\chi^{(3)}$ nonlinearities [34].

The phenomenon can be extended to systems in which the FP is not a spatial degree of freedom in the transverse plane. The first of such generalizations was made in [35], where the FP was a polarization degree of freedom of a degenerate type II OPO. This case will be properly addressed in Chapter 10. Continuing with a generalization to different symmetries, in the outlook section of the concluding chapter we will propose a new scheme in which the FP is associated to a temporal degree of freedom, hence closing the types of symmetries that the electromagnetic field has to offer.

7.2.2 The two-transverse-mode DOPO and spontaneous rotational symmetry breaking

The two-transverse-mode DOPO model

In order to introduce the phenomenon of squeezing induced by spontaneous symmetry breaking we consider a DOPO tuned to the first family of transverse modes at the signal frequency²; the DOPO is pumped by a TEM_{00} beam resonant with the pump mode, that is, $\omega_L = 2\omega_0$ in the nomenclature of the previous chapters. We would like to remind that the first family of transverse modes contains the Laguerre-Gauss modes $L_{0,\pm 1}(k_s; \mathbf{r}_\perp, z)$ which is the reason why we will call *two-transverse-mode DOPO* (2tmDOPO) to this system. Most of this thesis has been devoted to study several aspects of this system [32, 33, 36], as we have used it as a playground where analyzing spontaneous symmetry breaking at the quantum level.

Let us denote by \hat{a}_0 the annihilation operator for the pump mode, and by $\hat{a}_{\pm 1}$ the ones associated to the $L_{0,\pm 1}(k_s; \mathbf{r}_\perp, z)$ signal modes. Instead of using the Laguerre-Gauss basis, we can work in the most usual TEM_{mn} basis. Denoting by $H_{10}^\psi(k_s; \mathbf{r}_\perp, z)$ a TEM_{10} mode rotated an angle ψ with respect to the x axis and by $H_{01}^\psi(k_s; \mathbf{r}_\perp, z)$

² See [139, 140, 132] for related experimental configurations.

to its orthogonal, these are given by

$$H_{10}^\psi(k_s; \mathbf{r}_\perp, z) = \frac{1}{\sqrt{2}} [e^{-i\psi} L_{0,+1}(k_s; \mathbf{r}_\perp, z) + e^{i\psi} L_{0,-1}(k_s; \mathbf{r}_\perp, z)] = \sqrt{2} |L_{0,\pm 1}(k_s; \mathbf{r}_\perp, z)| \cos(\phi - \psi), \quad (7.18a)$$

$$H_{01}^\psi(k_s; \mathbf{r}_\perp, z) = \frac{1}{\sqrt{2i}} [e^{-i\psi} L_{0,+1}(k_s; \mathbf{r}_\perp, z) - e^{i\psi} L_{0,-1}(k_s; \mathbf{r}_\perp, z)] = \sqrt{2} |L_{0,\pm 1}(k_s; \mathbf{r}_\perp, z)| \sin(\phi - \psi). \quad (7.18b)$$

These relations can be inverted as

$$L_{0,\pm 1}(k_s; \mathbf{r}_\perp, z) = \frac{1}{\sqrt{2}} e^{\pm i\psi} [H_{10}^\psi(k_s; \mathbf{r}_\perp, z) \pm i H_{01}^\psi(k_s; \mathbf{r}_\perp, z)]. \quad (7.19)$$

The part of the signal field propagating along $+\mathbf{e}_z$ can be written as (Schrödinger picture is understood)

$$\hat{\mathbf{E}}_{s,\rightarrow}^{(+)}(\mathbf{r}) = i \sqrt{\frac{\hbar \omega_s}{4 \varepsilon_0 n_s L_s}} \mathbf{e}_e [\hat{a}_{+1} L_{0,+1}(k_s; \mathbf{r}_\perp, z) + \hat{a}_{-1} L_{0,-1}(k_s; \mathbf{r}_\perp, z)] e^{i n_s k_s z}, \quad (7.20)$$

Introducing the relation (7.19) between the Laguerre–Gauss and the Hermite–Gauss modes in this expression, we find the relation between their corresponding annihilation operators:

$$\hat{a}_{10,\psi} = \frac{1}{\sqrt{2}} (e^{i\psi} \hat{a}_{+1} + e^{-i\psi} \hat{a}_{-1}), \quad (7.21a)$$

$$\hat{a}_{01,\psi} = \frac{i}{\sqrt{2}} (e^{i\psi} \hat{a}_{+1} - e^{-i\psi} \hat{a}_{-1}). \quad (7.21b)$$

The quantum model for this OPO configuration was already introduced in Section 6.2; we just need to particularize the three–wave mixing Hamiltonian (6.42) to the case of operating in frequency degenerate type I conditions with only the $L_{0,\pm 1}(k_s; \mathbf{r}_\perp, z)$ present at the signal frequency³. Working as usual in a picture rotated to the frequency of the injected laser, which in this case is described by the operator

$$\hat{U}_0 = \exp[\hat{H}_0 t / i\hbar] \quad \text{with} \quad \hat{H}_0 = \hbar \omega_0 (2 \hat{a}_0^\dagger \hat{a}_0 + \hat{a}_{+1}^\dagger \hat{a}_{+1} + \hat{a}_{-1}^\dagger \hat{a}_{-1}), \quad (7.22)$$

the master equation of the system can be written in this case as

$$\frac{d\hat{\rho}_I}{dt} = [\chi \hat{a}_0 \hat{a}_{+1}^\dagger \hat{a}_{-1}^\dagger + \mathcal{E}_p \hat{a}_0^\dagger + \text{H.c.}, \hat{\rho}_I] + \sum_{j=0,\pm 1} \gamma_j (2 \hat{a}_j \hat{\rho}_I \hat{a}_j^\dagger - \hat{a}_j^\dagger \hat{a}_j \hat{\rho}_I - \hat{\rho}_I \hat{a}_j^\dagger \hat{a}_j), \quad (7.23)$$

where we will denote γ_0 by γ_p to match our previous notation, and will assume that $\gamma_{+1} = \gamma_{-1} = \gamma_s$ which is as to assume that the DOPO is invariant under rotations around the longitudinal axis, that is, rotationally symmetric in the transverse plane. As usual, we take \mathcal{E}_p as a positive real. On the other hand, the nonlinear coupling parameter χ can be found by particularizing (6.1.2) to the current situation; taking into account that

$$\int_0^{+\infty} r dr G(k_p; r) [\mathcal{R}_0^1(k_s; r)]^2 = \left(\frac{2}{\pi}\right)^{3/2} \int_0^{+\infty} dr \frac{2r^3}{w_p w_s^4} \exp\left[-\left(\frac{1}{w_p^2} + \frac{2}{w_s^2}\right) r^2\right] = \frac{1}{4\pi^{3/2} w_s} \quad (7.24)$$

where we have used that $w_p^2/w_s^2 = \lambda_p/\lambda_s = 1/2$, see (3.86b), we get

$$\chi = \frac{3}{2} \frac{l_c}{w_s} \chi_{\text{oee}}^{(2)}(2\omega_0; \omega_0, \omega_0) \sqrt{\frac{\hbar \omega_0^3}{8\pi^3 \varepsilon_0 n_c^3 L_{\text{opt}}^3}}. \quad (7.25)$$

The above master equation has exactly the same form as that modeling the OPO, see (6.92); this makes perfect sense, as even though the down–converted photons are indistinguishable in frequency and polarization, they are not in orbital angular momentum, and hence the 2tmDOPO is not a truly degenerate system. From an operational point of view this is very fortunate, as we can then directly take the Langevin equations that we already derived for the OPO, and

³ From the previous section we know now that the only important feature is that this process is the one with the highest gain, it doesn't matter if other processes are present (such as frequency non-degenerate processes or processes involving other transverse families), as long as these have a higher threshold.

rewrite them to match the notation of the current system. Using also the same scaling for the coherent amplitudes, the time, the noises, and the parameters as in Section 6.4.1, see (6.95) and (6.53), this allows us to write

$$\dot{\beta}_0 = \kappa[\sigma - \beta_0 - \beta_{+1}\beta_{-1}], \quad (7.26a)$$

$$\dot{\beta}_0^+ = \kappa[\sigma - \beta_0^+ - \beta_{+1}^+\beta_{-1}^+], \quad (7.26b)$$

$$\dot{\beta}_{+1} = -\beta_{+1} + \beta_0\beta_{-1}^+ + g\sqrt{\beta_0}\zeta(\tau), \quad (7.26c)$$

$$\dot{\beta}_{+1}^+ = -\beta_{+1}^+ + \beta_0^+\beta_{-1} + g\sqrt{\beta_0^+}\zeta^+(\tau), \quad (7.26d)$$

$$\dot{\beta}_{-1} = -\beta_{-1} + \beta_0\beta_{+1}^+ + g\sqrt{\beta_0}\zeta^*(\tau), \quad (7.26e)$$

$$\dot{\beta}_{-1}^+ = -\beta_{-1}^+ + \beta_0^+\beta_{+1} + g\sqrt{\beta_0^+}[\zeta^+(\tau)]^*. \quad (7.26f)$$

Let us finally remind that the squeezing spectrum of any signal mode can be evaluated from this normalized variables as

$$S(\hat{X}_m^\varphi; \Omega) = \frac{2}{g^2} \int_{-\infty}^{+\infty} d\tau' \exp(-i\tilde{\Omega}\tau') \langle \delta x_m^\varphi(\tau) \delta x_m^\varphi(\tau + \tau') \rangle_P, \quad (7.27)$$

with

$$x_m^\varphi(\tau) = e^{-i\varphi} \beta_m(\tau) + e^{i\varphi} \beta_m^+(\tau), \quad (7.28)$$

m referring to any of transverse modes resonating at the signal frequency.

Classical emission: Spontaneous rotational symmetry breaking

We now show that above threshold the two-transverse-mode DOPO shows the phenomenon of spontaneous symmetry breaking of its rotational invariance in the transverse plane.

Following the approach introduced in the previous chapter, the classical equations of the system are retrieved from the Langevin equations by neglecting the noise terms and making the correspondences $\beta_j^\pm \rightarrow \beta_j^*$ to come back to the classical phase space:

$$\dot{\beta}_0 = \kappa[\sigma - \beta_0 - \beta_{+1}\beta_{-1}], \quad (7.29a)$$

$$\dot{\beta}_{+1} = -\beta_{+1} + \beta_0\beta_{-1}^*, \quad (7.29b)$$

$$\dot{\beta}_{-1} = -\beta_{-1} + \beta_0\beta_{+1}^*. \quad (7.29c)$$

Now, from our previous treatment of the OPO (see Section 6.4.2) we can directly understand the classical emission properties of the current 2tmDOPO. For $\sigma \leq 1$ the signal modes are switched off, that is, its only long time term stable solution is

$$\bar{\beta}_0 = \sigma, \quad \bar{\beta}_{+1} = \bar{\beta}_{-1} = 0. \quad (7.30)$$

On the other hand, for $\sigma > 1$ the only stable solution is

$$\bar{\beta}_0 = 1, \quad \bar{\beta}_{\pm 1} = \rho \exp(\mp i\theta), \quad (7.31)$$

with $\rho = \sqrt{\sigma - 1}$ and where θ is arbitrary, as the classical equations are invariant under the change $\beta_{\pm 1} \rightarrow \exp(\mp i\theta)\beta_{\pm 1}$, that is, θ is the FP of the 2tmDOPO. Taking the expectation value of expression (7.20), and using⁴ $\langle \hat{a}_{\pm 1}(t) \rangle = \exp(-i\omega_0 t) \bar{\beta}_{\pm 1} / g$ within the classical limit, we get the form of the signal field as predicted by classical optics

$$\bar{\mathbf{E}}_{s,\rightarrow}^{(+)}(\mathbf{r}, t) = i \sqrt{\frac{\hbar\omega_s(\sigma - 1)}{4\varepsilon_0 n_s L_s g^2}} \mathbf{e}_e [e^{-i\theta} L_{0,+1}(k_s; \mathbf{r}_\perp, z) + e^{i\theta} L_{0,-1}(k_s; \mathbf{r}_\perp, z)] e^{-i\omega_0 t + i n_s k_s z} \propto H_{10}^\theta(k_s; \mathbf{r}_\perp, z), \quad (7.33)$$

that is, classical emission takes place in the form of a TEM₁₀ mode forming an angle θ with respect to the x axis (see Figure 7.1). Hence, the FP is identified in this case with the orientation of the transverse pattern which is formed above threshold, what finally shows that the rotational transverse symmetry of the 2tmDOPO is spontaneously broken.

In the following, we will call *bright mode* to $H_{10}^\theta(k_s; \mathbf{r}_\perp, z)$ —as it is classically excited— and *dark mode* to its orthogonal $H_{01}^\theta(k_s; \mathbf{r}_\perp, z)$ —as it is classically empty of photons—, and will define the collective indices $\mathbf{b} = (10, \theta)$ and $\mathbf{d} = (01, \theta)$ to simplify the notation.

⁴ Note that this result comes from the following chain of equalities:

$$\langle \hat{a}_{\pm 1}(t) \rangle = \text{tr}\{\hat{\rho}_1 \hat{U}_0^\dagger \hat{a}_{\pm 1} \hat{U}_0\} = \exp(-i\omega_0 t) \text{tr}\{\hat{\rho}_1 \hat{a}_{\pm 1}\} = \exp(-i\omega_0 t) \langle \alpha_{\pm 1} \rangle_P = \exp(-i\omega_0 t) \langle \beta_{\pm 1} \rangle_P / g \quad (7.32)$$

Quantum properties: Pattern diffusion and noncritical squeezing

The linearized Langevin equations. Just as we did with the DOPO, we are going to discuss the quantum properties of the down-converted field by inspection of the quantum Langevin equations (7.26) in the limit $\gamma_p \gg \gamma_s$, i.e., $\kappa \gg 1$, where the pump variables can be adiabatically eliminated. We will show in the next chapter that all the important properties found in this limit are valid in general.

As we already commented in Section 6.3.3, the deterministic procedure for adiabatically eliminating the pump modes (which consists in assuming that $\dot{\beta}_0 = \dot{\beta}_0^+ = 0$) is still valid in the stochastic case, but only if the equations are interpreted in the Ito sense. Hence, after applying this procedure, the Langevin equations read in Stratonovich form:

$$\dot{\beta}_{+1} = - (1 - g^2/4) \beta_{+1} + (\sigma - \beta_{+1}\beta_{-1})\beta_{-1}^+ + g\sqrt{\sigma - \beta_{+1}\beta_{-1}}\zeta(\tau), \quad (7.34a)$$

$$\dot{\beta}_{+1}^+ = - (1 - g^2/4) \beta_{+1}^+ + (\sigma - \beta_{+1}^+\beta_{-1}^+)\beta_{-1} + g\sqrt{\sigma - \beta_{+1}^+\beta_{-1}^+}\zeta^+(\tau), \quad (7.34b)$$

$$\dot{\beta}_{-1} = - (1 - g^2/4) \beta_{-1} + (\sigma - \beta_{+1}\beta_{-1})\beta_{+1}^+ + g\sqrt{\sigma - \beta_{+1}\beta_{-1}}\zeta^*(\tau), \quad (7.34c)$$

$$\dot{\beta}_{-1}^+ = - (1 - g^2/4) \beta_{-1}^+ + (\sigma - \beta_{+1}^+\beta_{-1}^+)\beta_{+1} + g\sqrt{\sigma - \beta_{+1}^+\beta_{-1}^+}[\zeta^+(\tau)]^*. \quad (7.34d)$$

In order to find analytic predictions from these equations we are going to linearize them. As explained in the previous chapter, the usual procedure begins by writing the amplitudes as $\beta_m = \bar{\beta}_m + \delta\beta_m$ and $\beta_m^+ = \bar{\beta}_m^+ + \delta\beta_m^+$, and treat the fluctuations as order g perturbations. This is in particular how we proceeded with the OPO. However, as already stated in the previous chapter and emphasized in the present one, we expect quantum noise to rotate the generated TEM₁₀ mode (that is, to make the phase difference between the opposite angular momentum modes diffuse), and hence fluctuations of the fields in an arbitrary direction of phase space could not be small (i.e., order g). Nevertheless, equations (7.34) can be linearized if the amplitudes are expanded as

$$\beta_{\pm 1}(\tau) = [\rho + b_{\pm 1}(\tau)] e^{\mp i\theta(\tau)} \quad (7.35a)$$

$$\beta_{\pm 1}^+(\tau) = [\rho + b_{\pm 1}^+(\tau)] e^{\pm i\theta(\tau)}, \quad (7.35b)$$

because as we will prove $\theta(\tau)$ carries the larger part of the fluctuations, while the b 's and $\dot{\theta}$ remain as order g quantities. In addition, expanding the fields in this way allows us to track the evolution of the classical pattern's orientation, as we take θ as an explicit quantum variable. Then, writing equations (7.34) up to order g , we arrive to the following linear system (arriving to this expression is not as straightforward as it might seem, there are some subtleties that we clarify in Appendix C)

$$-2i\rho\mathbf{w}_0\dot{\theta} + \dot{\mathbf{b}} = \mathcal{L}\mathbf{b} + g\boldsymbol{\zeta}(\tau), \quad (7.36)$$

with

$$\mathbf{b} = \begin{pmatrix} b_{+1} \\ b_{+1}^+ \\ b_{-1} \\ b_{-1}^+ \end{pmatrix}, \quad \boldsymbol{\zeta}(\tau) = \begin{pmatrix} \zeta(\tau) \\ \zeta^+(\tau) \\ \zeta^*(\tau) \\ [\zeta^+(\tau)]^* \end{pmatrix}, \quad (7.37)$$

and where \mathcal{L} is a real, symmetric matrix given by

$$\mathcal{L} = - \begin{pmatrix} \sigma & 0 & \sigma - 1 & -1 \\ 0 & \sigma & -1 & \sigma - 1 \\ \sigma - 1 & -1 & \sigma & 0 \\ -1 & \sigma - 1 & 0 & \sigma \end{pmatrix}, \quad (7.38)$$

with the following eigensystem

$$\begin{aligned} \lambda_0 &= 0, & \mathbf{w}_0 &= \frac{1}{2} \text{col}(1, -1, -1, 1) \\ \lambda_1 &= -2, & \mathbf{w}_1 &= \frac{1}{2} \text{col}(1, 1, -1, -1) \\ \lambda_2 &= -2(\sigma - 1), & \mathbf{w}_2 &= \frac{1}{2} \text{col}(1, 1, 1, 1) \\ \lambda_3 &= -2\sigma, & \mathbf{w}_3 &= \frac{1}{2} \text{col}(1, -1, 1, -1). \end{aligned} \quad (7.39)$$

Defining the projections $c_m(\tau) = \mathbf{w}_m \cdot \mathbf{b}(\tau)$, and projecting the linear system (7.36) onto these eigenmodes, we find the following set of decoupled linear equations (c_0 is set to zero, as otherwise it would just entail a redefinition of

θ)

$$\dot{\theta} = \frac{g}{2\rho}\eta_0(\tau) \quad (7.40a)$$

$$\dot{c}_1 = -2c_1 + ig\eta_1(\tau) \quad (7.40b)$$

$$\dot{c}_2 = -2(\sigma - 1)c_2 + g\eta_2(\tau) \quad (7.40c)$$

$$\dot{c}_3 = -2\sigma c_3 + g\eta_3(\tau), \quad (7.40d)$$

where the following real noises have been defined

$$\eta_0(\tau) = \mathbf{i}\mathbf{w}_0 \cdot \boldsymbol{\zeta}(\tau) = \text{Im} \{ \zeta^+(\tau) - \zeta(\tau) \} \quad (7.41a)$$

$$\eta_1(\tau) = -\mathbf{i}\mathbf{w}_1 \cdot \boldsymbol{\zeta}(\tau) = \text{Im} \{ \zeta^+(\tau) + \zeta(\tau) \} \quad (7.41b)$$

$$\eta_2(\tau) = \mathbf{w}_2 \cdot \boldsymbol{\zeta}(\tau) = \text{Re} \{ \zeta(\tau) + \zeta^+(\tau) \} \quad (7.41c)$$

$$\eta_3(\tau) = \mathbf{w}_3 \cdot \boldsymbol{\zeta}(\tau) = \text{Re} \{ \zeta(\tau) - \zeta^+(\tau) \}, \quad (7.41d)$$

which satisfy the usual statistical properties (2.82).

Note finally that in the long time term the solutions for the projections c_j will be of order g (see Appendix B), and hence so will be the b 's (note that this is not the case for θ , whose initial value is completely arbitrary, although its variation $\dot{\theta}$ is indeed of order g). This is consistent with the initial assumptions about the orders in g of the involved quantities.

Quantum diffusion of the classical pattern. Just as we commented in the previous sections, equation (7.40a) shows that the orientation of the bright mode (the FP of the system) diffuses with time ruled by quantum noise. How fast this diffusion is can be measured by evaluating the variance of θ . Using the statistical properties of noise (2.82), it is straightforward to obtain the following result

$$V_\theta(\tau) = \langle \delta\theta^2(\tau) \rangle_P = D\tau, \quad (7.42)$$

where $D = d/(\sigma - 1)$ with

$$d = g^2/4 = \chi^2/4\gamma_p\gamma_s. \quad (7.43)$$

Note that we have assumed that $V_\theta(0) = 0$, which is as saying that every time the 2tmDOPO is switched on, that is, on any stochastic realization, the bright mode appears with the same orientation; in Chapter 9 we will show that the pattern can be locked to a desired orientation by injecting a low-power TEM₁₀ seed at the signal frequency inside the cavity, and hence our assumption can be satisfied experimentally by switching on the 2tmDOPO with this seed present, and turning it off at one point so that quantum noise can start making the bright mode rotate arbitrarily.

Passing to quantitative matters, Eq. (7.42) shows that the delocalization of the pattern's orientation increases as time passes by, though for typical system parameters (see Section 6.3.3, where we argued that $g \approx 4 \times 10^{-6}$) one finds $d \simeq 4 \times 10^{-12}$, and hence the rotation of the pattern will be fast only when working extremely close to threshold.

Independent quadratures and noncritical squeezing. The first step towards analyzing the squeezing properties of the field within the framework presented above, is identifying a set of independent quadratures. As showed in the previous analysis, these appear naturally within our approach, as the eigenmodes $\{\mathbf{w}_m\}_{m=0,1,2,3}$ of the stability matrix give us a set of quadratures with well defined squeezing properties. In particular, from (7.35), (7.21), and (7.28), it is easy to find the following relations

$$x_b(\tau) = 2\sqrt{2}\rho + \sqrt{2}c_2(\tau) \quad (7.44a)$$

$$y_b(\tau) = -i\sqrt{2}c_3(\tau) \quad (7.44b)$$

$$x_d(\tau) = i\sqrt{2}c_0(\tau) \quad (7.44c)$$

$$y_d(\tau) = \sqrt{2}c_1(\tau), \quad (7.44d)$$

where $\{x_b, y_b\}$ and $\{x_d, y_d\}$ are the (normalized) X and Y quadratures of the bright and dark modes, $H_{10}^\theta(k_s; \mathbf{r}_\perp, z)$ and $H_{01}^\theta(k_s; \mathbf{r}_\perp, z)$, respectively.

The evolution of these quadratures can therefore be found from the equations satisfied by the projections (7.40), which are solved in Appendix B (remember that $c_0 = 0$). In particular, using the expression for the correlation

spectrum of the projections (B.6) as usual, it is straightforward to find the following results

$$V^{\text{out}}(\hat{X}_{\text{b}}; \Omega) = 1 + \frac{1}{(\sigma - 1)^2 + \tilde{\Omega}^2/4} \quad (7.45\text{a})$$

$$V^{\text{out}}(\hat{Y}_{\text{b}}; \Omega) = 1 - \frac{1}{\sigma^2 + \tilde{\Omega}^2/4} \quad (7.45\text{b})$$

$$V^{\text{out}}(\hat{X}_{\text{d}}; \Omega) = 1 \quad (7.45\text{c})$$

$$V^{\text{out}}(\hat{Y}_{\text{d}}; \Omega) = 1 - \frac{1}{1 + \tilde{\Omega}^2/4}. \quad (7.45\text{d})$$

We see that the quadratures of the bright mode have the same behavior as those of the single mode DOPO: The quadrature Y_{b} is perfectly squeezed ($V^{\text{out}} = 0$) at zero noise frequency ($\tilde{\Omega} = 0$) only at the bifurcation ($\sigma = 1$).

On the other hand, the dark mode has perfect squeezing in its Y quadrature at zero noise frequency. What is interesting is that this result is independent of the distance from threshold, and thus, it is a noncritical phenomenon.

This result was first shown in [32], and we can understand it by following the reasoning given in above: As the orientation θ of the classically excited pattern is undetermined in the long-time limit, its orbital angular momentum must be fully determined at low noise frequencies. On the other hand, the orbital angular momentum of the bright mode $H_{10}^{\theta}(k_{\text{s}}; \mathbf{r}_{\perp}, z)$ is nothing but its $\pi/2$ phase shifted orthogonal Hermite–Gauss mode, i.e., $-i\partial_{\phi}H_{10}^{\theta}(k_{\text{s}}; \mathbf{r}_{\perp}, z) = iH_{01}^{\theta}(k_{\text{s}}; \mathbf{r}_{\perp}, z)$, which used as a local oscillator in a homodyne detection experiment would lead to the observation of the Y_{d} quadrature fluctuations.

8. DEEP STUDY OF SPONTANEOUS SYMMETRY BREAKING THROUGH THE TWO-TRANSVERSE-MODE DOPO

In the previous chapter we have learned that spontaneous symmetry breaking allows for the obtention of noncritically squeezed light in OPOs. We have introduced this phenomenon by studying a particular example, the two-transverse-mode DOPO, in which the rotational invariance in the transverse plane is the symmetry broken by the TEM₁₀ signal field generated above threshold; the fundamental results at the quantum level have been that (i) this bright pattern rotates randomly in the transverse plane owed to quantum noise, and (ii) the dark mode consisting the the TEM₁₀ mode orthogonal to the generated one shows perfect squeezing on its Y quadrature irrespective of the distance to threshold.

In this chapter (and the next one) we answer some questions that appear naturally after the results of the previous chapter, and which are important both to get a clear understanding of the phenomenon, and to evaluate up to what point it is experimentally observable.

8.1 On canonical pairs and noise transfer

Although the noncritical squeezing of the dark mode coincide with what was intuitively expected after the arguments given in Section 7.2.1, a strange, unexpected result has appeared in (7.45): The quadratures of the dark mode seem to violate the uncertainty principle as $V^{\text{out}}(\hat{X}_d; \Omega = 0)V^{\text{out}}(\hat{Y}_d; \Omega = 0) = 0$.

Moreover, the noise spectrum of an arbitrary quadrature of the dark mode, which can be written in terms of its X and Y quadratures as $\hat{X}_d^\varphi = \hat{X}_d \cos \varphi + \hat{Y}_d \sin \varphi$, is

$$V^{\text{out}}(\hat{X}_d^\varphi; \Omega) = 1 - \frac{\sin^2 \varphi}{1 + \tilde{\Omega}^2/4}, \quad (8.1)$$

what shows that all the quadratures of the dark mode (except its X quadrature) are squeezed. Thus two orthogonal quadratures cannot form a canonical pair as they satisfy the relation

$$V^{\text{out}}(\hat{X}_d^\varphi; \Omega)V^{\text{out}}(\hat{Y}_d^\varphi; \Omega) < 1, \quad (8.2)$$

in clear violation of the uncertainty principle. This might look surprising, but one needs to keep in mind that the bright and dark modes are not true modes, as their orientation is not a fixed quantity, but a dynamical variable of the problem¹.

The natural question now is: Where does the excess of noise go if it is not transferred from one quadrature to its orthogonal one? The intuitive answer is that it goes to the pattern orientation, which is actually fully undetermined in the long term as we showed above (7.42). This section is devoted to prove this statement.

In particular we will prove that two orthogonal quadratures of the dark mode do not form a canonical pair, while the orientation θ is the canonical pair of all the squeezed quadratures. One way to prove this would be to evaluate the commutator between the corresponding quantum operators. However, θ is half the phase difference between the opposite orbital angular momentum modes $\hat{a}_{\pm 1}$, whose associated operator has a very difficult expression [141, 142], making the calculation of the needed commutators quite hard. Nevertheless, in [143] we gave evidences of this via a simple procedure based on the close relation between the quantum commutators and the classical Poisson brackets introduced in Section A.1, and this is the one we present here.

Let us then come back to a classical description of the system in which a pair of normal variables $\{\nu_m, \nu_m^*\}$ is associated to each mode of the field. The Poisson bracket between two phase space functions $f(\nu_m, \nu_m^*)$ and

¹ This gives rise to an even more important question: If the modes depend on the system variables, can we actually select them with a local oscillator? One can try to picture a detection scheme using some kind of feed-forward information in which the orientation of the local oscillator is locked somehow to the orientation of the bright or dark modes, but it seems highly unlikely. Nevertheless, we show along the next sections that this does not destroy the possibility of observing the phenomenon, or even of using it in applications.

$h(\nu_m, \nu_m^*)$ can be rewritten in terms of the normal variables (instead of the position and momenta) as

$$\{f, h\} = \sum_m \frac{2}{i\omega_m} \left(\frac{\partial f}{\partial \nu_m} \frac{\partial h}{\partial \nu_m^*} - \frac{\partial f}{\partial \nu_m^*} \frac{\partial h}{\partial \nu_m} \right), \quad (8.3)$$

where the sum covers all the cavity modes, being ω_m their corresponding frequencies.

As an example, the Poisson bracket between two orthogonal quadratures of a given mode $X_m = \sqrt{\omega_m/2\hbar}(\nu_m + \nu_m^*)$ and $Y_m = -\sqrt{\omega_m/2\hbar}(\nu_m - \nu_m^*)$ is found to be

$$\{X_m, Y_m\} = 2/\hbar, \quad (8.4)$$

which is consistent with the quantum commutator $[\hat{X}_m, \hat{Y}_m] = 2i$ given the correspondence $[\hat{X}_m, \hat{Y}_m] = i\hbar \{X_m, Y_m\}$.

Now, we say that two observables \hat{A} and \hat{B} are canonically related when their commutator is not an operator, but an imaginary number, that is, when $[\hat{A}, \hat{B}] = iK$ with $K \in \mathbb{R}$, as therefore they satisfy an uncertainty relation of the type $\Delta A \Delta B \geq K^2/4$. In an analogous way, given the relation between the commutators and the Poisson brackets, we will say that two classical observables $f(\nu_m, \nu_m^*)$ and $h(\nu_m, \nu_m^*)$ form a canonical pair if their Poisson bracket is a real number, that is, $\{f, h\} \in \mathbb{R}$.

In our case, the functions we are interested in are the classical counterparts of the dark mode quadratures, which using (7.21) with $\psi = \theta$ are written in terms of the normal variables of the Laguerre–Gauss modes as

$$X_d^\varphi = i\sqrt{\frac{\omega_s}{4\hbar}} [e^{-i\varphi} (e^{i\theta} \nu_{+1} - e^{-i\theta} \nu_{-1})] + \text{c.c.}, \quad (8.5)$$

with the orientation given by

$$\theta = \frac{1}{2i} \ln \left(\frac{\nu_{+1}^* \nu_{-1}}{|\nu_{+1}| |\nu_{-1}|} \right), \quad (8.6)$$

which is just half the phase difference between ν_{+1} and ν_{-1} .

Now, using the definition of the Poisson brackets (8.3) with $m = \pm 1$ and after some algebra, it is simple to show that

$$\{X_d^\varphi, Y_d^\varphi\} = -\frac{(|\nu_{+1}| - |\nu_{-1}|)^2}{2\hbar |\nu_{+1}| |\nu_{-1}|}, \quad (8.7)$$

and

$$\{X_d^\varphi, \theta\} = \frac{\exp(-i\varphi) (|\nu_{+1}| + |\nu_{-1}|) \sqrt{|\nu_{+1}| |\nu_{-1}|}}{4i\sqrt{\hbar}\omega_s |\nu_{+1}|^{3/2} |\nu_{-1}|^{3/2}} + \text{c.c.} \quad (8.8)$$

On the other hand, in the 2tmDOPO the number of photons with opposite orbital angular momentum is sensibly equal, that is, $|\nu_{+1}| \approx |\nu_{-1}|$; in particular, the steady state solution of the system above threshold (7.31) states that $|\nu_{\pm 1}| = \sqrt{2\hbar/\omega_s} |\langle \hat{a}_{\pm 1} \rangle| = \sqrt{2\hbar/\omega_s} |\beta_{\pm 1}/g| = \sqrt{2\hbar/\omega_s} \rho/g$, and thus the dominant term of the previous Poisson brackets will be

$$\{X_d^\varphi, X_d^{\varphi+\pi/2}\} \approx 0, \quad (8.9)$$

and

$$\{X_d^\varphi, \theta\} \approx -\frac{g \sin \varphi}{\sqrt{2\hbar}\rho}. \quad (8.10)$$

Hence, at least at the classical level two orthogonal dark quadratures X_d^φ and $X_d^{\varphi+\pi/2}$ do not form a canonical pair (moreover, they commute), while X_d^φ and θ do. This can be seen as an evidence of the same conclusion for the corresponding quantum operators.

8.2 Homodyne detection with a fixed local oscillator

So far we have considered the situation in which one is able to detect independently the bright and dark modes. However, as shown by Eq. (7.40a), these modes are rotating randomly, what means that a local oscillator field following that random rotation should be used in order to detect them separately. This might be a really complicated, if not impossible, task, so we analyze now the more realistic situation in which the local oscillator is matched to the orthogonal orientation of the emerging pattern only at the initial time, remaining then with the same orientation during the observation time T . We will show that even in this case, and as the rotation of the modes is quite slow (7.42), large levels of noise reduction can be obtained.

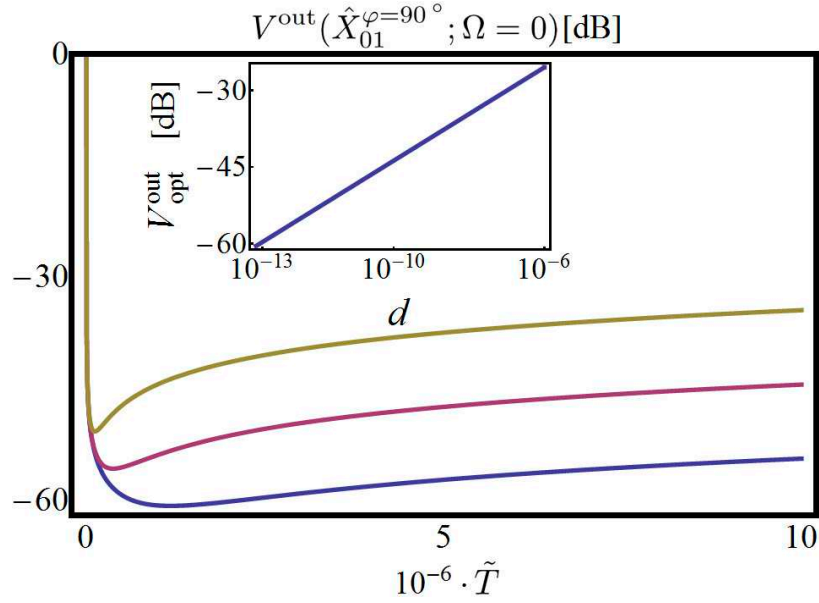


Fig. 8.1: Zero-frequency noise spectrum of the Y quadrature corresponding to a fixed TEM₀₁ mode as a function of the detection time \tilde{T} . Three different values of d are considered (10^{-11} , 10^{-12} and 10^{-13} from top to bottom). The inset shows also this spectrum at zero noise frequency, but evaluated at the optimum detection time T_{opt} and as a function of d (note that the d axis is in logarithmic scale). As mentioned in the text $\sigma = \sqrt{2}$.

Without loss of generality, we suppose that the bright mode emerges from the resonator at some initial time $\tau = 0$ oriented within the x axis, i.e., $\theta(0) = 0$. Hence, by using a TEM₀₁ local oscillator with a phase φ , the quadrature X_{01}^φ of a fixed $H_{01}(k_s; \mathbf{r}_\perp, z)$ mode (the initially dark mode) will be measured. In terms of the Gauss-Laguerre modes, the amplitude β_{01} of this mode is given by (7.21) with $\psi = 0$. Then, by using the expansion (7.35) of the amplitudes β_m as functions of the fluctuations b_m and the orientation θ , the normalized quadrature x_{01}^φ of this mode can be rewritten as

$$x_{01}^\varphi = 2\sqrt{2}\rho \cos \varphi \sin \theta + \sqrt{2}c_2 \cos \varphi \sin \theta + \sqrt{2}c_1 \sin \varphi \cos \theta - i\sqrt{2}c_3 \sin \varphi \sin \theta. \quad (8.11)$$

Hence, the two-time correlation function of x_{01}^φ yields (note that (7.40) show that c_1 , c_2 , c_3 , $\sin \theta$, and $\cos \theta$ are uncorrelated, as their corresponding noises are independent)

$$\langle x_{01}^\varphi(\tau_1) x_{01}^\varphi(\tau_2) \rangle = 2 \cos^2 \varphi [4\rho^2 + C_2(\tau_1, \tau_2)] S(\tau_1, \tau_2) + 2 \sin^2 \varphi [C_1(\tau_1, \tau_2) C(\tau_1, \tau_2) - C_3(\tau_1, \tau_2) S(\tau_1, \tau_2)], \quad (8.12)$$

with

$$S(\tau_1, \tau_2) = \langle \sin \theta(\tau_1) \sin \theta(\tau_2) \rangle \quad (8.13a)$$

$$C(\tau_1, \tau_2) = \langle \cos \theta(\tau_1) \cos \theta(\tau_2) \rangle \quad (8.13b)$$

$$C_m(\tau_1, \tau_2) = \langle c_m(\tau_1) c_m(\tau_2) \rangle. \quad (8.13c)$$

As shown in Appendices B and D, the latter correlation functions can be evaluated by using the linear evolution equations of the projections c_m and θ -see equations (B.5), (D.6), and (D.7)-; then from (8.12) the squeezing spectrum of a general quadrature of the $H_{01}(k_s; \mathbf{r}_\perp, z)$ mode can be found by using the general expression (5.52), which in terms of the normalized quadratures is written as

$$S(\hat{X}_{01}^\varphi; \Omega) = \frac{2}{\tilde{T}g^2} \int_0^{\tilde{T}} d\tau \int_0^{\tilde{T}} d\tau' \cos[\tilde{\Omega}(\tau - \tau')] \langle \delta x_{01}^\varphi(\tau) \delta x_{01}^\varphi(\tau + \tau') \rangle_P, \quad (8.14)$$

with $\tilde{T} = \gamma_s T$, as in this case the stationary expression (7.27) cannot be used because $S(\tau_1, \tau_2)$ and $C(\tau_1, \tau_2)$ don't reach a stationary state, see (D.6) and (D.7).

This integral is easily performed; however the resulting expression for $S(\hat{X}_{01}^\varphi; \Omega)$ is too lengthy, and a more compact approximated expression can be straightforwardly found in the limit of small d , leading to the following expression for the noise spectrum

$$V^{\text{out}}(\hat{X}_{01}^\varphi; \Omega) = 1 + S_{01}^0(\Omega) \cos^2 \varphi + S_{01}^{\pi/2}(\Omega) \sin^2 \varphi, \quad (8.15)$$

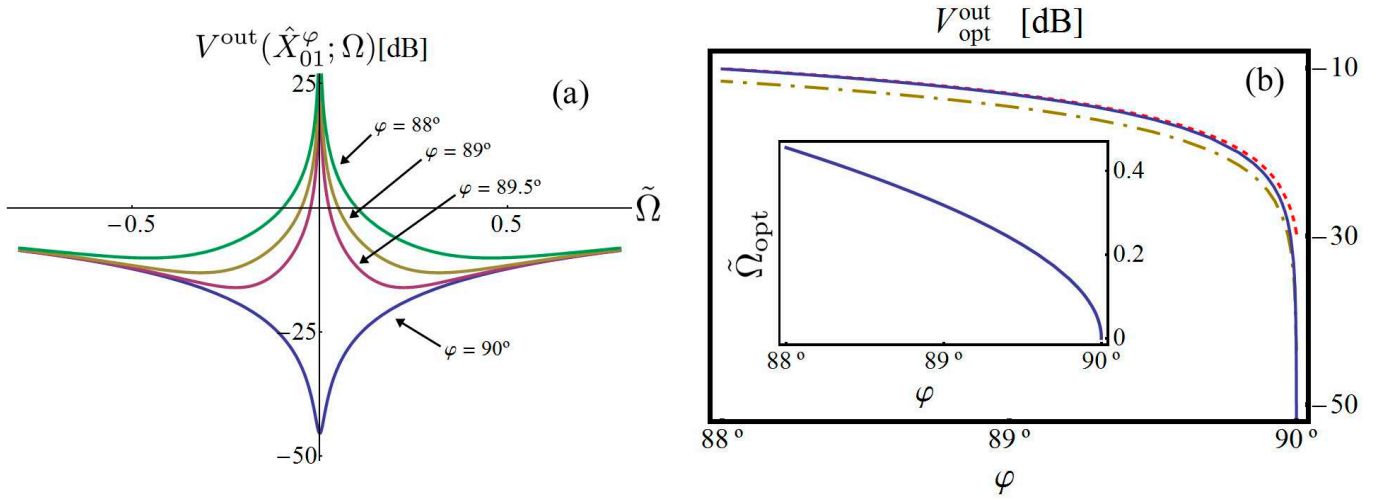


Fig. 8.2: (a) Noise spectrum of the fixed TEM_{01} mode as a function of the noise frequency $\tilde{\Omega}$, and for four different values of the local oscillator phase ($\varphi = 88, 89, 89.5$, and 90 from top to bottom curves). It can be appreciated how the infinite fluctuations of S_{01}^0 at zero noise frequency enter in the spectrum for any $\varphi \neq 90$. The rest of parameters are $\sigma = \sqrt{2}$, $d = 10^{-10}$, and $T = T_{\text{opt}}$, but the same behavior appears for any other election of the parameters. (b) Noise spectrum of the fixed TEM_{01} mode evaluated for the optimum parameters $\tilde{\Omega}_{\text{opt}}$ and \tilde{T}_{opt} as a function of φ ($d = 10^{-13}$ for the blue-solid curve and 10^{-6} for the red-dashed one, having both $\sigma = \sqrt{2}$). In addition, it is plotted the analogous curve for the single-mode DOPO (gold, dashed-dotted curve). The inset shows the dependence of the optimum frequency $\tilde{\Omega}_{\text{opt}}$ with the phase of the local oscillator φ .

with

$$S_{01}^0 = \frac{8}{\tilde{\Omega}^2} \left(1 - \text{sinc} \tilde{\Omega} T\right) - \frac{4d\tilde{T}}{\tilde{\Omega}^2(\sigma - 1)} \cdot \frac{6(\sigma - 1)^2 + \tilde{\Omega}^2}{4(\sigma - 1)^2 + \tilde{\Omega}^2} \quad (8.16)$$

and

$$S_{01}^{\pi/2} = \frac{8 - 2\tilde{\Omega}^2}{\tilde{T}(4 + \tilde{\Omega}^2)^2} - \frac{4}{4 + \tilde{\Omega}^2} + \frac{8d\tilde{T} [2(\sigma^2 + 1) + \tilde{\Omega}^2]}{(\sigma - 1)(4 + \tilde{\Omega}^2)(4\sigma^2 + \tilde{\Omega}^2)}, \quad (8.17)$$

where $\text{sinc} x = \sin(x)/x$. In the following we will fix σ to $\sqrt{2}$ (pump power twice above threshold), as the results are almost independent of its value as far as it is far enough from threshold. Hence, the free parameters will be the detection parameters \tilde{T} , $\tilde{\Omega}$ and φ , and the diffusion d which depends on the system parameters.

In this section, the results for $V^{\text{out}}(\hat{X}_{01}^{\varphi}; \Omega)$ are presented in dB units, defined through the relation $V^{\text{out}} [\text{dB}] = 10 \log V^{\text{out}}$ (hence, e.g., -10 dB and $-\infty$ dB correspond to 90% of noise reduction $-V^{\text{out}} = 0.1$ — and complete noise reduction $-V^{\text{out}} = 0$ — respectively.)

From expression (8.15) we see that the maximum level of squeezing is obtained at $\tilde{\Omega} = 0$ (see also Figure 8.2a) and when the phase of the local oscillator is tuned exactly to $\pi/2$. In Figure 8.1 we show the noise spectrum (8.15) for these parameters as a function of the detection time \tilde{T} for 3 different values of d . We see that in all cases there exist an optimum detection time for which squeezing is maximum. Minimizing Eq. (8.15) with $\tilde{\Omega} = 0$ and $\varphi = \pi/2$ with respect to \tilde{T} , it is straightforward to find that this optimum detection time is given by

$$\tilde{T}_{\text{opt}} = \sqrt{\frac{\sigma^2(\sigma - 1)}{d(\sigma^2 + 1)}}, \quad (8.18)$$

with an associated noise spectrum $V_{\text{opt}}^{\text{out}} = 1/\tilde{T}_{\text{opt}}$ (shown in the inset of Figure 8.1 as function of d).

These results show that large levels of noise reduction are obtained for the Y quadrature of the fixed TEM_{01} mode, even for values of the diffusion parameter d as large as 10^{-6} (remember that 10^{-12} is a more realistic value). However, in real experiments it is not possible to ensure that $\varphi = 90^\circ$ with an uncertainty below approximately 1.5° [5, 4, 6], and hence we proceed now to investigate the level of noise reduction predicted by (8.15) when the local oscillator phase is different from $\varphi = 90^\circ$.

Of course, when $\varphi \neq 90^\circ$ the noise frequency with maximum squeezing is no longer $\tilde{\Omega} = 0$, as in this case the infinite fluctuations of S_{01}^0 at zero noise frequency, due to the rotation noise, enter the noise spectrum (see Figure 8.2a). By numerical minimization of $V^{\text{out}}(\tilde{X}_{01}^\varphi; \Omega)$ with respect to $\tilde{\Omega}$ and \tilde{T} for different values of φ and d , it is possible to show that the optimum value of the detection time is almost independent of φ for small deviations of this from 90° , and hence it is still given to a good approximation by (8.18), although in this case this minimum is less pronounced than in the $\varphi = 90^\circ$ case shown in Figure 8.1 (i.e., the curve is almost horizontal around \tilde{T}_{opt}). On the other hand, the optimum noise frequency $\tilde{\Omega}_{\text{opt}}$ is independent of d and depends on φ as shown in the inset of Figure 8.2b.

As for the squeezing level, in Figure 8.2b we show the noise spectrum evaluated at \tilde{T}_{opt} and $\tilde{\Omega}_{\text{opt}}$ as a function of φ for 2 different values of the diffusion d . Together with these curves, we have plotted the noise spectrum of the single-mode DOPO² evaluated for its optimum parameters (in this case it is optimized respect to σ and $\tilde{\Omega}$) as a function of φ . We see that the noise reduction is independent of d as φ is taken apart from 90° . On the other hand, the squeezing level is similar to that of the single-mode DOPO, as the maximum difference between them are 1.5 dB (a factor 1.4 in the noise spectrum) in favor of the single-mode DOPO, with the advantage that in the 2tmDOPO this level is independent of the distance from threshold.

Therefore we see that the phenomenon of noncritical squeezing through spontaneous rotational symmetry breaking could be observed in the 2tmDOPO without the need of following the random rotation of the generated pattern, which makes its experimental realization feasible with currently available technology.

8.3 Beyond the considered approximations

8.3.1 Beyond the adiabatic elimination of the pump

The first assumption made in the search for the quantum properties of the system was that $\gamma_p \gg \gamma_s$, a limit that allowed the adiabatic elimination of the pump field. Now we are going to show analytically that the phenomenon of squeezing induced by spontaneous rotational symmetry breaking is still present even without this assumption, but still working within the linearized theory (in the next section we will check it via a numerical simulation of the complete nonlinear stochastic equations).

The way to show this is quite simple; starting from the complete equations (7.26), we expand the amplitudes β_m around the classical stationary solution (7.31) as we made in (7.35), but adding now a similar expression for the pump amplitudes: $\beta_0 = 1 + b_0$ and $\beta_0^+ = 1 + b_0^+$ (note that for the pump modes the b 's are directly small as the phase of this mode is locked to that of the injection \mathcal{E}_p). Then, linearizing these equations for the fluctuations and noises, we arrive to a linear system formally equal to (7.36), but with

$$\mathbf{b} = \begin{pmatrix} b_0 \\ b_0^+ \\ b_{+1} \\ b_{+1}^+ \\ b_{-1} \\ b_{-1}^+ \end{pmatrix}, \quad \boldsymbol{\zeta} = \begin{pmatrix} 0 \\ 0 \\ \zeta(\tau) \\ \zeta^+(\tau) \\ \zeta^*(\tau) \\ [\zeta^+(\tau)]^* \end{pmatrix}, \quad (8.19)$$

and a linear matrix

$$\mathcal{L} = \begin{pmatrix} -\kappa & 0 & -\rho & 0 & -\rho & 0 \\ 0 & -\kappa & 0 & -\rho & 0 & -\rho \\ \rho & 0 & -1 & 0 & 0 & 1 \\ 0 & \rho & 0 & -1 & 1 & 0 \\ \rho & 0 & 0 & 1 & -1 & 0 \\ 0 & \rho & 1 & 0 & 0 & -1 \end{pmatrix}. \quad (8.20)$$

Although in this case \mathcal{L} is not Hermitian, it can be checked that it possess a biorthonormal eigenbasis³, and in particular, the following two vectors are present in its eigensystem: $\mathbf{w}'_0 = \frac{1}{2} \text{col}(0, 0, 1, -1, -1, 1)$ and $\mathbf{w}'_1 = \frac{1}{2} \text{col}(0, 0, 1, 1, -1, -1)$, with corresponding eigenvalues $\lambda'_0 = 0$ and $\lambda'_1 = -2$. These eigenvectors have null projection onto the pump subspace, and coincide with \mathbf{w}_0 and \mathbf{w}_1 in what concerns to the signal subspace, see (7.39). Hence, all the properties derived from these vectors are still present without any change. In particular, as they account for the diffusion of θ and the squeezing properties of the dark mode, we can conclude that these properties are still present when working out of the limit $\gamma_p \gg \gamma_s$.

² In the single-mode DOPO the best levels of squeezing are found below threshold, where its noise spectrum can be written as $V^{\text{out}}(\tilde{X}_s^\varphi; \Omega) = 1 + S_+(\Omega) \cos^2 \varphi - S_-(\Omega) \sin^2 \varphi$, with $S_\pm(\Omega) = 4\sigma / [(\sigma \pm 1)^2 + \tilde{\Omega}^2]$, see (6.76).

³ This means that there exist a set of eigenvectors \mathbf{v}_m satisfying $\mathcal{L}\mathbf{v}_m = \lambda_m \mathbf{v}_m$, and another set \mathbf{w}_m satisfying $\mathcal{L}^\dagger \mathbf{w}_m = \lambda_m^* \mathbf{w}_m$, such that $\mathbf{w}_m^* \cdot \mathbf{v}_m = \delta_{mn}$.

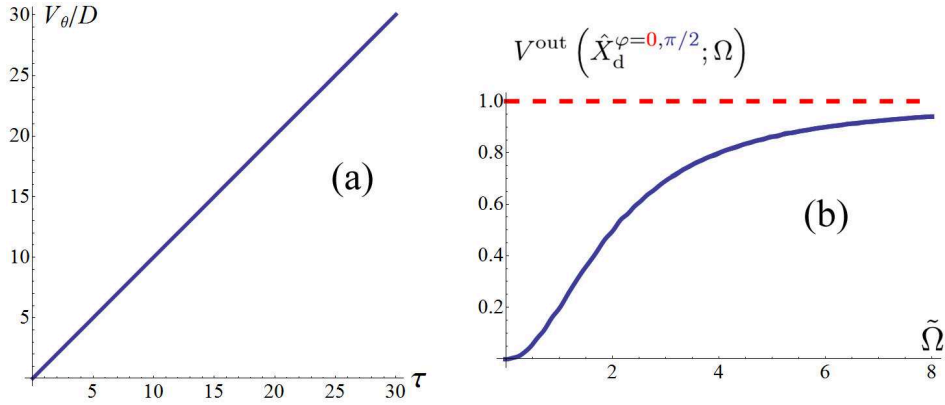


Fig. 8.3: (a) Evolution of the variance of the orientation θ given by the numerical simulation. It has been divided by the slope D predicted by the linearized theory (7.42), so the straight line obtained is in perfect agreement with this linear result. Quantitatively, a linear regression analysis shows that the slope obtained by the data is 0.99985, with standard error 7×10^{-5} . (b) Noise spectrum of the X (red-dashed curve) and Y (blue-solid curve) quadratures of the dark mode as obtained by the numerical simulation. The results are in perfect agreement with the ones predicted by the linearized theory (7.45). In particular, a nonlinear regression analysis of the numerical data respect to the function $(\omega/2)^2 / [b + a(\omega/2)^2]$, shows that $(a, b) = (0.9996, 1.0071)$ are the best fit parameters having standard errors $(1 \times 10^{-4}, 4 \times 10^{-4})$, which is in good agreement with the values $(a, b) = (1, 1)$ predicted by (7.45). Note finally that the small oscillations of the blue-solid line would disappear by increasing the number of stochastic trajectories Σ .

8.3.2 Numerical simulation of the nonlinear equations

In this section we will show that the diffusion of the orientation and the associated noncritical squeezing of the dark mode, which have been found by linearizing the Langevin equations, are also present when we consider the full nonlinear problem. To do so, we will solve numerically the complete stochastic equations (7.26) using the semi-implicit algorithm developed by Drummond and Mortimer in [144].

The details of the numerical simulation are explained in Appendix E. Here we just want to point out that the important parameters of the simulation are the step size $\Delta\tau$ used to arrive from $\tau = 0$ to the final integration time τ_{end} , and the number of stochastic trajectories, say Σ , which are used to evaluate stochastic averages. The initial conditions $\beta_m(0)$ are not relevant as the results in the stationary limit are independent of them. The system parameters which have been chosen for the simulation are $\sigma = \sqrt{2}$, $\kappa = 1$ (to show also numerically that the adiabatic elimination has nothing to do with the phenomenon), and $g = 10^{-3}$. We haven't chosen a smaller value for g (like 10^{-6} as followed from the physical parameters considered along the thesis) because such a small number can make the simulation fail; nevertheless all the results we are going to show should be independent of g and σ , and we have also checked that the same results are obtained for other values of these.

It is also important to note that we have defined a general quadrature of the rotating dark mode as (directly from (7.21) with $\beta = \theta$)

$$x_d^\varphi = \frac{i}{\sqrt{2}} [e^{-i\varphi} (e^{i\theta} \beta_{+1} - e^{-i\theta} \beta_{-1})] - \frac{i}{\sqrt{2}} [e^{i\varphi} (e^{-i\theta} \beta_{+1}^+ - e^{i\theta} \beta_{-1}^+)], \quad (8.21)$$

with θ defined within the positive P representation through

$$e^{2i\theta} = \frac{\beta_{-1} \beta_{+1}^+}{|\beta_{-1}| |\beta_{+1}^+|}. \quad (8.22)$$

Now let us show the results evaluated for the following simulation parameters: $\Delta\tau = 3 \cdot 10^{-3}$, $\tau_{\text{end}} = 30$ and $\Sigma = 7.5 \cdot 10^6$. This simulation has been compared with other ones having different values of these parameters to ensure convergence.

In Figure 8.3a we show the variance of θ as a function of time. The result has been normalized to D , so that the linear result (7.42) predicts a straight line forming 45° with respect to the time axis. It can be appreciated that this is indeed what the simulation shows (see also the caption of the figure).

In Figure 8.3b, we show the numerical results for the noise spectrum associated to the quadratures of the dark mode. Only times above $\tau = 10$ have been considered in the correlation function to ensure being working in the

stationary limit. Again, the results shown in Figure 8.3b are in reasonable agreement with the linear predictions (7.45c) and (7.45d), as explained quantitatively in the caption of Figure 8.3.

These results show that the phenomenon of noncritically squeezed light via spontaneous rotational symmetry breaking is not a product of the linearization.

9. THE TWO-TRANSVERSE-MODE DOPO WITH INJECTED SIGNAL

In this chapter we keep studying the properties of the 2tmDOPO, analyzing in particular how the injection of a TEM₁₀ mode at the signal frequency modifies its properties [36]. The study of this *signal seed* is motivated by two experimental issues. First, the arbitrariness of the initial orientation of the above-threshold pattern is highly inconvenient, since one cannot know in advance within which orientation it will rise at a particular realization of the experiment, what makes the matching of the local oscillator to the initial dark mode quite difficult; hence some means of fixing this orientation is called for, and we will show that this is exactly what the signal seed accomplishes. On the other hand, it is customary to inject a low intensity signal field in experiments to keep the cavity stable and locked to the desired frequency.

Note that this signal seed would break the rotational invariance of the system and hence a degradation of the squeezing level is expected. The goal of this chapter is then to determine the impact of the signal injection on the quantum properties of the 2tmDOPO.

In what follows, we will refer to this configuration as *driven* 2tmDOPO, denoting then by *free-running* 2tmDOPO the system without the injection at the signal frequency.

We will show that, fortunately, the 2tmDOPO still exhibits large levels of noncritical squeezing, even larger than those exhibited by the usual single-mode DOPO with injected signal, a result that is connected with the squeezing due to the spontaneous breaking of the rotational symmetry that exists in the absence of injection, but also to the existence of a new bifurcation in the system.

The current system is closely related to that analyzed by Protsenko *et al.* [145] who considered a single-mode DOPO with injected signal (see also [146, 147]). Indeed our model contains, as a limit, the model studied in [145], but we shall see that the existence of a second signal mode substantially modifies the properties of the system.

9.1 Model of the 2tmDOPO with injected signal

The system we are dealing with is exactly the same as the one we have already studied, with the exception that now the signal modes have also an injection term. In the previous chapters we wrote the system's equations in terms of the Laguerre–Gauss modes; now, however, it is quite recommendable to work in Hermite–Gauss basis, as we are injecting one of these modes. To this aim, we first use the relations (7.21) between the Laguerre–Gauss and the Hermite–Gauss boson operators to write the following relation between the corresponding normalized coherent amplitudes:

$$\beta_{\pm 1} = (\beta_x \mp i\beta_y) / \sqrt{2}, \quad (9.1)$$

where $\beta_{x/y}$ are the coherent amplitudes associated to the $H_{10/01}(k_s; \mathbf{r}_\perp, z)$ modes; then, we use these relations to rewrite the Langevin equations (7.26) which model the 2tmDOPO in terms of the $\beta_{x/y}$ amplitudes, arriving to

$$\dot{\beta}_0 = \kappa [\sigma - \beta_0 - (\beta_x^2 + \beta_y^2) / 2], \quad (9.2a)$$

$$\dot{\beta}_0^+ = \kappa [\sigma - \beta_0^+ - (\beta_x^{+2} + \beta_y^{+2}) / 2], \quad (9.2b)$$

$$\dot{\beta}_x = \varepsilon_i - \beta_x + \beta_0 \beta_x^+ + g\sqrt{\beta_0} \zeta_x(\tau), \quad (9.2c)$$

$$\dot{\beta}_x^+ = \varepsilon_i^* - \beta_x^+ + \beta_0^+ \beta_x + g\sqrt{\beta_0^+} \zeta_x^+(\tau), \quad (9.2d)$$

$$\dot{\beta}_y = -\beta_y + \beta_0 \beta_y^+ + g\sqrt{\beta_0} \zeta_y(\tau), \quad (9.2e)$$

$$\dot{\beta}_y^+ = -\beta_y^+ + \beta_0^+ \beta_y + g\sqrt{\beta_0^+} \zeta_y^+(\tau), \quad (9.2f)$$

where in addition to the usual dimensionless parameters, we have introduced the normalized injection parameter for the signal TEM₁₀ mode

$$\varepsilon_i = \frac{\chi \mathcal{E}_s}{\gamma_s \sqrt{\gamma_p \gamma_s}}, \quad (9.3)$$

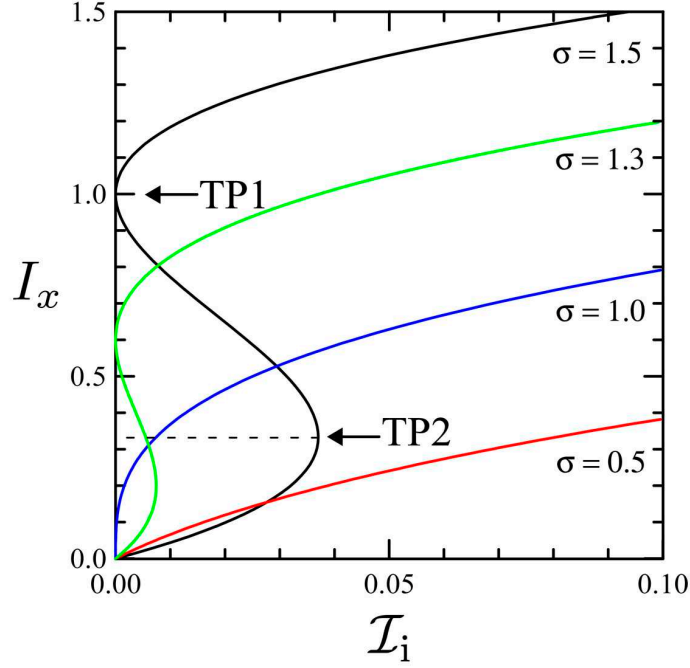


Fig. 9.1: Intensity of the TEM₁₀ mode for the ‘one-mode’ solution as a function of the injected field intensity \mathcal{I}_i for $\varphi_i = 0$ and the four indicated values of σ . Note that for $\sigma > 1$ the solution is three-valued. We have indicated the turning points TP1 and TP2 for the case $\sigma = 1.5$.

being \mathcal{E}_s the injection rate parameter appearing in the Hamiltonian piece corresponding to this signal injection, see (4.18).

9.2 Classical steady states and their stability

As discussed in depth in previous sections, the classical limit is recovered from the Langevin equations (9.2) by neglecting the noise terms and by making the identification $\beta_m^+ \rightarrow \beta_m^*$ ($m = 0, x, y$), arriving to

$$\dot{\beta}_0 = \kappa [\sigma - \beta_0 - (\beta_x^2 + \beta_y^2) / 2], \quad (9.4a)$$

$$\dot{\beta}_x = \varepsilon_i - \beta_x + \beta_0 \beta_x^*, \quad (9.4b)$$

$$\dot{\beta}_y = -\beta_y + \beta_0 \beta_y^*. \quad (9.4c)$$

In this section we study the steady states of this classical model, as well as their stability properties. Notice that by setting $\beta_y = 0$, equations (9.4) become those for a single-mode DOPO with injected signal. Such model (generalized by the presence of detunings) was studied in [148] for the case of real ε and then extended to arbitrary injection phases in [145].

A straightforward inspection of (9.4) leads to the conclusion that for $\varepsilon \neq 0$ there are only two types of classical solutions, either with $\beta_y = 0$ or with $\beta_y \neq 0$, both having $\beta_x \neq 0$. In the first case the intracavity signal field is single-mode and has the same shape as the injection; on the other hand, when $\beta_y \neq 0$ the intracavity field is in a coherent superposition of both transverse modes. We will refer to these two types of states as the *one-mode* and *two-mode* solutions, respectively.

In the following we decompose the fields into modulus and phase as

$$\varepsilon_i = \sqrt{\mathcal{I}_i} e^{i\varphi_i}, \quad \beta_m = \sqrt{I_m} e^{i\varphi_m}, \quad (9.5)$$

when needed.

9.2.1 The one-mode solution

We look first for a solution in which the non-injected mode $H_{01}(k_s; \mathbf{r}_\perp, z)$ is off ($\beta_y = 0$). This solution was the one analyzed in [145], and we refer to that work for the details. Using our notation, the intensity I_x of mode $H_{10}(k_s; \mathbf{r}_\perp, z)$

verifies the implicit relation

$$\mathcal{I}_i = \frac{2(\sigma^2 - X^2)^2(X - 1)}{\sigma^2 + X^2 + 2\sigma X \cos 2\varphi_i}, \quad (9.6)$$

where $X = 1 + \frac{1}{2}I_x$, which is a quintic polynomial in I_x , while its phase is given by

$$e^{i\varphi_x} = \pm \frac{\sigma e^{-i\varphi_i} + X e^{i\varphi_i}}{\sqrt{\sigma^2 + X^2 + 2\sigma X \cos 2\varphi_i}}, \quad (9.7)$$

where the plus and minus signs correspond, respectively, to cases $X > \sigma$ and $X < \sigma$. Finally, the intracavity pump field is given by

$$I_0 = \frac{1}{4}I_x^2 + \sigma^2 - \sigma I_x \cos 2\varphi_x, \quad (9.8a)$$

$$\varphi_0 = \arg(2\sigma - I_x e^{2i\varphi_x}). \quad (9.8b)$$

In Figure 9.1 we show the dependence of the intensity I_x on the injected intensity \mathcal{I}_i in the case $\varphi_i = 0$ (amplification regime) for various values of the pumping level σ as indicated. For $\sigma < 1$ (below the free-running 2tmDOPO threshold) the curve is single-valued, while for $\sigma > 1$ the curve is multivalued for small injection intensities. The location of the turning points (marked as TP1 and TP2) existing for $\sigma > 1$ can be obtained from Eq. (9.6) by solving $\partial\mathcal{I}_i/\partial I_x = 0$ (see [145] for more details). One of them is analytical,

$$I_x^{\text{TP1}} = 2(\sigma - 1), \quad (9.9)$$

which exists only if $\sigma > 1$, as expected. For $I_x = I_x^{\text{TP1}}$, $\mathcal{I}_i = 0$ as follows from (9.6), and then I_x^{TP1} corresponds to the upper turning points in Figure 9.1. The intensity I_x^{TP2} at the lower turning points in Figure 9.1 is given by a fourth order polynomial, which we do not present here as it gives no analytical information and, moreover, because it plays no effective role in the system behavior as is shown below in the stability analysis.

The final conclusion is simple: For $\sigma < 1$ Eq. (9.6) has a single real and positive solution, while for $\sigma > 1$ the solution is three-valued for small injection intensities.

As for the stability of this one-mode solution (see Figure 9.2 for a graphical summary of the discussion to follow), the stability matrix \mathcal{L} turns out to be block-diagonal (as usual, the switched off mode is decoupled from the rest). One submatrix affects only the subspace (β_y, β_y^*) and then governs the possible switching-on of mode $H_{01}(k_s; \mathbf{r}_\perp, z)$, while the other affects the rest of variables and is the same as the one considered in [145]. Accordingly, the characteristic polynomial is factorized into two.

The first polynomial, quadratic in λ , governs the evolution of the perturbations of the variables $\{\beta_y, \beta_y^*\}$ as commented, and gives the following two eigenvalues

$$\lambda_{1,2} = -1 \pm \sqrt{I_0}, \quad (9.10)$$

with I_0 given by Eq. (9.8a). Solving $\lambda_1 = 0$ gives two solutions, namely $I_x = I_x^{\text{TP1}}$, Eq. (9.9), which occurs at $\mathcal{I}_i = 0$, and

$$I_x = 2\sqrt{1 + \sigma^2 + 2\sigma \cos 2\varphi_i} \equiv I_x^{\text{PB}}, \quad (9.11)$$

which occurs at, using (9.6),

$$\mathcal{I}_i = 4 \left(1 + \sigma \cos 2\varphi_i + \sqrt{1 + 2\sigma \cos 2\varphi_i + \sigma^2} \right) \equiv \mathcal{I}_i^{\text{PB}}. \quad (9.12)$$

In a moment it will become clear why we denote by PB this new bifurcation.

The analyzed solution is stable (i.e., $\lambda_1 < 0$) for $I_x^{\text{TP1}} < I_x < I_x^{\text{PB}}$. For $I_x > I_x^{\text{PB}}$ or $I_x < I_x^{\text{TP1}}$, $\lambda_1 > 0$ and the one-mode solution is unstable. For $\sigma < 1$ the turning points TP1 and TP2 don't exist and the one-mode solution is stable all along its unique branch until $I_x = I_x^{\text{PB}}$. On the other hand, for $\sigma > 1$ the one-mode solution is stable only in the portion of its upper branch going from the turning point TP1 to the bifurcation PB; hence the branches lying below the turning point TP1 are unstable, including the turning point TP2 as anticipated.

Let us now understand the meaning of these two instabilities, having in mind that they affect the subspace corresponding to the (non-injected) TEM₀₁ mode $H_{01}(k_s; \mathbf{r}_\perp, z)$, which is off. The existence of an instability at the turning point TP1 is due to the fact that its corresponding injection intensity is null, i.e., $\mathcal{I}_i^{\text{TP1}} = 0$, Figure 9.1. In the absence of injection the system is rotationally symmetric in the transverse plane, and the 2tmDOPO can generate equally both modes $H_{10}(k_s; \mathbf{r}_\perp, z)$ and $H_{01}(k_s; \mathbf{r}_\perp, z)$; hence, at $\mathcal{I}_i = 0$ the solution with $\beta_y = 0$ is marginally unstable. On the other hand, the instability at PB is of a different nature as for injection intensities $\mathcal{I}_i > \mathcal{I}_i^{\text{PB}}$ the

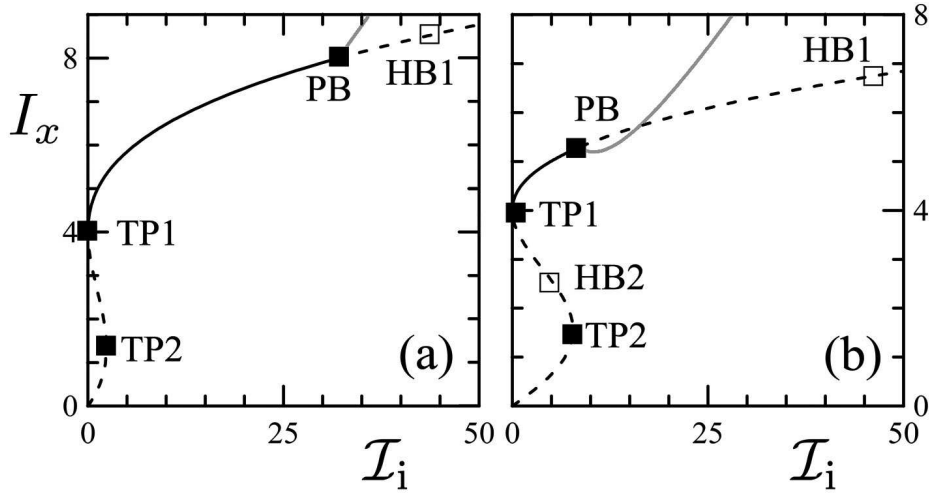


Fig. 9.2: Steady states of the system on the plane $\langle \mathcal{I}_i, I_{10} \rangle$. Continuous and dashed lines correspond to stable and unstable solutions, respectively. The black and grey lines correspond to the one-mode and two-mode solutions, respectively. The parameter values are $\sigma = 3$ and $\varphi_i = 0$, $\kappa = 0.25$ in (a) and $\varphi_i = \pi/3$, $\kappa = 1$ in (b). Notice that for $\mathcal{I}_i \neq 0$ the pitchfork bifurcation where the TEM₀₁ mode is switched on (marked as PB) is the only relevant bifurcation. TP1 and TP2 denote the turning points (see Figure 9.1) and HB1 and HB2 denote two different Hopf bifurcations (which are always preceded by the bifurcations occurring at points TP1 and PB, see text).

one-mode solution is no more stable. As this instability governs the growth of mode $H_{01}(k_s; \mathbf{r}_\perp, z)$ we conclude that at PB a pitchfork bifurcation takes place giving rise to a new steady state branch (the two-mode steady state, see Section 9.2.2). This instability is analogous to the one predicted in intracavity type II second harmonic generation, where the field orthogonal (in the polarization sense) to the injected one is generated at a pitchfork bifurcation [149, 150, 151, 152, 153, 154, 155, 156].

We show in the remainder of the section that TP1 and PB are the only relevant instabilities in the 2tmDOPO with injected signal.

As for the second polynomial it is, as commented, the one analyzed in [145]. We summarize next the results of that analysis and refer to [145] for the details. When $\sigma > 1$ an eigenvalue is null in correspondence with the turning point TP2 in Figure 9.1, as usual, but this point (as well as the whole lower and intermediate branches) is already unstable as stated above. On the other hand, a pair of complex-conjugate eigenvalues become purely imaginary (then with null real part) at an intensity $I_x = I_x^{\text{HB1}}$ existing at any value of σ , thus signalling a so-called Hopf bifurcation. In the case $\sigma > 1$ the Hopf bifurcation is located on the upper branches in Figure 9.1, and it is then relevant to ask if this bifurcation can play a role in the 2tmDOPO with injected signal. The expression for I_x^{HB1} is not analytical in general; however in the amplification regime ($\varphi_i = 0$), $I_x^{\text{HB1}} = 2(\kappa + \sigma + 1) > 2(\sigma + 1) = I_x^{\text{PB}}$, see (9.11). As $I_x^{\text{HB1}} > I_x^{\text{PB}}$, the Hopf bifurcation is always preceded by the pitchfork bifurcation and then the former never comes into play (note that $I_x^{\text{HB1}} \rightarrow I_x^{\text{PB}}$ for $\kappa \rightarrow 0$ though). On the other hand a second Hopf bifurcation (HB2) exists in the case $\sigma > 1$, but it is always located below the upper turning point TP1 in Figure 9.1 [145] and then affects an already unstable solution. In other words, the Hopf bifurcations of the one-mode solution, which coincide with those of the single-mode DOPO with injected signal, are always preceded by other bifurcations genuine of the driven 2tmDOPO, and then play no role in our case. While we have not extended this analytical proof to arbitrary values of φ_i , we have convinced ourselves through a numerical study, that its validity is general: The only bifurcations affecting the one-mode solution are the turning point bifurcation TP1, and the pitchfork bifurcation PB that gives rise to the switch on of the mode $H_{01}(k_s; \mathbf{r}_\perp, z)$. In Figure 9.2 we exemplify these results for two sets of parameters.

9.2.2 The two-mode solution

Next we consider the case $\beta_y \neq 0$, which is genuine of the present driven 2tmDOPO model. After simple but tricky algebra one finds $\beta_0 = -\exp(2i\varphi_i)$ (the intracavity pump intensity $|\beta_0|^2 = 1$ is clamped as usual in OPOs after a bifurcation is crossed),

$$\varphi_y = \varphi_i \pm \frac{\pi}{2}, \quad \tan(\varphi_x - \varphi_i) = -\frac{4\sigma}{\mathcal{I}_i} \sin(2\varphi_i), \quad (9.13)$$

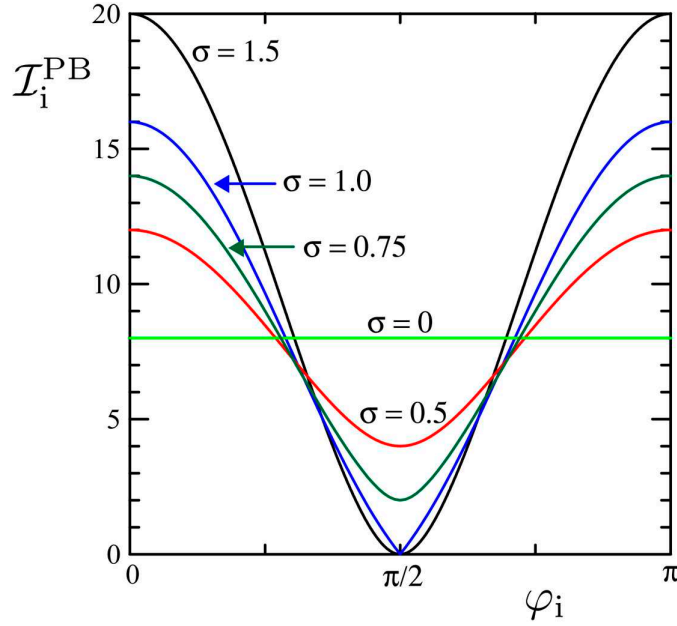


Fig. 9.3: $\mathcal{I}_i^{\text{PB}}$ as a function of the injected field phase φ for the indicated values of σ , see (9.11). Above this value of the injected intensity the non-injected TEM_{01} mode is switched on. Note that for $\sigma > 1$ and $\varphi = \pi/2$ there is no threshold for the generation of the TEM_{01} mode.

with the constrain $(\varphi_x - \varphi_i) \in [-\frac{\pi}{2}, \frac{\pi}{2}]$, and

$$I_x = \frac{\mathcal{I}_i}{4} + \frac{4\sigma^2}{\mathcal{I}_i} \sin^2 2\varphi_i, \quad (9.14a)$$

$$I_y = \frac{\mathcal{I}_i}{4} - \frac{4\sigma^2}{\mathcal{I}_i} \sin^2 2\varphi_i - 2[1 + \sigma \cos 2\varphi_i]. \quad (9.14b)$$

Note that the phase of the mode $H_{01}(k_s; \mathbf{r}_\perp, z)$, φ_y , can take any of two opposite values (this residual discrete symmetry survives even with the injection of the TEM_{10} mode), see (9.13); in other words, the sign of β_y can be either, as usual in DOPOs above threshold.

For this solution to exist I_y must be a positive real —note that $I_x > 0$ always, as follows from (9.14a)—. From (9.14b) the condition $I_y > 0$ is seen to be equivalent to $I_x > I_x^{\text{PB}}$ or, alternatively, $\mathcal{I}_i > \mathcal{I}_i^{\text{PB}}$, as expected: At the pitchfork bifurcation the two-mode solution is born.

In Figure 9.3 we show the dependence on φ_i of $\mathcal{I}_i^{\text{PB}}$ for several values of σ . In the absence of pump ($\sigma = 0$) $\mathcal{I}_i^{\text{PB}}$ is independent of the injection's phase φ_i as no reference phase exists in this case. For $\sigma \neq 0$ the threshold has a maximum in the case of amplification ($\varphi_i = 0$) and a minimum in the case of attenuation ($\varphi_i = \pi/2$). Interestingly, this minimum is zero when the external pump is above the free-running 2tmDOPO threshold ($\sigma > 1$). These results are actually quite intuitive: In the attenuation case, $\varphi_i = \pi/2$, the injected mode $H_x(\mathbf{r})$ is depleted as it has the ‘wrong’ phase, a fact that makes easier the amplification of the orthogonal mode $H_{01}(k_s; \mathbf{r}_\perp, z)$, while the amplification case $\varphi_i = 0$ is obviously detrimental for mode $H_{01}(k_s; \mathbf{r}_\perp, z)$ as mode $H_{10}(k_s; \mathbf{r}_\perp, z)$ is being amplified.

This two-mode solution does not correspond to a HG mode as it consists of the superposition of two orthogonal HG modes with different amplitudes and phases. Curiously, in the special case $\varphi_i = \pi/2$ and $\sigma = 1$, equations (9.14) imply that $\beta_x = \pm i\beta_y$, with $\beta_x = \frac{1}{2}\sqrt{\mathcal{I}_i}e^{i\varphi_i}$. This is also true for any φ_i value for sufficiently strong injection \mathcal{I}_i . This means that in these cases the emitted mode is a pure LG mode with +1 or -1 OAM, see Eq. (7.19), which is a somewhat unexpected result.

As for the linear stability analysis of this two-mode solution one gets a sixth order characteristic polynomial for the eigenvalue λ from which no conclusions can be drawn in general. However in the special cases $\varphi_i = 0$ and $\varphi_i = \pi/2$ the polynomial gets factorized giving rise to two cubic equations of the form $0 = P_{1,2}(\lambda)$, with

$$P_1(\lambda) = \lambda^3 + (\kappa + 2)\lambda^2 + \frac{\kappa}{2}(\mathcal{I}_i \mp 4\sigma)\lambda + \frac{\kappa}{2}\mathcal{I}_i, \quad (9.15)$$

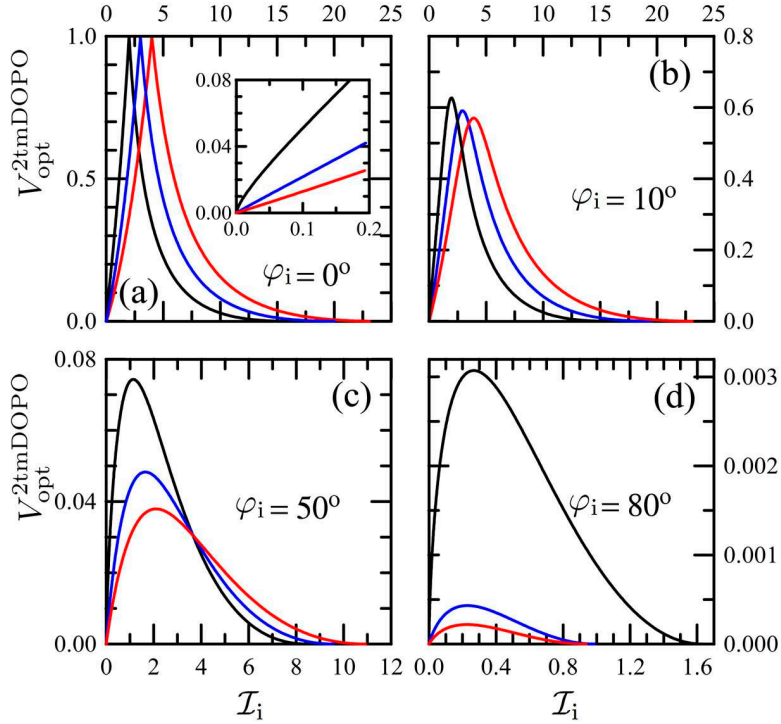


Fig. 9.4: Dependence of the optimal noise spectrum $V_{\text{opt}}^{2\text{tmDOPO}}$, Eq. (9.22b), on the injected intensity \mathcal{I}_i for the four values of the injection phase φ_i indicated at each figure. For each of φ_i , three values of σ have been plotted, namely $\sigma = 1$ (black), 1.5 (blue), and 2 (red), which correspond to the upper, middle and lower curves at the left of the maxima, respectively. Notice the different scales in each figure.

and $P_2(\lambda) = P_1(\lambda) \mp 4\kappa(\sigma + 1)$, where the upper (lower) signs of the polynomials correspond to the case $\varphi_i = 0$ ($\varphi_i = \pi/2$). It is now easy to demonstrate that all eigenvalues have negative real part when $\mathcal{I}_i > \mathcal{I}_i^{\text{PB}}$: By taking $\lambda = i\Omega$ in the above polynomials one obtains the frequency at the bifurcations (if any) and the values of the injected signal strength \mathcal{I}_i leading to instabilities. It is easy to see that these bifurcations occur for $\mathcal{I}_i < \mathcal{I}_i^{\text{PB}}$ (where the solution does not exist) and hence the two-mode solution is stable within its whole domain of existence. Through a numerical study of the characteristic polynomials for arbitrary injection phase φ_i we have convinced ourselves that this conclusion holds always.

9.2.3 Summary

In order to have a global picture of the steady states and their stability, what is necessary in order to perform the quantum analysis, we summarize the general results obtained up to now. After all, the picture is very simple, see Figure 9.2.

On one hand the one-mode solution (with mode $H_{01}(k_s; \mathbf{r}_\perp, z)$ off) is stable from the null injection point $\mathcal{I}_i = 0$ till the pitchfork bifurcation point at $\mathcal{I}_i = \mathcal{I}_i^{\text{PB}}$. For $\sigma < 1$ this comprises the single branch existing between these points (Figure 9.1), while for $\sigma > 1$ the stable domain extends from the turning point TP1 along the upper branch till the pitchfork bifurcation point PB (Figure 9.1). No other instabilities affect this solution. On the other hand the two-mode solution is born at the pitchfork bifurcation point $\mathcal{I}_i = \mathcal{I}_i^{\text{PB}}$ and is stable for any injection intensity $\mathcal{I}_i > \mathcal{I}_i^{\text{PB}}$.

9.3 Quantum properties of the non-injected mode

In this section we study the squeezing properties of the system by linearizing the Langevin equations (9.2). We are specially interested in the squeezing properties of the TEM₀₁ mode (as it corresponds to the dark mode in the free-running configuration). Moreover, once we move above the threshold for its classical generation, we expect it to approach a coherent state and hence we focus on the region where its mean field is still zero, that is, we focus on the one-mode solution (Section 9.2.1).

As usual, we write $\beta_m = \bar{\beta}_m + b_m$, where the overbar indicates steady state and b_m is an order g fluctuation. Then, considering the one-mode solution ($\bar{\beta}_y = 0$), the equations (9.2) can be linearized as

$$\dot{\mathbf{b}}_{0x} = \mathcal{L}_{0x} \mathbf{b}_{0x} + g\sqrt{I_0} \zeta_{0x}(t), \quad (9.16a)$$

$$\dot{\mathbf{b}}_y = \mathcal{L}_y \mathbf{b}_y + g\sqrt{I_0} \zeta_y(t), \quad (9.16b)$$

where $\mathbf{b}_{0x} = \text{col}(b_0, b_0^+, b_x, b_x^+)$, $\mathbf{b}_y = \text{col}(b_y, b_y^+)$,

$$\mathcal{L}_x = \begin{pmatrix} -\kappa & 0 & -\kappa\bar{\beta}_x & 0 \\ 0 & -\kappa & 0 & -\kappa\bar{\beta}_x^* \\ \bar{\beta}_x^* & 0 & -1 & \bar{\beta}_0 \\ 0 & \bar{\beta}_x & \bar{\beta}_0^* & -1 \end{pmatrix}, \quad (9.17a)$$

$$\mathcal{L}_y = \begin{pmatrix} -1 & \bar{\beta}_0 \\ \bar{\beta}_0^* & -1 \end{pmatrix}, \quad (9.17b)$$

and the noise vectors read

$$\zeta_{0x} = \text{col}\left(0, 0, e^{i\varphi_0/2} \zeta_x, e^{-i\varphi_0/2} \zeta_x^+\right), \quad (9.18a)$$

$$\zeta_y = \text{col}\left(e^{i\varphi_0/2} \zeta_y, e^{-i\varphi_0/2} \zeta_y^+\right). \quad (9.18b)$$

The procedure we follow below is the same we have used elsewhere in the previous chapters: We project quantum fluctuations onto the eigenvectors of the Hermitian matrix \mathcal{L}_y , as these projections are, up to a constant factor, the relevant quadratures of the output TEM₀₁ mode (those that are maximally squeezed or antisqueezed). The eigensystem of matrix \mathcal{L}_y ($\mathcal{L}_y \cdot \mathbf{w}_i = \lambda_i \mathbf{w}_i$) comprises the eigenvalues $\lambda_{1,2}$ given in (9.10) and the associated eigenvectors

$$\mathbf{w}_{1,2} = \left(e^{i\varphi_0/2}, \mp e^{-i\varphi_0/2}\right) / \sqrt{2}, \quad (9.19)$$

with φ_0 given by Eq. (9.8b). Defining the projections $c_y^{(j)} = \mathbf{w}_j^* \cdot \mathbf{b}_y$, we obtain the following decoupled equations

$$\dot{c}_y^{(j)} = \lambda_j c_y^{(j)} + g\sqrt{I_0} \zeta_y^{(j)}(t), \quad (9.20)$$

where we defined the standard real white Gaussian noises $\zeta_y^{(1,2)} = (\zeta_y \mp \zeta_y^+) / \sqrt{2}$. It is then trivial to obtain

$$x_y^{\varphi_0/2} = \sqrt{2} c_y^{(2)}, \quad x_y^{\varphi_0/2+\pi/2} = -i\sqrt{2} c_y^{(1)}. \quad (9.21)$$

After integration of (9.20) —see Appendix B— and substitution into the stationary squeezing spectrum (6.54), we obtain

$$V^{\text{out}}\left(\hat{X}_y^{\varphi_0/2}; \Omega\right) = 1 + \frac{4\sqrt{I_0}}{(1 - \sqrt{I_0})^2 + \tilde{\Omega}^2}, \quad (9.22a)$$

$$V^{\text{out}}\left(\hat{Y}_y^{\varphi_0/2}; \Omega\right) = 1 - \frac{4\sqrt{I_0}}{(1 + \sqrt{I_0})^2 + \tilde{\Omega}^2}. \quad (9.22b)$$

The only quadrature that can be perfectly squeezed ($V^{\text{out}} = 0$) is $Y_y^{\varphi_0/2}$ at $\Omega = 0$ when $I_0 = 1$ (quadrature $X_y^{\varphi_0/2}$ exhibits antisqueezing). According to (9.8) and (9.6) this happens only in two cases: Either at the turning point TP1 ($\mathcal{I}_i = 0$, no injection, where there exists perfect squeezing because of the rotational symmetry breaking occurring in the free-running 2tmDOPO at any $\sigma > 1$), or when $\mathcal{I}_i = \mathcal{I}_i^{\text{PB}}$, which corresponds to the pitchfork bifurcation where mode $H_{01}(k_s; \mathbf{r}_\perp, z)$ is switched on. Figure 9.4 shows the dependence on the injected intensity \mathcal{I}_i of the optimal squeezing level $V_{\text{opt}}^{\text{2tmDOPO}} \equiv V^{\text{out}}(\hat{Y}_y^{\varphi_0/2}; \Omega = 0)$, see Eq. (9.22b), for several values of the pump level σ and the injection phase φ_i .

In terms of the injection's external power, see (9.5), (9.3) and (4.40), the injection intensity parameter \mathcal{I}_i reads

$$\mathcal{I}_i = \frac{\chi^2 |\mathcal{E}_s|^2}{\gamma_s^3 \gamma_p} = 2 \frac{P_s}{P_{p,\text{thr}}}, \quad (9.23)$$

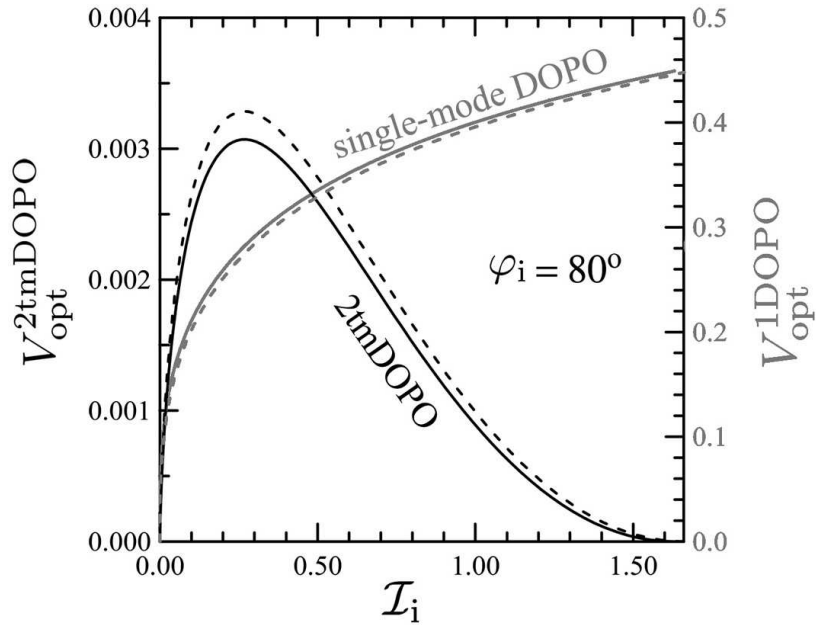


Fig. 9.5: Comparison between the optimum squeezing levels of the 2tmDOPO with injected signal, $V_{\text{opt}}^{2\text{tmDOPO}}$ (black lines, left vertical axis), and that of the single-mode DOPO, $V_{\text{opt}}^{1\text{DOPO}}$ (grey lines, right vertical axis), as a function of the injected intensity \mathcal{I}_i . We have taken $\varphi_i = 80^\circ$ and two values of σ : $\sigma = 1$ (full lines) and $\sigma = 0.99$ (dashed lines).

where $P_{p,\text{thr}}$ is the usual DOPO threshold pump power, that is, the pump power needed for making the signal field oscillate when no injection is used ($\mathcal{I}_i = 0$), which can be found from (4.40) with $|\mathcal{E}_{p,\text{thr}}|^2 = (\gamma_s \gamma_p / \chi)^2$ as follows from the threshold condition $\sigma = 1$; P_s is the actual injection power. In usual experiments, when the injected seed is used for active locking purposes, P_s is a small fraction of $P_{p,\text{thr}}$ (say 0.001 – 0.1); this is the reason why we show a zoom of the region $\mathcal{I}_i \in [0, 0.2]$ in Figure 9.4a (the enlargement is representative of what happens in the rest of cases represented in Figures 9.4). It is remarkable the very small squeezing degradation that the injected field induces in the 2tmDOPO model, specially close to attenuation ($\varphi_i = \pi/2$).

A relevant issue is how this squeezing level compares with the usual single-mode DOPO with injected signal, whose optimal squeezing level is calculated in [145], and is in particular given by Eq. (187) in that paper under the following substitutions, in order to adapt the expression to our notation: $\{A_0, A_1, \Delta_0, \Delta_1, E, e, \gamma, \} \rightarrow \{\beta_0, \beta_x/\sqrt{2}, 0, 0, \sigma, \varepsilon_i/\sqrt{2}, \kappa^{-1}\}$. This comparison is made in Figure 9.5, where we represent in the same plot the optimal squeezing level both for the 2tmDOPO and the single-mode DOPO with injected signal. That of the single-mode DOPO, $V_{\text{opt}}^{1\text{DOPO}}$, is shown in the limit $\kappa \rightarrow \infty$, which is a common limit from the experimental viewpoint and yields its best noise reduction (the 2tmDOPO squeezing level, on the other hand, does not depend on κ). As compared with the usual single-mode DOPO we observe that the squeezing level of the 2tmDOPO is quite insensitive to the injection (note the different scales for both quantities). As well as that, by increasing \mathcal{I}_i from zero, the squeezing first degrades but, in the 2tmDOPO, it improves again unlike the single-mode DOPO case. We want to stress that the squeezing level in a single-mode DOPO is highly sensitive to the pumping level σ (only very close to $\sigma = 1$ the squeezing is high), while in the case of the 2tmDOPO large squeezing levels can be found for any σ . This phenomenon is directly related to the rotational symmetry breaking which is the origin of the perfect, noncritical squeezing occurring for any $\sigma > 1$ for null injection. We can conclude that adding a small injection to a 2tmDOPO could be useful to improve the levels of squeezing available with single-mode DOPOs.

10. TYPE II OPO: POLARIZATION SYMMETRY BREAKING AND FREQUENCY DEGENERACY

In the previous chapters we have studied in depth the phenomenon of spontaneous symmetry breaking via a particular example: The rotational symmetry breaking which happens in the transverse plane of a 2tmDOPO (as well as any DOPO tuned to an odd family at the signal frequency, as proved in the next chapter). We have analyzed many features which are important both from the theoretical and experimental points of view, showing the phenomenon to be quite robust. It is then natural to try to generalize the phenomenon to other types of symmetries, in particular to symmetries whose associated free parameters are in the polarization or temporal degrees of freedom of the light coming out of the OPO.

In this chapter we introduce the phenomenon of spontaneous polarization symmetry breaking (the temporal one will be outlined in the next and final chapter, where we will discuss the outlook of the research developed in this thesis). The phenomenon will be analyzed in a system that we already dealt with: The frequency degenerate type II OPO introduced in Section 6.4. We will show it to be completely analogous to the 2tmDOPO, just changing the ± 1 orbital angular momentum modes by the two linearly polarized modes within the ordinary and extraordinary axes; the free parameter in this case will correspond to a continuous parameter in the polarization ellipse of the outgoing signal field. So much as in the 2tmDOPO, we will then be able to define bright and dark polarization modes, and rephrase all the properties that we found for them in the 2tmDOPO to the case of the frequency degenerate type II OPO.

The study of this system will also allow us to tackle a major problem in OPOs: It is quite difficult to ensure working at exact frequency degeneracy above threshold (both in type I and II), as we already discussed briefly in Section 6.1.2. In [157] it was proposed a way of locking the frequencies of the signal and idler modes in type II OPOs by introducing a wave-plate with its fast axis rotated respect to the ordinary-extraordinary axes (see also [158] for the quantum analysis of the system and [38] for the experiments); we will show that the same locking can be accomplished by injecting an external laser field with the right polarization.

10.1 Spontaneous polarization symmetry breaking

In Section 6.4 we already studied the properties of OPOs in which signal and idler are distinguishable, as is the case of frequency degenerate type II OPOs, where signal and idler have orthogonal linear polarizations. In that section we showed that signal and idler share EPR-like correlations below threshold, which become perfect exactly at threshold. Above threshold, we only studied the signal-idler intensity correlations, what we did by neglecting the quantum diffusion of their phase difference, arguing that it does not affect the results on intensity correlations at all. On the other hand, in Chapter 7, and Section 7.2.2 in particular, we developed a method for studying this phase diffusion when analyzing the 2tmDOPO, which actually has the same evolution equations as type II OPOs—just compare (7.26) with (6.96)—. In this section we are going to translate all the results found in the 2tmDOPO to the frequency degenerate type II OPO, showing how their properties can be interpreted in terms of spontaneous polarization symmetry breaking.

Let us first write the part of the down-converted (signal+idler) field propagating to the right as (Schrödinger picture is understood)

$$\hat{\mathbf{E}}_{\text{DC},\rightarrow}^{(+)}(\mathbf{r}) = i\sqrt{\frac{\hbar\omega_s}{4\epsilon_0 n_s L_s}}(\mathbf{e}_e \hat{a}_s + \mathbf{e}_o \hat{a}_i)G(k_s; \mathbf{r}_\perp, z)e^{in_s k_s z}, \quad (10.1)$$

where we have made the (unrealistic) approximation $n_s = n_i$ for simplicity, see (6.29); in a moment it will be clear that this approximation is not relevant at all, except for some quantitative considerations that we will explain later on.

Taking into account that the classical solution of the system above threshold is given by (6.99)

$$\bar{\beta}_p = 1, \quad \bar{\beta}_{s,i} = \sqrt{\sigma - 1} \exp(\mp i\theta), \quad (10.2)$$

where θ is arbitrary, that is, it is not fixed by the classical equations of motion, the form of the field in the classical limit can be obtained by taking the expectation value of (10.1) and making the correspondence $\langle \hat{a}_{s,i}(t) \rangle = \exp(-i\omega_0 t) \beta_{s,i}/g$, arriving to

$$\bar{\mathbf{E}}_{\text{DC},\rightarrow}^{(+)}(\mathbf{r}, t) = i \sqrt{\frac{\hbar \omega_s (\sigma - 1)}{4 \varepsilon_0 n_s L_s g}} (e^{-i\theta} \mathbf{e}_e + e^{+i\theta} \mathbf{e}_o) G(k_s; \mathbf{r}_\perp, z) e^{-i\omega_0 t + i n_s k_s z} \propto \boldsymbol{\varepsilon}(\theta, \varphi = \pi/4), \quad (10.3)$$

where the general parametrization of the polarization vector $\boldsymbol{\varepsilon}(\theta, \varphi)$ is given in (3.27). This shows that the down-converted field can arise with any of the polarizations depicted in Figure 3.2, that is, polarized along the $+45^\circ$ or -45° axis, and with arbitrary eccentricity and elicity. Hence, the system poses an invariance related to a polarization degree of freedom¹, which is spontaneously broken once the OPO starts emitting the down-converted field, just as commented above.

Just as in the 2tmDOPO, we can thus define a bright polarization mode $\boldsymbol{\varepsilon}(\theta, \varphi = \pi/4) = (e^{-i\theta} \mathbf{e}_e + e^{+i\theta} \mathbf{e}_o)/\sqrt{2}$ in which mean field emission takes place, and a dark polarization mode $\boldsymbol{\varepsilon}(\theta + \pi/2, \varphi = \pi/4) = -i(e^{-i\theta} \mathbf{e}_e - e^{+i\theta} \mathbf{e}_o)/\sqrt{2}$ which is empty of photons at the classical level.

As for the quantum properties of the down-converted field, they can also be directly enunciated without the need of further calculations by exploiting the analogy with the 2tmDOPO: (i) Quantum noise makes θ , and hence the polarization of the bright mode, diffuse (see Section 7.2.2); (ii) the dark mode has all the properties described in Section 7.2.2 and Chapter 8, for example, its Y quadrature—which is the one detected by a local oscillator with polarization $i\partial_\theta \boldsymbol{\varepsilon}(\theta, \varphi = \pi/4)$ —is perfectly squeezed irrespective of the system parameters. All these results are then in concordance with the general picture of spontaneous symmetry breaking introduced in Section 7.2.1.

This spontaneous polarization symmetry breaking phenomenon was introduced in [35], where we proposed its observation also in a Kerr resonator, where the generation of frequency degenerate cross-polarized twin beams has been accomplished without the need of breaking any invariance of the system [159], as opposed to the state of the art in OPOs, see below.

10.2 From nondegenerate to degenerate operation

In the previous section we have assumed that the type II OPO works at exact frequency degeneracy. As explained in 6.1.2 the phase-matching conditions ensuring that it is the degenerate process the one with larger gain (lowest threshold) are quite critical; for example, in the case of [160], where the authors are able to make the frequency difference between signal and idler as small as 150 kHz for a cavity with an 8 GHz free spectral range and a 6 MHz linewidth (loss rate), variations of the cavity length on the order of the nanometer can change the oscillation frequencies of signal and idler (mode-hopping).

In practice, this means that it is not possible to work at exact frequency degeneracy without additional locking techniques that break the phase invariance of the OPO. The pioneering example of such locking techniques was performed by Fabre and collaborators [157, 158, 38]. Their idea was to introduce in the resonator a $\lambda/4$ plate with its fast axis misaligned respect to the extraordinary axis of the nonlinear crystal. For small misalignments, the effect of this plate is to introduce a coupling between the signal and idler modes described by the Hamiltonian

$$\hat{H}_P = i\hbar(\mu_P \hat{a}_s \hat{a}_i^\dagger - \mu_P^* \hat{a}_s^\dagger \hat{a}_i), \quad (10.5)$$

where μ_P is some complex parameter. It was then shown in [157] that in a given region of the parameter space (in particular of the detunings of signal and idler) the frequencies of signal and idler get locked to half the pump frequency; this OPO is known as the *self-phase-locked OPO*, which was already tested experimentally in [38].

Note that, as mentioned above, this self-locking effect is accomplished by breaking the symmetry $\{\hat{a}_s, \hat{a}_i\} \rightarrow \{\exp(-i\theta)\hat{a}_s, \exp(i\theta)\hat{a}_i\}$ of the OPO—check that the Hamiltonian (10.5) does not possess this symmetry—, and hence a degradation of the signal-idler intensity correlations, as well as of the noncritical squeezing induced by spontaneous polarization symmetry breaking described above are to be expected. For example, in [38] the intensity-difference fluctuations were reduced by an 89% respect to the vacuum level prior to the introduction of the plate; then, after obtaining frequency degeneracy through the self-phase-locking mechanism this noise reduction fell down to a more humble 65%.

¹ When $n_s > n_i$ is taken into account, the situation is similar qualitatively, but not quantitatively. In particular, the polarization of the mean field is in this case

$$\boldsymbol{\varepsilon}(\theta_{\text{si}}, \varphi_{\text{si}}) = \mathbf{e}_e \exp[-i\theta_{\text{si}}(z)] \cos \varphi_{\text{si}} + \mathbf{e}_o \exp[i\theta_{\text{si}}(z)] \sin \varphi_{\text{si}}, \quad (10.4)$$

with $\theta_{\text{si}}(z) = \theta - (n_s - n_i)k_0 z/2$ and $\tan \varphi_{\text{si}} = \sqrt{n_s L_s / n_i L_i}$ ($\varphi_{\text{si}} \in [0, \pi/2]$). This means that the polarization has still a free parameter, θ , but is more complicated than the one explained in the text. Indeed, owed to z -dependence of θ_{si} , the polarization changes depending on the exact longitudinal point that we observe inside the crystal (this is actually a quite expected result, as the crystal is birefringent and hence the ordinary and extraordinary components of the field acquire different phases upon propagation through the crystal).

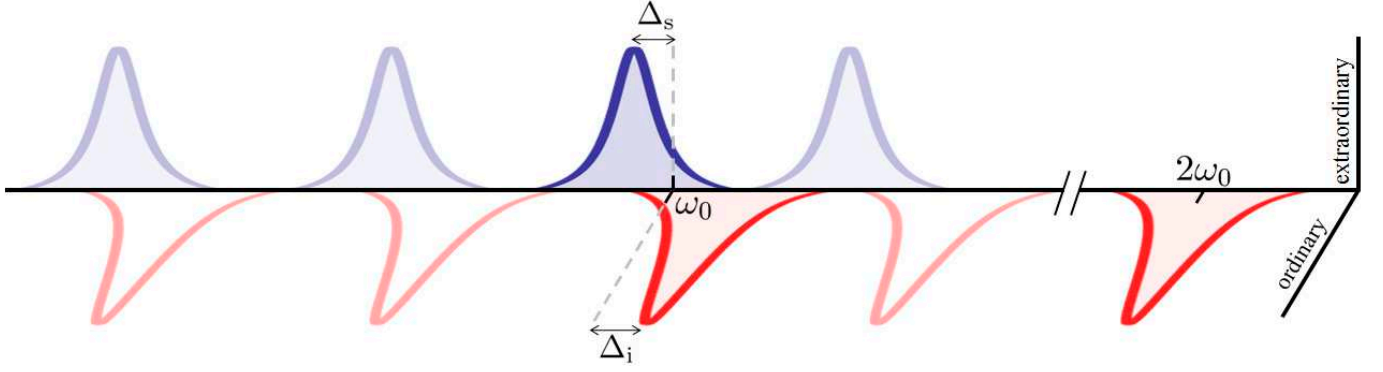


Fig. 10.1: Resonance scheme of the type II OPO in which we propose to obtain frequency degeneracy via an external injection at the degenerate frequency ω_0 .

In this section we introduce an alternative frequency–locking mechanism, based on the injection of an external beam at the degenerate frequency [37]. We will call *actively–phase–locked OPO* to such OPO configuration. The model for this system follows from the resonance scheme sketched in Figure 10.1. The signal and idler modes are already close to frequency degeneracy [160] and we inject an external laser field at the degenerate frequency ω_0 with arbitrary polarization $\boldsymbol{\varepsilon}_L = e^{-i\theta_L} \cos \varphi_L \mathbf{e}_e + e^{+i\theta_L} \sin \varphi_L \mathbf{e}_o$, see (3.27). In terms of the signal and idler boson operators, the corresponding injection Hamiltonian is given by

$$\hat{H}_{\text{inj-si}} = i\hbar(\mathcal{E}_s a_s^\dagger + \mathcal{E}_i a_i^\dagger) \exp(-i\omega_0 t) + \text{H.c.}, \quad (10.6)$$

with $\mathcal{E}_s = \mathcal{E}_L e^{-i\theta_L} \cos \varphi_L$ and $\mathcal{E}_i = \mathcal{E}_L e^{+i\theta_L} \sin \varphi_L$, where the injection parameter for the mode with polarization $\boldsymbol{\varepsilon}_L$ (which is fed by the whole power P_{inj} of the injected field) is denoted by $\mathcal{E}_L = \sqrt{2\gamma_s P_{\text{inj}}/\hbar\omega_0} \exp(i\phi_L)$. ϕ_L is the phase of this signal injection relative to the pump injection.

Moving to the interaction picture defined by the transformation operator

$$\hat{U}_0 = \exp[\hat{H}_0 t/i\hbar] \quad \text{with} \quad \hat{H}_0 = \hbar\omega_0(2\hat{a}_p^\dagger \hat{a}_p + \hat{a}_s^\dagger \hat{a}_s + \hat{a}_i^\dagger \hat{a}_i), \quad (10.7)$$

the master equation of the system can be written as

$$\frac{d\hat{\rho}_I}{dt} = \left[-i\Delta_s \hat{a}_s^\dagger \hat{a}_s + i\Delta_i \hat{a}_i^\dagger \hat{a}_i + \chi \hat{a}_p \hat{a}_s^\dagger \hat{a}_i^\dagger + \mathcal{E}_p a_p^\dagger + \mathcal{E}_s a_s^\dagger + \mathcal{E}_i a_i^\dagger + \text{H.c.}, \hat{\rho}_I \right] + \sum_{j=p,s,i} \gamma_j (2\hat{a}_j \hat{\rho}_I \hat{a}_j^\dagger - \hat{a}_j^\dagger \hat{a}_j \hat{\rho}_I - \hat{\rho}_I \hat{a}_j^\dagger \hat{a}_j), \quad (10.8)$$

where we take $\gamma_s = \gamma_i$ as in (6.92), and the detunings $\Delta_s = \omega_0 - \omega_s$ and $\Delta_i = \omega_i - \omega_0$ are taken as positive by convention. As usual, we take \mathcal{E}_p as a positive real. The stochastic Langevin equations associated to this master equation are

$$\dot{\alpha}_p = \mathcal{E}_p - \gamma_p \alpha_p - \chi \alpha_s \alpha_i, \quad (10.9a)$$

$$\dot{\alpha}_p^+ = \mathcal{E}_p - \gamma_p \alpha_p^+ - \chi \alpha_s^+ \alpha_i^+, \quad (10.9b)$$

$$\dot{\alpha}_s = \mathcal{E}_s - (\gamma_s + i\Delta_s) \alpha_s + \chi \alpha_p \alpha_i^+ + \sqrt{\chi \alpha_p} \xi(t), \quad (10.9c)$$

$$\dot{\alpha}_s^+ = \mathcal{E}_s - (\gamma_s - i\Delta_s) \alpha_s^+ + \chi \alpha_p^+ \alpha_i + \sqrt{\chi \alpha_p^+} \xi^+(t), \quad (10.9d)$$

$$\dot{\alpha}_i = \mathcal{E}_i - (\gamma_s - i\Delta_i) \alpha_i + \chi \alpha_p \alpha_s^+ + \sqrt{\chi \alpha_p} \xi^*(t), \quad (10.9e)$$

$$\dot{\alpha}_i^+ = \mathcal{E}_i - (\gamma_s + i\Delta_i) \alpha_i^+ + \chi \alpha_p^+ \alpha_s + \sqrt{\chi \alpha_p^+} [\xi^+(t)]^*, \quad (10.9f)$$

which are just as (6.93), but including the parameters associated to the external injection.

We will be interested only in the classical behavior of the system, as our main intention is to show that signal–idler frequency–locking can be accomplished with this scheme. Moreover, we will be working in the $\gamma_p \gg \gamma_s$ limit, where the pump variables can be adiabatically eliminated. Let us then directly write the classical equations governing the evolution of the system in this limit, which are obtained from the Langevin equations by setting the noises and the

pump time derivatives to zero, and making the identifications $\alpha_j^+ \rightarrow \alpha_j^*$. As usual, we also redefine time as $\tau = \gamma_s t$ and the coherent amplitudes as

$$\beta_s = g\alpha_s \exp(i\theta_L) \quad \text{and} \quad \beta_i = g\alpha_i \exp(-i\theta_L), \quad (10.10)$$

so that the final equations read

$$\dot{\beta}_s = \varepsilon_s e^{i\phi_L} - \left(1 + i\tilde{\Delta}_s\right) \beta_s + (\sigma - \beta_s \beta_i) \beta_i^*, \quad (10.11a)$$

$$\dot{\beta}_i = \varepsilon_i e^{i\phi_L} - \left(1 - i\tilde{\Delta}_i\right) \beta_i + (\sigma - \beta_s \beta_i) \beta_s^*, \quad (10.11b)$$

where we have defined the parameters

$$\varepsilon_s = \frac{g}{\gamma_s} |\mathcal{E}_L| \cos \varphi_L, \quad \varepsilon_i = \frac{g}{\gamma_s} |\mathcal{E}_L| \sin \varphi_L, \quad \text{and} \quad \tilde{\Delta}_j = \Delta_j / \gamma_s, \quad (10.12)$$

while the parameters g and σ are defined as usual, see (6.53). Note that these equations are invariant under changes of θ_L , and hence, the dynamics of the system are only sensitive to the parameter φ_L of the injection's polarization.

In order to get some analytic insight, we are going to simplify the problem to what we will call *symmetric configuration* of the actively-phase-locked OPO: We assume the detunings to be equal, $\tilde{\Delta}_s = \tilde{\Delta}_i = \tilde{\Delta}$, and inject with $\varphi_L = \pi/4$ (arbitrary polarization ellipse along the $\pm 45^\circ$ axis), so that signal and idler get equally pumped, $\varepsilon_s = \varepsilon_i \equiv \sqrt{\mathcal{I}}$. We also choose to inject in phase with the pump injection, that is, $\phi_L = 0$. With these simplifications equations (10.11) are reduced to

$$\dot{\beta}_s = \sqrt{\mathcal{I}} - \left(1 + i\tilde{\Delta}\right) \beta_s + (\sigma - \beta_s \beta_i) \beta_i^*, \quad (10.13a)$$

$$\dot{\beta}_i = \sqrt{\mathcal{I}} - \left(1 - i\tilde{\Delta}\right) \beta_i + (\sigma - \beta_s \beta_i) \beta_s^*. \quad (10.13b)$$

These equations have the symmetry $\{\beta_s \rightarrow \beta_i^*, \beta_i \rightarrow \beta_s^*\}$, what allows us to look for symmetric stationary solutions of the type

$$\bar{\beta}_s = \bar{\beta}_i^* = \sqrt{\mathcal{I}} \exp(i\varphi). \quad (10.14)$$

Note that whenever this solution exists (and is stable), the classical down-converted field emitted by the OPO will be

$$\bar{\mathbf{E}}_{\text{DC},\rightarrow}^{(+)}(\mathbf{r}) = i \sqrt{\frac{\hbar \omega_s \mathcal{I}}{4\varepsilon_0 n_s L_s g^2}} (e^{-i(\theta_L - \varphi)} \mathbf{e}_e + e^{i(\theta_L - \varphi)} \mathbf{e}_o) G(k_s; \mathbf{r}_\perp, z) e^{-i\omega_0 t + i n_s k_s z}, \quad (10.15)$$

where we have used (10.1) and made the correspondence $\langle \hat{a}_{s,i}(t) \rangle = \exp(-i\omega_0 t) \bar{\beta}_{s,i} / g$. As expected, this corresponds to a field oscillating at the degenerate frequency ω_0 . Moreover, the polarization of this field (which is always within the $\pm 45^\circ$ axis) can always be chosen as linear by selecting a proper θ_L tuned to φ . In the remaining of this section we study the conditions under which this solution exists and is stable.

It is completely trivial to show from (10.13) that the intensity I of the symmetric solution satisfies the third order polynomial

$$\mathcal{I} = [(I + 1 - \sigma)^2 + \tilde{\Delta}^2] I, \quad (10.16)$$

while its phase φ is uniquely determined from I as

$$\varphi = \arg\{I + 1 - \sigma - i\tilde{\Delta}\}. \quad (10.17)$$

Now, so much as happened in the previous chapter (see Figure 9.1), the polynomial (10.16) sometimes has a single positive definite solution, while sometimes its three roots are positive definite. By solving the equation $\partial \mathcal{I} / \partial I = 0$, it is simple to show that the turning points I_\pm have the expression

$$I_\pm = \frac{2}{3}(\sigma - 1) \pm \frac{1}{3} \sqrt{(\sigma - 1)^2 - 3\tilde{\Delta}^2} \quad (10.18)$$

and hence, they exist only for $\sigma > 1 + \sqrt{3}\tilde{\Delta}$. For $\sigma \leq 1 + \sqrt{3}\tilde{\Delta}$ the solution is therefore single-valued.

In order to analyze the stability of this symmetric solution, we will change to a new polarization basis

$$\varepsilon_b = \frac{1}{\sqrt{2}} (e^{-i(\theta_L - \varphi)} \mathbf{e}_e + e^{i(\theta_L - \varphi)} \mathbf{e}_o) \quad \text{and} \quad \varepsilon_d = \frac{1}{\sqrt{2}i} (e^{-i(\theta_L - \varphi)} \mathbf{e}_e - e^{i(\theta_L - \varphi)} \mathbf{e}_o), \quad (10.19)$$

where ε_b corresponds to the polarization mode excited by the symmetric solution (10.14) and ε_d to its orthogonal, that is, to the bright and dark modes of the system. The corresponding coherent amplitudes are written as

$$\beta_b = \frac{1}{\sqrt{2}}(e^{-i\varphi}\beta_s + e^{i\varphi}\beta_i) \quad \text{and} \quad \beta_d = \frac{i}{\sqrt{2}}(e^{-i\varphi}\beta_s - e^{i\varphi}\beta_i), \quad (10.20)$$

and satisfy the evolution equations

$$\dot{\beta}_b = \sqrt{2\mathcal{I}} \cos \varphi - \beta_b + \tilde{\Delta}\beta_d + (\sigma - \beta_b^2/2 - \beta_d^2/2)\beta_b^*, \quad (10.21a)$$

$$\dot{\beta}_d = -\sqrt{2\mathcal{I}} \sin \varphi - \beta_d - \tilde{\Delta}\beta_b + (\sigma - \beta_b^2/2 - \beta_d^2/2)\beta_d^*. \quad (10.21b)$$

In this new basis the symmetric solution reads

$$\bar{\beta}_b = \sqrt{2I}, \quad \bar{\beta}_d = 0, \quad (10.22)$$

and its associated stability matrix is

$$\mathcal{L} = \begin{bmatrix} -1 - 2I & \sigma - I & \tilde{\Delta} & 0 \\ \sigma - I & -1 - 2I & 0 & \tilde{\Delta} \\ -\tilde{\Delta} & 0 & -1 & \sigma - I \\ 0 & -\tilde{\Delta} & \sigma - I & -1 \end{bmatrix}. \quad (10.23)$$

The characteristic polynomial of this stability matrix can be factorized into two second order polynomials, namely $P_I(\lambda) = (\lambda + 1 + \sigma)^2 + \tilde{\Delta}^2 - I^2$ and $P_{II}(\lambda) = (\lambda + 1 - \sigma + 2I)^2 + \tilde{\Delta}^2 - I^2$. The bifurcation diagrams for the different parameter regions are shown in Figure 10.2; now we discuss them in depth.

Let us start by studying the instabilities predicted by the first polynomial, whose roots are given by

$$\lambda_{\pm}^I = -(1 + \sigma) \pm \sqrt{I^2 - \tilde{\Delta}^2}. \quad (10.24)$$

Therefore, the condition $\text{Re}\{\lambda_{\pm}^I\} = 0$ can only be satisfied for

$$I = \sqrt{(1 + \sigma)^2 + \tilde{\Delta}^2} \equiv I_{PB}. \quad (10.25)$$

The fact that the instability appears without imaginary part in the λ_{\pm}^I , and it is located in the upper branch of the S-shaped curve ($I_{PB} > I_+$ for any value of the parameters), signals that it corresponds to a Pitchfork bifurcation where a non-symmetric stationary solution $\{\beta_s = \sqrt{I_s} \exp(i\varphi_s), \beta_i = \sqrt{I_i} \exp(i\varphi_i)\}$ with $I_s \neq I_i$ borns (as we have checked numerically, see the grey lines in Figure 10.2). This bifurcation is equivalent to the one introduced in the previous chapter when studying the effects of a signal injection in the 2tmDOPO, and can be understood as a switching on of the dark mode.

As for the second polynomial, its roots are given by

$$\lambda_{\pm}^{II} = \sigma - 1 - 2I \pm \sqrt{I^2 - \tilde{\Delta}^2}. \quad (10.26)$$

Note that $\lambda_{\pm}^{II} = 0$ for $I = I_{\pm}$, that is, the turning points of the S-shaped curve signal an instability. It is then simple to check (for example numerically) that the whole middle branch connecting this instability points is unstable, as intuition says (see Figures 10.2c,d).

But λ_{\pm}^{II} has yet one more instability when

$$I = \frac{\sigma - 1}{2} \equiv I_{HB}. \quad (10.27)$$

At this instability the eigenvalues become purely imaginary, in particular, $\lambda_{\pm}^{II} = \pm i\omega_{HB}$ with $\omega_{HB} = \sqrt{\tilde{\Delta}^2 - (\sigma - 1)^2/4}$, and hence it corresponds to a Hopf bifurcation. Note that I_{HB} is negative for $\sigma < 1$, while ω_{HB} becomes imaginary for $\sigma > 1 + 2\tilde{\Delta}$, and hence the Hopf bifurcation only exists in the region $1 < \sigma < 1 + 2\tilde{\Delta}$. It is simple to check that I_{HB} is always below I_{PB} and I_- ; in particular, it borns at $I = 0$ for $\sigma = 1$, and climbs the $\mathcal{I} - I$ curve as σ increases until it dies at $I = I_-$ for $\sigma = 1 + 2\tilde{\Delta}$ (see Figures 10.2b,c,d). The portion of the curve with $I < I_{HB}$ is unstable, and no stationary solutions can be found there, as the stable states correspond in this case to periodic orbits (as we have checked numerically, see Figures 10.2b,c,d). This is also quite intuitive because when no injection is present, that is, for $\mathcal{I} = 0$, we know that the stable states of the OPO above threshold are the ones with the signal and idler beams oscillating at the non-degenerate frequencies $\omega_s = \omega_0 + \Delta$ and $\omega_i = \omega_0 - \Delta$, which in the picture we are working on means $\{\beta_s(\tau) \propto \exp(-i\tilde{\Delta}\tau), \beta_i(\tau) \propto \exp(i\tilde{\Delta}\tau)\}$.

This analysis proves that there exist regions in the parameter space where the frequencies of the signal and idler beams are locked to the degenerate one, and hence active-locking can be a good alternative to the self-locking technique already proposed for type II OPOs [157, 158, 38].

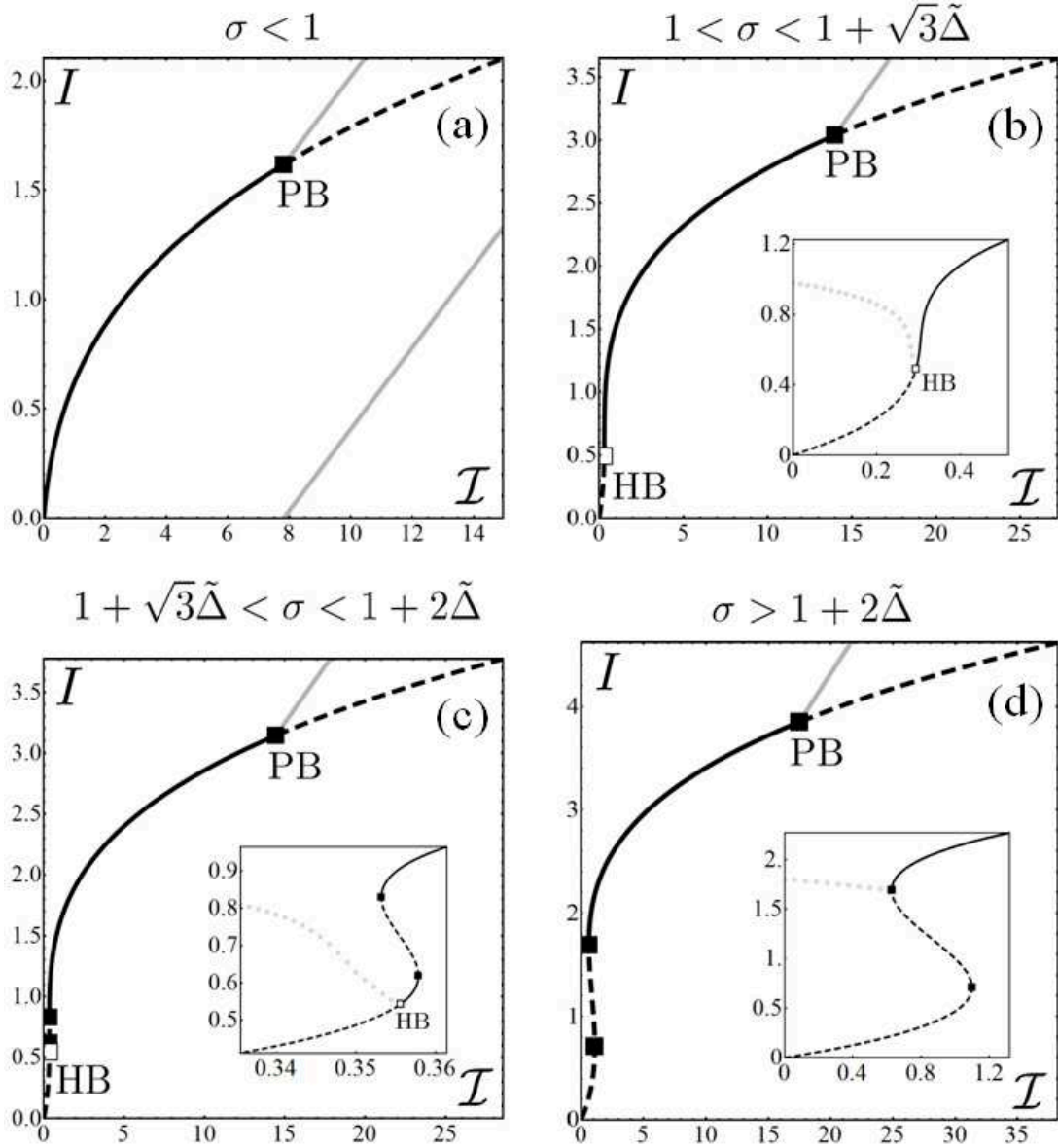


Fig. 10.2: Bifurcation diagrams of the type II OPO with an injected signal at the degenerate frequency, for the symmetric configuration $\tilde{\Delta}_s = -\tilde{\Delta}_i \equiv \tilde{\Delta}$ and $\varepsilon_s = \varepsilon_i \equiv \sqrt{\mathcal{I}}$; the value $\tilde{\Delta} = 0.6$ is chosen for all the figures (the same behavior is found for any other choice), while we set σ to 0.5 in (a), 1.98 in (b), 2.09 in (c), and 2.8 in (d). The black lines correspond to the intensity I of the stationary symmetric solution (10.14), the solid or dashed character of the lines meaning that this solution is stable or unstable, respectively. The upper and lower grey solid lines correspond to the values of $|\tilde{\beta}_b|^2/2$ and $|\tilde{\beta}_d|^2/2$, respectively, that is to half the intensity of the bright and dark (only showed in the $\sigma < 1$ case) modes; these lines have been found numerically, and show how above the pitchfork bifurcation (marked as PB in the figures) the symmetric solution (10.14) becomes unstable, and a new asymmetric solution is born. As explained in the text, for $\sigma > 1$ it is possible to find periodic solutions connecting the $\mathcal{I} = 0$ axis with the Hopf bifurcation (marked as HB in the figures); we have checked numerically that this periodic orbits exist, and moreover they are “symmetric”, that is, $\beta_s(t) = \beta_i^*(t)$. The grey circles correspond to the mean value of $|\beta_s|^2$ (half the sum between its maximum and its minimum of oscillation). Note that stable stationary solutions and periodic orbits coexist for $1 + \sqrt{3}\tilde{\Delta} < \sigma < 1 + 2\tilde{\Delta}$. Note also that after the Hopf bifurcation is extinguished ($\sigma > 1 + 2\tilde{\Delta}$) the periodic orbits are connected directly to the upper turning point of the S-shaped curve (it is to be expected that periodic orbits connecting the upper and lower turning points exist but become unstable when $\sigma > 1 + 2\tilde{\Delta}$, although we haven’t checked it numerically yet).

11. DOPOS TUNED TO ARBITRARY TRANSVERSE FAMILIES

So far we have studied DOPOs tuned to a fundamental TEM₀₀ mode (Section 6.3) and to the first family of transverse modes at the signal frequency (Section 7.2.2 and Chapters 8 and 9). The former was introduced as an example of a system showing bifurcation squeezing, while we proposed the later as a playground where studying the phenomenon of noncritical squeezing induced by spontaneous symmetry breaking. It is then natural to generalize the study to a DOPO tuned to an arbitrary family of transverse modes at the signal frequency, and this is what this final chapter is intended to do. We remind that a given family, say family f , posses $f + 1$ transverse modes having orbital angular momenta $\{\pm f, \pm(f-2), \dots, \pm l_0\}$, with l_0 equal to 0 for even families and 1 for the odd ones, so that the part signal field propagating along $+\mathbf{e}_z$ can be written in the Laguerre–Gauss basis as (from now on all the sums over l are assumed to run over the set $l \in \{f, f-2, \dots, l_0\}$)

$$\hat{\mathbf{E}}_{s,\rightarrow}^{(+)}(\mathbf{r}) = i\sqrt{\frac{\hbar\omega_s}{4\varepsilon_0 n_s L_s}} \mathbf{e}_e \sum_{\pm l} \hat{a}_l L_{(f-|l|)/2,l}(k_s; \mathbf{r}_\perp, z) e^{in_s k_s z}; \quad (11.1)$$

hence, for $f \geq 2$ this DOPO has more than one parametric down–conversion channel available, that is, a pump photon can decay into any pair of opposite angular momentum signal photons. Armed with the things that we have learned so far (bifurcation squeezing, pump clamping, and spontaneous symmetry breaking), the properties of such system will be quite intuitive; in fact, this is the system in which we originally predicted the phenomenon of OPO clamping [29] that was introduced in a general way in Section 7.1.

What is interesting about this particular implementation of a multi–mode DOPO that we may call *f–transverse–family DOPO* is that, as we will show in Section 11.4, by tuning the thickness of the pump mode (what can be done by using monolithic designs in which the cavities for the pump and signal modes are independent, or singly–resonant OPOs) one can find many transverse modes with large levels of squeezing, hence creating a highly nonclassical and multi–mode beam.

11.1 The model

As in the previous cases, the general model for intracavity down–conversion that we developed in Section 6.2 covers also the configuration that we are dealing with in this chapter. In particular, the down–conversion Hamiltonian can be obtained by particularizing (6.42) to the current scenario in which the set of transverse modes resonating at the signal frequency is the corresponding to the Laguerre–Gauss modes $\{L_{(f-l)/2,\pm l}(k; \mathbf{r}_\perp, z)\}_{l \in \{f, f-2, \dots, l_0\}}$. Denoting by \hat{a}_p and \hat{a}_l the annihilation operators for pump photons and signal photons with orbital angular momentum l , respectively, we get

$$\hat{H}_c = i\hbar \sum_l \frac{\chi_l}{1 + \delta_{0,l}} \hat{a}_p \hat{a}_l^\dagger \hat{a}_{-l}^\dagger + \text{H.c.}, \quad (11.2)$$

where

$$\chi_l = 3l_c \chi_{\text{oee}}^{(2)}(2\omega_0; \omega_0, \omega_0) \sqrt{\frac{\hbar\omega_0^3}{2\varepsilon_0 n_c^3 L_{\text{opt}}^3}} \int_0^{+\infty} r dr G(k_p; r) \left[\mathcal{R}_{(f-l)/2}^l(k_s; r) \right]^2. \quad (11.3)$$

Note that the larger is the OAM of the down–converted pair, the smaller is the overlapping between the square of $\mathcal{R}_{(f-l)/2}^l(k_s; r)$ and the Gaussian pump profile $G(k_p; r)$, what comes from the fact that the modes are thicker the larger their angular OAM is, and hence the following ordering of the couplings holds

$$\chi_f < \chi_{f-2} < \dots < \chi_{l_0}, \quad (11.4)$$

that is, the lowest OAM modes are the ones coupled more strongly to the pump.

The master equation associated to the f -transverse-family DOPO in a picture rotated to the laser frequency and in which everything is assumed to be resonant reads then

$$\frac{d\hat{\rho}_I}{dt} = \left[\sum_l \frac{\chi_l}{1 + \delta_{0,l}} \hat{a}_p \hat{a}_l^\dagger \hat{a}_{-l}^\dagger + \mathcal{E}_p a_p^\dagger + \text{H.c.}, \hat{\rho}_I \right] + \sum_{j=p,\pm l} \gamma_j (2\hat{a}_j \hat{\rho}_I \hat{a}_j^\dagger - \hat{a}_j^\dagger \hat{a}_j \hat{\rho}_I - \hat{\rho}_I \hat{a}_j^\dagger \hat{a}_j); \quad (11.5)$$

now, assuming that all the signal modes have the same loss rate γ_s , we can map this master equation into the following Langevin equations within the positive P representation:

$$\dot{\alpha}_p = \mathcal{E}_p - \gamma_p \alpha_p - \sum_l \frac{\chi_l}{1 + \delta_{0,l}} \alpha_l \alpha_{-l}, \quad (11.6a)$$

$$\dot{\alpha}_p^+ = \mathcal{E}_p - \gamma_p \alpha_p^+ - \sum_l \frac{\chi_l}{1 + \delta_{0,l}} \alpha_l^+ \alpha_{-l}^+, \quad (11.6b)$$

$$\dot{\alpha}_l = -\gamma_s \alpha_l + \chi_l \alpha_p \alpha_{-l}^+ + \sqrt{\chi_l \alpha_p} \xi_l(t), \quad (11.6c)$$

$$\dot{\alpha}_l^+ = -\gamma_s \alpha_l^+ + \chi_l \alpha_p^+ \alpha_{-l} + \sqrt{\chi_l \alpha_p^+} \xi_l^+(t), \quad (11.6d)$$

$$\dot{\alpha}_{-l} = -\gamma_s \alpha_{-l} + \chi_l \alpha_p \alpha_l^+ + \sqrt{\chi_l \alpha_p} \xi_l^*(t), \quad (11.6e)$$

$$\dot{\alpha}_{-l}^+ = -\gamma_s \alpha_{-l}^+ + \chi_l \alpha_p^+ \alpha_l + \sqrt{\chi_l \alpha_p^+} [\xi_l^+(t)]^*, \quad (11.6f)$$

where all the various complex noises satisfy the usual statistical properties (6.94) and are independent.

As usual, we now rewrite the equations in terms of the following normalized variables

$$\tau = \gamma_s t, \quad \beta_j(\tau) = \frac{\chi_{l_0}}{\gamma_s \sqrt{\gamma_p/\gamma_j}} \alpha_j(t), \quad \zeta_j(\tau) = \frac{1}{\sqrt{\gamma_s}} \xi_j(t), \quad (11.7)$$

arriving to

$$\dot{\beta}_p = \kappa \left[\sigma - \beta_p - \sum_l \frac{r_l}{1 + \delta_{0,l}} \beta_l \beta_{-l} \right], \quad (11.8a)$$

$$\dot{\beta}_p^+ = \kappa \left[\sigma - \beta_p^+ - \sum_l \frac{r_l}{1 + \delta_{0,l}} \beta_l^+ \beta_{-l}^+ \right], \quad (11.8b)$$

$$\dot{\beta}_l = -\beta_l + r_l \beta_p \beta_{-l}^+ + g \sqrt{r_l \beta_p} \zeta_l(\tau), \quad (11.8c)$$

$$\dot{\beta}_l^+ = -\beta_l^+ + r_l \beta_p^+ \beta_{-l} + g \sqrt{r_l \beta_p^+} \zeta_l^+(\tau), \quad (11.8d)$$

$$\dot{\beta}_{-l} = -\beta_{-l} + r_l \beta_p \beta_l^+ + \sqrt{r_l \alpha_p} \zeta_l^*(\tau), \quad (11.8e)$$

$$\dot{\beta}_{-l}^+ = -\beta_{-l}^+ + r_l \beta_p^+ \beta_l + \sqrt{r_l \beta_p^+} [\zeta_l^+(\tau)]^*, \quad (11.8f)$$

where in this case the parameters are defined as

$$\kappa = \gamma_p/\gamma_s, \quad \sigma = \chi_{l_0} \mathcal{E}_p/\gamma_p \gamma_s, \quad g = \chi_{l_0}/\sqrt{\gamma_p \gamma_s}, \quad r_l = \chi_l/\chi_{l_0}. \quad (11.9)$$

Note that $0 < r_l \leq 1$, where the equality holds only for $l = l_0$.

It will be convenient for future purposes to remind that instead of the Laguerre–Gauss basis, one could describe the system through the Hybrid Laguerre–Gauss modes $\{Y_{j,(f-l)/2,l}(k_s; \mathbf{r}_\perp, z)\}_{l \in \{f, f-2, \dots, l_0\}}^{j=c,s}$, see (3.49). For $l = 0$ the HLG and LG modes coincide and are rotationally symmetric, while for $l \neq 0$ the HLG modes have a well defined orientation in the transverse plane (see Figure 3.5). The annihilation operators for HLG photons are related to the LG ones by

$$\hat{a}_{c,l} = (\hat{a}_{+l} + \hat{a}_{-l})/\sqrt{2}, \quad \hat{a}_{s,l} = i(\hat{a}_{+l} - \hat{a}_{-l})/\sqrt{2}. \quad (11.10)$$

11.2 Classical emission

Based on the phenomenon of pump clamping that we introduced in Section 7.1, it is completely trivial to understand the classical behavior of the f -transverse-family DOPO; let's see this.

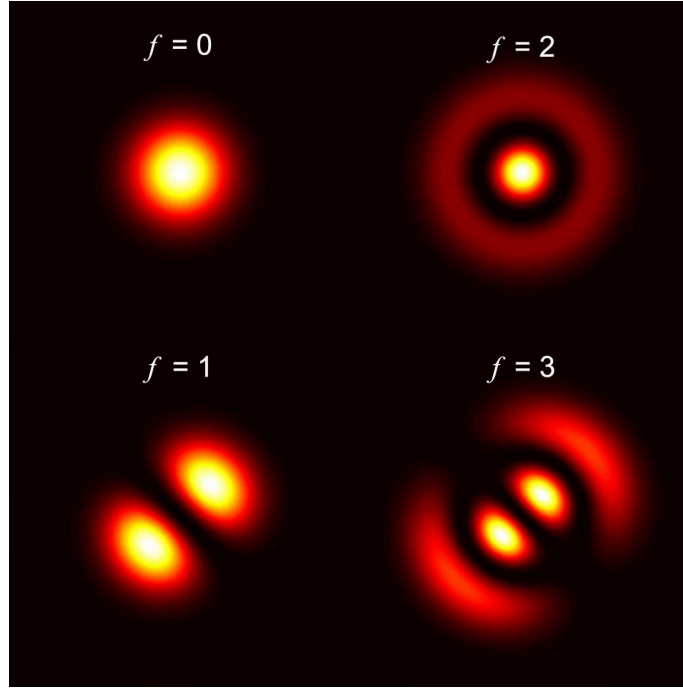


Fig. 11.1: Transverse profile of the signal field above threshold when the DOPO is tuned to the different families at the signal frequency.

The solution with the $\pm l$ couple of OAM modes switched on requires $\sigma > r_l^{-1}$ to exist; hence, the process involving the lowest OAM modes $\pm l_0$ is the one with the lowest oscillation threshold, which is obtained for $\sigma = 1$. As σ increases all the injected power is transferred then to the $\pm l_0$ couple, while the pump mode gets clamped to its value at threshold; the rest of the signal modes remain then switched off and feel that the DOPO is frozen at $\sigma = 1$.

Being more specific, the system has only two types of classical solutions: The below threshold solution

$$\bar{\beta}_p = \sigma, \quad \bar{\beta}_l = 0 \quad \forall l, \quad (11.11)$$

which is stable for $\sigma < 1$, and the above threshold solution, which reads

$$\bar{\beta}_p = 1, \quad \bar{\beta}_0 = \pm \sqrt{2(\sigma - 1)}, \quad \bar{\beta}_{\pm l} = 0 \quad \forall l \neq 0, \quad (11.12)$$

for even families, and

$$\bar{\beta}_p = 1, \quad \bar{\beta}_{\pm 1} = \sqrt{\sigma - 1} \exp(\mp i\theta), \quad \bar{\beta}_{\pm l} = 0 \quad \forall l \neq 1, \quad (11.13)$$

with θ arbitrary, for odd families.

Above threshold, the corresponding classical down-converted fields will be

$$\bar{\mathbf{E}}_{s,\rightarrow}^{(+)}(\mathbf{r}) = i \sqrt{\frac{\hbar\omega_s(\sigma - 1)}{2\varepsilon_0 n_s L_s g^2}} \mathbf{e}_e L_{f/2,0}(k_s; \mathbf{r}_\perp, z) e^{-i\omega_0 t + i n_s k_s z}, \quad (\text{even})$$

$$\bar{\mathbf{E}}_{s,\rightarrow}^{(+)}(\mathbf{r}) = i \sqrt{\frac{\hbar\omega_s(\sigma - 1)}{2\varepsilon_0 n_s L_s g^2}} \mathbf{e}_e Y_{c,(f-1)/2,1}(k_s; r, \phi - \theta, z) e^{-i\omega_0 t + i n_s k_s z}, \quad (\text{odd})$$

for even or odd families, respectively. The transverse profiles of these classical fields are plotted in Figure 11.1 for the first four transverse families. It can be appreciated that for even families the field preserves the rotational symmetry of the system, as $L_{f/2,0}(k_s; \mathbf{r}_\perp, z)$ is rotationally symmetric in the transverse plane. On the other hand, for odd families the field takes the form of a HLG mode with $l = 1$ and arbitrary orientation in the transverse plane, and hence the phenomenon of spontaneous rotational symmetry breaking appears in this case.

$f l$	2	4	6	8	10	12	$f l$	3	5	7	9	11	13
2	88.9						3	75.0					
4	96.0	49.0					5	88.9	33.1				
6	98.0	71.0	18.1				7	93.8	55.6	10.8			
8	98.8	81.6	36.8	5.6			9	96.0	69.1	24.9	3.1		
10	99.2	87.4	51.4	14.7	1.6		11	97.2	77.6	38.0	9.1	0.9	
12	99.4	90.9	62.1	24.9	5.1	0.4	13	98.0	83.0	49.0	16.6	3.0	0.2

Fig. 11.2: Percentage of noise reduction for the nonamplified hybrid modes $l \neq l_0$ lying in even (left table) and odd (right table) families. Note that large levels of squeezing are obtained for the lower angular momentum modes.

11.3 Quantum properties

Armed with all the background that we have learned in the previous chapters, the quantum properties of the f -transverse-family DOPO are as intuitive as the classical properties that we just found. First, remember that the dynamics of non-amplified down-conversion channels are decoupled (within the linearized theory) from the properties of the classically excited modes, and then we can discuss their properties separately.

For even families, the $l = 0$ mode will behave as the signal field of the single-mode DOPO, that is, it shows bifurcation squeezing. In particular, its Y quadrature is perfectly squeezed at zero noise frequency only at threshold, the squeezing level degrading as one moves far above or below this instability point (see Section 6.3).

For odd families, the $l = \pm 1$ modes behave as the signal modes of the 2tmDOPO, that is, their properties can be understood in terms of noncritical squeezing induced by spontaneous rotational symmetry breaking. Concretely, one can show that the orientation of the classically excited HLG mode diffuses with time driven by quantum noise, while the Y quadrature of the mode orthogonal to this one, $Y_{s,(f-1)/2,1}(k_s; r, \phi - \theta, z)$, is perfectly squeezed irrespective of the system parameters above threshold (see Section 7.2.2). All the properties that we have studied in Chapters 8 and 9 concerning the phenomenon of spontaneous symmetry breaking also apply to this case.

As for the modes with $l \neq l_0$, let us change to the HLG basis in order to formulate their quantum properties. The three-wave-mixing Hamiltonian (11.2) can be rewritten in this basis as

$$\hat{H}_c = i\hbar \sum_{l \neq l_0} \chi_l \hat{a}_p \left(\hat{a}_{c,l}^{\dagger 2} + \hat{a}_{s,l}^{\dagger 2} \right) / 2 + \text{H.c.}, \quad (11.15)$$

where we have not considered the lowest angular momentum modes, as their properties have been already discussed. Once the threshold $\sigma = 1$ is reached, these modes feel the DOPO as frozen at that point no matter how much we keep increasing σ . Hence, and given that the Hamiltonian in the HLG basis is a combination of down-conversion channels of indistinguishable pairs of photons, just as the case studied in Section 7.1.1, we can directly asses that the noise spectra of the different modes will be

$$V^{\text{out}}(\hat{X}_{c,l}; \Omega) = V^{\text{out}}(\hat{X}_{s,l}; \Omega) = \frac{(1 + r_l \bar{\beta}_p)^2 + \tilde{\Omega}^2}{(1 - r_l \bar{\beta}_p)^2 + \tilde{\Omega}^2}, \quad (11.16a)$$

$$V^{\text{out}}(\hat{Y}_{c,l}; \Omega) = V^{\text{out}}(\hat{Y}_{s,l}; \Omega) = \frac{(1 - r_l \bar{\beta}_p)^2 + \tilde{\Omega}^2}{(1 + r_l \bar{\beta}_p)^2 + \tilde{\Omega}^2}, \quad (11.16b)$$

see (7.15), and hence, all the $\{Y_{j,(f-l)/2,l}(k_s; \mathbf{r}_\perp, z)\}_{l \in \{f, f-2, \dots, l_0+2\}}^{j=c,s}$ modes have squeezing on their Y quadrature; in particular, the maximum levels of squeezing are obtained above threshold ($\bar{\beta}_p = 1$) and at zero noise frequency ($\tilde{\Omega} = 0$), and read

$$V^{\text{out}}(\hat{Y}_{c,l}; \Omega = 0) = V^{\text{out}}(\hat{Y}_{s,l}; \Omega = 0) = \frac{(1 - r_l)^2}{(1 + r_l)^2}. \quad (11.17)$$

Recall that as long as $r_l > 0.5$, this expression predicts more than 90% of noise reduction. Moreover, by defining the integral

$$I_l = \frac{[(f-l)/2]!}{[(f+l)/2]!} \int_0^{+\infty} du e^{-2u^2} u^{2l+1} \left[L_{(f-l)/2}^l(u^2) \right]^2, \quad (11.18)$$

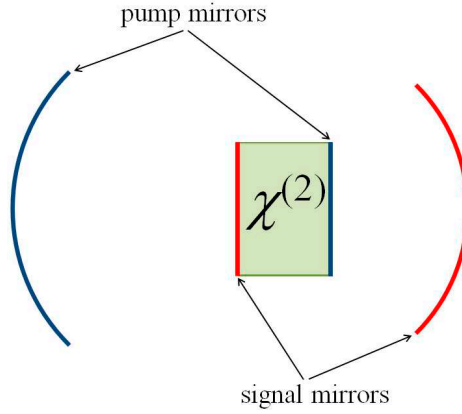


Fig. 11.3: Monolithic design in which the cavities for the pump and signal fields are independent. The pump (signal) mirrors are made completely transparent for the signal (pump) frequencies.

in terms of which the nonlinear couplings are written as (remember that $w_p^2/w_s^2 = \lambda_p/\lambda_s = 1/2$)

$$\chi_l = \frac{3}{2} \frac{l_c}{w_s} \chi_{\text{oeo}}^{(2)}(2\omega_0; \omega_0, \omega_0) \sqrt{\frac{8\hbar\omega_0^3}{\pi^3 \epsilon_0 n_c^3 L_{\text{opt}}^3}} I_l, \quad (11.19)$$

the actual ratios r_l can be evaluated for the different modes as

$$r_l = I_l/I_0; \quad (11.20)$$

in the tables of Figure 11.2 we show the noise reduction obtained for the different OAM pairs of the first families. Notice that the largest squeezing levels occur for large values of f and small values of l .

It is to be remarked that both the Hybrid mode $Y_{c,(f-l)/2,l}(k_s; \mathbf{r}_\perp, z)$ and its orthogonal $Y_{s,(f-l)/2,l}(k_s; \mathbf{r}_\perp, z)$ have the same squeezing properties. This means that the orientation of the mode is irrelevant, as an hybrid mode rotated an arbitrary angle ψ respect to the x axis, which is given by

$$Y_{c,(f-l)/2,l}(k_s; r, \phi - \psi, z) = Y_{c,(f-l)/2,l}(k_s; \mathbf{r}_\perp, z) \cos l\psi + Y_{s,(f-l)/2,l}(k_s; \mathbf{r}_\perp, z) \sin l\psi, \quad (11.21)$$

also has the same squeezing properties. This is in clear contrast to the perfectly squeezed mode in the $l = 1$ case which has not an arbitrary orientation but is orthogonal to the classically excited mode at every instant.

11.4 Tuning squeezing through the pump shape

In this last section of the chapter we would like to discuss how we can take r_l closer to one (and hence increase the squeezing levels of the non-amplified modes) by modifying the shape of the pump mode.

The idea comes from the following fact. The only difference between the nonlinear couplings (11.3) of the different OAM pairs is the three-mode overlapping integral

$$\int_0^{+\infty} r dr G(k_p; r) \left[\mathcal{R}_{(f-l)/2}^l(k_s; r) \right]^2 = \frac{1}{2\pi} \int_{\mathbb{R}^2} d^2\mathbf{r}_\perp G(k_p; \mathbf{r}_\perp, z=0) L_{(f-l)/2,l}(k_s; \mathbf{r}_\perp, z=0) L_{(f-l)/2,l}^*(k_s; \mathbf{r}_\perp, z=0); \quad (11.22)$$

now, if instead of the Gaussian profile $G(k_p; \mathbf{r}_\perp, z=0)$ the pump mode had a simple plane profile, that is, $G(k_p; \mathbf{r}_\perp, z=0) \rightarrow C \neq C(\mathbf{r}_\perp)$, the integral in the RHS of this expression would be transformed into the normalization of the Laguerre–Gauss modes, and hence all the modes would have the same nonlinear coupling to the pump field.

It is true that having a completely homogeneous pump profile is not possible because it is not physical. However, what we can actually do is design an OPO configuration in which the spot size of the pump mode exceeds the value $w_p = w_s/\sqrt{2}$ obtained when the pump and signal fields are resonating within the same cavity, which was the situation considered in the previous sections.

An obvious way of doing this is by using a singly-resonant DOPO, in which the cavity mirrors are completely transparent at the pump frequencies; was this the case, one could pump the crystal with a Gaussian mode of arbitrary

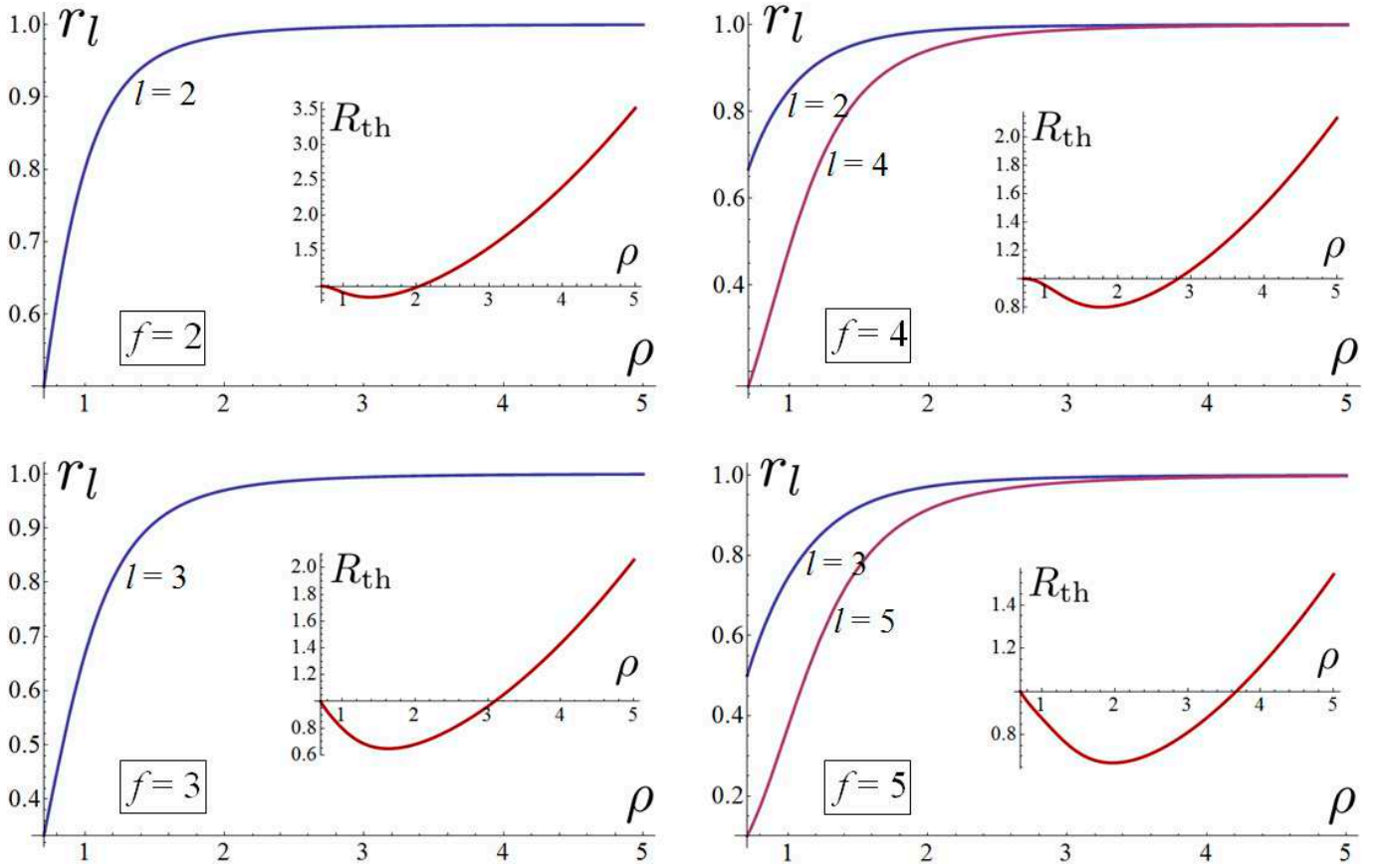


Fig. 11.4: Dependence of the ratios r_l on the ratio between the spot sizes of the pump and signal modes, ρ . The insets show how the threshold of the system changes with ρ .

thickness (or whatever shape one wanted!), as the pump does not have to match the profile of any mode resonating in the cavity at the pump frequency. The drawback of this configuration is that pump photons pass through the nonlinear crystal only once (*single-pass* down-conversion), and hence the threshold of the system is increased (see e.g., [130]).

In Figure 11.3 we sketch another configuration based on semi-monolithic OPOs which is interesting for the same purposes but in which both pump and signal are resonating. An OPO is said to be semi-monolithic if one of the faces of the nonlinear crystal acts itself as one of the mirrors of the cavity, what is accomplished by treating that face with an appropriate reflecting coating. Now, if we use one face of the crystal as a mirror for the pump, and the opposite face as a mirror for the signal as shown in Figure 11.3, the cavities for the pump and signal fields become independent, and we can tune the spot size of the pump and signal Gaussian modes independently.

Let us then assume that we can tune the ratio between the thickness of the pump and signal modes at will, and define the parameter $\rho = w_p/w_s$. Under these conditions, and following (11.19), the nonlinear couplings can be written as

$$\chi_l(\rho) = \frac{3}{2} \frac{l_c}{w_s} \chi_{\text{oe}}^{(2)}(2\omega_0; \omega_0, \omega_0) \sqrt{\frac{4\hbar\omega_0^3}{\pi^3 \epsilon_0 n_c^3 L_{\text{opt}}^3}} I_l(\rho), \quad (11.23)$$

where now

$$I_l(\rho) = \frac{1}{\rho} \frac{[(f-l)/2]!}{[(f+l)/2]!} \int_0^{+\infty} du e^{-u^2(1+1/2\rho^2)} u^{2l+1} \left[L_{(f-l)/2}^l(u^2) \right]^2, \quad (11.24)$$

and we have assumed that the lengths of the pump and signal cavities are similar. In Figure 11.4 we show how the ratios $r_l(\rho) = I_l(\rho)/I_0(\rho)$ change with ρ ; note that ρ does not need to be really big in order for r_l to approach unity (in fact, remember that with $r_l > 0.5$ we already find squeezing levels above 90%).

Of course, we should worry about what happens with the threshold of the system when changing the relation $w_p = w_s/\sqrt{2}$. In particular, the ratio between the power needed to make the signal field oscillate for an arbitrary ρ ,

and that for $\rho = 1/\sqrt{2}$ is given by

$$R_{\text{th}}(\rho) = \frac{P_{\text{th}}(\rho)}{P_{\text{th}}(\rho = 1/\sqrt{2})} = \frac{\chi_{l_0}^2(\rho = 1/\sqrt{2})}{\chi_{l_0}^2(\rho)} = \frac{I_{l_0}^2(\rho = 1/\sqrt{2})}{I_{l_0}^2(\rho)}, \quad (11.25)$$

as follows from (4.40), (11.9), and (11.23). This expression is plotted in the insets of Figure 11.4 for the different families. These figures show that the changes in the threshold are quite reasonable, and moreover, the threshold is even lowered respect to the $\rho = 1/\sqrt{2}$ case for small enough ratios ρ .

12. CONCLUSIONS AND OUTLOOK

12.1 Summary of the original research on OPOs

This thesis has been devoted to the study of some new properties of optical parametric oscillators (OPOs). Such devices consist of an optical cavity embedding a second order nonlinear crystal, which, when pumped with an external laser beam at frequency $\omega_p = 2\omega_0$, is able to generate light at frequencies ω_s and ω_i such that $\omega_p = \omega_s + \omega_i$, through the process of parametric down-conversion (the ω_p , ω_s , and ω_i fields are called, respectively, pump, signal, and idler). The down-conversion process is known as degenerate when the signal and idler modes have the same frequency ω_0 , and type I when they have the same polarization (if they are generated in orthogonal, linearly polarized modes, we talk then about type II down-conversion).

As stressed in the Introduction, the first two-thirds of the dissertation have consisted on a self-contained discussion about the basic physics behind these devices. Here we would like to remark the following well known properties of OPOs (see Section 1.2.1 for an extensive summary of this introductory part):

- From a classical point of view, the interplay between parametric down-conversion and cavity losses forces the pump power (denoted along the thesis by the dimensionless parameter σ) to go above some threshold level ($\sigma = 1$) in order to make the signal-idler fields oscillate. Hence, at $\sigma = 1$ the system shows a bifurcation in which the OPO passes from a steady state with the down-converted fields switched off, to a new steady state in which these are switched on (much like in the laser).
- Working with type I, degenerate down-conversion, we simply talk about a degenerate OPO (DOPO). If in addition the signal and idler modes are generated with in the same transverse mode (typically a TEM₀₀ mode), we talk about a single-mode DOPO. It is possible to show that in such system the down-converted field is in a squeezed state, that is, one of its quadratures has fluctuations below the vacuum (shot noise) level. However, this squeezing is only large when working close to the bifurcation: We say that it is a critical phenomenon.
- When the down-converted photons are distinguishable in frequency or/and polarization, we have shown that the joint state of the signal and idler modes corresponds to an entangled state in which these share correlations which go beyond what is classically allowed. Again, the entanglement level is large only when working close to threshold.
However, in this case there is one highly squeezed observable at any pump level above threshold: The signal-idler intensity difference. We say then that signal and idler are twin beams, as they have perfectly correlated photon numbers.

These well known results were the starting point of the research developed in this thesis; in the remaining of this section we make a summary of the main original results that we have found (numbering of this list follows the chapters and sections of the dissertation):

7. In the first completely original chapter we have introduced the concept of multi-mode OPO as that having several down-conversion channels available for a single pump mode. We have argued that this is actually the natural way in which OPOs operate, either because it is impossible to forbid the existence of other transverse modes close to the one in which we would like to operate, or because the phase matching curve is wide enough as to include more than a single signal-idler frequency pair.
We have then introduced two phenomena characteristic of multi-mode OPOs, phenomena which are considered by the PhD candidate as the most important contribution of the thesis: Pump clamping and spontaneous symmetry breaking. As we explain now, their main interest is that they offer new means for generating squeezed (or entangled) light, with the incentive that the squeezing is noncritical, that is, independent of the system parameters.

7.1. Let us first explain the key points describing the phenomenon of pump clamping:

- * In general, the different down-conversion channels of the multi-mode OPO will have different thresholds, depending these on the coupling to the pump, the detuning, and the loss rates of the modes involved in the particular process.
- * Classically, only the channel with the lowest threshold can be amplified, that is, the processes with higher thresholds remain switched off no matter how much we increase σ .
- * What is interesting is that once the lowest threshold mode is generated, the non-amplified modes feel as if the OPO was frozen at the bifurcation, even if we change the actual pump injection. This applies also to their quantum properties, that is, the modes of the non-amplified channels will have the squeezing or entanglement that they are supposed to have below their oscillation threshold, irrespective of the system parameters.

Hence, our first prediction has been that, above threshold, apart from the bright signal-idler modes which behave as the ones in the single-channel OPO (bifurcation squeezing or entanglement), the output of a general OPO has a lot more signal-idler pairs with some squeezing or entanglement, their actual levels depending on the distance between their thresholds and the lowest threshold of the system (the true threshold).

7.2.1. We have introduced the basic idea behind spontaneous symmetry breaking in an abstract way as follows:

- * Suppose that we work with an OPO which is invariant under changes of some continuous degree of freedom of the down-converted field, say ϵ , which we have denoted by “free parameter” all along the dissertation. Above threshold, the down-converted field, say $\bar{\mathbf{E}}_\epsilon(\mathbf{r}, t)$ —we explicitly introduce the free parameter in the field—, is not zero, and when the OPO starts emitting it, a particular value of the free parameter is chosen according to the particular fluctuations from which the field is built up. We say that ϵ is chosen through spontaneous symmetry breaking.
- * Let’s think now about what quantum theory might introduce to this classical scenario. First, as variations of the FP do not affect the system (what mathematically is reflected in the appearance of a Goldstone mode in the matrix governing the linear evolution of the system, that is, a mode with null eigenvalue), quantum noise is expected to make it fluctuate without opposition, eventually making it become completely undetermined.
- * Then, invoking now the uncertainty principle, the complete indetermination of a system’s variable allows for the perfect determination of its corresponding momentum, meaning this that we could expect perfect squeezing in the quadrature selected by the local oscillator $-i\partial_\epsilon \bar{\mathbf{E}}_\epsilon(\mathbf{r}, t)$ in an homodyne detection scheme.
- * Finally, as this process relies only on the generation of the down-converted field, this perfect squeezing is expected to be independent of the distance to threshold, as long as we are above the bifurcation point.

The first proof of such an intuitive reasoning was offered through the study of a DOPO with plane mirrors [30, 31], where transverse patterns as well as cavity solitons have been predicted to appear above threshold [137, 138], hence breaking the translational symmetry of the system. Most of the present thesis has been devoted to study several aspects of the phenomenon of spontaneous symmetry breaking, but we have designed a much more simple (and realistic) DOPO configuration for that matter.

7.2.2,8. The system we have used to study in depth the phenomenon of spontaneous symmetry breaking is a DOPO (hence signal and idler have the same frequency and polarization) pumped by a TEM_{00} mode, and whose cavity is tuned so that the first family of transverse modes resonates at the down-converted frequency. Under this circumstances the down-converted photons are created in opposite orbital angular momentum (OAM) Laguerre-Gauss modes, and, consequently, we have called two-transverse-mode DOPO (2tmDOPO) to this system.

Let us summarize now the main results that we have found in this system.

7.2.2. In connection with the general picture of 7.2.1, these are the properties of the system:

- * A weighted superposition of two ± 1 Laguerre-Gauss modes can be seen as a TEM_{10} mode, whose orientation in the transverse plane is given by half the phase-difference between the underlying Laguerre-Gauss modes. Hence, owed to the rotational invariance of the cavity, classical emission takes place in a TEM_{10} mode with an arbitrary orientation in the transverse plane (mathematically this is clear because the 2tmDOPO classical equations are invariant against changes in the relative phase between the Laguerre-Gauss modes).

Hence, once the threshold is crossed and the orientation is chosen according to the particular initial fluctuations, the rotational symmetry is spontaneously broken, and we can talk about a bright mode (the generated one which breaks the symmetry) and a dark mode (the mode orthogonal to the generated one).

- * Quantum noise is able to make the bright TEM_{10} mode rotate randomly in the transverse plane. Mathematically, this is reflected in the appearance of a Goldstone mode in the matrix governing the linear evolution of the fluctuations above threshold. The null eigenvalue of this mode allows quantum noise to change the orientation of the bright mode without opposition. Though continuously increasing with time, this rotation of the classically excited pattern is quite slow when working above threshold.
- * As for the squeezing properties, it has been proved that the bright mode has the same behavior as the single-mode DOPO, i.e., large levels of squeezing appear only close to threshold. On the other hand, accompanying the Goldstone mode it appears another mode whose associated eigenvalue takes the minimum possible value (-2).

Together, the Goldstone mode and the maximally damped mode are responsible of the remarkable properties of the dark mode: Its Y quadrature is perfectly squeezed at any pump level above threshold, while its X quadrature carries only with vacuum fluctuations (in apparent violation of the uncertainty principle).

This is in full agreement with the abstract picture of the phenomenon offered in 7.2.1, as the dark mode coincides (up to a $\pi/2$ phase) with the OAM of the bright mode.

- 8.1. We have proved that the apparent violation of the uncertainty principle is just that, apparent, as the conjugate pair of the squeezed quadrature is not another quadrature but the orientation of the bright mode, which in fact is completely undetermined in the long time term.
 - 8.2. Next we have pointed out that in order to measure the quantum properties of the dark mode via homodyne detection, one has to use a TEM_{10} local oscillator that is perfectly matched to the orientation of this mode at any time. However, the mode is rotating randomly, which seems to make impossible the perfect matching. For this reason we have studied the situation in which the local oscillator is matched to the dark mode's orientation only at the initial time, remaining fixed during the detection time. We have shown that arbitrarily large levels of noise reduction can be obtained even in this case if the phase of the local oscillator is exactly $\pi/2$. We then considered phase deviations up to 2° (1.5° seems to be the current experimental limit [5, 6]), comparing the results with those predicted for the single-mode DOPO; similar levels are obtained for both, with the advantage that in the 2tmDOPO this level is independent of the distance from threshold, and hence, noncritical.
 - 8.3. We have also shown that the assumptions made in order to analytically solve the problem are not the responsible for the quantum properties of the dark mode. In particular, we have used numerical simulations to show that these analytic predictions coincide with those of the complete nonlinear stochastic equations describing the system.
9. In this chapter we have studied the classical and quantum dynamics of the 2tmDOPO when a TEM_{10} beam is injected at the signal frequency. This study was motivated by experimental reasons: On one hand, this injection is customarily used in real DOPOs to stabilize the cavity, so that, in particular, the signal resonance is locked to the desired value (active locking); on the other, in the 2tmDOPO, and given that down-conversion is a stimulated process, we think that the injection of a TEM_{10} mode could also lock the orientation of the bright mode, what seems highly recommendable from the detection point of view.

These are the main results that we have found:

- 9.2. Let's start with the classical dynamics. For signal injections below some threshold, the system possesses a unique, stable solution in which the TEM_{01} (the non-injected mode) remains switched off. However, above this injection threshold both the TEM_{10} and TEM_{01} modes become populated. Hence, the system possesses a new bifurcation linked to the switching on of the non-injected mode.

This bifurcation is present for any σ , and in particular it exists also for $\sigma = 0$, when the DOPO runs as a second harmonic generator (as in this case the $2\omega_0$ field is generated from the ω_0 injection); of course in this case the threshold is independent of the injection's phase, as there is no other phase reference. For $\sigma > 0$ this is no longer the case: The threshold is maximum (minimum) when the signal injection is in phase (anti-phase) with the pump injection.

Surprisingly, working in anti-phase and when $\sigma \geq 1$, there is no threshold for the generation of the TEM_{01} mode. On the other hand, in the in-phase case there exists a clear threshold below which the bright mode is locked to the injected TEM_{10} mode, just as we wanted to prove.

9.3. As for the quantum properties, we have proved that the TEM_{01} mode has large levels of squeezing in all the region below their generation threshold, hence proving that the TEM_{10} injection does not degrade too much the squeezing capabilities of the 2tmDOPO.

This insensitivity to the injection (in particular we have proved that it is far much insensitive to the injection than the single-mode DOPO, the configuration customarily used in experiments) comes from the fact that the TEM_{01} mode shows perfect squeezing at the instability point leading to its activation.

10. In this chapter we have studied type II OPOs tuned to the TEM_{00} mode for all the frequencies involved in the down-conversion process. We had a twofold intention:

10.1. On one hand, we wanted to generalize the phenomenon of spontaneous symmetry breaking to the polarization degrees of freedom of light. In particular, we have shown that when the down-conversion process is also frequency degenerate, the system is isomorphic to the 2tmDOPO, where the role of the opposite orbital angular momenta are now played by the orthogonal linear polarizations of the signal-idler modes.

We have then proved that the behavior expected after the general reasoning of Section 7.2.1 applies: Classical emission takes place in an elliptically polarized mode, and the free parameter of this system (the relative phase between signal and idler) is related now to the eccentricity of the corresponding polarization ellipse; quantum noise is responsible for a diffusion process of this polarization parameter, which eventually becomes completely undetermined; the Y quadrature of the dark mode, which in this case consists on the mode orthogonally polarized to the bright one, has perfect squeezing at any pump level above threshold.

10.2. However, we have pointed out that in real experiments it seems not possible to obtain frequency degeneracy in OPOs. In the case of type II operation, frequency degeneracy can be obtained by introducing a birefringent element inside the cavity (self-phase-locked type II OPOs), but this breaks the polarization symmetry of the system, hence destroying the phenomenon of spontaneous symmetry breaking. Nevertheless, we have argued that a residual squeezing should be present after this explicit symmetry breaking, and that it was actually observed (but not interpreted a residue of the symmetry breaking) some years ago [38].

We then show that frequency degeneracy might as well be obtained by injecting an external laser beam at the degenerate frequency (actively-phase-locked type II OPOs). Moreover, we have studied the complete bifurcation diagram of this system in the simple case of having opposite detunings for the signal and idler modes, showing that there are regimes in which stationary solutions coexist with periodic orbits.

11. Motivated by the fact that we already studied DOPOs tuned to the fundamental TEM_{00} mode at the subharmonic (single-mode DOPOs), as well as DOPOs tuned to the first family of transverse modes (2tmDOPOs), in the last original chapter of the thesis we have studied what happens when the DOPO is tuned to an arbitrary family of transverse modes at the signal frequency. Note that family f contains Laguerre-Gauss modes with orbital angular momenta $\{\pm f, \pm(f-2), \dots, \pm l_0\}$, with l_0 equal to 0 for even families and 1 for the odd ones. The results have been actually very intuitive based on the phenomena that we studied in the previous chapters. In particular:

11.2. Given that the lowest orbital angular momenta of the family are the ones which couple the strongest to the pump (so that they have the lowest threshold), they will be the ones classically amplified above threshold, while the rest of modes will remain switched off.

For even families this means that the bright mode will consist in a 0 OAM mode, and hence the rotational symmetry of the system will be preserved; on the other hand, the bright mode for the case of odd families will consist in a superposition of two ± 1 OAM modes (a Hybrid Laguerre-Gauss mode), and hence the rotational symmetry will be spontaneously broken.

11.3. As for the quantum properties, they are very simple to guess as well. First, and given that the dynamics of the non-amplified modes decouple from the ones of the amplified ones, the 0 OAM mode of the even-family case will behave as the signal field of the single-mode DOPO (bifurcation squeezing); similarly, the ± 1 OAM modes of the odd-family case will behave as the ones in the 2tmDOPO (the Hybrid Laguerre-Gauss mode generated above threshold and its orthogonal will behave, respectively, as the bright and dark modes of the 2tmDOPO).

On the other hand, and this is the most relevant result, the properties of the higher OAM modes are dictated by the phenomenon of pump clamping, that is, the Hybrid Laguerre-Gauss modes associated to the opposite OAM modes will show noncritical squeezing, the particular squeezing levels depending on the distance of their corresponding thresholds to that of the lowest OAM modes.

11.4. In the last section of the chapter we have shown that the thresholds of the higher OAM modes can be brought closer to that of the lowest OAM modes by pumping with a TEM_{00} mode wider than the one expected for the doubly resonant cavity (in particular, in the limit of infinite transverse thickness of the pump, the couplings of these to the different OAM pairs become all equal). We have suggested that this might be implemented either by using singly resonant DOPOs (in which the cavity is transparent at the pump frequency, and therefore the shape of the pump can be arbitrary), or by using clever monolithic cavity designs in which the pump and signal cavities become independent.

This offers the possibility to generate multi-mode beams with a large number of squeezed modes within it, what could be interesting for quantum information protocols requiring multipartite entanglement (quantum correlations shared between more than two parties).

12.2 Outlook

There are several ideas related to the research summarized in the previous section which we have started to analyze, but which I have decided not to include in the main text either because they are not completely developed, or just to keep the dissertation at a reasonable size. This section is devoted to summarize some of these ideas.

12.2.1 Temporal symmetry breaking

In the thesis we have studied the phenomenon of noncritical squeezing generated via spontaneous symmetry breaking by means of examples involving spatial and polarization degrees of freedom. It is then natural to try generalizing the phenomenon to the last kind of degrees of freedom that light can hold: the temporal ones. Time is a very subtle variable in quantum mechanics, and hence it seems interesting to find out whether our general reasoning introduced in Section 7.2.1 applies to symmetries involving it or not.

The idea can be explained as follows. Suppose that we work with an OPO which poses in some parameter region a dynamic mean field or classical solution (in the sense that the intensity of the field is not stationary, contrary to most of the examples that we have analyzed in the thesis); assume for simplicity that the solution is periodic. Now, as the classical equations of the OPO are invariant under time translations, the periodic solution can start at any point of its allowed values. We then expect quantum noise to make this parameter fluctuate randomly, eventually making it become completely undetermined; physically, this means that in the long time term, it won't be possible to determine at which point of its oscillation the mean field is. Based on the results found for the spatial and polarization symmetries, it seems interesting to analyze whether a local oscillator with the temporal profile of the $\pi/2$ phase-shifted time derivative of the bright field will measure perfect, noncritical squeezing in some quadrature of the field coming out of the cavity.

We have already analyzed these ideas in one of the most simple temporal instabilities that can be found in OPOs: The temporal instability associated to second harmonic generation. In particular, it is simple to show that when only the degenerate signal field is pumped externally, there exists a threshold value of this injection at which the stationary solution becomes unstable through a Hopf bifurcation. Therefore, for injected intensities above this threshold, the solution becomes time dependent, and in particular periodic when working close enough to the bifurcation. We advance that, unfortunately, the general reasoning explained above does not seem to apply to this case, that is, the squeezing of the $\pi/2$ phase-shifted time derivative of the bright field is not perfect, as happens in the case of spontaneous spatial or polarization symmetry breaking.

We believe that the problem lies in the fact that the instability of the stationary solution leading to the periodic solutions involves not only the signal field, but also the pump field (that is, the eigenvectors of the stability matrix have projections both onto the pump and signal subspaces), and it is well known that the pump mode never has large squeezing in OPOs.

In this sense, the actively-phase-locked OPO introduced in Section 10.2 seems a perfect candidate, in particular in the parameter region where non-stationary, periodic solutions exist (see Figure 10.2), as in this case the pump fluctuations are completely decoupled from the signal-idler fluctuations as long as one works in the adiabatic limit $\gamma_p \gg \gamma_s$ (a limit that cannot be taken in second harmonic generation because then the Hopf bifurcation goes to infinity, and the stationary solution becomes stable for finite external injection).

What makes the actively-phase-locked OPO even a more suited candidate for the study of this phenomenon, is that it connects directly with the free-running OPO when no injection at the degenerate frequency is present ($\mathcal{I} = 0$ in the notation of Chapter 10), and hence, one knows what to expect at that exact point.

We have just started the analysis, and then hope to offer new results soon enough.

12.2.2 Self-phase-locked two-transverse-mode type II OPO

In order to study in depth the phenomenon of noncritical squeezing induced by spontaneous symmetry breaking, we have made extensive use of the two-transverse-mode DOPO, in which signal and idler are degenerate in frequency and polarization, but have opposite orbital angular momenta. Even though there is nothing fundamental preventing experimentalists to operate OPOs in such configuration, it is quite hard to ensure that this particular down-conversion channel wins the nonlinear competition, and then in real experiments frequency-degeneracy might not be possible to achieve.

However, we believe to have found a way to bring the phenomenon of spontaneous symmetry breaking to observable grounds. The idea is to work with a type II non-degenerate OPO tuned to the first family of transverse modes at the signal and idler frequencies¹, and then use the self-phase-locking mechanism introduced at the beginning of Section 10.2 to lock the signal and idler frequencies to the degenerate one [157, 158, 38]; we believe that a residual continuous symmetry in the orbital angular momentum degree of freedom of signal and idler will be present, and hence in the frequency locking region one should be able to study the phenomenon of spontaneous rotational symmetry breaking.

In order to show explicitly how this is so, let us reason from the Hamiltonian of the system. Let us denote by $\hat{a}_{s,\pm 1}$ and $\hat{a}_{i,\pm 1}$ the annihilation operators for signal and idler photons with ± 1 orbital angular momentum, respectively. The parts of the Hamiltonian corresponding to the down-conversion process and the mixing induced by the $\lambda/4$ plate misaligned respect to the extraordinary axis of the nonlinear crystal can be written for this configuration as

$$\hat{H}_{\text{DC}} = i\hbar\chi\hat{a}_{\text{p}}(\hat{a}_{s,+1}^\dagger\hat{a}_{i,-1}^\dagger + \hat{a}_{s,-1}^\dagger\hat{a}_{i,+1}^\dagger) + \text{H.c.} \quad (12.1a)$$

$$\hat{H}_{\text{P}} = i\hbar\varepsilon(\hat{a}_{s,+1}\hat{a}_{i,+1}^\dagger + \hat{a}_{s,-1}\hat{a}_{i,-1}^\dagger) + \text{H.c.} \quad (12.1b)$$

As in the case in which the OPO is tuned to the fundamental Gaussian modes at the signal-idler frequencies [157, 158, 38], we expect \hat{H}_{P} to be able to lock the frequencies of signal and idler to the degenerate in a certain parameter region. On the other hand, there is a continuous symmetry still present in these Hamiltonian terms, namely

$$\begin{aligned} & \{\hat{a}_{s,+1}, \hat{a}_{s,-1}, \hat{a}_{i,+1}, \hat{a}_{i,-1}\} \\ & \quad \downarrow \\ & \{\exp(-i\theta)\hat{a}_{s,+1}, \exp(i\theta)\hat{a}_{s,-1}, \exp(-i\theta)\hat{a}_{i,+1}, \exp(i\theta)\hat{a}_{i,-1}\}, \end{aligned} \quad (12.2)$$

and hence, the phenomenon of spontaneous symmetry breaking should still be present in the system.

In simple terms, we believe that the polarization degree of freedom will allow us to make OPO become frequency degenerate through the self-phase-locking mechanism, while the extra orbital angular momentum degree of freedom will allow for the existence of a residual continuous symmetry in the system, which will be spontaneously broken above threshold once the mean field is switched on.

We have already started the analysis of this idea, although it might take a while to understand the parameter region where frequency locking is present, as the classical equations related to the system involve six modes, and are therefore hard to extract information from.

12.2.3 Effect of anisotropy

Another thing that we have been studying is how robust is the phenomenon of squeezing induced by spontaneous symmetry breaking against imperfections of the system's symmetry, what feels important as no perfect symmetry is present in real physical systems. Note that we have already answered this question partly, as in Chapter 9 we studied the 2tmDOPO with an injected signal beam which explicitly breaks the rotational symmetry of the system, showing that the squeezing levels of the dark mode can still be very large for reasonable injection intensities. This is the main reason why, in an effort to save some space in an already lengthy dissertation as this is, we have decided not to introduce the detailed study of symmetry imperfections in the main text; nevertheless, let us spend now a few words on how we have made this analysis, and what new interesting features of the phenomenon of spontaneous symmetry breaking can we learn from it.

As usual, we have used the 2tmDOPO as the platform where studying symmetry imperfections. In particular, we have considered two sources of anisotropy in the transverse plane which might actually appear in experiments².

¹ This system, but under the assumption of frequency degeneracy, was recently studied in the context of hyperentanglement, that is, entanglement between two independent degrees of freedom (polarization and orbital angular momentum in this case) of signal and idler [161].

² In the original paper where we considered the 2tmDOPO we already showed the robustness of the phenomenon by allowing the TEM₁₀ and TEM₀₁ modes to have different damping rates through the partially transmitting mirror. However, while mathematically this anisotropy model is very easy to handle, physically it is no justified why these modes could have different damping rates.

First, we have allowed the mirrors to not be perfectly spherical, in particular taking them as ellipsoids with some finite ellipticity. Then, we have allowed the nonlinear crystal to be misaligned respect to the cavity axis, what may not only correspond experimental imperfections, but may even be interesting in order to achieve angular phase-matching (see Section 6.1.2).

We have already developed the 2tmDOPO model including this sources of anisotropy, and we are currently trying to find the best way to characterize the robustness of squeezing against the degree of anisotropy. A preliminary, not exhaustive inspection of the resulting squeezing spectrum of the dark mode shows that, as expected, still large levels of noise reduction can be found for a reasonably large degree of anisotropy.

Concerning new physics, the most interesting feature that can be studied in this context is how the phase difference θ between the Laguerre–Gauss modes (that is, the orientation of the bright TEM_{10} mode) gets locked as the anisotropy increases, and the relation of this locking to the loss of squeezing in the dark mode. Our preliminary analysis shows that the variance of θ , which is infinite in the long time term when the rotational symmetry in the transverse plane is perfect, see (7.42), becomes finite when the anisotropy kicks in; of course, this variance tends to zero as the anisotropy increases, what means that the bright and dark modes get locked to a certain orientation in the transverse plane. Similarly, the noncritical squeezing of the dark mode, which can be perfect when no anisotropy is present, see (7.45d), is degraded as the anisotropy increases. What we are trying to understand now is if the scaling of this squeezing degradation with the degree of anisotropy is the same as that of the θ 's variance, what will be a further prove of the canonical relation existing between θ and the quadratures of the dark mode (see Section 8.1).

APPENDIX

A. QUANTUM DESCRIPTION OF PHYSICAL SYSTEMS

The purpose of this appendix is the introduction of the fundamental laws (axioms) of quantum mechanics as are used throughout this thesis. In an effort to make this thesis as self-contained as possible, the Hamiltonian formalism of classical mechanics (which is needed to fully understand and motivate the transition to quantum mechanics), as well as the theory of Hilbert spaces (which is the fundamental mathematical language in terms of which quantum theory is formulated), are briefly exposed.

A.1 Classical mechanics

The framework offered by quantum mechanics is far from intuitive, but somehow feels reasonable once one understands the context in which it was created. This aims to understand (i) the theories which were used to describe physical systems prior to its development, and (ii) the experiments which did not fit in this context.

In this section we make a brief introduction to classical mechanics¹, with emphasis in analyzing the Hamiltonian formalism and how it treats observable magnitudes. We will see that a proper understanding of this formalism is needed to make the transition to quantum mechanics.

A.1.1 The Lagrangian formalism

In classical mechanics the state of a system is specified by the position of its constituent particles at all times, $\mathbf{r}_j(t) = [x_j(t), y_j(t), z_j(t)]$ with $j = 1, 2, \dots, N$, being N the number of particles. Defining the linear momentum of the particles as $\mathbf{P}_j = m_j \dot{\mathbf{r}}_j$ (m_j is the mass of particle j), the evolution of the system is found from a set of initial positions and velocities by solving the Newtonian equations of motion $\dot{\mathbf{P}}_j = \mathbf{F}_j$, being \mathbf{F}_j the forces acting onto particle j .

Most physical systems have further constraints that have to fulfil (for example, the distance between the particles of a rigid body cannot change with time, that is, $|\mathbf{r}_j - \mathbf{r}_l| = \text{const}$), and therefore the positions $\{\mathbf{r}_j\}_{j=1, \dots, N}$ are no longer independent, what makes Newton's equations hard to solve. This calls for a new, simpler theoretical framework: the so-called *analytical mechanics*.

In analytical mechanics the state of the system at any time is specified by a vector $\mathbf{q}(t) = [q_1(t), q_2(t), \dots, q_n(t)]$; n is the number of degrees of freedom of the system (the total number of coordinates, $3N$, minus the number of constraints), and the q_j 's are called the *generalized coordinates* of the system, which are compatible with the constraints and related with the usual coordinates of the particles by some smooth functions $\mathbf{q}(\mathbf{r}_j) \Leftrightarrow \{\mathbf{r}_j(\mathbf{q})\}_{j=1, \dots, N}$. In the following, we will call *coordinate space* to the space formed by the generalized coordinates, and $\mathbf{q}(t)$ a *trajectory* on it.

The basic object in analytical mechanics is the *Lagrangian*, $L[\mathbf{q}(t), \dot{\mathbf{q}}(t), t]$, which is a function of the generalized coordinates and velocities, and can even have some explicit time dependence. In general, the Lagrangian must be built based on general principles like symmetries; however, if the forces acting on the particles of the system are conservative, that is, $\mathbf{F}_j = \nabla_j V[\{\mathbf{r}_l\}_{l=1, \dots, N}] = (\partial_{x_j} V, \partial_{y_j} V, \partial_{z_j} V)$ for some *potential* $V[\{\mathbf{r}_l\}_{l=1, \dots, N}]$, it takes the simple form $L = T(\dot{\mathbf{q}}, \mathbf{q}) - V(\mathbf{q})$, being $T(\dot{\mathbf{q}}, \mathbf{q}) = \sum_{j=1}^N m_j \dot{\mathbf{r}}_j^2(\mathbf{q})/2$ the kinetic energy of the system and $V(\mathbf{q}) = V[\{\mathbf{r}_j(\mathbf{q})\}_{j=1, \dots, n}]$. The dynamic equations of the system are then formulated as a *variational principle* on the *action*

$$S = \int_{t_1}^{t_2} dt L[\mathbf{q}(t), \dot{\mathbf{q}}(t), t], \quad (\text{A.1})$$

by asking the trajectory of the system $\mathbf{q}(t)$ between two fixed points $\mathbf{q}(t_1)$ and $\mathbf{q}(t_2)$ to be such that the action is an extremal, $\delta S = 0$. From this principle, it is straightforward to arrive to the well known Euler-Lagrange equations

$$\frac{\partial L}{\partial q_j} - \frac{d}{dt} \frac{\partial L}{\partial \dot{q}_j} = 0, \quad (\text{A.2})$$

¹ For a deeper lecture concerning this topic we recommend Goldstein's book [162], as well as Greiner's books [163, 164]

which are a set of second order differential equations for the generalized coordinates \mathbf{q} , and together with the conditions $\mathbf{q}(t_1)$ and $\mathbf{q}(t_2)$ provide the trajectory $\mathbf{q}(t)$.

A.1.2 The Hamiltonian formalism

As we have seen, the Euler–Lagrange equations are a set of second order differential equations which allow us to find the trajectory $\mathbf{q}(t)$ on coordinate space. We could reduce the order of the differential equations by taking the velocities $\dot{\mathbf{q}}$ as dynamical variables, arriving then to a set of $2n$ first order differential equations. This is, however, a very naïve way of reducing the order, which leads to a non-symmetric system of equations for \mathbf{q} and $\dot{\mathbf{q}}$. In this section we review Hamilton’s approach to analytical mechanics, which leads to a symmetric-like first order system of equations, and is of major importance to understand the transition from classical to quantum mechanics.

Instead of using the velocities, the Hamiltonian formalism considers the *generalized momenta*

$$p_j = \frac{\partial L}{\partial \dot{q}_j}, \quad (\text{A.3})$$

as the dynamical variables. Note that this definition establishes a relation between these generalized momenta and the velocities $\dot{\mathbf{q}}(\mathbf{q}, \mathbf{p}) \Leftrightarrow \mathbf{p}(\mathbf{q}, \dot{\mathbf{q}})$. Note also that when the usual Cartesian coordinates of the system’s particles are taken as the generalized coordinates these momenta coincide with those of Newton’s approach.

The theory is then built in terms of a new object called the *Hamiltonian*, which is defined as a Legendre transform of the Lagrangian,

$$H(\mathbf{q}, \mathbf{p}) = \mathbf{p}\dot{\mathbf{q}}(\mathbf{q}, \mathbf{p}) - L[\mathbf{q}, \dot{\mathbf{q}}(\mathbf{q}, \mathbf{p}), t], \quad (\text{A.4})$$

and coincides with the total energy for conservative systems, that is, $H(\mathbf{q}, \mathbf{p}) = T(\mathbf{q}, \mathbf{p}) + V(\mathbf{q})$, with $T(\mathbf{q}, \mathbf{p}) = T[\mathbf{q}, \dot{\mathbf{q}}(\mathbf{q}, \mathbf{p})]$. Differentiating this expression and using the Euler–Lagrange equations (or using again the variational principle on the action), it is then straightforward to obtain the equations of motion for the generalized coordinates and momenta (the *canonical equations*),

$$\dot{q}_j = \frac{\partial H}{\partial p_j} \quad \text{and} \quad \dot{p}_j = -\frac{\partial H}{\partial q_j}, \quad (\text{A.5})$$

which together with some initial conditions $\{\mathbf{q}(t_0), \mathbf{p}(t_0)\}$ allow us to find the trajectory $\{\mathbf{q}(t), \mathbf{p}(t)\}$ in the space formed by the generalized coordinates and momenta, which we will call *phase space*.

Another important object in the Hamiltonian formalism is the *Poisson bracket*; given two functions of the coordinates and momenta $F(\mathbf{q}, \mathbf{p})$ and $G(\mathbf{q}, \mathbf{p})$, their Poisson bracket is defined as

$$\{F, G\} = \sum_{j=1}^N \frac{\partial F}{\partial q_j} \frac{\partial G}{\partial p_j} - \frac{\partial F}{\partial p_j} \frac{\partial G}{\partial q_j}. \quad (\text{A.6})$$

The importance of this object is reflected in the fact that the evolution equation of any quantity $g(\mathbf{q}, \mathbf{p}, t)$ can be written as

$$\frac{dg}{dt} = \{g, H\} + \frac{\partial g}{\partial t}, \quad (\text{A.7})$$

and hence, if the quantity doesn’t depend on time and *commutes* with the Hamiltonian, that is, its Poisson bracket with the Hamiltonian is zero, it is a *constant of motion*.

Of particular importance for the transition to quantum mechanics are the *fundamental Poisson brackets*, that is, the Poisson brackets of the coordinates and momenta,

$$\{q_j, p_l\} = \delta_{jl}, \quad \{q_j, q_l\} = \{p_j, p_l\} = 0. \quad (\text{A.8})$$

A.1.3 Observables and their mathematical structure

In this last section concerning classical mechanics, we would like to explain the mathematical structure in which observables are embedded within the Hamiltonian formalism. We will show that the mathematical objects corresponding to physical observables form a well defined mathematical structure, a real Lie algebra. Moreover, the position and momentum will be shown to be the generators of a particular Lie group, the Heisenberg group. Understanding this internal structure of *classical observables* will give us the chance to introduce the quantum description of observables in a reasonable way. Let us start by defining the concept of Lie algebra.

A *real Lie algebra* is a real vector space² \mathcal{L} equipped with an additional operation, the *Lie product*, which takes two vectors f and g from \mathcal{L} , to generate another vector also in \mathcal{L} denoted by $\{f, g\}$; this operation must satisfy the following properties:

1. $\{f, g + h\} = \{f, g\} + \{f, h\}$ (linearity)
2. $\{f, f\} = 0 \xrightarrow{\text{together with 1}} \{f, g\} = -\{g, f\}$ (anticommutativity)
3. $\{f, \{g, h\}\} + \{g, \{h, f\}\} + \{h, \{f, g\}\} = 0$ (Jacobi identity)

Hence, in essence a real Lie algebra is basically a vector space equipped with a linear, non-commutative, non-associative product. They have been subject of study for many years, and now we know a lot about the properties of these mathematical structures. They appear in many branches of physics and geometry, specially connected to continuous symmetry transformations, whose associated mathematical structures are actually called *Lie groups*. In particular, it is possible to show that given any Lie group with p parameters (like, e.g., the three-parameter groups of translations or rotations in real space), any transformation onto the system in which it is acting can be generated from a set of p elements of a Lie algebra $\{g_1, g_2, \dots, g_p\}$, called the *generators* of the Lie group, which satisfy some particular relations

$$\{g_j, g_k\} = \sum_{l=1}^p c_{jkl} g_l; \quad (\text{A.9})$$

these relations are called the *algebra–group relations*, and the *structure constants* c_{jkl} are characteristic of the particular Lie group (for example, the generators of translations and rotations in real space are the momenta and angular momenta, respectively, and the corresponding structure constants are $c_{jkl} = 0$ for the translation group and $c_{jkl} = i\epsilon_{jkl}$ for the rotation group³).

Coming back to the Hamiltonian formalism, we start by noting that *observables*, being *measurable* quantities, must be given by continuous, real functions in phase space; hence they form a real vector space with respect to the usual addition of functions and multiplication of a function by a real number. It also appeared naturally in the formalism a linear, non-commutative, non-associative operation between phase space functions, the Poisson bracket, which applied to real functions gives another real function. It is easy to see that the Poisson bracket satisfies all the requirements of a Lie product, and hence, observables form a Lie algebra within the Hamiltonian formalism.

Moreover, the fundamental Poisson brackets (A.8) show that the generalized coordinates \mathbf{q} and momenta \mathbf{p} , together with the identity in phase space, satisfy particular algebra–group relations, namely⁴ $\{q_j, p_k\} = \delta_{jk} 1$ and $\{q_j, 1\} = \{p_j, 1\} = 0$, and hence can be seen as the generators of a Lie group; this group is known as the *Heisenberg group*⁵.

Therefore, we arrive to the main result of this section:

[The mathematical framework of Hamiltonian mechanics associates physical observables with elements of a Lie algebra, being the phase space coordinates themselves the generators of the Heisenberg group.]

Maintaining this structure for observables will help to develop the laws of quantum mechanics.

² The concept of complex vector space is defined in the next section; the definition of a real vector space is the same, but changing complex numbers by real numbers.

³ ϵ_{jkl} is the Levi-Civita symbol, which has $\epsilon_{123} = \epsilon_{312} = \epsilon_{231} = 1$ and is completely antisymmetric, that is, changes its sign after permutation of any pair of indices.

⁴ Ordering the generators as $\{\mathbf{q}, \mathbf{p}, 1\}$, the structure constants associated to this algebra–group relations are explicitly

$$c_{jkl} = \begin{cases} \Omega_{jk} \delta_{l, 2n+1} & j, k = 1, 2, \dots, 2n \\ 0 & j = 2n + 1 \text{ or } k = 2n + 1 \end{cases}, \quad (\text{A.10})$$

being $\Omega = \begin{pmatrix} 0_{n \times n} & I_{n \times n} \\ -I_{n \times n} & 0_{n \times n} \end{pmatrix}$, with $I_{n \times n}$ and $0_{n \times n}$ the $n \times n$ identity and null matrices, respectively.

⁵ This group was introduced by Weyl when trying to prove the equivalence between the Schrödinger and Heisenberg pictures of quantum mechanics. It was later shown to have connections with the symplectic group, which is the basis of many physical theories. We could have taken the Poisson brackets between the angular momenta associated to the possible rotations in the system of particles (which are certainly far more intuitive transformations than the one related to the Heisenberg group) as the fundamental ones; however, we have chosen the Lie algebra associated to the Heisenberg group just because it deals directly with position and momenta, allowing for a simpler connection to quantum mechanics.

A.2 The mathematical language of quantum mechanics: Hilbert spaces

Just as classical mechanics is formulated in terms of the mathematical language of differential calculus and its extensions, quantum mechanics takes linear algebra (and Hilbert spaces in particular) as its fundamental grammar. In this section we introduce the concept of Hilbert space, and discuss the properties of some operators which will play important roles in the formalism of quantum mechanics.

A.2.1 Finite-dimensional Hilbert spaces

In essence, a Hilbert space is a *complex vector space* in which an *inner product* is defined. Let us define first these terms as will be used in this thesis.

A *complex vector space* is a set \mathcal{V} , whose elements will be called *vectors* or *kets* and will be denoted by $\{|a\rangle, |b\rangle, |c\rangle, \dots\}$ (a, b , and c may correspond to any suitable label), in which the following two operations are defined: the *vector addition*, which takes two vectors $|a\rangle$ and $|b\rangle$ and creates a new vector inside \mathcal{V} denoted by $|a\rangle + |b\rangle$; and the *multiplication by a scalar*, which takes a complex number $\alpha \in \mathbb{C}$ (in this section Greek letters will represent complex numbers) and a vector $|a\rangle$ to generate a new vector in \mathcal{V} denoted by $\alpha|a\rangle$.

The following additional properties must be satisfied:

1. The vector addition is commutative and associative, that is, $|a\rangle + |b\rangle = |b\rangle + |a\rangle$ and $(|a\rangle + |b\rangle) + |c\rangle = |a\rangle + (|b\rangle + |c\rangle)$.
2. There exists a null vector $|null\rangle$ such that $|a\rangle + |null\rangle = |a\rangle$.
3. $\alpha(|a\rangle + |b\rangle) = \alpha|a\rangle + \alpha|b\rangle$.
4. $(\alpha + \beta)|a\rangle = \alpha|a\rangle + \beta|a\rangle$.
5. $(\alpha\beta)|a\rangle = \alpha(\beta|a\rangle)$.
6. $1|a\rangle = |a\rangle$.

From these properties it can be proved that the null vector is unique, and can be built from any vector $|a\rangle$ as $0|a\rangle$; hence, in the following we denote it simply by $|null\rangle \equiv 0$. It can also be proved that any vector $|a\rangle$ has a unique *antivector* $|-a\rangle$ such that $|a\rangle + |-a\rangle = 0$, which is given by $(-1)|a\rangle$ or simply $-|a\rangle$.

An *inner product* is an additional operation defined in the complex vector space \mathcal{V} , which takes two vectors $|a\rangle$ and $|b\rangle$ and associates them a complex number. It will be denoted by $\langle a|b\rangle$ or sometimes also by $(|a\rangle, |b\rangle)$, and must satisfy the following properties:

1. $\langle a|a\rangle > 0$ if $|a\rangle \neq 0$.
2. $\langle a|b\rangle = \langle b|a\rangle^*$.
3. $(|a\rangle, \alpha|b\rangle) = \alpha\langle a|b\rangle$.
4. $(|a\rangle, |b\rangle + |c\rangle) = \langle a|b\rangle + \langle a|c\rangle$.

The following additional properties can be proved from these ones:

- $\langle null|null\rangle = 0$.
- $(\alpha|a\rangle, |b\rangle) = \alpha^*\langle a|b\rangle$.
- $(|a\rangle + |b\rangle, |c\rangle) = \langle a|c\rangle + \langle b|c\rangle$.
- $|\langle a|b\rangle|^2 \leq \langle a|a\rangle\langle b|b\rangle$

Note that for any vector $|a\rangle$, one can define the object $\langle a| \equiv (|a\rangle, \cdot)$, which will be called a *dual vector* or a *bra*, and which takes a vector $|b\rangle$ to generate the complex number $(|a\rangle, |b\rangle) \in \mathbb{C}$. It can be proved that the set formed by all the dual vectors corresponding to the elements in \mathcal{V} is also a vector space, which will be called the *dual space* and will be denoted by \mathcal{V}^+ . Within this picture, the inner product can be seen as an operation which takes a bra $\langle a|$ and a ket $|b\rangle$ to generate the complex number $\langle a|b\rangle$, a *bracket*. This whole *bra-c-ket* notation is due to Dirac.

In the following we assume that any time a bra $\langle a|$ is applied to a ket $|b\rangle$, the complex number $\langle a|b\rangle$ is formed, so that objects like $|b\rangle\langle a|$ generate kets when applied to kets from the left, $(|b\rangle\langle a|)|c\rangle = (\langle a|c\rangle)|b\rangle$, and bras when applied to bras from the right, $\langle c|(|b\rangle\langle a|) = (\langle c|b\rangle)\langle a|$. Technically, $|b\rangle\langle a|$ is called an *outer product*.

A vector space equipped with an inner product is called an *Euclidean space*. In the following we give some important definitions and properties which are needed in order to understand the concept of Hilbert space:

- The vectors $\{|a_1\rangle, |a_2\rangle, \dots, |a_m\rangle\}$ are said to be *linearly independent* if the relation $\alpha_1|a_1\rangle + \alpha_2|a_2\rangle + \dots + \alpha_m|a_m\rangle = 0$ is satisfied only for $\alpha_1 = \alpha_2 = \dots = \alpha_m = 0$, as otherwise one of them can be written as a linear combination of the rest.
- The *dimension* of the vector space is defined as the maximum number of linearly independent vectors, and can be finite or infinite.
- If the dimension of an Euclidean space is $d < \infty$, it is always possible to build a set of d orthonormal vectors $E = \{|e_j\rangle\}_{j=1,2,\dots,d}$ satisfying $\langle e_j|e_l\rangle = \delta_{jl}$, such that any other vector $|a\rangle$ can be written as a linear superposition of them, that is, $|a\rangle = \sum_{j=1}^d a_j |e_j\rangle$, being the a_j 's some complex numbers. This set is called an *orthonormal basis* of the Euclidean space \mathcal{V} , and the coefficients a_j of the expansion can be found as $a_j = \langle e_j|a\rangle$. The column formed with the expansion coefficients, which is denoted by $\text{col}(a_1, a_2, \dots, a_d)$, is called a *representation* of the vector $|a\rangle$ in the basis E .

Note that the set $E^+ = \{\langle e_j|\}_{j=1,2,\dots,d}$ is an orthonormal basis in the dual space \mathcal{V}^+ , so that any bra $\langle a|$ can be expanded then as $\langle a| = \sum_{j=1}^d a_j^* \langle e_j|$. The representation of the bra $\langle a|$ in the basis E corresponds to the row formed by its expansion coefficients, and is denoted by $(a_1^*, a_2^*, \dots, a_d^*)$. Note that if the representation of $|a\rangle$ is seen as a $d \times 1$ matrix, the representation of $\langle a|$ can be obtained as its $1 \times d$ conjugate–transpose matrix.

Note finally that the inner product of two vectors $|a\rangle$ and $|b\rangle$ reads $\langle a|b\rangle = \sum_{j=1}^d a_j^* b_j$ when represented in the same basis, which is the matrix product of the representations of $\langle a|$ and $|b\rangle$.

For finite dimension, an Euclidean space is a *Hilbert space*. However, in most applications of quantum mechanics (and certainly in quantum optics), one has to deal with infinite–dimensional vector spaces. We will treat them after the following section.

A.2.2 Linear operators in finite–dimensional Hilbert spaces

We now discuss the concept of linear operator, as well as analyze the properties of some important classes of operators. Only finite–dimensional Hilbert spaces are considered in this section, we will generalize the discussion to infinite–dimensional Hilbert spaces in the next section.

We are interested in maps \hat{L} (operators will be denoted with ‘ $\hat{}$ ’ throughout the thesis) which associate to any vector $|a\rangle$ of a Hilbert space \mathcal{H} another vector denoted by $\hat{L}|a\rangle$ in the same Hilbert space. If the map satisfies

$$\hat{L}(\alpha|a\rangle + \beta|b\rangle) = \alpha\hat{L}|a\rangle + \beta\hat{L}|b\rangle, \quad (\text{A.11})$$

then it is called a *linear operator*. For our purposes this is the only class of interesting operators, and hence we will simply call them *operators* in the following.

Before discussing the properties of some important classes of operators, we need some definitions:

- Given an orthonormal basis $E = \{|e_j\rangle\}_{j=1,2,\dots,d}$ in a Hilbert space \mathcal{H} with dimension $d < \infty$, any operator \hat{L} has a representation; while bras and kets are represented by $d \times 1$ and $1 \times d$ matrices (rows and columns), respectively, an operator \hat{L} is represented by a $d \times d$ matrix with *elements* $L_{jl} = (|e_j\rangle, \hat{L}|e_l\rangle) \equiv \langle e_j|\hat{L}|e_l\rangle$. An operator \hat{L} can then be expanded in terms of the basis E as $\hat{L} = \sum_{j,l=1}^d L_{jl} |e_j\rangle\langle e_l|$. It follows that the representation of the vector $|b\rangle = \hat{L}|a\rangle$ is just the matrix multiplication of the representation of \hat{L} by the representation of $|a\rangle$, that is, $b_j = \sum_{l=1}^d L_{jl} a_l$.
- The *addition* and *product* of two operators \hat{L} and \hat{K} , denoted by $\hat{L} + \hat{K}$ and $\hat{L}\hat{K}$, respectively, are defined by their action onto any vector $|a\rangle$: $(\hat{L} + \hat{K})|a\rangle = \hat{L}|a\rangle + \hat{K}|a\rangle$ and $\hat{L}\hat{K}|a\rangle = \hat{L}(\hat{K}|a\rangle)$. It follows that the representation of the addition and the product are, respectively, the sum and the multiplication of the corresponding matrices, that is, $(\hat{L} + \hat{K})_{jl} = L_{jl} + K_{jl}$ and $(\hat{L}\hat{K})_{jl} = \sum_{k=1}^d L_{jk} K_{kl}$.
- Note that while the addition is commutative, the product is not in general. This leads us to the notion of *commutator*, defined for two operators \hat{L} and \hat{K} as $[\hat{L}, \hat{K}] = \hat{L}\hat{K} - \hat{K}\hat{L}$. When $[\hat{L}, \hat{K}] = 0$, we say that the operators *commute*.

- Given an operator \hat{L} , its *trace* is defined as the sum of the diagonal elements of its matrix representation, that is, $\text{tr}\{\hat{L}\} = \sum_{j=1}^d L_{jj}$. It may seem that this definition is basis-dependent, as in general the elements L_{jj} are different in different bases. However, we will see that the trace is invariant under any change of basis.

The trace has two important properties. It is *linear* and *cyclic*, that is, given two operators \hat{L} and \hat{K} , $\text{tr}\{\hat{L} + \hat{K}\} = \text{tr}\{\hat{L}\} + \text{tr}\{\hat{K}\}$ and $\text{tr}\{\hat{L}\hat{K}\} = \text{tr}\{\hat{K}\hat{L}\}$, as is trivially proved.

- We say that a vector $|l\rangle$ is an *eigenvector* of an operator \hat{L} if $\hat{L}|l\rangle = \lambda|l\rangle$; $\lambda \in \mathbb{C}$ is called its associated *eigenvalue*. The set of all the eigenvalues of an operator is called its *spectrum*.

We can pass now to describe some classes of operators which play important roles in quantum mechanics.

The identity operator. The *identity operator*, denoted by \hat{I} , is defined as the operator which maps any vector onto itself. Its representation in any basis is then $I_{jl} = \delta_{jl}$, so that it can be expanded as

$$\hat{I} = \sum_{j=1}^d |e_j\rangle \langle e_j|. \quad (\text{A.12})$$

This expression is known as the *completeness relation* of the basis E ; alternatively, it is said that the set E forms a *resolution of the identity*.

Note that the expansion of a vector $|a\rangle$ and its dual $\langle a|$ in the basis E is obtained just by application of the completeness relation from the left and the right, respectively. Similarly, the expansion of an operator \hat{L} is obtained by application of the completeness relation both from the right and the left at the same time.

The inverse of an operator. The *inverse* of an operator \hat{L} , denoted by \hat{L}^{-1} , is defined as that satisfying $\hat{L}^{-1}\hat{L} = \hat{L}\hat{L}^{-1} = \hat{I}$.

An operator function. Consider a real function $f(x)$ which can be expanded in powers of x as $f(x) = \sum_{m=0}^{\infty} f_m x^m$; given an operator \hat{L} , we define the *operator function* $\hat{f}(\hat{L}) = \sum_{m=0}^{\infty} f_m \hat{L}^m$, where \hat{L}^m means the product of \hat{L} with itself m times.

The adjoint of an operator. Given an operator \hat{L} , we define its *adjoint*, and denote it by \hat{L}^\dagger , as that satisfying $(|a\rangle, \hat{L}|b\rangle) = (\hat{L}^\dagger|a\rangle, |b\rangle)$ for any two vectors $|a\rangle$ and $|b\rangle$. Note that the representation of \hat{L}^\dagger corresponds to the conjugate transpose of the matrix representing \hat{L} , that is $(\hat{L}^\dagger)_{jl} = L_{lj}^*$. Note also that the adjoint of a product of two operators \hat{K} and \hat{L} is given by $(\hat{K}\hat{L})^\dagger = \hat{L}^\dagger\hat{K}^\dagger$.

Self-adjoint operators. We say that \hat{H} is a *self-adjoint* if it coincides with its adjoint, that is, $\hat{H} = \hat{H}^\dagger$. A property which will be shown to be of major importance for the construction of the laws of quantum mechanics is that the spectrum $\{h_j\}_{j=1,2,\dots,d}$ of a self-adjoint operator is real. Moreover, its associated eigenvectors⁶ $\{|h_j\rangle\}_{j=1,2,\dots,d}$ form an orthonormal basis of the Hilbert space.

The representation of any operator function $\hat{f}(\hat{H})$ in the *eigenbasis* of \hat{H} is then $[\hat{f}(\hat{H})]_{jl} = f(h_j) \delta_{jl}$, from which follows

$$\hat{f}(\hat{H}) = \sum_{j=1}^d f(h_j) |h_j\rangle \langle h_j|. \quad (\text{A.13})$$

This result is known as the *spectral theorem*.

Unitary operators. We say that \hat{U} is a *unitary operator* if $\hat{U}^\dagger = \hat{U}^{-1}$. The interest of this class of operators is that they preserve inner products, that is, for any two vectors $|a\rangle$ and $|b\rangle$ the inner product $(\hat{U}|a\rangle, \hat{U}|b\rangle)$ coincides with $\langle a|b\rangle$. Moreover, it is possible to show that given two orthonormal bases $E = \{|e_j\rangle\}_{j=1,2,\dots,d}$ and $E' = \{|e'_j\rangle\}_{j=1,2,\dots,d}$, there exists a unique unitary matrix \hat{U} which connects them as $\{|e'_j\rangle\rangle = \hat{U}|e_j\rangle\}_{j=1,2,\dots,d}$, and then any basis of the Hilbert space is unique up to a unitary transformation.

We can now prove that the trace of an operator is basis-independent. Let us denote by $\text{tr}\{\hat{L}\}_E$ the trace of an operator \hat{L} in the basis E ; the trace of this operator in the transformed basis can be written then as $\text{tr}\{\hat{L}\}_{E'} =$

⁶ We will assume that the spectrum of any operator is non-degenerate, that is, only one eigenvector corresponds to a given eigenvalue, as all the operators that appear in this thesis have this property.

$\text{tr}\{\hat{U}^\dagger \hat{L} \hat{U}\}_E$, or using the cyclic property of the trace and the unitarity of \hat{U} , $\text{tr}\{\hat{L}\}_{E'} = \text{tr}\{\hat{U} \hat{U}^\dagger \hat{L}\} = \text{tr}\{\hat{L}\}_E$, which proves that the trace is equal in both bases.

Note finally that a unitary operator \hat{U} can always be written as the exponential of i -times a self-adjoint operator \hat{H} , that is, $\hat{U} = \exp(i\hat{H})$.

Projection operators. In general, any self-adjoint operator \hat{P} satisfying $\hat{P}^2 = \hat{P}$ is called a *projector*. We are interested only in those projectors which can be written as the outer product of a vector $|a\rangle$ with itself, that is, $\hat{P}_a = |a\rangle \langle a|$; when applied to a vector $|b\rangle$, this gets *projected* along the ‘direction’ of $|a\rangle$ as $\hat{P}_a |b\rangle = (\langle a|b\rangle) |a\rangle$.

Note that given an orthonormal basis E , we can use the projectors $\hat{P}_j = |e_j\rangle \langle e_j|$ to extract the components of a vector $|c\rangle$ as $\hat{P}_j |c\rangle = c_j |e_j\rangle$. Note also that the completeness and orthonormality of the basis E implies that $\sum_{j=1}^d \hat{P}_j = \hat{I}$ and $\hat{P}_j \hat{P}_l = \delta_{jl} \hat{P}_j$, respectively.

Density operators. A self-adjoint operator $\hat{\rho}$ is called a *density operator* if it is *positive semidefinite*, that is $\langle a | \hat{\rho} | a \rangle \geq 0$ for any vector $|a\rangle$, and has unit trace.

The interesting property of density operators is that they ‘hide’ probability distributions in the diagonal of its representation. To see this just note that given an orthonormal basis E , the self-adjointness and positivity of $\hat{\rho}$ ensure that all its diagonal elements $\{\rho_{jj}\}_{j=1,2,\dots,d}$ are either positive or zero, that is, $\rho_{jj} \geq 0 \forall j$, while the unit trace makes them satisfy $\sum_{j=1}^d \rho_{jj} = 1$. Hence, the diagonal elements of a density operator have all the properties required by a *probability distribution*.

It is possible to show that a density operator can always be expressed as a *statistical* or *convex mixture* of projection operators, that is, $\hat{\rho} = \sum_{k=1}^M w_k |a_k\rangle \langle a_k|$, where $\sum_{k=1}^M w_k = 1$ and the vectors $\{|a_k\rangle\}_{k=1}^M$ are normalized to one, but don’t need not to be orthogonal (note that in fact M doesn’t need to be equal to d). Hence, another way of specifying a density matrix is by a set of normalized vectors together with some statistical rule for mixing them. When only one vector $|a\rangle$ contributes to the mixture, $\hat{\rho} = |a\rangle \langle a|$ is completely specified by just this single vector, and we say that the density operator is *pure*; otherwise, we say that it is *mixed*.

A.2.3 Generalization to infinite dimensions

As shown in the thesis (see Chapters 2 and 3), the natural Euclidean space for quantum optics is infinite-dimensional. Unfortunately, not all the previous concepts and objects that we have introduced for the finite-dimensional case are trivially generalized to infinite dimensions; in this section we discuss this generalization.

The first problem that we meet when dealing with infinite-dimensional Euclidean spaces is that the existence of a basis $\{|e_j\rangle\}_{j=1,2,\dots}$ in which any other vector can be represented as $|a\rangle = \sum_{j=1}^{\infty} a_j |e_j\rangle$ is not granted. The class of infinite-dimensional Euclidean spaces in which these infinite but countable bases exist are called *Hilbert spaces*, and are the ones that will be appearing in quantum mechanics.

The conditions which ensure that an infinite-dimensional Euclidean space is indeed a Hilbert space can be found in, for example, reference [165]. Here we just want to stress that quite intuitively, any infinite-dimensional Hilbert space⁷ is *isomorphic* to the space called $l^2(\infty)$, which is formed by the column vectors $|a\rangle \equiv \text{col}(a_1, a_2, \dots)$ where the set $\{a_j \in \mathbb{C}\}_{j=1,2,\dots}$ satisfies the restriction $\sum_{j=1}^{\infty} |a_j|^2 < \infty$, and has the operations $|a\rangle + |b\rangle = \text{col}(a_1 + b_1, a_2 + b_2, \dots)$, $\alpha |a\rangle = \text{col}(\alpha a_1, \alpha a_2, \dots)$, and $\langle a|b\rangle = \sum_{j=1}^{\infty} a_j^* b_j$.

Most of the previous definitions are directly generalized to Hilbert spaces by taking $d \rightarrow \infty$ (dual space, representations, operators,...). However, there is one crucial property of self-adjoint operators which doesn’t hold in this case: its eigenvectors may not form an orthonormal basis of the Hilbert space. The remainder of this section is devoted to deal with this problem.

Just as in finite dimension, given an infinite-dimensional Hilbert space \mathcal{H} , we say that one of its vectors $|d\rangle$ is an eigenvector of the self-adjoint operator \hat{H} if $\hat{H}|d\rangle = \delta|d\rangle$, where $\delta \in \mathbb{C}$ is called its associated eigenvalue. Nevertheless, it can happen in infinite-dimensional spaces that some vector $|c\rangle$ not contained in \mathcal{H} also satisfies the condition

⁷ An example of infinite-dimensional complex Hilbert space consists in the vector space formed by the complex functions of real variable, say $|f\rangle = f(x)$ with $x \in \mathbb{R}$, with integrable square, that is

$$\int_{\mathbb{R}} dx |f(x)|^2 < \infty, \quad (\text{A.14})$$

with the inner product

$$\langle g|f\rangle = \int_{\mathbb{R}} dx g^*(x) f(x). \quad (\text{A.15})$$

This Hilbert space is known as the $L^2(x)$ space.

$\hat{H}|c\rangle = \chi|c\rangle$, in which case we call it a *generalized eigenvector*, being χ its *generalized eigenvalue*⁸. The set of all the eigenvalues of the self-adjoint operator is called its *discrete* (or *point*) *spectrum* and is a countable set, while the set of all its generalized eigenvalues is called its *continuous spectrum* and is uncountable, that is, forms a continuous set [165] (see also [166]).

In quantum optics we find two extreme cases: either the observable, say \hat{H} , has a pure discrete spectrum $\{h_j\}_{j=1,2,\dots}$; or the observable, say \hat{X} , has a pure continuous spectrum $\{x\}_{x\in\mathbb{R}}$. It can be shown that in the first case the eigenvectors of the observable form an orthonormal basis of the Hilbert space, so that we can build a resolution of the identity as $\hat{I} = \sum_{j=1}^{\infty} |h_j\rangle\langle h_j|$, and proceed along the lines of the previous sections.

In the second case, the set of generalized eigenvectors cannot form a basis of the Hilbert space in the strict sense, as they do not form a countable set and do not even belong to the Hilbert space. Fortunately, there are still ways to treat the generalized eigenvectors of \hat{X} ‘as if’ they were a basis of the Hilbert space. The idea was introduced by Dirac [167], who realized that normalizing the generalized eigenvectors as⁹ $\langle x|y\rangle = \delta(x-y)$, one can define the following integral operator

$$\int_{\mathbb{R}} dx |x\rangle\langle x| = \hat{I}_c, \quad (\text{A.19})$$

which acts as the identity onto the generalized eigenvectors, that is, $\hat{I}_c|x\rangle = |x\rangle$; it is then assumed that \hat{I}_c coincides with the identity in \mathcal{H} , so that any other vector $|a\rangle$ or operator \hat{L} in the Hilbert space can be expanded as

$$|a\rangle = \int_{\mathbb{R}} dx a(x) |x\rangle \quad \text{and} \quad \hat{L} = \int_{\mathbb{R}^2} dx dy L(x, y) |x\rangle\langle y| \quad (\text{A.20})$$

where the elements $a(x) = \langle x|a\rangle$ and $L(x, y) = \langle x|\hat{L}|y\rangle$ of this *continuous representations* form complex functions defined in \mathbb{R} and \mathbb{R}^2 , respectively. From now on, we will call *continuous basis* to the set $\{|x\rangle\}_{x\in\mathbb{R}}$.

Dirac introduced this continuous representations as a ‘limit to the continuum’ of the countable case; even though this approach was very intuitive, it lacked of mathematical rigor. Some decades after Dirac’s proposal, Gel’fand showed how to generalize the concept of Hilbert space to include these generalized representations in full mathematical rigor [168]. The generalized spaces are called *rigged Hilbert spaces* (in which the algebra of Hilbert spaces joins forces with the theory of continuous probability distributions), and working on them it is possible to show that given any self-adjoint operator, one can use its eigenvectors and generalized eigenvectors to expand any vector of the Hilbert space.

Note finally that given two vectors $|a\rangle$ and $|b\rangle$ of the Hilbert space, and a continuous basis $\{|x\rangle\}_{x\in\mathbb{R}}$, we can use their generalized representations to write their inner product as

$$\langle a|b\rangle = \int_{\mathbb{R}} dx a^*(x) b(x). \quad (\text{A.21})$$

It is also easily proved that the trace of any operator \hat{L} can be evaluated from its continuous representation on $\{|x\rangle\}_{x\in\mathbb{R}}$ as

$$\text{tr}\{\hat{L}\} = \int_{\mathbb{R}} dx L(x, x). \quad (\text{A.22})$$

This has important consequences for the properties of density operators, say $\hat{\rho}$ for the discussion which follows. We explained at the end of the last section that when represented on an orthonormal basis of the Hilbert space, its diagonal elements (which are real owed to its self-adjointness) can be seen as a probability distribution, because they satisfy $\sum_{j=1}^{\infty} \rho_{jj} = 1$ and $\rho_{jj} \geq 0 \forall j$. Similarly, because of its unit trace and positivity, the diagonal elements of its continuous representation satisfy $\int_{\mathbb{R}} dx \rho(x, x) = 1$ and $\rho(x, x) \geq 0 \forall x$, and hence, the real function $\rho(x, x)$ can be seen as a *probability density function*.

⁸ In $L^2(x)$ we have two simple examples of self-adjoint operators with eigenvectors not contained in $L^2(x)$: the so-called \hat{X} and \hat{P} , which, given an arbitrary vector $|f\rangle = f(x)$, act as $\hat{X}|f\rangle = xf(x)$ and $\hat{P}|f\rangle = -idf/dx$, respectively. This is simple to see, as the equations

$$xf_X(x) = Xf_X(x) \quad \text{and} \quad -i\frac{d}{dx}f_P(x) = Pf_P(x), \quad (\text{A.16})$$

have

$$f_X(x) = \delta(x-X) \quad \text{and} \quad f_P(x) = \exp(iPx), \quad (\text{A.17})$$

as solutions, which are not square-integrable, and hence do not belong to $L^2(x)$.

⁹ This $\delta(x)$ function the so-called *Dirac-delta distribution* which is defined by the conditions

$$\int_{x_1}^{x_2} dx \delta(x-y) = \begin{cases} 1 & \text{if } y \in [x_1, x_2] \\ 0 & \text{if } y \notin [x_1, x_2] \end{cases}. \quad (\text{A.18})$$

A.2.4 Composite Hilbert spaces

In many moments of this thesis, we find the need associate a Hilbert space to a composite system, the Hilbert spaces of whose parts we now. In this section we show how to build a Hilbert space \mathcal{H} starting from a set of Hilbert spaces $\{\mathcal{H}_A, \mathcal{H}_B, \mathcal{H}_C \dots\}$.

Let us start with only two Hilbert spaces \mathcal{H}_A and \mathcal{H}_B with dimensions d_A and d_B , respectively (which might be infinite); the generalization to an arbitrary number of Hilbert spaces is straightforward. Consider a vector space \mathcal{V} with dimension $\dim(\mathcal{V}) = d_A \times d_B$. We define a map called the *tensor product* which associates to any pair of vectors $|a\rangle \in \mathcal{H}_A$ and $|b\rangle \in \mathcal{H}_B$ a vector in \mathcal{V} which we denote by $|a\rangle \otimes |b\rangle \in \mathcal{V}$. This tensor product must satisfy the following properties:

1. $(|a\rangle + |b\rangle) \otimes |c\rangle = |a\rangle \otimes |c\rangle + |b\rangle \otimes |c\rangle$.
2. $|a\rangle \otimes (|b\rangle + |c\rangle) = |a\rangle \otimes |b\rangle + |a\rangle \otimes |c\rangle$.
3. $(\alpha|a\rangle) \otimes |b\rangle = |a\rangle \otimes (\alpha|b\rangle)$.

If we endorse the vector space \mathcal{V} with the inner product $(|a\rangle \otimes |b\rangle, |c\rangle \otimes |d\rangle) = \langle a|c\rangle \langle b|d\rangle$, it is easy to show it becomes a Hilbert space, which in the following will be denoted by $\mathcal{H} = \mathcal{H}_A \otimes \mathcal{H}_B$. Given the bases $E_A = \{|e_j^A\rangle\}_{j=1,2,\dots,d_A}$ and $E_B = \{|e_l^B\rangle\}_{l=1,2,\dots,d_B}$ of the Hilbert spaces \mathcal{H}_A and \mathcal{H}_B , respectively, a basis of the *tensor product Hilbert space* $\mathcal{H}_A \otimes \mathcal{H}_B$ can be built as $E = E_A \otimes E_B = \{|e_j^A\rangle \otimes |e_l^B\rangle\}_{j=1,2,\dots,d_A, l=1,2,\dots,d_B}$ (note that the notation in the first equality is symbolical).

We will use a more economic notation for the tensor product, namely $|a\rangle \otimes |b\rangle = |a, b\rangle$, except when the explicit tensor product symbol is needed for any reason. With this notation the basis of the tensor product Hilbert space is written as $E = \{|e_j^A, e_l^B\rangle\}_{j=1,2,\dots,d_A, l=1,2,\dots,d_B}$.

The tensor product also maps operators acting on \mathcal{H}_A and \mathcal{H}_B to operators acting on \mathcal{H} . Given two operators \hat{L}_A and \hat{L}_B acting on \mathcal{H}_A and \mathcal{H}_B , the *tensor product operator* $\hat{L} = \hat{L}_A \otimes \hat{L}_B$ is defined in \mathcal{H} as that satisfying $\hat{L}|a, b\rangle = (\hat{L}_A|a\rangle) \otimes (\hat{L}_B|b\rangle)$ for any pair of vectors $|a\rangle \in \mathcal{H}_A$ and $|b\rangle \in \mathcal{H}_B$. When explicit subindices making reference to the Hilbert space on which operators act on are used, so that there is no room for confusion, we will use the shorter notations $\hat{L}_A \otimes \hat{L}_B = \hat{L}_A \hat{L}_B$, $\hat{L}_A \otimes \hat{I} = \hat{L}_A$, and $\hat{I} \otimes \hat{L}_B = \hat{L}_B$.

Note that the tensor product preserves the properties of the operators; for example, given two self-adjoint operators \hat{H}_A and \hat{H}_B , unitary operators \hat{U}_A and \hat{U}_B , or density operators $\hat{\rho}_A$ and $\hat{\rho}_B$, the operators $\hat{H}_A \otimes \hat{H}_B$, $\hat{U}_A \otimes \hat{U}_B$, and $\hat{\rho}_A \otimes \hat{\rho}_B$ are self-adjoint, unitary, and a density operator in \mathcal{H} , respectively. Note that this doesn't mean that any self-adjoint, unitary, or density operator acting on \mathcal{H} can be written in a simple tensor product form $\hat{L}_A \otimes \hat{L}_B$.

A.3 The laws of quantum mechanics

A.3.1 A brief historical introduction

By the end of the XIX century there was a great feeling of security among the physics community: analytical mechanics (together with statistical mechanics) and Maxwell's electromagnetism, (in the following *classical physics* altogether) seem to explain the whole range of physical phenomena that one could observe, and hence, in a sense, the foundations of physics were completed. There were, however, a couple of experimental observations which lacked explanation within this 'definitive' framework, which actually lead to the construction of a whole new way of understanding physical phenomena: quantum mechanics.

Among these experimental evidences, the shape of the spectrum of the radiation emitted by a black body, the photoelectric effect which showed that only light exceeding some frequency can release electrons from a metal irrespective of its intensity, and the discrete set of spectral lines of hydrogen, were the principal triggers of the revolution to come in the first quarter of the XX century. The first two lead Planck and Einstein to suggest that electromagnetic energy is not continuous but divided in small packages of energy $\hbar\omega$ (ω being the frequency of the radiation), while Bohr succeed in explaining the latter by assuming that the electron orbiting the nucleus can occupy only a discrete set of orbits with angular momenta proportional to \hbar . The constant $\hbar = h/2\pi \sim 10^{-34} \text{J} \cdot \text{s}$, where h is now known as the Planck constant, appeared in both cases as somehow the 'quantization unit', the value separating the quantized values that energy or angular momentum are able to take.

Even though the physicists of the time tried to understand this quantization of the physical magnitudes within the framework of classical physics, it was soon realized that it would need a complete new theory to do it. The first attempts to build such a theory (which actually worked for some particular scenarios) were based on applying ad-hoc quantization rules to various mechanical variables of systems, but with a complete lack of physical interpretation for

such rules [169]. However, between 1925 and 1927 the first real formulations of the needed theory were developed: the *wave mechanics* of Schrödinger [170] and the *matrix mechanics* of Heisenberg, Born and Jordan [171, 172, 173] (see [169] for English translations), which received also independent contributions by Dirac [174]. Even though in both theories the quantization of various observable quantities appeared naturally and in correspondence with experiments, they seem completely different, at least until Schrödinger showed the equivalence between them both.

The new theory was later formalized mathematically using vector spaces by Dirac [167] (though not very rigorously), and a little after by von Neumann with full mathematical rigor using Hilbert spaces [175] ([176] for an English version); they developed the laws of *quantum mechanics* basically as we know it now [177, 178, 179, 180, 181].

A.3.2 The axioms of quantum mechanics

In this section we will introduce the basic postulates which describe how quantum mechanics treats physical systems. Being the basic blocks that build the theory, these axioms cannot be *proved*; they can only be formulated following *plausibility arguments* based on the *observation* of physical phenomena and the *connection* of the theory with previous theories which are known to work in some limit. We will try to motivate (and justify to a point) these axioms as much as possible.

Along these lines, the experimental evidence for the tendency of observable physical quantities to be quantized at the microscopic level motivates the first axiom:

Axiom I. [Any physical observable quantity A corresponds to a self-adjoint operator \hat{A} acting on an abstract Hilbert space; after a measurement of A , the only possible outcomes are the eigenvalues of \hat{A} .]

The quantization of physical observables is therefore directly introduced in the theory by this postulate. Note that it doesn't say anything about the dimension d of the Hilbert space corresponding to a given observable, and it even leaves open the possibility of observables having a continuous spectrum, not a discrete one. The problem of how to make the proper correspondence between observables and self-adjoint operators will be addressed in an axiom to come.

In the following we will use the name 'observable' for both the physical quantity A and its associated self-adjoint operator \hat{A} indistinctly. Observables having pure discrete spectrum or pure continuous spectrum will be referred to as *countable* and *continuous observables*, respectively.

Now we introduce the second axiom. It follows from the following question: the eigenvalues of an observable are the only values that can appear when measuring it, but what about the statistics of such a measurement? We know a class of operators in Hilbert spaces which act as probability distributions for the eigenvalues of any self-adjoint operator, density operators. This motivates the second axiom:

Axiom II. [The state of the system is completely specified by a density operator $\hat{\rho}$. When measuring an observable A having a complete orthonormal set of eigenvectors $\{|a_j\rangle\}_{j=1,2,\dots,d}$ (d might be infinite), it is associated to the possible outcomes $\{a_j\}_{j=1,2,\dots,d}$ a probability distribution $\{p_j = \rho_{jj}\}_{j=1,2,\dots,d}$ which determines the statistics of the experiment.

Similarly, when measuring an observable X having a complete set of generalized continuous eigenvectors $\{|x\rangle\}_{x \in \mathbb{R}}$, the probability density function $P(x) = \rho(x, x)$ is associated to the possible outcomes $\{x\}_{x \in \mathbb{R}}$ in the experiment.]

This postulate has deep consequences that we analyze now. Contrary to classical mechanics (and intuition), even if the system is in a fixed state, the value of an observable is in general not well defined; we can only specify with what probability a given value of the observable will come out in a measurement. Hence, this axiom proposes a change of paradigm, determinism must be abandoned: theory is no longer able to predict with certainty the outcome of a single experiment in which an observable is measured, but rather gives the statistics that will be extracted after a large number of such experiments.

To be fair, there is a case in which the theory allows us to predict the outcome of the measurement of an observable with certainty: When the system is prepared such that its state is an eigenvector of the observable. This seems much like when in classical mechanics the system is prepared with a given value of its observables. One can show however that it is impossible to find a common eigenvector to *all* the available observables of a system, and hence the difference between classical and quantum mechanics is that in the later it is impossible to prepare the system in a state which would allow us to predict with certainty the outcome of a measurement of each of its observables. Let us try to elaborate on this in a more rigorous fashion.

Let us define the *expectation value* of a given operator \hat{B} as

$$\langle \hat{B} \rangle \equiv \text{tr}\{\hat{\rho}\hat{B}\}. \quad (\text{A.23})$$

In the case of a countable observable \hat{A} or a continuous observable \hat{X} , this expectation value can be written in their own eigenbases as

$$\langle \hat{A} \rangle = \sum_{j=1}^d \rho_{jj} a_j \quad \text{and} \quad \langle \hat{X} \rangle = \int_{-\infty}^{+\infty} dx \rho(x, x) x, \quad (\text{A.24})$$

which correspond to the mean value of the outcomes registered in large number of measurements of the observables. We define also the *variance* of the observable as the expectation value of the square of its *fluctuation operator* $\delta \hat{A} = \hat{A} - \langle \hat{A} \rangle$, that is,

$$V(A) \equiv \text{tr} \left\{ \hat{\rho} (\delta \hat{A})^2 \right\} = \langle \hat{A}^2 \rangle - \langle \hat{A} \rangle^2, \quad (\text{A.25})$$

from which we obtain the *standard deviation* or *uncertainty* as $\Delta A = V(A)^{1/2}$, which measures how much the outcomes of the experiment deviate from the mean, and hence, somehow specifies how ‘well defined’ is the value of the observable A.

Note that the probability of obtaining the outcome a_j when measuring A can be written as the expectation value of the projection operator $\hat{P}_j^A = |a_j\rangle\langle a_j|$, that is $p_j = \langle \hat{P}_j^A \rangle$. Similarly, the probability density function associated to the possible outcomes $\{x\}_{x \in \mathbb{R}}$ when measuring X can be written as $P(x) = \langle \hat{P}_x^X \rangle$, where $\hat{P}_x^X = |x\rangle\langle x|$.

Having written all these objects (probabilities, expectation values, and variances) in terms of traces is really important, as traces can be evaluated in any basis we want to work with, see Section A.2.2.

These axioms have one further unintuitive consequence. It is possible to prove that irrespective of the state of the system, the following relation between the variances of two non-commuting observables A and B is satisfied:

$$\Delta A \Delta B \geq \frac{1}{2} |\langle [\hat{A}, \hat{B}] \rangle|. \quad (\text{A.26})$$

According to this inequality, known as the *uncertainty principle* (which was first derived by Heisenberg), the only way in which the observable A can be perfectly defined ($\Delta A \rightarrow 0$) is by making completely undefined observable B ($\Delta B \rightarrow \infty$), or vice-versa. Hence, in the quantum formalism one cannot, in general, build a state of the system such that all its observables are well defined, what is completely opposite to our everyday experience. This property of quantum mechanics will play a major role in this thesis.

Before going to the third axiom, let us comment one last thing. When the state of the system is given by a pure density operator $\hat{\rho} = |\psi\rangle\langle\psi|$, we say that the system is in a *pure state* $|\psi\rangle$ (if the density operator is mixed we then say that the system is in a *mixed state*). In this case, the expectation value of an operator \hat{B} takes the simple form $\langle \psi | \hat{B} | \psi \rangle$. Moreover, the pure state can be expanded in the countable and continuous bases of the observables \hat{A} and \hat{X} as

$$|\psi\rangle = \sum_{j=1}^d \psi_j |a_j\rangle \quad \text{and} \quad |\psi\rangle = \int_{-\infty}^{+\infty} dx \psi(x) |x\rangle, \quad (\text{A.27})$$

respectively, being $\psi_j = \langle a_j | \psi \rangle$ and $\psi(x) = \langle x | \psi \rangle$. In this case, the probability distribution for the discrete outcomes $\{a_j\}_{j=1,2,\dots,d}$ and the probability density function for the continuous outcomes $\{x\}_{x \in \mathcal{D}}$ are given by $\{p_j = |\psi_j|^2\}_{j=1,2,\dots,d}$ and $P(x) = |\psi(x)|^2$, respectively.

The introduction of the third axiom is motivated by the following fact. The class of self-adjoint operators forms a real vector space with respect to the addition of operators and the multiplication of an operator by a real number. Using the commutator we can also build an operation which takes two self-adjoint operators \hat{A} and \hat{B} to generate another self-adjoint operator $\hat{C} = i[\hat{A}, \hat{B}]$, which in addition satisfies all the properties required by a Lie product. Hence, even if classical and quantum theories seem fundamentally different, it seems that observables are treated similarly within their corresponding mathematical frameworks: They are elements of a Lie algebra.

On the other hand, we saw that the generalized coordinates and momenta have a particular mathematical structure in the Hamiltonian formalism, they are the generators of the Heisenberg group. It seems then quite reasonable to ask for the same in the quantum theory, so that at least in what concerns to observables both theories are equivalent. This motivates the third axiom:

Axiom III. [Consider a physical system described classically within a Hamiltonian formalism by a set of generalized coordinates $\mathbf{q} = \{q_j\}_{j=1}^n$ and momenta $\mathbf{p} = \{p_j\}_{j=1}^n$; within the quantum formalism, the corresponding observables $\hat{\mathbf{q}} = \{\hat{q}_j\}_{j=1}^n$ and $\hat{\mathbf{p}} = \{\hat{p}_j\}_{j=1}^n$ satisfy the commutation relations

$$[\hat{q}_j, \hat{p}_l] = i\hbar \delta_{jl} \quad \text{and} \quad [\hat{q}_j, \hat{q}_l] = [\hat{p}_j, \hat{p}_l] = 0. \quad (\text{A.28})$$

The constant \hbar is included because, while the Poisson bracket $\{q_j, p_l\}$ has no units, the commutator $[\hat{q}_j, \hat{p}_l]$ has units of action; that the proper constant is \hbar is seen only once the theory is compared with experiments.

We can now discuss how to build the self-adjoint operator corresponding to a given observable. Suppose that in the Hamiltonian formalism the observable A is represented by the phase space function $A(\mathbf{q}, \mathbf{p})$. It seems quite natural to use then $A(\hat{\mathbf{q}}, \hat{\mathbf{p}})$ as the corresponding quantum operator; however, this correspondence faces a lot of troubles derived from the fact that while coordinates and momenta commute in classical mechanics, they do not in quantum mechanics. For example, given the classical observable $A = qp = pq$, we could be tempted to assign it any of the quantum operators $\hat{A}_1 = \hat{q}\hat{p}$ or $\hat{A}_2 = \hat{p}\hat{q}$; these two operators are different and they are not even self-adjoint, and hence, cannot represent observables. One possible solution to this problem, at least for observables with a series expansion, is to always symmetrize the classical expressions with respect to coordinates and momenta, so that the resulting operator is self-adjoint. Applied to our previous example, we should take $\hat{A} = (\hat{p}\hat{q} + \hat{q}\hat{p})/2$ according to this rule. This simple procedure leads to the correct results most of the times, and when it fails (for example, if the classical observable doesn't have a series expansion) it was proved by Groenewold [182] that it is possible to make a faithful systematic correspondence between classical observables and self-adjoint operators by using more sophisticated correspondence rules.

Of course, when the observable corresponds to a degree of freedom which is not defined in a classical context (like spin), it must be built from scratch based on observations and first principles. Nevertheless, we won't be working with observables having no classical analog in this thesis.

Note that the commutation relations between coordinates and momenta makes them satisfy the uncertainty relation $\Delta q \Delta p \geq \hbar/2$, and hence if one of them is well defined in the system, the other must have statistics very spread around the mean. We will examine this relation in depth when studying the harmonic oscillator in the next section.

The three previous axioms have served to define the mathematical structure of the theory and its relation to physical systems. We haven't said anything yet about how quantum mechanics treats the evolution of the system. Just as with the last axiom, it feels pretty reasonable to keep the analogy with the Hamiltonian formalism, a motivation which comes also from the fact that, as stated, quantum mechanics must converge to classical mechanics in some limit. In the Hamiltonian formalism, observables evolve according to (A.7), so that making the correspondence between the classical and quantum Lie products as in the third axiom, we enunciate the fourth axiom (for simplicity, we assume no explicit time dependence of observables):

Axiom IV. [The evolution of an observable \hat{A} is given by

$$i\hbar \frac{d\hat{A}}{dt} = [\hat{A}, \hat{H}], \quad (\text{A.29})$$

which is known as the Heisenberg equation, and where \hat{H} is the self-adjoint operator corresponding to the Hamiltonian of the system.]

For the case of a time-independent Hamiltonian, this evolution equation admits the explicit solution

$$\hat{A}(t) = \hat{U}^\dagger(t) \hat{A}(0) \hat{U}(t), \text{ being } \hat{U}(t) = \exp[\hat{H}t/i\hbar], \quad (\text{A.30})$$

a unitary operator called the *evolution operator*. For time-dependent Hamiltonians it is still possible to solve explicitly the Heisenberg equation, but we won't worry about this case, as it won't appear throughout the thesis.

Note that within this formalism the state $\hat{\rho}$ of the system is fixed in time, the observables are the ones which evolve. On the other hand, we have seen that on what concerns to observations (experiments), only expectation values of operators are relevant, and for an observable \hat{A} at time t , this can be written as

$$\langle \hat{A}(t) \rangle = \text{tr}\{\hat{\rho}\hat{A}(t)\} = \text{tr}\{\hat{U}(t)\hat{\rho}\hat{U}^\dagger(t)\hat{A}(0)\}, \quad (\text{A.31})$$

where in the last equality we have used the cyclic property of the trace. This expression shows that, instead of treating the observable as the evolving operator, we can define a new state at time t given by

$$\rho(t) = \hat{U}(t)\hat{\rho}(0)\hat{U}^\dagger(t), \quad (\text{A.32})$$

while keeping fixed the operator. In differential form, this expression reads

$$i\hbar \frac{d\hat{\rho}}{dt} = [\hat{H}, \hat{\rho}], \quad (\text{A.33})$$

which is known as the *von Neumann equation*. When the system is in a pure state $|\psi\rangle$, the following evolution equation is derived for the state vector itself

$$i\hbar \frac{d}{dt} |\psi\rangle = \hat{H} |\psi\rangle, \quad (\text{A.34})$$

which is known as the *Schrödinger equation*, from which the state at time t is found as $|\psi(t)\rangle = \hat{U}(t) |\psi(0)\rangle$.

Therefore, we have two different but equivalent evolution formalisms. In one, which we shall call *Heisenberg picture*, the state of the system is fixed, while observables evolve according to the Heisenberg equation. In the other, which we will denote by *Schrödinger picture*, observables are fixed, while states evolve according to the von Neumann equation.

We can even define intermediate pictures in which both the state and the observables evolve, the so-called *interaction pictures*. To show how this is done, let us denote by \hat{A}_S and $\hat{\rho}_S(t)$, an observable and the state of the system in the Schrödinger picture.

Suppose that we are in the Schrödinger picture, so that the expectation value of an observable A is written as $\text{tr}\{\hat{\rho}_S(t)\hat{A}_S\}$, and want to go to a new picture in which both the state and the operator evolve; all we need to do is define a unitary operator $\hat{U}_c = \exp[\hat{H}_c t / i\hbar]$, with \hat{H}_c some self-adjoint operator, and then a transformed state $\hat{\rho}_I = \hat{U}_c^\dagger \hat{\rho}_S \hat{U}_c$ and a transformed observable $\hat{A}_I = \hat{U}_c^\dagger \hat{A}_S \hat{U}_c$. This transformation leaves invariant the expectation value, which can be evaluated as $\text{tr}\{\hat{\rho}_I(t)\hat{A}_I(t)\}$, but now the evolution equations of the state and the observable read

$$i\hbar \frac{d\hat{\rho}_I}{dt} = [\hat{H}_I, \hat{\rho}_I] \quad \text{and} \quad i\hbar \frac{d\hat{A}_I}{dt} = [\hat{A}_I, \hat{H}_c], \quad (\text{A.35})$$

so that within this new picture states evolve according to the *interaction Hamiltonian* $\hat{H}_I = \hat{U}_c^\dagger \hat{H} \hat{U}_c - \hat{H}_c$, while observables evolve according to the *transformation Hamiltonian* \hat{H}_c .

The last axiom specifies how the theory accommodates dealing with composite systems within its mathematical framework. Of course, a composition of two systems is itself another system subject to the laws of quantum mechanics; the question is how can we build it.

Axiom V. [Consider two systems A and B with associated Hilbert spaces \mathcal{H}_A and \mathcal{H}_B ; then, the state of the composite system $\hat{\rho}_{AB}$ as well as its observables act onto the tensor product Hilbert space $\mathcal{H}_{AB} = \mathcal{H}_A \otimes \mathcal{H}_B$.]

This axiom has the following consequence. Imagine that the systems A and B interact during some time in such a way that they cannot be described anymore by independent states $\hat{\rho}_A$ and $\hat{\rho}_B$ acting on \mathcal{H}_A and \mathcal{H}_B , respectively, but by a state $\hat{\rho}_{AB}$ acting on the joint space \mathcal{H}_{AB} . After the interaction, system B is kept isolated of any other system, but system A is given to an observer, who is therefore able to measure observables defined in \mathcal{H}_A only, and might not even know that system A is part of a larger system. The question is, is it possible to reproduce the statistics of the measurements performed on system A with some state $\hat{\rho}_A$ defined in \mathcal{H}_A only? This question has a positive and *unique* answer: this state is given by the *reduced density operator* $\hat{\rho}_A = \text{tr}_B\{\hat{\rho}_{AB}\}$, that is, by performing the partial trace respect system's B subspace onto the joint state.

These five axioms (together with the definitions of the previous sections) define quantum mechanics as we use it throughout the thesis.

We would like to note finally, that in most of the textbooks about quantum mechanics one can find two more axioms. The first one refers to how multi-particle states have to be built: For indistinguishable integer (half-integer) spin particles the state must be symmetric (antisymmetric) with respect to the permutation of any two particles; we haven't incorporated this axiom mainly because we don't use it. In any case it finds full justification in the context of quantum field theory via the *spin-statistics theorem*, so we do not find it a true foundational axiom

The second one is more controversial [181] (see also the Appendix E of [166]): It states that if the value a_j is observed for observable A in an experiment, then immediately after the measurement the state of the system *collapses* to $|a_j\rangle$. Even though this axiom leads to predictions in full agreement with observations, it somehow creates an inconsistency in the theory because of the following argument. According to Axiom IV the evolution of a closed system is *reversible* (unitary); on the other hand, the *collapse* axiom states that when the system is put in contact with a measurement device and an observable is measured, the state of the system collapses to some other state in a *non-reversible* way. However, coming back to Axiom IV, the whole measurement process could be described reversibly by considering, in addition to the system's particles, the evolution of all the particles forming the measurement device (or even the human who is observing the measurement outcome!), and a Hamiltonian for the whole 'observed system + measurement device' system. Hence, it seems that, when including the collapse axiom, quantum mechanics allows for two completely different descriptions of the measurement process, one reversible and one irreversible, without giving a clear rule for when to apply each. This is the sense in which there is an inconsistency in the theory.

There are three main lines of thought regarding to how this inconsistency might be solved. First, there are the ones who believe that the collapse is real, and that, even though we still don't know it, there exists a rule explaining under which circumstances one has to apply unitary evolution or the collapse of the state. The second line of thought suggests that the collapse should be derivable from unitary evolution according with some procedure yet to be devised; for example, when the density of particles in the system exceeds some value, one cannot expect to track the reversible evolution of each single particle, and this "missing information" could give rise to the irreversible collapse. A third possible approach states that the collapse is just an operationally convenient way of describing measurements, but it is far from real; instead, the measurement is described as a joint unitary transformation onto the system and the measurement apparatus, leading to a final entangled state of these in which the eigenstates of the system's observable are in one-to-one correspondence with a set of macroscopic states of the measurement device [181].

Real or not real, the collapse postulate offers the easiest successful way of analyzing schemes involving measurements, and hence we apply it when needed. Nevertheless, during practically all the thesis we consider only measurements in which the observed system is destroyed after its observation, the so-called *destructive measurements*, so we won't need to worry about the state of the system after the measurement.

B. LINEAR STOCHASTIC EQUATIONS WITH ADDITIVE NOISE

In this Appendix we explain how to deal with one of the most simple examples of an stochastic equation: A one-variable linear equation with additive noise. This type of equation appears all along the thesis, see equations (6.74) and (6.105) for example, which indeed match the general form

$$\dot{c} = -\lambda c + \Gamma \eta(\tau), \quad (\text{B.1})$$

where $c(\tau)$ is the stochastic variable, λ is a positive real parameter, Γ might be complex, and $\eta(\tau)$ is a real noise with zero mean and two-time correlation $\langle \eta(\tau) \eta(\tau') \rangle = \delta(\tau - \tau')$.

The solution of the equation is readily found by making the variable change $z(\tau) = c(\tau) \exp(\lambda\tau)$, what leads to $\dot{z}(\tau) = \Gamma \exp(\lambda\tau) \eta(\tau)$, and hence to

$$c(\tau) = c(0) e^{-\lambda\tau} + \Gamma \int_0^\tau d\tau_1 \eta(\tau_1) e^{\lambda(\tau_1 - \tau)}, \quad (\text{B.2})$$

or in the $\tau \gg \lambda^{-1}$ limit

$$c(\tau) = \Gamma \int_0^\tau d\tau_1 \eta(\tau_1) e^{\lambda(\tau_1 - \tau)}. \quad (\text{B.3})$$

Note that in this limit the solution does not depend on its initial value, and hence we can expect the process to be stationary in this limit [20].

The stochastic variable $c(\tau)$ has then zero mean in the stationary limit, that is, $\langle c(\tau \gg \lambda^{-1}) \rangle = 0$. On the other hand, the two-time correlation function of $c(\tau)$ can be written for $\tau \gg \lambda^{-1}$ as

$$\langle c(\tau) c(\tau') \rangle = \Gamma^2 e^{-\lambda(\tau + \tau')} \int_0^\tau d\tau_1 \int_0^{\tau'} d\tau_2 \delta(\tau_1 - \tau_2) e^{\lambda(\tau_1 + \tau_2)}. \quad (\text{B.4})$$

Considering separately the cases $\tau' > \tau$ and $\tau' < \tau$, this integral is easily carried out, yielding (again in the limit $\tau \gg \lambda^{-1}$)

$$\langle c(\tau) c(\tau') \rangle = \frac{\Gamma^2}{2\lambda} e^{-\lambda|\tau' - \tau|}, \quad (\text{B.5})$$

where we see that this function depends only on the time difference $|\tau' - \tau|$, and hence $c(\tau)$ arrives indeed to a stationary state for large enough times [20] (it is invariant under changes of the time origin).

The quantity we are usually interested in is the correlation spectrum of $c(\tau)$, which is finally evaluated in the stationary limit as the integral

$$\tilde{C}(\tilde{\Omega}) = \int_{-\infty}^{+\infty} d\tau' e^{-i\tilde{\Omega}\tau'} \langle c(\tau) c(\tau + \tau') \rangle = \frac{\Gamma^2}{2\lambda} \left[\int_0^{+\infty} d\tau' e^{-(\lambda + i\tilde{\Omega})\tau'} + \int_{-\infty}^0 d\tau' e^{(\lambda - i\tilde{\Omega})\tau'} \right] = \frac{\Gamma^2}{\lambda^2 + \tilde{\Omega}^2}. \quad (\text{B.6})$$

We make extensive use of this last result all along the thesis.

C. LINEARIZATION OF THE TWO-TRANSVERSE-MODE DOPO LANGEVIN EQUATIONS

Following the linearization procedure we explained in 7.2.2 leads not to Eq. (7.36) directly, but to the following one

$$i(\mathcal{G}\mathbf{b} - 2\rho\mathbf{w}_0)\dot{\boldsymbol{\theta}} + \dot{\mathbf{b}} = \mathcal{L}\mathbf{b} + g\mathcal{K}(\boldsymbol{\theta})\boldsymbol{\zeta}(\tau), \quad (\text{C.1})$$

where

$$\begin{aligned} \mathcal{K}(\boldsymbol{\theta}) &= \text{diag}(e^{i\theta}, e^{-i\theta}, e^{-i\theta}, e^{i\theta}), \\ \mathcal{G} &= \text{diag}(-1, 1, 1, -1), \end{aligned}$$

and the rest of vectors and symbols were defined in the corresponding section. Note that the differences between this system of equations and the one used throughout the thesis (7.36) are the matrix $\mathcal{K}(\boldsymbol{\theta})$ and the $i\mathcal{G}\mathbf{b}\dot{\boldsymbol{\theta}}$ term. The latter is of order g^2 (as the b 's and $\dot{\boldsymbol{\theta}}$ are of order g), and hence it can be simply removed within the linearized theory.

Understanding why $\mathcal{K}(\boldsymbol{\theta})$ can be removed from the linearized equations is a little more involved. Projecting these equations onto the eigensystem of \mathcal{L} (7.39) and defining the vector $\mathbf{c} = \text{col}(\boldsymbol{\theta}, c_1, c_2, c_3)$ leads to the following system of equations (remember that we set $c_0 = 0$)

$$\dot{\mathbf{c}} = -\Lambda\mathbf{c} + g\mathcal{B}\mathcal{R}(\boldsymbol{\theta})\boldsymbol{\eta}(\tau) \quad (\text{C.2})$$

with

$$\begin{aligned} \Lambda &= 2\text{diag}(0, 1, \sigma - 1, \sigma), \\ \mathcal{B} &= \text{diag}(1/2\rho, i, 1, 1), \\ \mathcal{R}(\boldsymbol{\theta}) &= \mathcal{R}_{1,3}(\boldsymbol{\theta})\mathcal{R}_{2,4}(-\boldsymbol{\theta}), \end{aligned}$$

being $\mathcal{R}_{i,j}(\boldsymbol{\theta})$ the two-dimensional rotation matrix of angle $\boldsymbol{\theta}$ acting on the $i - j$ subspace, and where the components of vector $\boldsymbol{\eta}(\tau)$ are real, independent noises satisfying the usual statistical properties (2.82). Now, we will prove that this system, and the same with $\mathcal{R}(\boldsymbol{\theta} = 0)$ are equivalent within the linearized theory, and hence (C.1) and (7.36) are equivalent too.

To show this, we just write the Fokker-Planck equation (2.80) corresponding to this stochastic system (which we remind is in Stratonovich form), whose drift vector and diffusion matrix are found to be

$$\vec{\mathcal{A}} = \Lambda\mathbf{c} + \frac{g^2}{4\rho}\text{col}(0, 0, 1, 0), \quad (\text{C.3})$$

and

$$\mathcal{D} = g^2\mathcal{B}\mathcal{B}^T, \quad (\text{C.4})$$

respectively. Note that in the last equation we have used that $\mathcal{R}(\boldsymbol{\theta})$ is an orthogonal matrix.

The proof is completed by writing the stochastic system corresponding to this Fokker-Planck equation up to the linear order in g , which reads

$$\dot{\mathbf{c}} = -\Lambda\mathbf{c} + g\mathcal{B}\boldsymbol{\eta}(\tau), \quad (\text{C.5})$$

corresponding to (C.2) with $\mathcal{R}(\boldsymbol{\theta} = 0)$ as we wanted to prove.

Hence, removing $\mathcal{K}(\boldsymbol{\theta})$ and neglecting the $i\mathcal{G}\mathbf{b}\dot{\boldsymbol{\theta}}$ term from (C.1) doesn't change its equivalent Fokker-Planck equation within the linearized description, and thus equation (7.36) must lead to the same predictions as (C.1).

D. CORRELATION FUNCTIONS OF $\cos \theta(\tau)$ AND $\sin \theta(\tau)$

In this appendix we evaluate the correlation functions $S(\tau_1, \tau_2) = \langle \sin \theta(\tau_1) \sin \theta(\tau_2) \rangle$ and $C(\tau_1, \tau_2) = \langle \cos \theta(\tau_1) \cos \theta(\tau_2) \rangle$ starting from

$$\theta(\tau) = \sqrt{D} \int_0^\tau d\tau' \eta_0(\tau'), \quad (\text{D.1})$$

which is found by integrating equation (7.40a), and assuming that $\theta(0) = 0$ at any stochastic realization, as explained in the main text.

The correlation functions are easy to find by noticing that, as $\eta_0(\tau)$ is a Gaussian noise, $\theta(\tau)$ is a Gaussian variable, that is, all its moments are determined from the first and second ones. Under these conditions, it is straightforward to show (for example by performing a series expansion) that the following property holds

$$\left\langle e^{\pm i\theta(\tau)} \right\rangle_P = e^{-\langle \theta^2(\tau) \rangle_P / 2}, \quad (\text{D.2})$$

or, as the combinations $\theta(\tau_1) \pm \theta(\tau_2)$ are also Gaussian variables,

$$\left\langle e^{\pm i[\theta(\tau_1) \pm \theta(\tau_2)]} \right\rangle_P = e^{-\langle [\theta(\tau_1) \pm \theta(\tau_2)]^2 \rangle_P / 2}. \quad (\text{D.3})$$

Now, given that

$$\langle \theta(\tau_1) \theta(\tau_2) \rangle_P = D \int_0^{\tau_1} d\tau \int_0^{\tau_2} d\tau' \delta(\tau - \tau') = D \min(\tau_1, \tau_2), \quad (\text{D.4})$$

we get

$$\left\langle [\theta(\tau_1) \pm \theta(\tau_2)]^2 \right\rangle = D [\tau_1 + \tau_2 \pm 2 \min(\tau_1, \tau_2)], \quad (\text{D.5})$$

and finally

$$S(\tau_1, \tau_2) = \langle \sin \theta(\tau_1) \sin \theta(\tau_2) \rangle = -\frac{1}{4} \left\langle e^{i[\theta(\tau_1) + \theta(\tau_2)]} \right\rangle_P + \frac{1}{4} \left\langle e^{i[\theta(\tau_1) - \theta(\tau_2)]} \right\rangle_P + \text{c.c.} = e^{-\frac{D}{2}(\tau_1 + \tau_2)} \sinh[D \min(\tau_1, \tau_2)], \quad (\text{D.6})$$

and

$$C(\tau_1, \tau_2) = \langle \cos \theta(\tau_1) \cos \theta(\tau_2) \rangle = \frac{1}{4} \left\langle e^{i[\theta(\tau_1) + \theta(\tau_2)]} \right\rangle_P + \frac{1}{4} \left\langle e^{i[\theta(\tau_1) - \theta(\tau_2)]} \right\rangle_P + \text{c.c.} = e^{-\frac{D}{2}(\tau_1 + \tau_2)} \cosh[D \min(\tau_1, \tau_2)]. \quad (\text{D.7})$$

E. DETAILS ABOUT THE NUMERICAL SIMULATION OF THE TWO-TRANSVERSE-MODE DOPO EQUATIONS

In this appendix we want to briefly summarize the details concerning the numerical simulation of the Langevin equations (7.26) which model the 2tmDOPO.

The first important property of these equations is that, irrespective of the initial conditions, the amplitudes corresponding to opposite orbital angular momentum modes become complex-conjugate after a short transitory time, i.e., $(\beta_{-1}, \beta_{-1}^+) \rightarrow (\beta_{+1}^*, [\beta_{+1}^+]^*)$. Hence, if the initial conditions are chosen so this property is already satisfied, we can be sure that these amplitudes will remain complex-conjugate during the evolution. In particular, we have chosen the above threshold stationary solution (7.31) with $\theta = 0$ as the initial condition. Under these conditions, the 6 Langevin equations (7.26) get reduced to the following 4 (which we write in matrix form):

$$\dot{\boldsymbol{\beta}} = \mathbf{A}(\boldsymbol{\beta}) + \mathcal{B}(\boldsymbol{\beta}) \cdot \boldsymbol{\zeta}(\tau), \quad (\text{E.1})$$

with

$$\boldsymbol{\beta} = \begin{pmatrix} \beta_0 \\ \beta_0^+ \\ \beta_{+1} \\ \beta_{+1}^+ \end{pmatrix}, \quad \boldsymbol{\zeta}(\tau) = \begin{pmatrix} 0 \\ 0 \\ \zeta(\tau) \\ \zeta^+(\tau) \end{pmatrix}, \quad (\text{E.2})$$

$$\mathbf{A}(\boldsymbol{\beta}) = \begin{pmatrix} \sigma - \beta_0 - |\beta_{+1}|^2 \\ \sigma - \beta_0^+ - |\beta_{+1}^+|^2 \\ -\beta_{+1} + \beta_0 [\beta_{+1}^+]^* \\ -\beta_{+1}^+ + \beta_0^+ \beta_{+1}^* \end{pmatrix},$$

$$\mathcal{B}(\boldsymbol{\beta}) = g \text{diag} \left(0, 0, \sqrt{\beta_0}, \sqrt{\beta_0^+} \right).$$

In order to solve numerically these equations we use the semi-implicit algorithm developed in [144]. This algorithm is a finite-differences based method in which the total integration time τ_{end} (the integration is supposed to begin always at $\tau = 0$) is divided in N segments, creating hence a lattice of times $\{\tau_n\}_{n=0,1,\dots,N}$ separated by time steps $\Delta\tau = \tau_{\text{end}}/N$. Then, a recursive algorithm starts in which the amplitudes at time τ_n , say $\boldsymbol{\beta}_n$, are found from the amplitudes $\boldsymbol{\beta}^{n-1}$ at an earlier time τ_{n-1} from

$$\boldsymbol{\beta}^n = \boldsymbol{\beta}^{n-1} + \Delta\tau \mathbf{A}(\tilde{\boldsymbol{\beta}}^n) + \mathcal{B}(\tilde{\boldsymbol{\beta}}^n) \cdot \mathbf{W}^n, \quad (\text{E.3})$$

where $\tilde{\boldsymbol{\beta}}^n$ is an approximation to the amplitudes at the mid-point between τ_{n-1} and τ_n (hence the name ‘‘semi-implicit’’ for the algorithm) and the components of \mathbf{W}^n are independent discrete noises W_j^n with null mean and satisfying the correlations

$$\langle W_j^m, [W_k^n]^* \rangle = \Delta\tau \delta_{mn} \delta_{jk}. \quad (\text{E.4})$$

The mid-point approximation is found from the following iterative algorithm

$$\tilde{\boldsymbol{\beta}}^{n,p} = \boldsymbol{\beta}^{n-1} + \frac{1}{2} \left[\Delta\tau \mathbf{A}(\tilde{\boldsymbol{\beta}}^{n,p-1}) + \mathcal{B}(\tilde{\boldsymbol{\beta}}^{n,p-1}) \cdot \mathbf{W}^n \right], \quad (\text{E.5})$$

where $\tilde{\boldsymbol{\beta}}^{n,0} = \boldsymbol{\beta}^{n-1}$, being p the iteration index (two iterations are carried in all our simulations), while the discrete noises can be simulated at any step as [183]

$$W_j^n = \sqrt{\Delta\tau} \left[r(z_j, z'_j) + i r(y_j, y'_j) \right], \quad (\text{E.6})$$

with

$$r(z, z') = \sqrt{-\log z} \cos(2\pi z'), \quad (\text{E.7})$$

being z_j, z'_j, y_j and y'_j independent random numbers uniformly distributed along the interval $[0, 1]$.

This algorithm allows us to simulate one stochastic trajectory. Then, by repeating it Σ times, the stochastic average of any function can be approximated by the arithmetic mean of its values evaluated at the different stochastic trajectories.

BIBLIOGRAPHY

- [1] P. Meystre and D. F. Walls, Eds., *Nonclassical Effects in Quantum Optics*. American Institute of Physics, 1991.
- [2] R. E. Slusher, L. W. Hollberg, B. Yurke, J. C. Mertz, and J. F. Valley, “Observation of squeezed states generated by four-wave mixing in an optical cavity,” *Phys. Rev. Lett.*, vol. 55, p. 2409, 1985.
- [3] P. D. Drummond and F. Zbigniew, Eds., *Quantum squeezing*. Springer Verlag, 2004.
- [4] M. Mehmet, H. Vahlbruch, N. Lastzka, K. Danzmann, and R. Schnabel, “Observation of squeezed states with strong photon-number oscillations,” *Phys. Rev. A*, vol. 81, p. 013814, 2010.
- [5] H. Vahlbruch, M. Mehmet, S. Chelkowski, B. Hage, A. Franzen, N. Lastzka, S. Goßler, K. Danzmann, and R. Schnabel, “Observation of squeezed light with 10-db quantum-noise reduction,” *Phys. Rev. Lett.*, vol. 100, p. 033602, 2008.
- [6] Y. Takeno, M. Yukawa, H. Yonezawa, and A. Furusawa, “Observation of -9 db quadrature squeezing with improvement of phase stability in homodyne measurement,” *Opt. Express*, vol. 15, pp. 4321–4327, 2007.
- [7] S. L. Braunstein and P. van Loock, “Quantum information with continuous variables,” *Rev. Mod. Phys.*, vol. 77, pp. 513–577, 2005.
- [8] C. Weedbrook, S. Pirandola, R. García-Patrón, N. Cerf, T. C. Ralph, J. H. Shapiro, and S. Lloyd, “Gaussian quantum information,” to appear in *Reviews of Modern Physics*.
- [9] P. van Loock and S. L. Braunstein, “Multipartite entanglement for continuous variables: A quantum teleportation network,” *Phys. Rev. Lett.*, vol. 84, pp. 3482–3485, 2000.
- [10] T. Aoki, N. Takei, H. Yonezawa, K. Wakui, T. Hiraoka, A. Furusawa, and P. van Loock, “Experimental creation of a fully inseparable tripartite continuous-variable state,” *Phys. Rev. Lett.*, vol. 91, p. 080404, 2003.
- [11] N. Treps, U. Andersen, B. Buchler, P. K. Lam, A. Maître, H.-A. Bachor, and C. Fabre, “Surpassing the standard quantum limit for optical imaging using nonclassical multimode light,” *Phys. Rev. Lett.*, vol. 88, p. 203601, 2002.
- [12] N. Treps, N. Grosse, W. P. Bowen, C. Fabre, H.-A. Bachor, and P. K. Lam, “A quantum laser pointer,” *Science*, vol. 301, pp. 940–943, 2003.
- [13] H. Vahlbruch, S. Chelkowski, B. Hage, A. Franzen, K. Danzmann, and R. Schnabel, “Demonstration of a squeezed-light-enhanced power- and signal-recycled michelson interferometer,” *Phys. Rev. Lett.*, vol. 95, p. 211102, 2005.
- [14] K. Goda, O. Miyakawa, E. E. Mikhailov, S. Saraf, R. Adhikari, K. McKenzie, R. Ward, S. Vass, A. J. Weinstein, and N. Mavalvala, “A quantum-enhanced prototype gravitational-wave detector,” *Nat. Phys.*, vol. 4, pp. 472–476, 2008.
- [15] W. H. Louisell, *Quantum statistical properties of radiation*. John Wiley & Sons, 1973.
- [16] C. Cohen-Tannoudji, J. Dupont-Roc, and J. Grynberg, *Photons and atoms: Introduction to quantum electrodynamics*. John Wiley & Sons, 1989.
- [17] H. J. Carmichael, *An open systems approach to quantum optics*. Springer Verlag, 1993.
- [18] —, *Statistical methods in quantum optics 1: Master equations and Fokker–Planck equations*. Springer Verlag, 1999.
- [19] —, *Statistical methods in quantum optics 2: Non-classical fields*. Springer Verlag, 2008.

- [20] L. Mandel and E. Wolf, *Optical coherence and quantum optics*. Cambridge University Press, 1995.
- [21] M. O. Scully and M. S. Zubairy, *Quantum optics*. Cambridge University Press, 1997.
- [22] W. P. Schleich, *Quantum optics in phase space*. Wiley-VCH, 2001.
- [23] C. C. Gerry and P. L. Knight, *Introductory quantum optics*. Cambridge University Press, 2005.
- [24] G. Grynberg, A. Aspect, and C. Fabre, *Introduction to quantum optics*. Cambridge University Press, 2010.
- [25] D. F. Walls and G. J. Milburn, *Quantum optics*. Springer, 1994.
- [26] C. Navarrete-Benlloch, R. García-Patrón, J. H. Shapiro, and N. Cerf, “Enhancing entanglement by photon addition and subtraction,” in preparation.
- [27] R. García-Patrón, C. Navarrete-Benlloch, J. H. Shapiro, S. Lloyd, and N. Cerf, “A new approach towards proving the minimum output entropy conjecture for bosonic channels,” in preparation.
- [28] C. Navarrete-Benlloch, I. de Vega, D. Porras, and J. I. Cirac, “Simulating quantum-optical phenomena with cold atoms in optical lattices,” *New J. Phys.*, vol. 13, p. 023024, 2011.
- [29] C. Navarrete-Benlloch, G. J. de Valcárcel, and E. Roldán, “Generating highly squeezed hybrid laguerre-gauss modes in large-fresnel-number degenerate optical parametric oscillators,” *Phys. Rev. A*, vol. 79, p. 043820, 2009.
- [30] I. Pérez-Arjona, E. Roldán, and G. J. de Valcárcel, “Quantum squeezing of optical dissipative structures,” *Europhys. Lett.*, vol. 74, p. 247, 2006.
- [31] I. Pérez-Arjona, E. Roldán, and G. J. de Valcárcel, “Theory of quantum fluctuations of optical dissipative structures and its application to the squeezing properties of bright cavity solitons,” *Phys. Rev. A*, vol. 75, p. 063802, 2007.
- [32] C. Navarrete-Benlloch, E. Roldán, and G. J. de Valcárcel, “Noncritically squeezed light via spontaneous rotational symmetry breaking,” *Phys. Rev. Lett.*, vol. 100, p. 203601, 2008.
- [33] C. Navarrete-Benlloch, A. Romanelli, E. Roldán, and G. J. de Valcárcel, “Noncritical quadrature squeezing in two-transverse-mode optical parametric oscillators,” *Phys. Rev. A*, vol. 81, p. 043829, 2010.
- [34] F. V. Garcia-Ferrer, C. Navarrete-Benlloch, G. J. de Valcárcel, and E. Roldán, “Squeezing via spontaneous rotational symmetry breaking in a four-wave mixing cavity,” *IEEE J. Quantum Electron.*, vol. 45, p. 1404, 2008.
- [35] F. V. Garcia-Ferrer, C. Navarrete-Benlloch, G. J. de Valcárcel, and E. Roldán, “Noncritical quadrature squeezing through spontaneous polarization symmetry breaking,” *Opt. Lett.*, vol. 35, pp. 2194–2196, 2010.
- [36] C. Navarrete-Benlloch, E. Roldán, and G. J. de Valcárcel, “Squeezing properties of a two-transverse-mode degenerate optical parametric oscillator with an injected signal,” *Phys. Rev. A*, vol. 83, p. 043812, 2011.
- [37] —, “Actively-phase-locked optical parametric oscillators: from non-degenerate to degenerate operation,” in preparation.
- [38] J. Laurat, L. Longchambon, C. Fabre, and T. Coudreau, “Experimental investigation of amplitude and phase quantum correlations in a type II optical parametric oscillator above threshold: from nondegenerate to degenerate operation,” *Opt. Lett.*, vol. 30, pp. 1177–1179, 2005.
- [39] A. Einstein, B. Podolsky, and N. Rosen, “Can quantum-mechanical description of physical reality be considered complete?” *Phys. Rev.*, vol. 47, pp. 777–780, 1935.
- [40] J. S. Bell, “On the einstein podolsky rosen paradox,” *Physics*, vol. 1, pp. 195–200, 1964.
- [41] P. W. Shor, “Polynomial-time algorithms for prime factorization and discrete logarithms on a quantum computer,” *SIAM J. Comput.*, vol. 26, p. 14841509, 1997.
- [42] L.-M. Duan, G. Giedke, J. I. Cirac, and P. Zoller, “Inseparability criterion for continuous variable systems,” *Phys. Rev. Lett.*, vol. 84, p. 2722, 2000.

-
- [43] R. Simon, “Peres-horodecki separability criterion for continuous variable systems,” *Phys. Rev. Lett.*, vol. 84, p. 2726, 2000.
- [44] M. D. Reid, “Demonstration of the einstein-podolsky-rosen paradox using nondegenerate parametric amplification,” *Phys. Rev. A*, vol. 40, pp. 913–923, 1989.
- [45] J. Wenger, R. Tualle-Brouri, and P. Grangier, “Non-gaussian statistics from individual pulses of squeezed light,” *Phys. Rev. Lett.*, vol. 92, p. 153601, 2004.
- [46] A. Zavatta, S. Viciani, and M. Bellini, “Quantum-to-classical transition with single-photon-added coherent states of light,” *Science*, vol. 306, pp. 660–662, 2004.
- [47] A. Zavatta, V. Parigi, and M. Bellini, “Experimental nonclassicality of single-photon-added thermal light states,” *Phys. Rev. A*, vol. 75, p. 052106, 2007.
- [48] V. Parigi, A. Zavatta, M. Kim, and M. Bellini, “Probing quantum commutation rules by addition and subtraction of single photons to/from a light field,” *Science*, vol. 317, pp. 1890–1893, 2007.
- [49] A. Zavatta, V. Parigi, M. S. Kim, H. Jeong, and M. Bellini, “Experimental demonstration of the bosonic commutation relation via superpositions of quantum operations on thermal light fields,” *Phys. Rev. Lett.*, vol. 103, p. 140406, 2009.
- [50] J. Eisert, “Entanglement in quantum information theory,” PhD dissertation; arXiv:quant-ph/061025.
- [51] M. A. Nielsen and I. L. Chuang, *Quantum information and quantum computation*. Cambridge University Press, 2000.
- [52] V. Giovannetti, S. Guha, S. Lloyd, L. Maccone, J. H. Shapiro, and H. P. Yuen, “Classical capacity of the lossy bosonic channel: The exact solution,” *Phys. Rev. Lett.*, vol. 92, p. 027902, 2004.
- [53] V. Giovannetti, S. Guha, S. Lloyd, L. Maccone, and J. H. Shapiro, “Minimum output entropy of bosonic channels: A conjecture,” *Phys. Rev. A*, vol. 70, p. 032315, 2004.
- [54] A. S. Holevo, M. Sohma, and O. Hirota, “Capacity of quantum gaussian channels,” *Phys. Rev. A*, vol. 59, pp. 1820–1828, 1999.
- [55] A. S. Holevo and R. F. Werner, “Evaluating capacities of bosonic gaussian channels,” *Phys. Rev. A*, vol. 63, p. 032312, 2001.
- [56] E. Wigner, “On the quantum correction for thermodynamic equilibrium,” *Phys. Rev.*, vol. 40, p. 749, 1932.
- [57] K. Husimi, “Some formal properties of the density matrix,” *Proc. Phys. Math. Soc. Jpn.*, vol. 22, pp. 264–314, 1940.
- [58] R. J. Glauber, “Photon correlations,” *Phys. Rev. Lett.*, vol. 10, p. 84, 1963.
- [59] E. C. G. Sudarshan, “Equivalence of semiclassical and quantum mechanical descriptions of statistical light beams,” *Phys. Rev. Lett.*, vol. 10, pp. 277–279, 1963.
- [60] P. D. Drummond and C. W. Gardiner, “Generalized P -representations in quantum optics,” *J. Phys. A: math. gen.*, vol. 13, pp. 2353–2368, 1980.
- [61] C. W. Gardiner, *Stochastic Methods: A Handbook for the Natural and Social Sciences*, 4ed. Springer, 2009.
- [62] J. C. Maxwell, “A dynamical theory of the electromagnetic field,” *Philosophical Transactions of the Royal Society of London*, vol. 155, p. 459512, 1865.
- [63] H. R. Hertz, *Electric waves: being researches on the propagation of electric action with finite velocity through space*. Macmillan and Co., 1893.
- [64] O. Heaviside, *Electrical papers, Volume II*. Macmillan and Co., 1894.
- [65] J. Jackson, *Classical electrodynamics*. John Wiley & Sons, 1962.
- [66] M. Born and E. Wolf, *Principles of optics*, 6ed. Pergamon press, 1980.

- [67] D. J. Griffiths, *Introduction to electrodynamics, 3ed.* Prentice Hall, 1999.
- [68] I. de Vega, D. Porras, and J. I. Cirac, “Matter-wave emission in optical lattices: Single particle and collective effects,” *Phys. Rev. Lett.*, vol. 101, p. 260404, 2008.
- [69] H.-P. Breuer and F. Petruccione, *The theory of open quantum systems.* Oxford University Press, 2002.
- [70] D. Jaksch, C. Bruder, J. I. Cirac, C. W. Gardiner, and P. Zoller, “Cold bosonic atoms in optical lattices,” *Phys. Rev. Lett.*, vol. 81, p. 3108, 1998.
- [71] M. Greiner, O. Mandel, T. Esslinger, T. W. Hänsch, and I. Bloch, “Quantum phase transition from a superfluid to a Mott insulator in a gas of ultracold atoms,” *Nature*, vol. 415, pp. 39–44, 2002.
- [72] D. Jaksch and P. Zoller, “The cold atom Hubbard toolbox,” *Ann. Phys.*, vol. 315, pp. 52–79, 2004.
- [73] M. Lewenstein, A. Sanpera, V. Ahufinger, B. Damski, A. Sen(De), and U. Sen, “Ultracold atomic gases in optical lattices: mimicking condensed matter physics and beyond,” *Adv. Phys.*, vol. 56, pp. 243–379, 2007.
- [74] I. Bloch, J. Dalibard, and W. Zwerger, “Many-body physics with ultracold gases,” *Rev. Mod. Phys.*, vol. 80, p. 885, 2008.
- [75] U. Schneider, L. Hackermüller, S. Will, T. Best, I. Bloch, T. A. Costi, R. W. Helmes, D. Rasch, and A. Rosch, “Metallic and insulating phases of repulsively interacting fermions in a 3D optical lattice,” *Science*, vol. 322, p. 1524, 2008.
- [76] Z. Hadzibabic, P. Krüger, M. Cheneau, B. Battelier, and J. Dalibard, “Berezinskii-Kosterlitz-Thouless crossover in a trapped atomic gas,” *Nature*, vol. 441, pp. 1118–1121, 2006.
- [77] M. Anderlini, P. J. Lee, B. L. Brown, J. Sebby-Strabley, W. D. Phillips, and J. V. Porto, “Controlled exchange interaction between pairs of neutral atoms in an optical lattice,” *Nature*, vol. 448, pp. 452–456, 2007.
- [78] R. H. Dicke, “Coherence in spontaneous radiation processes,” *Phys. Rev.*, vol. 93, p. 99, 1954.
- [79] M. Gross and S. Haroche, “Superradiance: An essay on the theory of collective spontaneous emission,” *Physics Reports*, vol. 93, pp. 301 – 396, 1982.
- [80] V. Ernst and P. Stehle, “Emission of radiation from a system of many excited atoms,” *Phys. Rev.*, vol. 176, pp. 1456–1479, 1968.
- [81] G. S. Agarwal, “Master-equation approach to spontaneous emission,” *Phys. Rev. A*, vol. 2, pp. 2038–2046, 1970.
- [82] N. E. Rehler and J. H. Eberly, “Superradiance,” *Phys. Rev. A*, vol. 3, pp. 1735–1751, 1971.
- [83] C. Chin, R. Grimm, P. Julienne, and E. Tiesinga, “Feshbach resonances in ultracold gases,” *Rev. Mod. Phys.*, vol. 82, pp. 1225–1286, 2010.
- [84] B. Paredes, A. Widera, V. Murg, O. Mandel, S. Fölling, I. Cirac, G. V. Shlyapnikov, T. W. Hänsch, and I. Bloch, “Tonks-Girardeau gas of ultracold atoms in an optical lattice,” *Nature*, vol. 429, pp. 277–281, 2004.
- [85] W. Greiner and J. Reinhardt, *Field quantization.* Springer Verlag, 1996.
- [86] R. Friedberg, S. R. Hartmann, and J. T. Manassah, “Limited superradiant damping of small samples,” *Physics Letters A*, vol. 40, pp. 365 – 366, 1972.
- [87] R. Friedberg and S. R. Hartmann, “Temporal evolution of superradiance in a small sphere,” *Phys. Rev. A*, vol. 10, no. 5, pp. 1728–1739, 1974.
- [88] B. R. Mollow, “Quantum theory of field attenuation,” *Phys. Rev.*, vol. 168, pp. 1896–1919, 1968.
- [89] H. J. Carmichael, “Spectrum of squeezing and photocurrent shot noise: a normally ordered treatment,” *J. Opt. Soc. Am. B*, vol. 4, pp. 1514–1519, 1987.
- [90] P. L. Kelley and W. H. Kleiner, “Theory of electromagnetic field measurement and photoelectron counting,” *Phys. Rev.*, vol. 136, pp. A316–A334, 1964.

-
- [91] L. Mandel, "Fluctuations of photon beams and their correlations," *Proc. Phys. Soc. (London)*, vol. 72, p. 1037, 1958.
- [92] —, "Fluctuations of photon beams: The distribution of the photo-electrons," *Proc. Phys. Soc. (London)*, vol. 74, p. 933, 1959.
- [93] R. W. Boyd, *Nonlinear optics*. Academic Press, 2003.
- [94] J. Seres, "Dispersion of second-order nonlinear optical coefficient," *App. Phys. B*, vol. 73, pp. 705–709, 2001.
- [95] M. Hillery, "An introduction to the quantum theory of nonlinear optics," *Acta Physica Slovaca*, vol. 59, p. 180, 2009.
- [96] P. D. Drummond, "Quantum theory of nonlinear optics," 2001.
- [97] M. J. Collett and C. W. Gardiner, "Squeezing of intracavity and traveling-wave light fields produced in parametric amplification," *Phys. Rev. A*, vol. 30, pp. 1386–1391, 1984.
- [98] G. Milburn and D. F. Walls, "Production of squeezed states in a degenerate parametric amplifier," *Optics Communications*, vol. 39, pp. 401 – 404, 1981.
- [99] K. J. McNeil and C. W. Gardiner, "Quantum statistics of parametric oscillation," *Phys. Rev. A*, vol. 28, pp. 1560–1566, 1983.
- [100] H. Yuen and J. H. Shapiro, "Optical communication with two-photon coherent states—Part I: Quantum-state propagation and quantum-noise," *IEEE Trans. Inf. Theory*, vol. 24, p. 657, 1978.
- [101] J. Shapiro, H. Yuen, and A. Mata, "Optical communication with two-photon coherent states—Part II: Photoemissive detection and structured receiver performance," *IEEE Trans. Inf. Theory*, vol. 25, p. 179, 1979.
- [102] H. Yuen and J. H. Shapiro, "Optical communication with two-photon coherent states—Part III: Quantum measurements realizable with photoemissive detectors," *IEEE Trans. Inf. Theory*, vol. 26, pp. 78–92, 1980.
- [103] C. M. Caves, "Quantum-mechanical noise in an interferometer," *Phys. Rev. D*, vol. 23, pp. 1693–1708, 1981.
- [104] B. Yurke and J. S. Denker, "Quantum network theory," *Phys. Rev. A*, vol. 29, pp. 1419–1437, 1984.
- [105] S. Chaturvedi, K. Dechoum, and P. D. Drummond, "Limits to squeezing in the degenerate optical parametric oscillator," *Phys. Rev. A*, vol. 65, p. 033805, 2002.
- [106] P. D. Drummond, K. Dechoum, and S. Chaturvedi, "Critical quantum fluctuations in the degenerate parametric oscillator," *Phys. Rev. A*, vol. 65, p. 033806, 2002.
- [107] C. Fabre, E. Giacobino, A. Heidmann, L. Lugiato, S. Reynaud, M. VDACCHINO, and W. KAIGE, "Squeezing in detuned degenerate optical parametric oscillators," *Quantum Optics: Journal of the European Optical Society Part B*, vol. 2, p. 159, 1990.
- [108] C. M. Savage and D. F. Walls, "Squeezing by parametric oscillation and intracavity four-wave mixing," *J. Opt. Soc. Am. B*, vol. 4, pp. 1514–1519, 1987.
- [109] M. D. Reid and P. D. Drummond, "Quantum correlations of phase in nondegenerate parametric oscillation," *Phys. Rev. Lett.*, vol. 60, pp. 2731–2733, 1988.
- [110] P. D. Drummond and M. D. Reid, "Correlations in nondegenerate parametric oscillation. II. below threshold results," *Phys. Rev. A*, vol. 41, pp. 3930–3949, 1990.
- [111] Z. Y. Ou, S. F. Pereira, H. J. Kimble, and K. C. Peng, "Realization of the Einstein-Podolsky-Rosen paradox for continuous variables," *Phys. Rev. Lett.*, vol. 68, pp. 3663–3666, 1992.
- [112] S. Reynaud, C. Fabre, and E. Giacobino, "Quantum fluctuations in a two-mode parametric oscillator," *J. Opt. Soc. Am. B*, vol. 4, pp. 1520–1524, 1987.
- [113] A. Heidmann, R. J. Horowicz, S. Reynaud, E. Giacobino, C. Fabre, and G. Camy, "Observation of quantum noise reduction on twin laser beams," *Phys. Rev. Lett.*, vol. 59, pp. 2555–2557, 1987.

- [114] A. S. Lane, M. D. Reid, and D. F. Walls, “Quantum analysis of intensity fluctuations in the nondegenerate parametric oscillator,” *Phys. Rev. A*, vol. 38, pp. 788–799, 1988.
- [115] M. D. Reid and P. D. Drummond, “Correlations in nondegenerate parametric oscillation: Squeezing in the presence of phase diffusion,” *Phys. Rev. A*, vol. 40, pp. 4493–4506, 1989.
- [116] K. Dechoum, P. D. Drummond, S. Chaturvedi, and M. D. Reid, “Critical fluctuations and entanglement in the nondegenerate parametric oscillator,” *Phys. Rev. A*, vol. 70, p. 053807, 2004.
- [117] M. I. Kolobov and I. V. Sokolov, *Sov. Phys. JETP*, vol. 69, p. 1097, 1989.
- [118] —, “Squeezed states of light and noise-free optical images,” *Physics Letters A*, vol. 140, pp. 101 – 104, 1989.
- [119] —, “Multimode squeezing, antibunching in space and noise-free optical images,” *Europhys. Lett.*, vol. 15, p. 271, 1991.
- [120] A. La Porta and R. E. Slusher, “Squeezing limits at high parametric gains,” *Phys. Rev. A*, vol. 44, pp. 2013–2022, 1991.
- [121] L. A. Lugiato and F. Castelli, “Quantum noise reduction in a spatial dissipative structure,” *Phys. Rev. Lett.*, vol. 68, pp. 3284–3286, 1992.
- [122] L. A. Lugiato and A. Gatti, “Spatial structure of a squeezed vacuum,” *Phys. Rev. Lett.*, vol. 70, pp. 3868–3871, 1993.
- [123] G. Grynberg and L. Lugiato, “Quantum properties of hexagonal patterns,” *Optics Communications*, vol. 101, pp. 69 – 73, 1993.
- [124] A. Gatti and L. Lugiato, “Quantum images and critical fluctuations in the optical parametric oscillator below threshold,” *Phys. Rev. A*, vol. 52, pp. 1675–1690, 1995.
- [125] L. A. Lugiato and G. Grynberg, “Quantum picture of optical patterns: Complementarity and wave-particle aspects,” *Europhys. Lett.*, vol. 29, p. 675, 1995.
- [126] R. E. Slusher, P. Grangier, A. LaPorta, B. Yurke, and M. J. Potasek, “Pulsed squeezed light,” *Phys. Rev. Lett.*, vol. 59, pp. 2566–2569, 1987.
- [127] R. M. Shelby and M. Rosenbluh, “Generation of pulsed squeezed light in a mode-locked optical parametric oscillator,” *Applied Physics B: Lasers and Optics*, vol. 55, pp. 226–232, 1992.
- [128] D. K. Serkland, M. M. Fejer, R. L. Byer, and Y. Yamamoto, “Squeezing in a quasi-phase-matched LiNbO₃ waveguide,” *Opt. Lett.*, vol. 20, pp. 1649–1651, 1995.
- [129] G. J. de Valcárcel, G. Patera, N. Treps, and C. Fabre, “Multimode squeezing of frequency combs,” *Phys. Rev. A*, vol. 74, p. 061801, 2006.
- [130] G. Patera, N. Treps, C. Fabre, and G. J. de Valcárcel, “Quantum theory of synchronously pumped type I optical parametric oscillators: characterization of the squeezed supermodes,” *Eur. Phys. J. D*, vol. 56, pp. 123–140, 2010.
- [131] A. E. B. Nielsen and K. Mølmer, “Multimode analysis of the light emitted from a pulsed optical parametric oscillator,” *Phys. Rev. A*, vol. 76, p. 033832, 2007.
- [132] B. Chalopin, F. Scazza, C. Fabre, and N. Treps, “Multimode nonclassical light generation through the optical-parametric-oscillator threshold,” *Phys. Rev. A*, vol. 81, p. 061804, 2010.
- [133] G.-L. Oppo, M. Brambilla, and L. A. Lugiato, “Formation and evolution of roll patterns in optical parametric oscillators,” *Phys. Rev. A*, vol. 49, p. 2028, 1994.
- [134] G.-L. Oppo, M. Brambilla, D. Camesasca, A. Gatti, and L. A. Lugiato, “Spatiotemporal dynamics of optical parametric oscillators,” *Journal of Modern Optics*, vol. 41, p. 1151, 1994.
- [135] K. Staliunas, “Transverse pattern formation in optical parametric oscillators,” *Journal of Modern Optics*, vol. 42, p. 1261, 1995.

-
- [136] G. J. de Valcárcel, K. Staliunas, E. Roldán, and V. J. Sánchez-Morcillo, “Transverse patterns in degenerate optical parametric oscillation and degenerate four-wave mixing,” *Phys. Rev. A*, vol. 54, p. 1609, 1996.
- [137] K. Staliunas and V. J. Sánchez-Morcillo, “Localized structures in degenerate optical parametric oscillators,” *Optics Communications*, vol. 139, pp. 306 – 312, 1997.
- [138] S. Longhi, “Localized structures in optical parametric oscillation,” *Physica Scripta*, vol. 56, p. 611, 1997.
- [139] M. Lassen, G. Leuchs, and U. L. Andersen, “Continuous variable entanglement and squeezing of orbital angular momentum states,” *Phys. Rev. Lett.*, vol. 102, p. 163602, 2009.
- [140] J. Janousek, K. Wagner, J.-F. Morizur, N. Treps, P. K. Lam, C. C. Harb, and H.-A. Bachor, “Optical entanglement of co-propagating modes,” *Nature photonics*, vol. 3, pp. 399–402, 2009.
- [141] A. Luis and L. L. Sánchez-Soto, “Phase-difference operator,” *Phys. Rev. A*, vol. 48, pp. 4702–4708, 1993.
- [142] S. Yu, “Quantized phase difference,” *Phys. Rev. Lett.*, vol. 79, pp. 780–783, 1997.
- [143] C. Navarrete-Benlloch, E. Roldán, and G. J. de Valcárcel, “On canonical pairs and noise transfer in 2-transverse-mode DOPOs,” 2008, arXiv: 0802.4356.
- [144] P. D. Drummond and I. K. Mortimer, “Computer simulations of multiplicative stochastic differential equations,” *Journal of Computational Physics*, vol. 93, pp. 144 – 170, 1991.
- [145] I. E. Protsenko, L. A. Lugiato, and C. Fabre, “Spectral analysis of the degenerate optical parametric oscillator as a noiseless amplifier,” *Phys. Rev. A*, vol. 50, pp. 1627–1645, 1994.
- [146] B. Coutinho dos Santos, K. Dechoum, A. Z. Khoury, L. F. da Silva, and M. K. Olsen, “Quantum analysis of the nondegenerate optical parametric oscillator with injected signal,” *Phys. Rev. A*, vol. 72, p. 033820, 2005.
- [147] B. Coutinho dos Santos, C. E. R. Souza, K. Dechoum, and A. Z. Khoury, “Phase conjugation and adiabatic mode conversion in a driven optical parametric oscillator with orbital angular momentum,” *Phys. Rev. A*, vol. 76, p. 053821, 2007.
- [148] P. Drummond, K. McNeil, and D. Walls, “Bistability and photon antibunching in sub/second harmonic generation,” *Optics Communications*, vol. 28, pp. 255 – 258, 1979.
- [149] Z. Y. Ou, “Quantum-nondemolition measurement and squeezing in type-II harmonic generation with triple resonance,” *Phys. Rev. A*, vol. 49, pp. 4902–4911, 1994.
- [150] A. Eschmann and M. D. Reid, “Squeezing of intensity fluctuations in frequency summation,” *Phys. Rev. A*, vol. 49, pp. 2881–2890, 1994.
- [151] M. W. Jack, M. J. Collett, and D. F. Walls, “Asymmetrically pumped nondegenerate second-harmonic generation inside a cavity,” *Phys. Rev. A*, vol. 53, pp. 1801–1811, 1996.
- [152] U. L. Andersen and P. Buchhave, “Squeezing and entanglement in doubly resonant, type II, second-harmonic generation,” *J. Opt. Soc. Am. B*, vol. 20, pp. 1947–1958, 2003.
- [153] —, “Polarization squeezing and entanglement produced by a frequency doubler,” *Journal of Optics B: Quantum and Semiclassical Optics*, vol. 5, p. S486, 2003.
- [154] Z. Zhai, Y. Li, and J. Gao, “Entanglement characteristics of subharmonic modes reflected from a cavity for type-II second-harmonic generation,” *Phys. Rev. A*, vol. 69, p. 044301, 2004.
- [155] Z. Zhai, H. Zou, J. Zhang, and J. Gao, “Bright entanglement characteristics of subharmonic modes reflected from cavity for type ii second-harmonic generation,” *J. Opt. Soc. Am. B*, vol. 22, pp. 878–883, 2005.
- [156] Y. Luo, Y. Li, C. Xie, Q. Pan, and K. Peng, “Simultaneous experimental generation of vacuum squeezing and bright amplitude squeezing from a frequency doubler,” *Opt. Lett.*, vol. 30, pp. 1491–1493, 2005.
- [157] L. Longchambon, J. Laurat, T. Coudreau, and C. Fabre, “Non-linear and quantum optics of a type II OPO containing a birefringent element,” *The European Physical Journal D - Atomic, Molecular, Optical and Plasma Physics*, vol. 30, pp. 279–285, 2004.

- [158] —, “Non-linear and quantum optics of a type II OPO containing a birefringent element,” *The European Physical Journal D - Atomic, Molecular, Optical and Plasma Physics*, vol. 30, pp. 287–293, 2004.
- [159] M. Vallet, M. Pinard, and G. Grynberg, “Generation of twin photon beams in a ring four-wave mixing oscillator,” *Europhys. Lett.*, vol. 11, pp. 739–744, 1990.
- [160] S. Feng and O. Pfister, “Stable nondegenerate optical parametric oscillation at degenerate frequencies in a χ^2 crystal,” *Journal of Optics B: Quantum and Semiclassical Optics*, vol. 5, p. 262, 2003.
- [161] B. C. dos Santos, K. Dechoum, and A. Z. Khoury, “Continuous-variable hyperentanglement in a parametric oscillator with orbital angular momentum,” *Phys. Rev. Lett.*, vol. 103, p. 230503, 2009.
- [162] H. Goldstein, C. Poole, and J. Safko, *Classical mechanics, 3ed.* Addison Wesley, 2001.
- [163] W. Greiner, *Classical mechanics: Point particles and relativity.* Springer Verlag, 1989.
- [164] W. Greiner and J. Reinhardt, *Classical mechanics: Systems of particles and Hamiltonian dynamics.* Springer Verlag, 1989.
- [165] E. Prugovečky, *Quantum mechanics in Hilbert space.* Academic Press, 1971.
- [166] A. Galindo and P. Pascual, *Quantum Mechanics I.* Springer Verlag, 1990.
- [167] P. A. M. Dirac, *The principles of quantum mechanics.* Oxford university press, 1930.
- [168] I. M. Gelfand and N. Y. Vilenkin, *Generalized Functions, Vol. IV.* Academic Press, 1964.
- [169] B. L. van der Waerden, *Sources of Quantum Mechanics.* Dover Publications, 1968.
- [170] E. Schrödinger, “An undulatory theory of the mechanics of atoms and molecules,” *Phys. Rev.*, vol. 28, pp. 1049–1070, 1926.
- [171] W. Heisenberg, “über quantentheoretische umdeutung kinematischer und mechanischer beziehungen,” *Zs. f. Phys.*, vol. 33, pp. 879–893, 1925.
- [172] M. Born and P. Jordan, “Zur quantenmechanik,” *Zs. f. Phys.*, vol. 34, pp. 858–888, 1925.
- [173] M. Born, W. Heisenberg, and P. Jordan, “Zur quantenmechanik ii,” *Zs. f. Phys.*, vol. 35, pp. 557–615, 1926.
- [174] P. A. M. Dirac, “The fundamental equations of quantum mechanics,” *Proc. Roy. Soc. A*, vol. 109, pp. 642–653, 1926.
- [175] J. von Neumann, *Mathematische Grundlagen der Quantenmechanik.* Springer Verlag, 1932.
- [176] —, *Mathematical foundations of quantum mechanics.* princeton university press, 1955.
- [177] C. Cohen-Tannoudji, B. Diu, and F. Laloë, *Quantum mechanics, Vol. I.* Hermann and John Wiley & Sons, 1977.
- [178] —, *Quantum mechanics, Vol. II.* Hermann and John Wiley & Sons, 1977.
- [179] W. Greiner and B. Müller, *Quantum mechanics: An introduction.* Springer Verlag, 1989.
- [180] W. Greiner, *Quantum mechanics: Symmetries.* Springer Verlag, 1989.
- [181] J.-L. Basdevant and J. Dalibard, *Quantum mechanics.* Springer Verlag, 2002.
- [182] H. J. Groenewold, “On the principles of elementary quantum mechanics,” *Physica*, vol. 12, pp. 405–460, 1946.
- [183] R. F. Fox, I. R. Gatland, R. Roy, and G. Vemuri, “Fast, accurate algorithm for numerical simulation of exponentially correlated colored noise,” *Phys. Rev. A*, vol. 38, pp. 5938–5940, 1988.